MARINA MILITARE

IMEKO TC-19 INTERNATIONAL WORKSHOP ON
METROLOGY FOR THE SEA

Learning to measure sea health parameters

MetroSea
#Naples2020

Virtual Conference

MetroSea2020

For further information, visit the website
www.metrosea.org

BOOK OF ABSTRACTS

ATHENA SRL
Business and technology consulting

MetroSea 2020 - Welcome Message

On behalf of the Organizing Committee, we cordially welcome you to the **2020 IMEKO International Workshop on Metrology for the Sea** (*MetroSea 2020*).

The Sea is the medium that allowed people to travel from one continent to another using vessels and even today despite the use of aircraft. It has been acting also as a great reservoir and source of foods for all living beings. However, for many generations it served as a landfill for depositing conventional and nuclear wastes, especially in its seabed and there is a race to exploit minerals and resources, different from foods, encompassed in it. Its heath is a very challenge for the survival of all humanity since it is one the most important environmental components targeted by the global warming.

"Learning to measure sea health parameters" is a challenge for the whole humanity. This is underlined by the growing interest for the marine sciences. In this field new technologies and analysis techniques have recently improved the combined use of numerical approach and metrology systems to get more detailed marine data. For example, advances in computer science, data acquisition and modelling, new spectrometric techniques, analysis and remote sensing have encouraged interactions among these scientific disciplines based on measurement data and marine data interpretations.

The benefits of a multidisciplinary approach have reduced the level of uncertainty in marine technical studies. The 2020 IMEKO International Workshop on Metrology for the Sea aims to gather people who work in developing instrumentation and measurement methods for the sea. Attention is paid, but not limited to, at new technology for sea environment monitoring, metrology-assisted production in sea industry, ship component measurement, sensors and associated signal conditioning for the sea, and calibration methods for electronic test and measurement for marine applications.

This edition of MetroSea was originally planned to be held in Naples (Italy) hosted by the Università degli Studi di Napoli “Parthenope” as part of the celebrations for the 100th anniversary of its foundation; however, due to the COVID-19 emergency, we were forced to organize this 4th edition as a virtual conference. We do hope that, soon, there will be another chance to host you all in Naples. The virtual Workshop has been planned in order to make an online conference not so different from a live event. It was challenging to set up a web platform to maintain live the presentations and we thank the colleagues of the organizing team, who professionally addressed this issue.

Despite the COVID-19 occurrence, we received 60 extended abstracts from all over the world. Due to the time limits of the workshop, only 45 papers have been selected after a meticulous activity of the program committee and additional reviewers. We like to thank all people who contributed to this process with opinions, comments, and suggestions to choose the best papers and improve their quality.

Authors of all the above contributions are also welcome to submit an extended version to the Special Issues on ACTA IMEKO Journal, MDPI Geosciences, MDPI Sensors and MDPI Journal of Marine Science and Engineering.

The Workshop Technical Program consists of 15 oral sessions scheduled over three days. The technical program encompasses several events and activities. With the wide range of technical sessions covering the many fields of metrology for the sea we are happy to welcome you to the variety of technical presentations that await you this year.

The keynote speeches will be held by experts in the field of metrology for the sea. Cosimo Solidoro and Rajesh Nair, both from National institute for Oceanography and Applied Geophysics OGS, Italy, will speak about “*Filling a gap: metrology in marine observation and data*”. Marcos Portabella, Institut de Ciències del Mar (ICM-CSIC), Spain, will present “*Scatterometer-derived stress-equivalent wind fields: retrievals and applications*”. We are honored to have them as plenary speakers and thank them in advance for coming to our conference to share their knowledge and experiences with us.

This edition of the Workshop includes:

- “**Military Metrology for the Sea**”, organized by Italian Navy and AFCEA Naples Chapter, October 5, 09:30 CET
- **Tutorials** offering three subjects:
  - “Integrated remote coastal and seabed mapping”, S.V.T. Luca Labella, Italian Navy;
  - “Multidimensional marine geophysical data acquisition using Autonomous Surface Vehicles”, Dr Luca Gasperini, Institute of Marine Science - National Research Council, Italy
  - “Satellite remote sensing of the ocean: applications in temperate and polar regions”, Dr Giuseppe Aulicino, University of Naples "Parthenope", Italy

Several Awards offered by International Institution and Companies will be assigned, in particular to young researchers.

With the aim of providing a common ground for researches to share their findings on the metrology for the sea, the Workshop was improved by adding a significant number of Special Sessions. This allows a spontaneous aggregation providing a forum of discussion close to the single research field. We wish to thank the organizers of these Special Sessions for their cooperation and support to the Workshop organization.

The 2020 IMEKO International Workshop on Metrology for the Sea is about to begin.

Giorgio Budillon, Parthenope University of Naples, Italy
Pasquale Daponte, University of Sannio, Italy
Luigi Sinapi, Italian Navy, Italy

MetroSea 2020 General Chairs

MetroSea 2020 Committee

HONORARY CHAIR
Aimé Lay-Ekuakille, *University of Salento, Italy*

GENERAL CO-CHAIRS
Giorgio Budillon, *University of Naples "Parthenope", Italy*
Pasquale Daponte, *University of Sannio, Italy*
Luigi Sinapi, *Italian Hydrographic Institute - Italian Navy, Italy*

TECHNICAL PROGRAMME CO-CHAIRS
Salvatore Gaglione, *University of Naples "Parthenope", Italy*
Donatella Insinga, *ISMAR-CNR, Italy*

AWARD CHAIR
Maria Rosaria Senatore, *University of Sannio, Italy*

SPECIAL SESSION CHAIR
Fabio Conversano, *Stazione Zoologica Anton Dohrn of Naples, Italy*

TREASURY CHAIR
Sergio Rapuano, *University of Sannio, Italy*

INTERNATIONAL PROGRAM COMMITTEE
Francesco Adamo, *Polytechnic University of Bari, Italy*
Gregorio Andria, *Polytechnic University of Bari, Italy*
Leopoldo Angrisani, *University of Naples Federico II, Italy*
Antonio Angrisano, *University of Benevento "G. Fortunato", Italy*
Flavio Balsamo, *University of Naples Federico II, Italy*
Yvan Baudoin, *Royal Military Academy, Belgium*
Paul L. Bishop, *University of Rhode Island, USA*
Vittorio Bucci, *University of Trieste, Italy*
Francesca Budillon, *CNR-IAMC Napoli, Italy*
Bertrand Calpini, *Federal Polytechnic School of Lausanne, Switzerland*
Roberto Carlucci, *University of Bari Aldo Moro, Italy*
Francesco Chiocci, *University of Roma "La Sapienza", Italy*
Roland Collay, *Ecole des Mines de Saint-Etienne, France*
Daniele Contini, *ISAC - CNR, Italy*
Francesco Crenna, *University of Genova, Italy*
Claudio De Capua, *University Mediterranea of Reggio Calabria, Italy*
Silvio Del Pizzo, *University of Naples "Parthenope", Italy*
Attilio Di Nisio, *Polytechnic University of Bari, Italy*

Nicola Donato, *Università degli studi di Messina, Italy*
Marc Dubois, *Institute of Chemistry of Clermont-Ferrand, France*
Ivana Durickovic, *University Paul Verlaine, France*
Artur Dybko, *Warsaw Univ of Technology, Poland*
Marc Fontana, *University of Lorraine and Supélec, France*
Cristian Fosalau, *"Gheorghe Asachi" Technical Universiy of Iasi, Romania*
Fabiano Gamberi, *CNR-ISMAR, Italy*
Pedro Girao, *Superior Technical Institute, Lisbon*
Athar Hussain, *GGSIPU Civil Engineering, India*
Satoshi Ikezawa, *Earthquake Research Institute, Japan*
Marina Iorio, *IAMC, Italy*
Olfa Kanoun, *Chemnitz University of Technology, Germany*
Theodore Laopoulos, *Aristotle University of Thessaloniki, Greece*
Anna M. L. Lanzolla, *Polytechnic University of Bari, Italy*
Martin Lloyd, *Farside Technology, United Kingdom*
Sabino Maggi, *IRSA - CNR, Italy*
Ennio Marsella, *IAMC-CNR, Naples, Italy*
Alessandro Massaro, *CNR-IMIP, Italy*
Janusz Mindykowski, *Gdynia Maritime University, Poland*
Danilo Morelli, *University of Genova, Italy*
Rosario Morello, *University Mediterranea of Reggio Calabria, Italy*
Michele Mossa, *Polytechnic University of Bari, Italy*
Marco Mugnaini, *University of Siena, Italy*
Rosaria E. Musumeci, *University of Catania, Italy*
Marina Paolucci, *University of Sannio, Italy*
Lorenzo Papa, *University of Genova, Italy*
Nicola Pasquino, *University of Naples Federico II, Italy*
Giuseppe Passarella, *IRSA - CNR, Italy*
Armin Pavic, *University of Zagreb, Croazia*
Silvia Pennino, *University of Naples "Parthenope", Italy*
Vincenzo Piscopo, *Parthenope University of Naples, Italy*
Octavian Postolache, *Superior Technical Institute, Portugal*
Peter Princz, *Institute of Geosciences, HUN*
Alberto Quagli, *University of Genova, Italy*
Janaina M. Rodrigues, *INMETRO, Brazil*
Bianca Russo, *University of Napoli Federico II, Italy*
Guido Sassi, *University of Torino, Italy*
Mario Savino, *Polytechnic University of Bari, Italy*
Emiliano Schena, *Università Campus Bio-Medico, Italy*
Paulo R. Martins Silva, *Brazil*
Giovanni Satta, *University of Genoa, Italy*
Joao Sousa, *Portugal*
Maurizio Spadavecchia, *Polytechnic University of Bari, Italy*
Attilio Sulli, *University of Palermo, Italy*
Tong Sun, *City University of London, London*

Tiziana Tambosso, *IEEE Italy Section, Italy*
Alessio Tei, *Newcastle University, UK*
Maurizio Torrente, *University of Sannio, Italy*
Andrea Trucco, *University of Genoa, Italy*
Angelo Tursi, *University of Bari, Italy*
Shabana Urooj, *Gautam Buddha University, India*
Henry Vallius, *Geological Survey of Finland (GTK), Finland*
Leo Van Biesen, *Vrije Universiteit Brussel, Belgium*
Ramiro Velazquez, *Universidad Panamericana, Mexico*
Jari Walden, *Finnish Meteorological Institute, Finland*
Sunao Yamashita, *DKK-TOA Corporation, Japan*

MetroSea 2020 Plenary Speakers

Tuesday, October 6, 2020 - 09.30 CET

Filling a gap: Metrology in Marine Observation and Data

Cosimo Solidoro, Rajesh Nair

National Institute of Oceanography and Applied Geophysics, Italy

ABSTRACT

The European Union's Marine Strategy Framework Directive (2008) states that "Provision should be made for the adoption of methodological standards for the assessment of the status of the marine environment, monitoring, environmental targets and the adoption of technical formats for the purposes of transmission and processing of data […]". In its 2010 Communication to the European parliament and Council on the Marine Knowledge 2020 initiative within the framework of the European Union's Integrated Maritime Policy, the European Commission highlighted that "Fragmented standards, formats and nomenclature, lack of information on precision and accuracy, the pricing policy of some providers and insufficient temporal or spatial resolution are further barriers [to the exploitation of collected data in developing new products and services]".

The above institutional excerpts are testimony to the pressing need to begin building a strong metrological basis for marine measurements in Europe, making it an integral part of the region's marine observing and data management sectors. The metrological approach represents an established way to assure traceability of measurements to the Système International d'Unités (SI) and achieve true inter-comparability of data at the transnational level. Such traceability is essential to ensure:

- the relation of acquired measurements to recognized standards;
- the conformity of measurement practices amongst laboratories to acknowledged guidelines at both the national and international levels;
- the provision of documentation to handle sensors and data properly.

However, metrology is rarely discussed in marine observing circles and in the marine data management community despite its intimate link to sensor performance, data quality and data usability issues. This disregard arises from ignorance concerning the rigor required of modern measuring activity and the complexity of the underlying metrological system supporting it. It must be said that the situation is also a heritage of the historical evolution of marine observing activity, which developed outside the umbrellas of national metrological institutions (NMIs) and formally recognized international metrological frameworks. Unfortunately, in today's reality, where marine measurements and data are no longer viewed solely as a scientific tool but also as a valuable multiple-use commercial commodity and a resource for social change, this state of affairs is no longer tenable and needs to be addressed.

At the present time, there are very few scientists working formally in the field of metrology applied expressly to marine measurements (perhaps even < 10 persons per country in Europe). But, over the past

few years, these small groups are beginning to work together to try to lay the foundation for a pan-European marine calibration grid in coordination with the system of NMIs and industry. Most of this activity is being, or has been, attempted indirectly, and only in small ways, within the framework of European projects and programmes, most notably, ENV05, JERICO, JERICO-NEXT and JPI-Oceans. There is a strong necessity to inform the marine observing community and the European Commission of the need for specific attention and investments on this topic as it will be fundamental to fulfilling central European policy goals such as the Marine Strategy Framework Directive and Blue Growth.

SPEAKERS BIOGRAPHY

Cosimo Solidoro is research director and currently head of the Oceanography Section of the National institute for Oceanography and Applied Geophysics OGS . Research activities include developments, analysis and use of a variety of numerical methodologies, ecological models and ocean models of different complexity. Recent research activities expand further over the human dimensions and the integration among different components of marine systems. Scientific Coordinator of Sharemd, a EU project on pollution and environmental threats and of ICCC, a PRIN project on pollutants and biogeochemical cycles in a changing climate. President of the International Society of Ecological Modelling - European Chapter, member of the executive board of the european consortium EUROCEANS.

Rajesh Nair (male) has nearly 30 years of experience in Oceanography and the Marine Sciences, with a strong experimental background, extensive field skills and "hands-on" knowledge of a wide variety of marine instrumentation. As part of the permanent staff of the Centro di Taratura e Metrologia Oceanografica (CTMO), the oceanographic calibration facility of the INOGS which he helped set up in 2002, his present activities and interests focus on marine observing technologies, including calibration, control and testing of instrumentation, and the application of metrological principles to measurement quality assurance both in the laboratory and in the field. Mr. Nair is actively involved in marine research at both the national and EU levels, and internationally. He co-led Work Package 2 ("Harmonization of technologies and methodologies - technical strategy) of the EU H2020 project, JERICO-NEXT (Joint European Research Infrastructure network for Coastal Observatory - Novel European eXpertise for coastal observaTories; 2015 - 2019), and was the leader of Work Package 5 ("Data management and distribution") of the EU FP7 project, JERICO (Towards a Joint European Research Infrastructure network for Coastal Observatories, 2011 - 2015). Mr. Nair currently co-chairs the Technology Panel Working Group (TPWG) of the European Global Ocean Observing System (EuroGOOS), the European component of the Global Ocean Observing System (GOOS), and is also a National Representative in the EU's JPI Oceans (Joint Programming Initiative - Healthy and Productive Seas and Oceans) European Marine Sensor Calibration Network Joint Action.

Wednesday, October 7, 2020 - 09:30 CET

Scatterometer-derived stress-equivalent wind fields: retrievals and applications

Marcos Portabella

Institut de Ciències del Mar (ICM-CSIC), Spain

ABSTRACT

Spaceborne scatterometers (real-aperture radars) are known for their near-surface wind sensing capabilities over the ocean. Their derived stress-equivalent wind field observations are increasingly used in a wide variety of atmospheric, oceanographic and climate applications. An introduction to the physical principles of scatterometry, followed by an overview of the wind retrieval processing chain will be presented and discussed. The radar antenna geometry, the measurement noise, as well as non-linearities in the relationship between the measurements and the wind vector complicate the wind retrieval process. In addition, scatterometers are sensitive to geophysical phenomena other than wind, such as confused sea state, rain, and land/ice contamination of the radar footprint. These phenomena can distort the wind signal, leading to poor quality retrieved winds. As such, elimination of poor quality data is a prerequisite for the successful use of the retrieved winds. The differences between sea-surface C-band and Ku-band radar signatures will also be discussed in the context of sensor inter-calibration efforts.

The main applications of the scatterometer-derived stress-equivalent winds will also be presented. Besides the obvious atmospheric applications, such as nowcasting and global and regional Numerical Weather Prediction (NWP) data assimilation, scatterometer winds can provide very useful information on NWP model errors. They are also used to well characterize the extreme wind stress divergence and vorticity (missed by NWP models) associated to extreme rain events in the tropics. In addition, these observations are also required to drive ocean circulation, wave and surge models, and are used to compute sea surface currents and air-sea fluxes. Recent developments show that a modified NWP output using scatterometer-based corrections can introduce true smaller scale signal into the model output, which corresponds to the physical processes absent or misrepresented by the model, e.g., strong current effects (such as WBCS, highly stationary), wind effects associated with the ocean mesoscales (SST), coastal effects (land see breezes, katabatic winds), parameterization errors, and large-scale circulation effects, e.g., at the ITCZ. Finally, recent efforts to consolidate an in situ high and extreme wind reference for improving current and future scatterometer extreme wind calibration and validation will be discussed in the context of improved monitoring and prediction of extreme wind events, such as tropical and extra-tropical cyclones, and polar lows.

SPEAKER BIOGRAPHY

Marcos Portabella was born in Barcelona, Spain, in 1970. He received the B.Sc. degree in physics from the University of Barcelona, Barcelona, Spain, in 1994, the M.Sc. degree in remote sensing from the Institute of Space Studies of Catalonia, Barcelona, in 1995, and the Ph.D. degree in physics from the University of Barcelona. He is currently with the Institut de Ciències del Mar (ICM-CSIC), Barcelona, where he leads the Satellite Winds Group. He is involved in satellite remote sensing, and in particular, scatterometry and L-band radiometry.

MetroSea 2020 Patronages

MARINA MILITARE

Consiglio Nazionale delle Ricerche

CoNISMa
Consorzio Nazionale Interuniversitario per le Scienze del Mare

UNIVERSITÀ DEGLI STUDI DEL SANNIO
Benevento

1920 - 2020
UNIVERSITÀ DEGLI STUDI DI NAPOLI PARTHENOPE
100° ANNIVERSARIO

LEGA NAVALE ITALIANA

Sistema Nazionale per la Protezione dell'Ambiente

SOCIETÀ GEOLOGICA ITALIANA
1881
MENTE ET MALLEO

associazione italiana
gme
gruppo misure
elettriche ed elettroniche

MMT
Gruppo Nazionale

CARMELO

MetroSea 2020 Sponsors

Indice

1

General Session
Metrology for the Sea 2020

Albacore: A Sub Drone for Shallow Waters A preliminary study

Enrico Petritoli, Fabio Leccese
Science Department, Università degli Studi "Roma Tre"
Via Della Vasca Navale n°84, 00146
Rome, Italy
e_petritoli@libero.it - ORCID: 0000-0002-6135-8386
fabio.leccese@uniroma3.it - ORCID: 0000-0002-8152-2112

***Abstract*—In this paper the idea to develop an underwater drone optimized for shallow water, inland ports and small inlets is shown. The vehicle should be simple and robust: a mathematical part is included on the vertical balance to be able to size weights and payload volumes.**

Keywords - AUV; Drone; Shallow; Water.

I. INTRODUCTION

This paper is part of several preliminary studies by Underwater Drones Group (UDG) of the Science Department of the Università degli Studi "Roma Tre", which is developing a series of advanced Autonomous Underwater Vehicles (AUVs) for the exploration of the sea at high depths. The final aim of the general project is to create several platforms for underwater scientific research that can accommodate a wide range of different payloads optimized for the most usual tasks [1]-[12]. The underwater vehicle was named *Albacore* (*Thunnus Alalunga*) due to the extreme similarity in both size and shape with the tuna well widespread in the Mediterranean: it was designed for use in shallow, high turbulence waters, often in the presence of natural obstacles (rocks and shoals) but also wrecks or breakwaters, etc. For all this reasons, it has been equipped with two powerful engines that operate counter-rotating propellers and an elliptical wing, sturdy and stiff [13]-[18].

II. THE VEHICLE

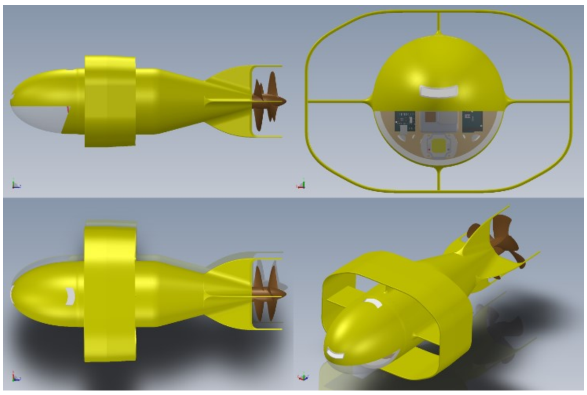

Figure 1. Four views of the AUV Albacore.

The vehicle is a cylindrical AUV, with an annular wing and propelled by a double electric motor. Let's look at its detailed description (see Figure 1).

A. The Fuselage

The fuselage of the Albacore (see Figure 2) is roughly cylindrical, composed of milled aluminium 6061 class: in the front, we have an elliptical radome act to contain the payload that consists on several biochemical sensors arranged in a "nostril" that has the purpose of protecting the instrumentation without exposing it directly to the outside [19]-[27].

In the lower section, there is a transparent porthole in polymethylmethacrylate (Plexiglas): it is the window for the camera (GoPro class) and the relative lighting system.

The central part supports the supports of the elliptical wing and is further stiffened by a series of internal battens. The terminal cone (this too stiffened in the same way) supports the fletching and the thrust of two counter-rotating propellers [28]-[35].

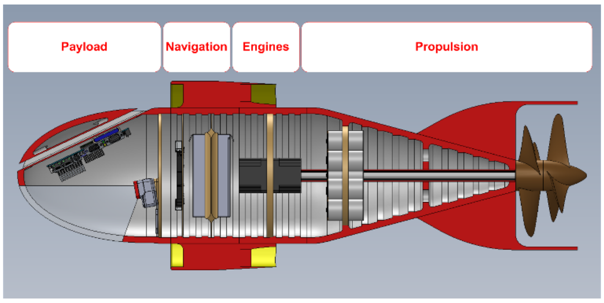

Figure 2. Cross section of the AUV Albacore: the interior arrangement of the vehicle is visible.

The fuselage is composed by four coaxial cylindrical compartments (or bays):

- Payload bay
- Navigation bay
- Engines bay and
- Propulsion bay.

B. Payload Bay

The Payload Bay is, in essence, a "radome", which contains the "nostril" (see Figure 3) whose channel in turn houses the chemical and biological sensors: the data collected are managed by a PC-104 computer card, which also has the task of sending them to the central computer (Arduino) [36]-[42]. The nostril is inclined of 20° so that its flow is the least disturbed possible and its discharge flow does not create turbulence or disturbance to the flow of the elliptical wing. Below, there is the corresponding window of a digital camera

(Go-Pro class): in anticipation of its use for visual inspection and automatic recognition of objects at depths, which, although modest, could be lacking in sufficient light, on the bulkhead will be mounted a 10^6 candle, flat LED. Lighting for the camera is important in the case of operation in the low waters of the ports, notoriously turbid or in co-current sources coming from silty river mouths [43]-[46].

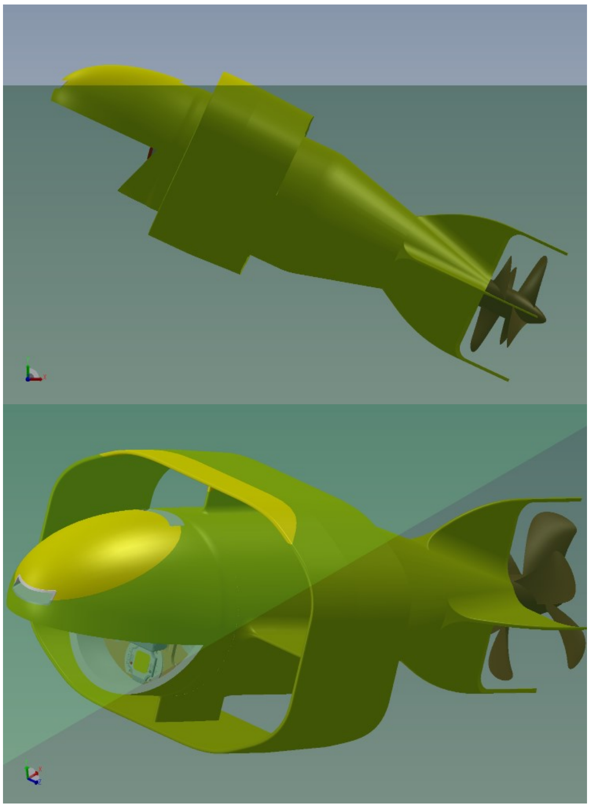

Figure 3. The drone in "nose up" attitude (upper) side view; (lower) prospective view.

C. Navigation Bay

The Navigation Bay contains two Arduino units: due to their quality level COTS (Commercial Off-The-Shelf), it was decided to put them in Main and Redundant configuration. The second unit (redundant) is placed in "hot strand by", that is to say, despite being fed and while managing the same data flow, it is not called to play the role of OBDH (On Board Computer and Data Handling) as instead the Main Unit does: this allows, in the event of a malfunction, to take over the latter in a completely transparent manner to the rest of the devices to which they are interfaced (see Figure 4). The bay also contains the two main rechargeable batteries: one supplies power to the ODBH and the other to the payload. The differentiation was necessary due to the fact that, in the event of a serious failure of the first battery, the second, disconnecting all non-essential services, can supply the energy needed by the Arduino computer to be able to lead the vehicle to the surface and to manage any recovery procedures.

D. Engines Bay

The engine bay contains two identical but counter-rotating electric motors (CW and CCW) which in turn operate the two propellers, also these counter-rotating. The movement is transmitted by two concentric drive shafts: the first (CW) is internal and moves the propeller at the end, the second (CCW) is hollow and allows the rotation of the first and moves the propeller closer to the hull. Due to the length of the drive shafts, two bearings were placed to attenuate any vibrations, one at the auxiliary battery cluster and another near the tail.

E. Propulsion Bay

The propulsion bay contains first and foremost the battery cluster, the drive shafts of the engines, the fletching and the two counter-rotating propellers. The battery cluster is composed of a canister that supports 12 "D" type accumulators of a completely different technology compared to the two main batteries so that, given the same environment, it has a completely different reliability (electromechanical degradation) response. Thanks to a small engine, it is possible to slide the chassis backwards so that the centre of mass of the vehicle moves quite far from the hydrostatic centre and so the hull can assume the "nose up" position for biochemical measurements (see Fig. 4).

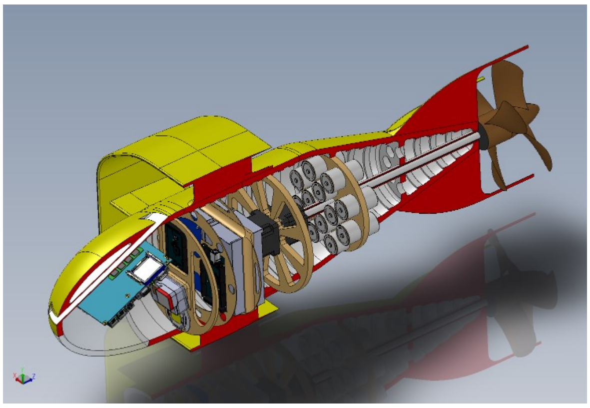

Figure 4. Prospective cross section of the AUV Albacore: the interior sections and supports are visible.

The cruciform flutes have no dihedral and have been prolonged to act as a guard for the propellers, thus preventing them from being sized in the presence of tufts of algae or wandering nets. Finally, the propellers are counter-rotating in order to counteract the strong torque of the engines, which are especially slow-moving because we are in the absence of a large wingspan that can counteract them. The terminal propeller has an angle of attack greater than the previous one in order to have the same performance as the previous one, being lapped by a flow already in rotation.

F. The Wing

Following a careful study, an elliptical annular wing was chosen for the vehicle: the peculiarity of the configuration was dictated by very strict requirements. First of all, with this solution we have practically halved the wingspan, greatly reducing the moment of inertia on the longitudinal axis: this apparent "introduction of instability" is largely compensated for the presence of spoilers that guarantee the vehicle's dynamic stability. One of the possible applications of the AUV is that of the underwater inspection of fishing nets, submerged systems and submarine cables: the fact of having a ring-shaped wing guarantees the fact that it does not get caught in possible underwater obstacles [47]-[50].

Among the main requirements, it was considered that the vehicle can be used by unskilled personnel with equipment not specially adapted: it will be sufficient, therefore, to be able to set sail on board, to have a simple winch: in this case the wing has been strengthened to operate as a "bumper" and withstand without damage possible minor bumps against the ship's rail. Last but not least, the elliptical annular wing gives the vehicle great dynamic stability, a modest induced resistance, a dimensional compactness: this is supported by four cross-shaped bracing that also act as a further element of stability.

III. Dynamic Force Balance

In this section, we consider the drone emerging at constant speed (see Fig. 5).

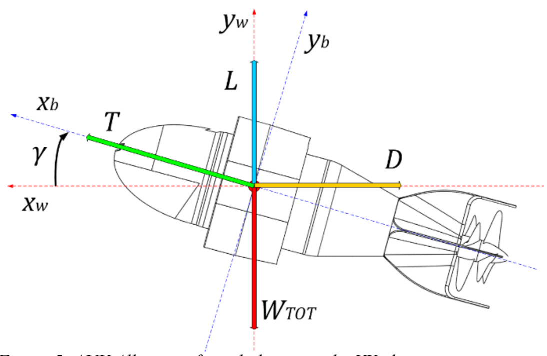

Figure 5. AUV Albacore: force balance on the XY plane.

At the equilibrium, the dynamic on the x_w and y_w axis are, at constant speed:

$$\begin{cases} 0 = T\cos\gamma - D \\ 0 = T\sin\gamma + L - W_{tot} \end{cases} \tag{1}$$

Where

T : thrust

D : drag due to the shape of the vehicle

v : drone relative speed (refer to water)

L : lift

γ : angle of attack

W_{tot} : total weight

The complete expression for the *drag* is:

$$D = \frac{1}{2}\rho v^2 S C_D \tag{2}$$

where:

ρ : seawater density (average 1.025 kg/L)

S : drone wing surface

v : drone relative speed (refer to water)

C_D : coefficient of drag

According to Taylor method [51], the last member can be separated in:

$$C_D = C_{D_0} + C_{D_\gamma}\gamma \tag{3}$$

where:

C_{D_0} : coefficient of drag at $\gamma = 0$

C_{D_γ} : coefficient of drag at $\gamma \neq 0$

so the (2) becomes:

$$D = \frac{1}{2}\rho v^2 S\left(C_{D_0} + C_{D_\gamma}\gamma\right) \tag{4}$$

The expression for the *lift* is:

$$L = \frac{1}{2}\rho v^2 S C_L \tag{5}$$

where:

C_L : coefficient of lift

According to Taylor method as per Eq. (3):

$$C_L = C_{L_0} + C_{L_\gamma}\gamma \tag{6}$$

where:

C_{L_0} : coefficient of lift at $\gamma = 0$

C_{L_γ} : coefficient of lift at $\gamma \neq 0$

so the (5) becomes:

$$L = \frac{1}{2}\rho v^2 S\left(C_{L_0} + C_{L_\gamma}\gamma\right) \tag{7}$$

For the weight we have

$$W_{tot} = W_{DW} - B_{GB} \tag{8}$$

where

W_{DW} : dry weight of the drone

B_{GB} : buoyancy of the drone

so, for the (1) we have:

$$\begin{cases} 0 = T\cos\gamma - \frac{1}{2}\rho v^2 S\left(C_{D_0} + C_{D_\gamma}\gamma\right) \\ 0 = T\sin\gamma + \frac{1}{2}\rho v^2 S\left(C_{L_0} + C_{L_\gamma}\gamma\right) - W_{DW} + B_{GB} \end{cases} \tag{9}$$

Now we evidence the thrust:

$$\begin{cases} T\cos\gamma = +\frac{1}{2}\rho v^2 S\left(C_{D_0} + C_{D_\gamma}\gamma\right) \\ T\sin\gamma = -\frac{1}{2}\rho v^2 S\left(C_{L_0} + C_{L_\gamma}\gamma\right) + W_{DW} - B_{GB} \end{cases} \tag{10}$$

so:

$$\begin{cases} T = \dfrac{+\frac{1}{2}\rho v^2 S\left(C_{D_0} + C_{D_\gamma}\gamma\right)}{\cos\gamma} \\ T = \dfrac{-\frac{1}{2}\rho v^2 S\left(C_{L_0} + C_{L_\gamma}\gamma\right) + W_{DW} - B_{GB}}{\sin\gamma} \end{cases} \tag{11}$$

Upper and lower member are the same, so:

$$\frac{+\frac{1}{2}\rho v^2 S\left(C_{D_0} + C_{D_\gamma}\gamma\right)}{\cos\gamma} = \frac{-\frac{1}{2}\rho v^2 S\left(C_{L_0} + C_{L_\gamma}\gamma\right) + W_{DW} - B_{GB}}{\sin\gamma} \tag{12}$$

Now, in order to isolate the angle of attack:

$$\frac{\sin\gamma}{\cos\gamma} = \frac{-\frac{1}{2}\rho v^2 S\left(C_{L_0} + C_{L_\gamma}\gamma\right) + W_{DW} - B_{GB}}{+\frac{1}{2}\rho v^2 S\left(C_{D_0} + C_{D_\gamma}\gamma\right)} \tag{13}$$

Then

$$\tan\gamma = \frac{-\frac{1}{2}\rho v^2 S\left(C_{L_0} + C_{L_\gamma}\gamma\right) + W_{DW} - B_{GB}}{+\frac{1}{2}\rho v^2 S\left(C_{D_0} + C_{D_\gamma}\gamma\right)} \quad (14)$$

In case of "straight and level" trajectory we have $\gamma = 0$ so

$$0 = \frac{-\frac{1}{2}\rho v^2 S C_{L_0} + W_{DW} - B_{GB}}{+\frac{1}{2}\rho v^2 S C_{D_0}} \quad (15)$$

and

$$0 = -\frac{1}{2}\rho v^2 S C_{L_0} + W_{DW} - B_{GB} \quad (16)$$

Posing

$$\kappa = \frac{1}{2}\rho S C_{L_0} \quad (17)$$

we have:

$$\kappa \cdot v^2 = W_{DW} - B_{GB} \quad (18)$$

so for the speed:

$$v = \sqrt{\frac{W_{DW} - B_{GB}}{\kappa}} \quad (19)$$

In, the graph in fig. 6, we see the trend of the function:

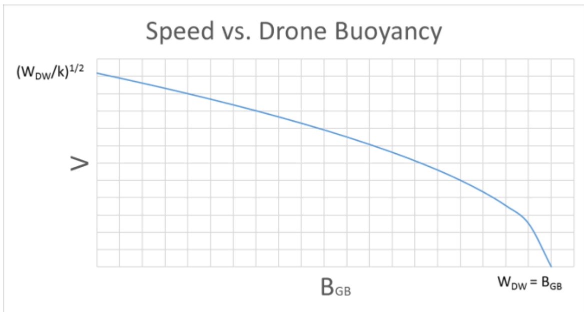

Figure 6. Qualitative trend of the function Speed vs. drone buoyancy.

The limits for v are:

$$0 < v < \sqrt{\frac{W_{DW}}{\kappa}} \quad (20)$$

the speed goes from zero to the maximum: this does not mean that the drone cannot go at higher speeds but only that it is the limit for leveled "flight". To reach higher speeds in horizontal paths it is necessary to choose negative angles of attack because the lift of the wing would bring the vehicle upwards.

The limits for B_{GB} are:

$$0 < B_{GB} < W_{DW} \quad (21)$$

The variation B_{GB} of buoyancy is obtained by means of a small external bladder which is filled and emptied of oil if necessary by means of a small electric pump. Its limits are absolutely evident: a bladder that gives a hydrostatic thrust greater than the weight itself would lead the drone to float on the surface without construct. The zero limit, on the other hand, can be overcome by appropriately ballasting the drone and obtaining a negative buoyancy: also in this case we will have that the vehicle is over ballasted and would sink directly. This type of set-up is allowed for a sub-glider but not for a classic drone.

IV. Conclusions

In this paper we have defined the general architecture for an underwater drone that is optimized for shallow water, inland ports, small inlets. The vehicle is simple and robust and divided into four main sections: Payload bay, Navigation bay, Engines bay and Propulsion bay. The study of balance on the vertical plane shows that the volume of the bladder must be well calculated otherwise it could interfere with the maximum vehicle speed.

References

[1] C. S. Draper. "Origins of inertial navigation", Journal of Guidance, Control, and Dynamics, Vol. 4, No. 5 (1981), pp. 449-463. https://doi.org/10.2514/3.19748.

[2] Woithe, H.C.; Tilkidjieva, D.; Kremer, U. Towards a resource-aware programming architecture for smart autonomous underwater vehicles; Technical Report, DCS-TR-637; Rutgers University: New Brunswick, NJ, USA, 2008.

[3] Petritoli, E., Leccese, F., Leccisi, M. Inertial navigation systems for UAV: Uncertainty and error measurements (2019) 2019 IEEE International Workshop on Metrology for AeroSpace, MetroAeroSpace 2019 - Proceedings, art. no. 8869618, pp. 218-222. DOI: 10.1109/MetroAeroSpace.2019.8869618.

[4] Hussain, N.A.A.; Ali, S.S.A.; Saad, M.N.M.; Nordin, N. Underactuated nonlinear adaptive control approach using U-model for multivariable underwater glider control parameters. In Proceedings of the 2016 IEEE International Conference on Underwater System Technology: Theory and Applications (USYS), Penang, Malaysia, 13–14 December 2016; pp. 19–25, doi:10.1109/USYS.2016.7893947.

[5] Leccese, F.; Cagnetti, M.; Giarnetti, S.; Petritoli, E.; Luisetto, I.; Tuti, S.; Đurović-Pejčev, R.; Đorđević, T.; Tomašević, A.; Bursić, V.; et al. A Simple Takagi-Sugeno Fuzzy Modelling Case Study for an Underwater Glider Control System. In Proceedings of the 2018 IEEE International Workshop on Metrology for the Sea; Learning to Measure Sea Health Parameters (MetroSea), Bari, Italy, 8–10 October 2018, pp. 262–267, doi:10.1109/MetroSea.2018.8657877.

[6] C. Jekeli "Inertial Navigation Systems with Geodetic Applications" Walter de Gruyter Berlin New York 2001.

[7] Petritoli, E.; Leccese, F.; Cagnetti, M. A High Accuracy Buoyancy System Control for an Underwater Glider. In Proceedings of the 2018 IEEE International Workshop on Metrology for the Sea; Learning to Measure Sea Health Parameters (MetroSea), Bari, Italy, 8–10 October 2018; pp. 257–261. doi:10.1109/MetroSea.2018.8657831.

[8] Lennart Ljung, "System Identification Theory for the User," Second Edition. USA: Prentice Hall, 1999.

[9] Leonard and Graver, "Model based feedback control of autonomous underwater glider," IEEE Journal of Oceanic Engineering, Vol. 26, No 4, pp.633-644, 2001.

[10] B. Etkin," Dynamic of Flight," New York and London: John Wiley and Sons, 1959.

[11] Xiaobo Tan, Drew Kim, Nathan Usher, Dan Laboy, Joel Jackson, Azra Kapetanovic, Jason Rapai, Beniamin Sabadus, Xin Zhou, "An Autonomous Robotic Fish for Mobile Sensing", Intelligent Robots and Systems 2006 IEEE/RSJ International Conference on, pp. 5424-5429, 2006.

[12] Ryan N. Smith, Arvind Pereira, Yi Chao, Peggy P. Li, David A. Caron, Burton H. Jones, Gaurav S. Sukhatme, "Autonomous Underwater Vehicle trajectory design coupled with predictive ocean models: A case study", Robotics and Automation (ICRA) 2010 IEEE International Conference on, pp. 4770-4777, 2010, ISSN 1050-4729.

[13] Smith Chao Jones Caron Li Sukhatme – "Trajectory Design for Autonomous Underwater Vehicles based on Ocean Model Predictions for Feature Tracking" Field and Service Robotics Volume 62 of the series Springer Tracts in Advanced Robotics pp 263-273.

[14] R. Austin "Unmanned Aircraft Systems" Wiley. (2010).

[15] Petritoli, E., Leccese, F. A high accuracy navigation system for a tailless underwater glider (2017) IMEKO TC19 Workshop on Metrology for the Sea, MetroSea 2017: Learning to Measure Sea Health Parameters, 2017-October, pp. 127-132.

[16] Bong-Huat Jun, Jin-Yeong Park, Fill-Youb Lee, Pan-Mook Lee, Chong-Moo Lee, Kihun Kim, Young-Kon Lim, Jun-Ho Oh. "Development of the AUV 'ISiMI' and free running test in an ocean engineering basin," Ocean Engineering, v 36, n 1, pp. 2-14, January 2009

[17] Petritoli, E., Leccese, F. High accuracy attitude and navigation system for an autonomous underwater vehicle (AUV) (2018) Acta IMEKO, 7 (2), pp. 3-9. DOI: 10.21014/acta_imeko.v7i2.535.

[18] M. Arima, N. Ichihashi, T. Ikebuchi, "Motion characteristics of an underwater glider with independently controllable main wings,"OCEAN '08 MTS/IEEE Kobe-Techno-Ocean'08-Voyage toward Future, OTO'08, 2008.

[19] Roger E.O, Genderson JG, Smith W.S, Denny G.F, Farley P.J., "Underwater acoustic glider," Geoscience and Remote Sensing Symposium, IGARSS '04. Proceedings. IEEE International Vol. 3, pp. 2241-2244, 2004.

[20] H. C. Woithe, Ulrich Kremer, "A programming architecture for smart autonomous underwater vehicles", Intelligent Robots and Systems 2009. IROS 2009. IEEE/RSJ International Conference on, pp. 4433-4438, 2009.

[21] H. C. Woithe, Denitsa Tilkidjieva, Ulrich Kremer, "Towards a resource-aware programming architecture for smart autonomous underwater vehicles," Technical Report, DCS-TR-637, Dept. of Computer Science, Rutgers Univ.

[22] John F. Gardner, "Simulation of Machines, Using MATLAB and Simulink," Canada: Wadsworth Group, 2001.

[23] Daniel L. Rudnick, Russ E. Davis, David M. Fratantoni, Mary Jane Perry, "Underwater Gliders for Ocean Research," Marine Technology Society Journal, v 38, n 2, pp 73-84, Summer 2004.

[24] Laszlo Techy, Kristi A. Morganseny, Craig A. Woolseyz, "Long-baseline acoustic localization of the Seaglider underwater glider", American Control Conference (ACC) 2011, pp. 3990-3995, 2011, ISSN 2378-5861.

[25] Nur Afande Ali Hussain, Syed Saad Azhar Ali, Mohamad Naufal Mohamad Saad, Nadira Nordin, "Underactuated nonlinear adaptive control approach using U-model for multivariable underwater glider control parameters", Underwater System Technology: Theory and Applications (USYS) IEEE International Conference on, pp. 19-25, 2016.

[26] Pengyao Yu, Yong Zhao, Tianlin Wang, Han Zhou, Shaojuan Su, Chunbo Zhen, "Steady-state spiral motion simulation and turning speed analysis of an underwater glider", Information Cybernetics and Computational Social Systems (ICCSS) 2017 4th International Conference on, pp. 372-377, 2017.

[27] Tony Bloch, P.S. Krishnaprasad, Naomi Leonard, Richard Murray, "Jerrold Eldon Marsden [Obituaries]", Control Systems IEEE, vol. 31, pp. 105-108, 2011, ISSN 1066-033X.

[28] C.D. Williams, "AUV systems research at the NRC-IOT: an update", Underwater Technology 2004. UT '04. 2004 International Symposium on, pp. 59-73, 2004.

[29] Adamo, Francesco; Andria, Gregorio; Di Nisio, Attilio; Calò Carducci, Carlo Guarnieri; Lay-Ekuakille, Aimé; Mattencini, Giuseppe; Spadavecchia, Maurizio "Designing And Prototyping A Sensors Head For Test And Certification Of Uav Components" International Journal on Smart Sensing & Intelligent Systems . Sep2017, Vol. 10 Issue 3, p646-672. 27p.

[30] Petritoli, E., Leccese, F., Ciani, L. Reliability assessment of UAV systems (2017) 4th IEEE International Workshop on Metrology for AeroSpace, MetroAeroSpace 2017 - Proceedings, art. no. 7999577, pp. 266-270. DOI: 10.1109/MetroAeroSpace.2017.7999577.

[31] Pasquali, V., D'Alessandro, G., Gualtieri, R., Leccese, F. A new data logger based on Raspberry-Pi for Arctic Notostraca locomotion investigations (2017) Measurement: Journal of the International Measurement Confederation, 110, pp. 249-256. DOI: 10.1016/j.measurement.2017.07.004

[32] Leccese, F., Cagnetti, M., Di Pasquale, S., Giarnetti, S., Caciotta, M. A new power quality instrument based on raspberry-pi (2016) Electronics (Switzerland), 5 (4), art. no. 64, . DOI: 10.3390/electronics5040064

[33] Pasquali, V., Gualtieri, R., D'Alessandro, G., Leccese, F., Cagnetti, M. Experimental in field reliability test for data logger based on Raspberry-Pi for extreme scenarios: A first step versus aerospace applications (2016) 3rd IEEE International Workshop on Metrology for Aerospace, MetroAeroSpace 2016 - Proceedings, art. no. 7573242, pp. 365-370. DOI: 10.1109/MetroAeroSpace.2016.7573242.

[34] Pasquali, V., Gualtieri, R., D'Alessandro, G., Granberg, M., Hazlerigg, D., Cagnetti, M., Leccese, F. Monitoring and analyzing of circadian and ultradian locomotor activity based on Raspberry-Pi (2016) Electronics (Switzerland), 5 (3), art. no. 58, . DOI: 10.3390/electronics5030058.

[35] Leccese, F., Cagnetti, M., Calogero, A., Trinca, D., di Pasquale, S., Giarnetti, S., Cozzella, L. A new acquisition and imaging system for environmental measurements: An experience on the Italian cultural heritage (2014) Sensors (Switzerland), 14 (5), pp. 9290-9312. DOI: 10.3390/s140509290.

[36] J. G. Graver, J. Liu, C. Woolsey et al., "Design and Analysis of an Underwater Vehicle for Controlled Gliding," in Conference on Information Sciences and Systems (CISS), Princeton, 1998.

[37] H. Stommel "The Slocum Mission" Oceanography, pp. 22 - 25, April 1989

[38] J.G. Graver. Underwater Gliders: Dynamics, Control and Design. PhD thesis, Princeton University, 2005.

[39] Sherman, J., R. E. Davis, W. B. Owens, and J. Valdes, 2001: The autonomous underwater glider "Spray". IEEE J Oceanic Eng. 26:437-446.

[40] D. L. Rudnick, R. E. Davis, C.C. Eriksen et al., "Underwater Gliders for Ocean Research," Marine Technology Society Journal, vol. 38, no. 1, Spring, 2004.

[41] A. Pereira, H. Heidarsson, D.A. Caron, B.H. Jones, and G.S. Sukhatme. An implementation of a communication framework for the cost-effective operation of slocum gliders in coastal regions. In Proceedings of The 7th International Conference on Field and Service Robotics, Cambridge, MA, July, 2009.

[42] Y.C. Lee, D.G. O'Laughlin "A Performance Analysis of a Tightly Coupled GPS INS For two integrity monitoring Methods" The MITRE Corporation, Center for Advanced Aviation System Development (CAASD).

[43] D. Küchemann "The Aerodynamic Design of Aircraft" Pergamon international library of science, technology, engineering, and social studies, 1978. Oxford: Pergamon Press. ISBN 0-08-020515-1.

[44] D. Meyer "Glider Technology for Ocean Observations: A Review" Ocean Sci. Discuss., doi: 10.5194/os-2016-40, 2016.

[45] Davis, R. E., D. C. Webb, L. A. Regier and J. Dufour. 1992. "The Autonomous Lagrangian Circulation Explorer (ALACE)." J Atmos Oceanic Technol. 9:264-285.

[46] G.Parthasarathy, Degala Shravya Sree, B.Lakshmi Manasa – "Design Mathematical Modeling and Analysis of Underwater Glider" International Journal of Science and Research (IJSR) ISSN (Online): 2319-7064.

[47] V.F. Strachan "A Review of the implications of the Johns Hopkins University Applied Physics Laboratory GPS Risk Assessment Study" Litton Aero Products, April 5th, 1999.

[48] RTCM Special Committee n.104 "RTCM Recommended standards for differential Navstar GPS Service" Ver.2.0, Jan.1, 1990.

[49] Davis, R. E., C. C. Eriksen and C. P. Jones. 2003. Autonomous buoyancy-driven underwater gliders. In: Technology and Applications of Autonomous Underwater Vehicles, ed. G. Griffiths, pp. 37-58. Taylor and Francis.

[50] Y.C. Lee, D.G. O'Laughlin "A Performance Analysis of a Tightly Coupled GPS INS For two integrity monitoring Methods" The MITRE Corporation, Center for Advanced Aviation System Development (CAASD).

[51] Warren F. Philips "Mechanics of Flight" Ed Wiley India. Ed 2009. ISBN-13: 978-8126538515

2020 IMEKO TC-19 International Workshop on
Metrology for the Sea
Naples, Italy, October 5-7, 2020

A Brief Survey on Underwater Optical Wireless Communications

Giuseppe Schirripa Spagnolo[1], Lorenzo Cozella[1], Fabio Leccese[3]

[1] *Dipartimento di Matematica e Fisica - Università degli Studi "Roma Tre" - Roma, Italy*
[2] *Dipartimento di Scienze - Università degli Studi "Roma Tre" - Roma, Italy*

***Abstract* – Acoustic, radio frequency (RF) and optical waves systems are the technologies that are used to carry out underwater wireless communications. In scientific, military and industrial sectors, the development of robust and efficient submarine wireless communication links is of enormous interest. To achieve secure short-range wireless communications, the Underwater Optical Wireless Communication (UOWC), which uses the 450-550 nm spectral range of the electromagnetic spectrum, is a good technology. Recently, UOWC applications have been proposed for environmental monitoring, offshore exploration, and military operations. There are many review articles published on this topic. However, research in this field evolves rapidly as does existing literature. The article deals with current and potentially available UWOC technologies in the near future. It is aimed at those who want to undertake studies in this field. Obviously, this paper does not attempt to cover every single aspect of UWOC.**

I. INTRODUCTION

Underwater wireless communication (UWC) has many potential applications in the military, industrial and scientific research fields, but, for practical applications significant data bandwidth is required [1-3].

Generally, underwater wireless communication takes place via acoustic waves due to their relatively low attenuation. Unfortunately, acoustic systems have low bandwidth and high latency. Therefore, they are not suitable for applications that require data-intensive information exchange and real-time response processing in real time. However, since acoustic transmission is the only technology capable of ensuring communication over long distances, extensive studies are continuously conducted to improve the performance of the acoustic communication channels [4-6]. Anyhow, acoustic underwater communication is susceptible to malicious attacks [7].

Therefore, complementary technology capable of achieving secure broadband underwater communications is required. Wireless communication via radio frequency (RF) waves is the most widespread technology in terrestrial communications. Unfortunately, this technology is not suitable for underwater use; in fact, in the water, the radio frequency waves are strongly attenuated [8].

Optical communication is defined as remote communication using light to carry information. Potentially, it can solve the problem of broadband and low latency submarine wireless transmission. Recently, in terrestrial application, Visible-Light Communication (VLC) technology was developed to provide both lighting and data transfer with the same infrastructure [9-10]. VLC techniques transmit information wirelessly by rapidly pulsing visible light using Light Emitting Diodes (LEDs); recent work has shown the possibility of replacing the Wi-Fi connection, based on radio frequency waves, with a VLC link. Generally, the information data is overlaid on the LED light without introducing flickering. The exhaustion of low-frequency bands to cope with the exponential growth for the high-speed wireless access is another reason for exploring new technologies. The visible light spectrum is unlicensed and hardware readily available, which can be used for data transmission. Furthermore, the exponential improvement in the high-power light emitting diodes is an enabler for high data rate VLC Network. Like VLC systems are the Underwater Optical Wireless Communications (UOWCs) [11-13], where potential light sources are Laser Diodes (LDs) instead of LEDs. Both are extremely interesting, LDs for their feature higher modulation bandwidth respect to LEDs, while, these latest, for their higher power efficiency, lower cost, and longer lifetime, seem more suitable for medium bit rate applications.

Optical communication is defined as communication at a distance using light to carry information. An optical fiber is the most common type of channel for optical communications, as well as the only medium that can meet the needs for enormous bandwidth in such an information age. Replacing the channel from an optical fiber to free-space underwater, we achieve UOWC that can be regarded as the underwater transmission of unguided optical signals.

Compared to acoustic and radio frequency communication, UWOC has great potential; with it, we can make communications with high bit rate and very low latency. Currently, the performance of UOWC systems is limited to short range applications [14]. Submarine optical communication systems are starting to be commercially available [15,16]. However, in-depth studies are still necessary to create systems that can be used in real operational scenarios. Researches are needed to allow submarine optical transmission even over long distances.

Figure 1 compares the performance of acoustic, RF and UOWC, based on the transmission range and the data speed (bandwidth).

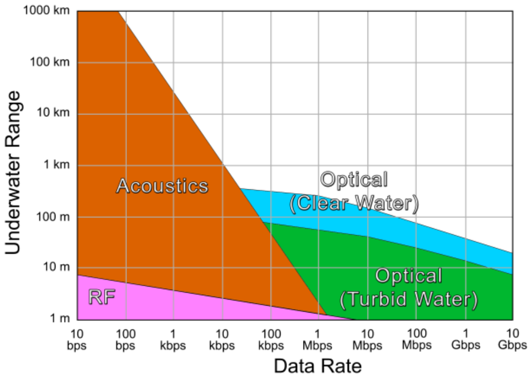

Fig. 1. Theoretical communication performance of acoustics, RF and optical underwater communication technologies.

In order provide a basic overview, we will go through and provide summary is to highlight the prospects of UOWC technologies. The focus of this is to examine current technologies and those potentially available in the next few years, for UOWC. The study in this field can open great opportunities since current optical underwater communication solutions are still of large dimension, expensive and power-consuming.

Military field is one of the fastest growing related to this innovative communication technology, due to its intrinsic security and superior bandwidth availability. One possible application is divers direct communication. During military incursions with divers, it is very important for the command to have secure communications that are difficult to locate. Figure 2 shows a typical behavior where two divers have the necessity to exchange tactical information.

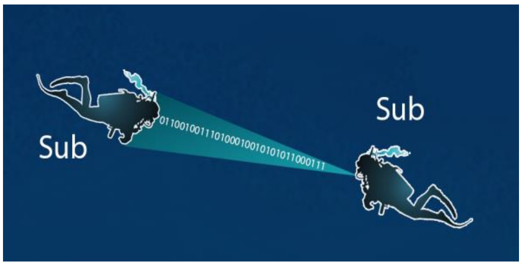

Fig. 2. Secure optical communication between subs.

In this scenario, UOWC is an excellent technology. It has the advantage that it cannot be intercepted and, in any case, it can be encrypted. This specific application does not require long range and high band communications. Therefore, the systems can have implemented are simple, small, lightweight and with low power.

Figure 3. It is a Dynamic Positioning Buoy [17], capable of communicating with satellite and via bidirectional UOWC with optical surveillance station positioned on the seabed. The surveillance station can be powered by nuclear batteries [18] and in real time control, through digital optical correlation [19,20], if something intrudes into the monitored area. In case of suspect object (e.g. a submarine) the image and related alert is sent back to the buoy and, from it, to the ground costal station via satellite link. This application can grand a very accurate underwater video surveillance.

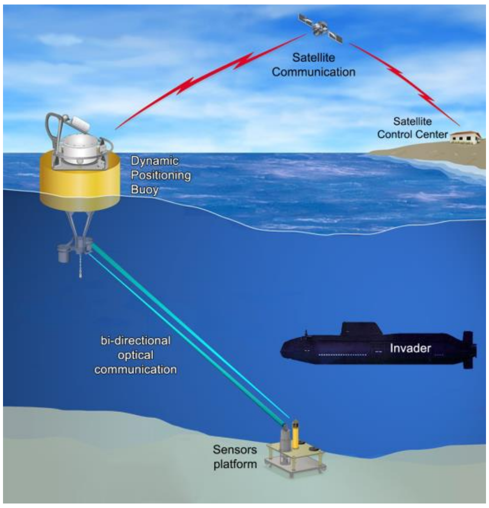

Fig. 3. Underwater video surveillance scenario.

Figure 4 shows a typical UOWC scenario. It shows several platforms (divers, ships, submarines, submarine sensors, etc.) connected by beams of light.

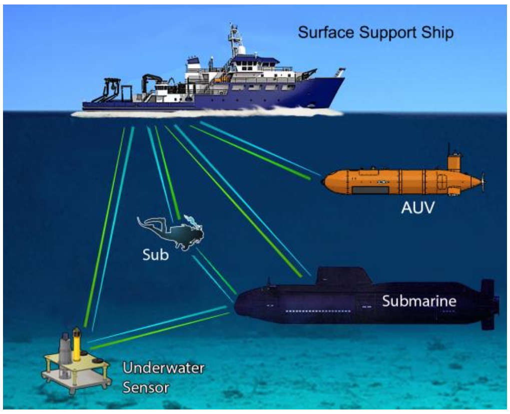

Fig. 4. Typical application scenarios of UWOC.

II. OPTICAL TRANSMISSION IN WATER

The optical channel model is defined by means of Beer-Lambert. After the beam propagates z length, the propagation loss factor (L_P) is:

$$L_P = h \cdot \exp[-c \cdot z] \quad (1)$$

where c in m^{-1} is the total attenuation coefficient, and h is a constant. The total attenuation coefficient is a sum of the effects of the absorption coefficient and of the scattering one, respectively called a and b:

$$c = a + b \quad (2)$$

The absorption and scattering coefficients, with inverse meter units, are determined by the contribution of water molecules, particulate algal/sediment matters and colored organic contents dissolved [21,22].

The spectral attenuation of radiation depends upon the constituents and their concentration in a volume of seawater. Generally, in turbid harbor, the attenuation is minimum in the spectral region 550 to 600 nm. For coastal ocean, the wave band is 520 to 570 nm and for clear ocean, the minimum attenuation wave band shifts to still lower wavelength region i.e. 450 to 500 nm.

In this way, the absorption coefficient a and the scattering coefficient b can be expressed as a function of the wavelength λ and the concentration of chlorophyll C_{chlor} [23]:

$$a(\lambda) = [a_w(\lambda) + 0.06 \cdot a_c(\lambda) \cdot C_{chlor}^{0.65}]\{1 + 0.2 \cdot \exp[-0.014(\lambda - 440)]\} \quad (3)$$

$$b(\lambda) = 0.30 \frac{550}{\lambda} C_{chlor}^{0.62} \quad (4)$$

where, a_w points out the pure water absorption coefficient while, a_c is a nondimensional number, statistically derived that points out the absorption coefficient specific for the chlorophyll.

Therefore, the chlorophyll concentration C, expressed in $mg \cdot m^{-3}$, can be used as the free parameter to calculate $a(\lambda)$ and $b(\lambda)$.

The measured values for the absorption $a(\lambda)$, for the total scattering $b(\lambda)$ and for the extinction $c(\lambda)$ are outlined in Table 1.

Table 1. Table caption.

Water types	$a(\lambda)$ [m^{-1}]	$b(\lambda)$ [m^{-1}]	$c(\lambda)$ [m^{-1}]	Operate Wavelength
Clear Ocean	0.114	0.037	0.151	450-500 nm
Coastal Ocean	0.179	0.220	0.339	520-570 nm
Turbid Harbour	0.366	1.829	2.195	550-600 nm

Seawater light transmission model is shown in Figure 5.

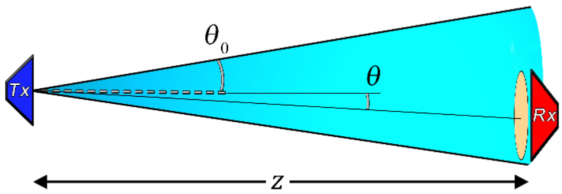

Fig. 5. Seawater light transmission model.

The optical power reaching the receiver can be written as [24]:

$$P_{Rx} = P_{Tx} \cdot \eta_{Tx} \cdot \eta_{Tx} \cdot \exp\left[-\frac{c(\lambda) \cdot z}{\cos\theta}\right] \cdot \frac{A_{R_x} \cdot \cos\theta}{2\pi \cdot z^2 (1 - \cos\theta_0)} \quad (5)$$

where P_{Tx} is the transmitted power, η_{Tx} and η_{Rx} are the optical efficiencies of the Tx and Rx correspondingly, $c(\lambda)$ is total attenuation coefficient, z is the perpendicular distance between the Tx plane and the Rx plane, θ_0 is the Tx beam divergence angle, θ is the angle between the perpendicular to the Rx plane and the Tx-Rx trajectory, and A_{Rx} is the receiver aperture area.

The transmitted power is limited by the energy that can be used by the transmitter apparatus. It is essential that this energy be as small as possible. In this way, it is possible to have low power supply, very useful in underwater applications.

The Eq. 5 shows that for the same energy used by the transmitter, if you want to increase the transmission distance, it is essential, among other things, to improve the efficiency of the transmitter and receiver.

Obviously, the transmission distance can also be increased by using reception systems capable of capturing, theoretically, even the single photon.

As far as light sources are concerned, the technology offers increasingly efficient and reliable devices. Current LED systems have excellent efficiency, high reliability and low cost. On the contrary, as far as the receiver is concerned, much research work still needs to be done.

III. BASIC COMPONENTS OF UOWC

A UOWC link can be schematized in three parts, the transmitter unit, the water channel, and the receiver module. The schematic in Fig. 6 shows the components of a typical system.

The transmitter, which consists of four principal components: a modulator and pulse shape circuit, a driver circuit, converts the electrical signal to an optical signal suitable for transmission and a lens to realize optical link configuration.

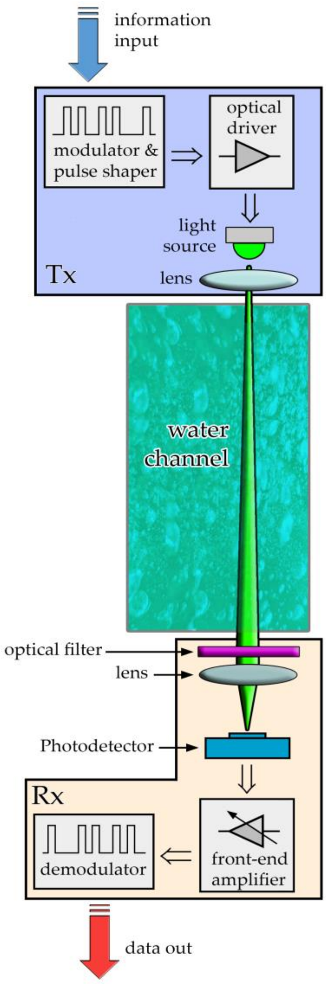

Fig. 1. Schematic of a typical UOWC link. The transmitter (TX) is composed of a modulator, optical driver, light source and projection lens. The receiver (RX) is made of optical bandpass filter, photodetector Low noise electronics and demodulator.

The function of the transmitter is to transform the electrical signal in optical one, projecting the carefully aimed light pulses into the water. The optical light sources are based on LED or LD one [25-29]. Compared to LEDs, Laser Diode switch faster and support a higher optical power output. On other hand, the LEDs systems are cheaper, simpler and more reliable. In addition, the LEDs can switch fast enough to allow large band optical underwater communications. Diode lasers are preferable for long distance communications. Instead, at short distances, communications via LEDs are preferable. Finally, since LEDs can be used for bi-directional communication, they can be employed to make simple, cheap short-range communication systems between divers.

Joined to the specific requirements and considering that underwater systems are obliged to respect power and mass constraints, the choice of one of the two optical available technologies, LED or laser, in specific blue-green portion of the spectrum, could be conditioned by the research of the maximum efficiency. Generally, blue-green LEDs are the better choice for buoy system operating in shallow water. Instead, for systems operating in deep clear ocean water, the laser-based transmission systems are preferred.

The receiver has the task of capturing the transmitted optical signal and transforming it into an electrical signal. In many applications, it is important to select a specific wavelength that impact on the light detector [30]. The light coming on the receiver should have no noise introduced by sunlight and the presence of other light sources [31]. To try to solve this problem, the wavelength band (the one transmitted) is selected by using a narrow optical band-pass filter [32].

There are many different types of photo detectors currently commonly used, e.g., the photodiodes. These devices, for their characteristics of small size, suitable material, high sensitivity and fast response time, are commonly used in optical communication applications. There are two types of photodiodes: the PIN photodiode and the Avalanche Photodiode (APD). Unfortunately, due to the high detection threshold and high noise intensity, linked to Trans-Conductance Amplifier, that limit their practical application, photodiodes are not advisable for long distance UOWC systems. For traditional detection devices and methods, due to the exponential attenuation of the water, the optical communication distance is less than 100 m. This constraint severely limits the performance of UOWC systems. Especially for the management of AUVs and remote control vehicles (ROV) [33, 34].

Recent researches are focused on the possible application of Single Photon Avalanche Diodes (SPADs) technology to UOWC systems. The Avalanche Photodiodes have a similar structure of the PIN ones and operate at a much higher reversed bias. This physical characteristic allows to a single photon to produce a significant avalanche of electrons. This way of operation is called the single-photon avalanche mode or even the Geiger's mode [35-37]. The great advantage of SPADs is that their detectors do not need to a Trans-Conductance Amplifier.

IV. CONCLUSIONS

Recently many studies have been conducted to use UOWC technology to transmit information safely with high data rate in underwater environment. Today, UOWC systems usable in real operating conditions (with some exceptions) are not yet available. Therefore, a lot of research in this area has yet to be done. In particular:

- Currently, an inevitable phenomenon for UOWC Link is the misalignment between transmitter and receiver.

Although some researches on smart transceivers to limit the impact of the link misalignments have been proposed, the need to develop more intelligent UOWC transceivers is pressing.

- The design innovative modulation and coding schemes that can adapt the characterizations of underwater environment.
- Since most UOWC systems are integrated into a battery-powered platform, energy efficiency is therefore important. The systems must be designed with energy efficiency optimization.
- Possibility of simultaneously using different colored source light to increase data transfer rate and/or consent simultaneous use by multiple users.
- Development of new underwater communication channel modeling. When environmental conditions deviate from ideality, the light signal rapidly degrades. It is essential to study the propagation of the light beam with models that simulate real conditions as much as possible (even in "difficult" environments). All this to allow the optimization of transmission and reception techniques, both in terms of transmitter and sensor used as receiver.

Finally, almost all the studies available in the literature are conducted by simulation or by laboratory experiments. Studies in real marine environment are needed.

The interest in UOWC is mainly outside the academic field. In fact, the possibility to use UOWC is on the basis of future military application for secure Under Water Telephones (UWTs), necessary for allowing secure communications between vessels and submarines, taking into account the possibility to use both direct and spread light channels. In addition, the usage of Point-to-Point optical communications can allow a better usage of torpedoes, not specifically for their guidance, but for reporting sonar information back to the basis with a high rate, even in case of not wire-guided solution.

REFERENCES

[1] I.F. Akyildiz, D. Pompili, T. Melodia, "Underwater acoustic sensor networks: research challenges," Ad Hoc Networks, vol. 3, no. 3, pp. 257 – 279, 2005. https://doi.org/10.1016/j.adhoc.2005.01.004

[2] C.M.G. Gussen, P.S.R. Diniz, M.L.R. Campos, W.A. Martins, F.M. Costa, J.N. Gois, "A survey of underwater wireless communication technologies," J. of Commun. and Info. Sys., vol. 31, no. 1, pp. 242–255, 2016. https://doi.org/10.14209/jcis.2016.22

[3] M.F. Ali, D.N.K. Jayakody, Y.A. Chursin, S. Affes; S. Dmitry, "Recent Advances and Future Directions on Underwater Wireless Communications", Archives of Computational Methods in Engineering, pp. 1-34. 2019 https://doi.org/10.1007/s11831-019-09354-8

[4] E. Demirors, G. Sklivanitis, G.E. Santagati, T. Melodia, S.N. Batalama, "High-Rate Software-Defined Underwater Acoustic Modem with Real-Time Adaptation Capabilities", IEEE Access, vol. 6, pp. 18602-18615. 2018. https://doi.org/10.1109/ACCESS.2018.2815026

[5] D. Centelles, A. Soriano-Asensi, J.V. Martí, R. Marín, R.; P.J. Sanz, "Underwater Wireless Communications for Cooperative Robotics with UWSim-NET," Appl. Sci. vol. 9, 3526. 2019doi:10.3390/app9173526

[6] M. J. Bocus, A. Doufexi, D.Agr afiotis, "Performance of OFDM-based massive MIMO OTFS systems for underwater acoustic communication," IET Communications, vol. 14, no. 4, pp. 588-593, 2020. https://doi.org/10.1049/iet-com.2019.0376

[7] M.C. Domingo, "Securing underwater wireless communication networks," IEEE Wireless Communications, vol. 18, no. 1, pp. 22-28, 2011. https://doi.org/10.1109/MWC.2011.5714022

[8] X. Che, I. Wells, G. Dickers, P. Kear, X. Gong, "Re-evaluation of RF electromagnetic communication in underwater sensor networks," IEEE Commun. Mag. vol. 48, no 12, 2010, pp. 143–151. https://doi.org/10.1109/MCOM.2010.5673085

[9] Z. Ghassemlooy, L.N. Alves, S. Zvanovec, M.A. Khalighi, "Visible light communications: theory and applications," CRC press, Boca Raton,FL,USA, 2017. https://doi.org/10.1201/9781315367330-3

[10] S.U. Rehman, S. Ullah, P.H.J. Chong, S. Yongchareon, D. Komosny, "Visible Light Communication: A System Perspective - Overview and Challenges," Sensors vol.19, no. 5, 1153, 2019. https://doi.org/10.3390/s19051153

[11] G. Schirripa Spagnolo, L. Cozzella, F. Leccese, "Underwater Optical Wireless Communications: Overview," Sensors, vol. 20, 2261, 2020

[12] H.M. Oubei, C. Shen, A. Kammoun, E. Zedini, K.H. Park, X. Sun, G. Liu, C.H. Kang, T.K. Ng, N.S. Alouini, "Light based underwater wireless communications," Japanese Journal of Applied Physics, vol. 57, no. 8S2, 08PA06, 2018 https://doi.org/10.7567/JJAP.57.08PA06

[13] Z. Zeng, S. Fu, H. Zang, Y. Dong, J. Cheng, "A survey of underwater optical wireless communications," IEEE Commun. Surv. Tutorials, vol. 19, no. 1, pp. 204–238, 2017. https://doi.org/10.1109/COMST.2016.2618841

[14] B. Cochenour, K. Dunn, A. Laux, L. Mullen, "Experimental measurements of the magnitude and phase response of high-frequency modulated light underwater," Appl. Opt. vol. 56, no. 14, pp. 4019-4024, 2017. https://doi.org/10.1364/AO.56.004019

[15] BlueComm Underwater Optical Communication. Available online at: https://www.sonardyne.com/product/bluecomm-underwater-optical-communication-system/ [Accessed May 2020]

[16] SA Photonics - Neptune™ FSO, Available online at: https://www.saphotonics.com/communications-

sensing/optical-communications/ [Accessed May 2020]

[17] Introduction to Dynamic Positioning (DP) Systems Available online at: https://www.dco.uscg.mil/Portals/9/OCSNCOE/References/Custom%20Ref%20Books/Introduction%20to%20DP%20Systems%20Dec2019.pdf?ver=2019-12-11-135125-197 [Accessed May 2020]

[18] I. Hamilton, N. Patel, "Nuclear Batteries for Maritime Applications," Marine Technology Society Journal, vol. 53, no, 4, pp. 26-28, 2019. https://doi.org/10.4031/MTSJ.53.4.5

[19] H. Ma, Y. Liu, "Correlation based video processing in video sensor networks," In International Conference on Wireless Networks, Communications and Mobile Computing (Vol. 2, pp. 987-992), Maui: HI, USA, 3-16 June 2005. https://doi.org/10.1109/WIRLES.2005.1549547

[20] G. Schirripa Spagnolo, L. Cozzella, F. Leccese, "Phase correlation functions: FFT vs. FHT," ACTA IMEKO, vol. 8, no. 1, pp. 87-92, 2019. http://dx.doi.org/10.21014/acta_imeko.v8i1.604

[21] C.F. Bohren, D.R.; Huffman, "Absorption and Scattering of Light by Small Particles," Wiley: New York, NY (USA), 1988. https://doi.org/10.1002/9783527618156

[22] S.K. Sahu, P. Shanmugam, "A study on the effect of scattering properties of marine particles on underwater optical wireless communication channel characteristics," In OCEANS 2017: Aberdeen UK. https://doi.org/10.1109/OCEANSE.2017.8084720

[23] J. Xu, Y. Song, X. Yu, A. Lin, M. Kong, J. Han, N. Deng, "Underwater wireless transmission of high-speed QAM-OFDM signals using a compact red-light laser," Optics express, vol. 24, no. 8, pp. 8097-8109. 2016. https://doi.org/10.1364/OE.24.008097

[24] L.K. Gkoura, G.D. Roumelas, H.E. Nistazakis, H.G. Sandalidis, A. Vavoulas, A.D. Tsigopoulos, G.S. Tombras, "Underwater Optical Wireless Communication Systems: A Concise Review, Turbulence Modelling Approaches - Current State, Development Prospects, Applications," Konstantin Volkov, IntechOpen, July 26th 2017. https://doi.org/10.5772/67915.

[25] Gabriel, C.; Khalighi, M.A.; Bourennane, S.; Léon, P.; Rigaud, V. Investigation of suitable modulation techniques for underwater wireless optical communication. Proceedings of International Workshop on Optical Wireless Communications (pp. 1-3). 22-22 Oct. 2012 Pisa, ltaly https://doi.org/10.1109/IWOW.2012.6349691

[26] G. Schirripa Spagnolo, F. Leccese, M. Leccisi, "LED as Transmitter and Receiver of Light: A Simple Tool to Demonstration Photoelectric Effect," Crystals, vol. 9, 531, 2019. https://doi.org/10.3390/cryst9100531

[27] T. Wu, Y. Chi, H. Wang, C. Tsai, G. Lin, "Blue Laser Diode Enables Underwater Communication at 12.4 Gbps," Sci Rep, 7, 40480, 2017 https://doi.org/10.1038/srep40480

[28] P. Tian, X. Liu, S. Yi, Y. Huang, S. Zhang, X. Zhou, L. Hu, L. Zheng, R. Liu, "High-speed underwater optical wireless communication using a blue GaN-based micro-LED," Optics Express, vol. 25, no. 2, 1193. 2017. http://dx.doi.org/10.1364/OE.25.001193

[29] H. Kaushal, G. Kaddoum, "Underwater Optical Wireless Communication," IEEE Access, vol. 4, pp. 1518-1547, 2016. https://doi.org/10.1109/ACCESS.2016.2552538

[30] G. Schirripa Spagnolo, D. Papalillo, C. Malta, S. Vinzani, "LED Railway Signal vs full Compliance with colorimetric Specification, Int. J. Transp. Dev. Integr., vol. 1, no. 3, pp. 568–577. 2017. https://doi.org/ 10.2495/TDI-V1-N3-568-577

[31] T. Hamza, M.A. Khalighi, S. Bourennane, P. Léon, J. Opderbecke, "Investigation of solar noise impact on the performance of underwater wireless optical communication links. Opt. Express, vol. 24, no. 22, pp. 25832-25845, 2016. https://doi.org/10.1364/OE.24.025832

[32] J. Sticklus, M. Hieronymi, P.A. Hoeher, "Effects and Constraints of Optical Filtering on Ambient Light Suppression in LED-Based Underwater Communications," Sensors, vol. 18, no. 11, 3710, 2018. https://doi.org/10.3390/s18113710

[33] E. Petritoli, F. Leccese, M. Cagnetti, "High accuracy buoyancy for underwater gliders: The uncertainty in the depth control," Sensors,vol. 19, no.8, 1831, 2019 https://doi.org/10.3390/s19081831.

[34] E. Petritoli, F.; Leccese, "High accuracy attitude and navigation system for an autonomous underwater vehicle (AUV)," Acta IMEKO, vol.7, no. 2, pp. 3-9, 2018. https://doi.org/10.1109/10.21014/acta_imeko.v7i2.535

[35] C. Wang, H.Y. Yu, Y.J. Zhu, "A Long Distance Underwater Visible Light Communication System With Single Photon Avalanche Diode," IEEE Photonics Journal, vol. 8, no. 5, 7906311 (11 pp), 2016. https://doi.org/10.1109/JPHOT.2016.2602330

[36] Q. Yan, Z. Li, Z. Hong, T. Zhan and Y. Wang, "Photon-Counting Underwater Wireless Optical Communication by Recovering Clock and Data From Discrete Single Photon Pulses," in *IEEE Photonics Journal*, vol. 11, no. 5, pp. 1-15, Oct. 2019, Art no. 7905815, doi: 10.1109/JPHOT.2019.2936833.

F. Zappa, S. Tisa, A. Tosi, S. Cova, "Principles and features of single-photon avalanche diode arrays," Sensors and Actuators A: Physical, vol. 140, no. 1, pp. 103-112, 2007. https://doi.org/10.1016/j.sna.2007.06.02

2020 IMEKO TC-19 International Workshop on
Metrology for the Sea
Naples, Italy, October 5-7, 2020

Triggering Cyber-electronic Attacks in Naval Radar Systems

Walmor Cristino Leite Junior[1,2], Alan Oliveira de Sá[1,2]

[1] *Brazilian Naval War College, Rio de Janeiro, Brazil, walmor.clj@outlook.com*
[2] *Admiral Wandenkolk Instruction Center, Rio de Janeiro, Brazil, alan.oliveira@gmail.com*

Abstract **– The present paper discusses relevant aspects related to hybrid attacks involving cyber warfare and electronic warfare in naval radar systems. It addresses how such attacks can be implemented, showing that Electronic Attacks (EA) can be used to remotely trigger a cyber threat hosted in a radar computational system. The concept is demonstrated through simulations where a template matching technique is used to acknowledge the EA and, thus, trigger the cyber threat. The results show the effectiveness of the technique as a tool for activating malicious code previously installed in a radar system.**

I. INTRODUCTION

Cyber Warfare (CW), which seeks to explore and manipulate digital information, is becoming increasingly relevant in the international context. Advanced cyber attacks have been documented and the studies generated for their understanding shows the feasibility of development of others even more powerful and with great potential to achieve strategic objectives [1]. Among these attacks are the malwares, *i.e.* malicious codes that aim to interfere with the functioning of systems. Stuxnet [2], an example of malware supposedly produced by Nation-States, was able to delay a country's nuclear program by a few years [3]. In the military operation *Orchard*, according to the literature [4], the Israeli air force attacked a Syrian facility without being noticed thanks to a malicious cyber mechanism installed in the Syrian radar system. One hypothesis raised in the literature [4] regards to the possibility that an Electronic Attack (EA) – *i.e.* an attack performed in the electromagnetic spectrum – was used to unleash a cyber attack capable of hindering the radar computational process. Such integration of electronic and cyber attacks presents itself as a new trend in modern warfare, where the resulting *cyber-electronic* attacks represent a novel class of threats to be addressed [5].

In the maritime sector, radar systems are used as relevant sensors for navigation safety or as a source of information for integrated navigation systems. Note that a compromised radar system may result in serious risks to the vessels' safety, with possible impacts in a wide range of areas (*e.g.* economic, environmental, defense, etc.). For this reason, it is important to study how such kind of cyber-electronic attacks can be implemented and seek for possible countermeasures.

This paper presents how a template matching technique can be used in a cyber-electronic offensive [5] to detect specific EA patterns and, thus, use this information to trigger a malicious cyber process in a radar system. The main contribution of this paper is to demonstrate, for the sake of awareness, a mechanism that can be used as a link between an EA and a cyber weapon. More specifically, the mechanism is used to allow an EA to trigger a cyber weapon previously installed in the naval radar system. The effectiveness of the proposed mechanism is assessed through simulations in Python, where the target is a generic radar system used for maritime navigation.

The rest of this work is organized as follows: Section II presents the related works. Section III describes the mechanism proposed in in this work to allow the communication between the EA and the cyberattack in a radar system. Section IV presents the simulation results. Finally, Section V brings the conclusions.

II. RELATED WORKS

The disclosure of the Stuxnet malware in 2010 showed the details of a worm endowed with a surprising level of complexity [3]. Its refinement raised concerns about the development of specialized, high skilled and complex cyber weapons, with multidisciplinary design. The literature [2,3] shows that it would not be possible to develop such a sophisticated weapon without extensive technical support of highly qualified human resources from different technical fields (*e.g.* Information and Communication Technology, Control Engineering and Nuclear Engineering). It would have been created by State institutions to achieve strategic objectives in the international environment [3]. The target of Stuxnet was an Iranian nuclear enrichment plant that had its operation impaired, delaying the country's nuclear program by some years. Today, several studies on it are available, showing that such attack model can be used as inspiration for individuals with malicious intentions against other critical targets. The same concept of multidisciplinary attack can be used to impair other platforms, including systems and sensors used in naval environments, which may have cyber vulnerabilities – intentionally implanted or not.

In [5], the authors discuss the concepts of hybrid attacks in the scope of sea power, where the cyber, electronic and kinetic warfare can be integrated to accomplish specific tactical and strategic purposes. The separate application of these kinds of warfare has been usual in modern military operations, however it is noticed that there is a trend for these warfare dimensions to merge so that actions in one of them cause effects in the others. An example of hybrid attack is sown in [6], where the authors demonstrate an EA (more specifically a GPS spoofing attack) that is able to produce a kinetic effect on a ship navigation.

Among the possible kinds of hybrid attacks discussed in [5], this paper focuses on the cyber-electronic attack. More specifically, it addresses a particular attack against naval radar systems which, to the best of our knowledge, is not explored in the literature. According to [5], a cyber-electronic attack is an offensive where Electronic Warfare (EW) actions seek not only to manipulate the tactical information obtained through the electromagnetic spectrum (as in the traditional EW), but also to manipulate the computational process of the target system.

In [7], the authors present an EA technique able to forge multiple false targets, with different ranges, within the radar detection range. The purpose of their technique is to produce multiple fabricated targets and, thus, make the radar operator unable to distinguish between the real target and the false targets. Note that in their case, the target detection information is manipulated, but the radar computational process continues to run normally. To make such EA able to manipulate the computational process, it would be necessary to have in the radar system a mechanism prepared to acknowledge the false information produced by the EA as a command to trigger the malicious cyber mechanism responsible for manipulating the system behavior.

Note that for such a cyber-electronic attack, it is necessary to have a cyber component previously implanted in the radar computing system. On this aspect, the literature report vulnerabilities implanted in air gapped systems (which is often the case of naval radar systems). These vulnerabilities can be implemented either in software, as in the Stuxnet [8], or in hardware through supply chain attacks, as in [4,9]. Special attention should be given to the operation *Orchard*. According to [4], commercial off-the-shelf microprocessors contained in the Syrian radar might have been purposely fabricated with a hidden hardware backdoor (referred to as *kill switch*) which, by receiving a preprogrammed code had its functions disrupted and temporarily blocked the radar.

In this context, the aim of this work is to show – for awareness purpose – how the electronic and cyber warfare can be linked. As previously discussed, in [7] the authors present an EA able to produce multiple forged echoes for radar systems. In [4], the author presents clues about the implantation of a cyber vulnerability to affect radar systems, but not explain how such vulnerability can be triggered as the convenience of the attacker, especially if radar computers are air gapped and the only path to send commands to a previously installed vulnerability is through the radar antenna. In this work we demonstrate a mechanism that can be used to link the electronic and cyber warfare domains – a key element for the construction of a cyber-electronic attack.

III. MECHANISM FOR CYBER-ELECTRONIC ATTACK

In the cyber-electronic attack addressed in this work, it is assumed that the electromagnetic spectrum is used by the attacker to send a sequence of forged pulses to the radar receiver, as in [7], which is coded in time/range to represent a command to the cyber mechanism hosted in the radar. Once the command is acknowledged, the cyber component of the attack can start to manipulate the radar computational process to perform malicious actions, such as reset the system, stop to update the Plan Position Indicator (PPI), or even record and replay scenarios. The focus of this work is not on the generation of the forged radar echoes (an action in the EW domain represented in Figure 1), neither in the details about the manipulation of the radar computational process (an action in the CW domain represented in Figure 1). The focus of this work is on the linking mechanism that lies between both domains to make a cyber-electronic attack feasible in a naval radar system. The mechanism herein proposed for this task is based on a template matching technique [10].

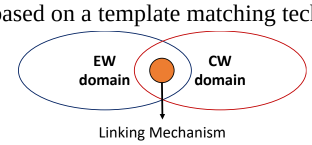

Fig. 1. Linking mechanism between EW and CW domains

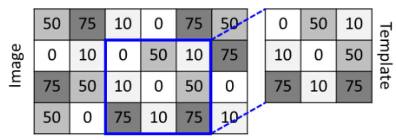

Fig. 2. Example of a template matching

The template matching technique is used in image processing to find small parts of an image that correspond to a model (template) image. To do so, it is defined a template to be searched in a main image. The main image in analysis and the template are divided in pixels, as shown in Figure 2. Then the template is moved over the main image, in a search process throughout all the main image's area. For each position assumed by the template in this scanning process over the main image, a similarity index is computed. The similarity index quantifies the similitude between the template and the piece of the main image being compared. If the index is higher than a previously defined threshold, then the template image is considered to be detected in the main image. This exhaustive search operation demands a considerable computational cost, proportional to the sizes of the images. On the other hand, it provides a high degree of effectiveness in searching for patterns in images [10].

Note that the degree of similarity between the template and a piece of the main image is established by comparing intensity values of each of their pixels. Among the available methods to compute the similarity coefficient, there are: the Sum of Absolute Differences (SAD), the Sum of Squared Differences (SSD), and normalized cross correlation. In this paper, the Pearson cross correlation (PCC) [10] is used (1):

$$corr = \frac{\sum_{i=1}^{N}(p_i + p)(a_i - a)}{\sqrt{\sum_{i=1}^{N}(p_i - p)^2}\sqrt{\sum_{i=1}^{N}(a_i - a)^2}} \qquad (1)$$

wherein, p_i is the intensity of pixel i in the template; p is the average intensity of the pixels of the template; a_i is the intensity of the pixel i in the patch of the image; a is the average intensity of the pixels in the patch of the image; N is the number of pixels. Note that this method presents a normalizing term in the denominator, which gives it invariance to global changes in brightness [10], and the results always lie within a defined range $[-1, 1]$.

IV. RESULTS

The mechanism for cyber-electronic attack described in Section III was evaluated through simulations on a computer with an Intel i7 processor of 2.5 Ghz, 8G RAM DDR3 memory, running Microsoft Windows 10, 64 bits. The radar environment was simulated in the Cinematic Radar Simulator v.2.0 and the template matching mechanism for cyber-electronic attack was implemented and simulated in Python.

It is assumed that the cyber component of the attack (the malware) is already installed in the radar, given that the exploitation mechanisms to install it in the radar computational system is out of the scope of this paper. Also, considering that the implementation of the EA component of the attack is not in the scope of this paper, it is assumed that the remote command (a sequence of false echoes) is generated and transmitted through a Digital Radio Frequency Memory (DRFM) technique [7]. The command is received and processed by the radar, and displayed as an image in the PPI screen, such as any other received echoes (false or not).

In the simulations herein presented, the Python code scans the graphical interface (the PPI) produced by the radar simulator in order to identify the attack commands received from the EA component of the offensive. To evaluate the effectiveness of the proposed mechanism, in this work, the chosen attack command consists of a sequence of five false echoes, which produces a sequence of five points displayed in the direction where the DRFM transmitter is. Once this pattern is detected, it can be used to trigger a malicious action in the naval radar system.

To validate this hypothesis and test the effectiveness of the command detection method, 30 fictitious scenarios were generated using the radar simulation software in order to represent real situations where a naval platform could be. Clutter/target echoes that might affect the command detection were randomly inserted in the PPI. Figure 3 shows an example of scenario used in the simulations. The triggering command is highlighted.

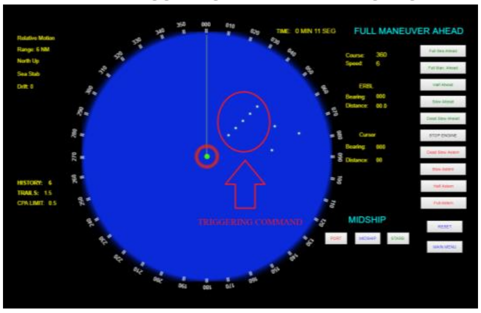

Fig. 3. Example of radar screen used in the simulations

```python
import numpy as np
import cv2
from PIL import Image

import time

ini = time.time()

for i in range(179):

 print (i)

 colorImage = Image.open('tamplate.png')

 rotated = colorImage.rotate(i)

 rotated.save('tamplate 2.png')

 img_bgr = cv2.imread('Imagem teste 5.png')
 img_gray = cv2.cvtColor(img_bgr, cv2.COLOR_BGR2GRAY)

 template = cv2.imread('tamplate 2.png',0)
 w, h = template.shape[::-1]

 res = cv2.matchTemplate(img_gray,template,cv2.TM_CCOEFF_NORMED)
 threshold = 0.7
 loc = np.where(res >= threshold)

for pt in zip(*loc[::-1]):
     cv2.rectangle(img_bgr, pt, (pt[0]+w, pt[1]+h), (0,255,255), 2)
     cv2.imshow('detected', img_bgr)

fim = time.time()

print ("Tempo de execução: ", fim-ini)
```

Fig. 4 Triggering mechanism implementation in Python.

It is worth mentioning that the attacker is transmitting the EA signal that generates triggering command shown in the screen, and that the signal can come from any direction, depending on the DRFM transmitter location. Thus, it is necessary to consider different angles from which the triggering command could be received. For the sake of simplicity, variations of 1 degree are considered, so the attacker could emit from the directions 000, 001, 002, 003 and so on. Considering these possible different Angles Of Arrival (AOA), the template containing the triggering command pattern is also rotated in steps of 1 degree during the search process throughout the PPI. This template matching search is executed throughout all the PPI screen until the algorithm finds a match or until all possibilities along the screen are tested. During the search process, the test image (*i.e.*, the PPI screen) is read and converted to grayscale. This serves to eliminate possible color variations, performing only the analysis of the pixel intensity. The template is also processed in grayscale for the comparison. To implement the algorithm, the libraries Numpy, cv2 and Pillow were used. The implementation is shown in Figure 4.

Five threshold levels were assessed: 0.3, 0.4, 0.5, 0.6, 0.7. Recall that the computed PCCs are compared with the threshold levels in order to decide if a match was found or not (see Section III). Each threshold level was assessed using the set of 30 different scenarios. The values corresponding to the confusion matrix for each threshold level are compiled in Table 1. The performance of the triggering mechanism for each threshold level is also depicted in Figure 5.

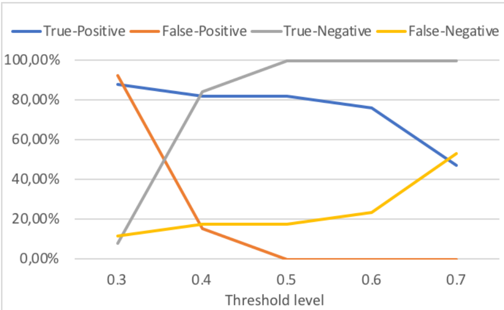

Fig. 5. Performance of the triggering mechanism

Table 1. Performance Rates

Threshold	TP	FP	TN	FN
0.3	88.24%	92.31%	7.69%	11,76%
0.4	82.35%	15.38%	84.62%	17,65%
0.5	82.35%	0%	100%	17,65%
0.6	76.47%	0%	100%	23,53%
0.7	47.06%	0%	100%	52,94%

The situation of True-Positive (TP) refers to the case where the triggering command is present in the PPI and there is a match with the template. False-Positive (FP) is the case in which the triggering command is not present in the PPI, but there is a match with the template. True-Negative (TN) occurs when the triggering command is not present in the PPI and is there is no match with the template. Finally, the False-Negative (FN) occurs when the triggering command is in the PPI but it is not detected. Based on the results, lowering the threshold increases the TP rate, but also increases the FP rate (which may cause fortuitous and unwanted attack activations). On the other hand, increasing the threshold decreases the FP rate, but also decreases the TP rate (which reduces the attack effectiveness). According to the results, the best threshold from the attacker point of view is 0.5. Note that with this threshold the attacker is able to obtain the maximum TP rate (82.35%) without false positives. It means that, with this threshold, considering the evaluated scenarios, the probability of an accidental attack activation tends to 0% (which is important to avoid the attack disclosure) and the attacker has 82.35% of probability in successfully activating the cyber component of the attack in the first attempt. Note that, with two attempts the probability of having the attack properly activeted in at least one of the attempts increases to 96.88%.

V. CONCLUSIONS

Considering the theoretical framework presented and the simulations carried out, it is possible to realize that EA and cyberattacks can be linked to each other, forming a cyber-electronic attack capable of affecting naval radar systems. The attack exploits the fact that the radar, as a sensor, can be considered an open door for commands. It is possible to use image processing techniques to trigger a malicious code previously installed on a naval radar system with a good accuracy and effectiveness, maintaining the due safety against accidental activations. Even with all the information security devices, all computer systems are subject to the risk of being infected by malware. This mechanism can be used for the benefit of a naval operation, being activated at the most opportune moment for the attacking force. For future work we plan to evaluate the performance of the proposed mechanism in a real system and investigate countermeasures to mitigate this threat – such as tools to verify the integrity of the software used in naval radars.

REFERENCES

[1] S. McLaughlin et al., "The Cybersecurity Landscape in Industrial Control Systems," in Proceedings of the IEEE, vol. 104, no. 5, pp. 1039-1057, May 2016.

[2] R. Langner, "Stuxnet: Dissecting a Cyberwarfare Weapon," in IEEE Security & Privacy, vol. 9, no. 3, pp. 49-51, May-June 2011.

[3] K. Zetter, “Countdown to Zero Day: Stuxnet and the launch of the world’s first digital weapon”, Broadway books, 2014.

[4] S. Adee, "The Hunt For The Kill Switch," in IEEE Spectrum, vol. 45, no. 5, pp. 34-39, May 2008.

[5] A. O. Sá, R. C. S. Machado, N. N. Almeida, “The Convergence of Cyber, Electronic and Kinetic Warfare Within the Scope of Sea Power”, Journal of the Brazilian Naval War College, vol. 25, pp. 89-128, 2018.

[6] J. Bhatti, T. Humphreys, “Hostile Control of Ships via False GPS Signals: Demonstration and Detection”, Navigation, vol. 64, pp.51-66, 2017.

[7] A. Almslmany, C. Wang and Q. Cao, "Advanced deceptive jamming model based on DRFM Sub-Nyquist sampling," 2016 13th International Bhurban Conference on Applied Sciences and Technology (IBCAST), Islamabad, 2016, pp. 727-730.

[8] N. Falliere, L. O. Murchu, E. Chien, “W32. stuxnet dossier”, Symantec, 2010.

[9] J. Robertson, M. Riley, “The big hack: how China used a tiny chip to infiltrate US companies”, Bloomberg Businessweek, vol. 4, 2018.

[10] Y. M. Tavares, N. Nedjah, L. M. Mourelle, “Embedded implementation of template matching using correlation and particle swarm optimization”, International Journal of Bio-Inspired Computation, 2018 Vol.11 No.2, pp.102 – 109.

2020 IMEKO TC-19 International Workshop on
Metrology for the Sea
Naples, Italy, October 5-7, 2020

The European Metrology Network for Climate and Ocean Observation: updates and perspectives

Francesca Rolle[1], Michela Sega[1], Paola Fisicaro[2], Emma Woolliams[3], Miruna Dobre[4], Steffen Seitz[5]

1) Istituto Nazionale di Ricerca Metrologica (INRIM), Strada delle Cacce 91, 10135, Torino (Italy)

2) Laboratoire national de métrologie et d'essais (LNE) 1 rue Gaston Boissier, 75015 Paris (France)

3) National Physical Laboratory (NPL), Hampton Road, Teddington, TW11 0LW, UK

4) FPS Economy, Metrology Division (SMD), Boulevard du Roi Albert II 16, 1000 Brussels (Belgium)

5) Physikalisch-Technische Bundesanstalt (PTB), Bundesallee 100, 38116 Braunschweig (Germany)

***Abstract* – In the present paper, the EURAMET European Metrology Network for Climate and Ocean Observation (ClimOcNet), established in 2019, is presented. The EMN is focused on three different thematic areas, among which is ocean observation and metrology for EOVs. The main goal of the network is to establish a solid, long-term, European infrastructure to enhance the cooperation between the metrological and the oceanographic communities, to support the global understanding of climate change and the sustainable use of the oceans. The structure and the objectives of the EMN are described, together with an overview of the outputs of the first year of the EMN.**

I. INTRODUCTION

Climate change and its impact on oceans, land, atmosphere and biosphere, led the United Nations to ratify in 2015 the "Sustainable Development Goals" (SDGs) [1]. Amongst these, goal 13 states: "Take urgent action to combat climate change and its impacts" and SDG 14 states: "Conserve and use the oceans, seas and marine resources for sustainable development".

The Global Climate Observing System (GCOS) has defined a set of more than 50 Essential Climate Variables (ECVs), physical, chemical, and biological, that characterise Earth's climate. Each variable poses challenging measurement accuracy targets, to enable the global observation of small climate trends [2].

Metrology can provide expertise and a sound basis for the reliable monitoring of the ECVs over the long timescales needed to detect and understand climate trends.

The Global Ocean Observing System (GOOS) has similarly defined Essential Ocean Variables (EOVs), including both the GCOS oceanic ECVs and additional EOVs that support the economic and social applications of the ocean system [3].

The European Association of National Metrology Institutes (EURAMET) [4] has recently established European Metrology Networks (EMNs) to support its vision to ensure that Europe's metrology capability meets the rapidly advancing needs of end users. The European Metrology Network for Climate and Ocean Observation (ClimOcNet) is one of the first six EMNs established by EURAMET.

EMNs will analyse the European and global metrology needs and address these both in coordinating the research and services of European metrology institutes and in providing a single point of contact for information, to underpin regulation and standardisation and to promote metrological practice [5].

Fig. 1. The EMN for Climate and Ocean Observation logo

II. METROLOGICAL REQUIREMENTS FOR EOVs OBSERVATIONS

GCOS recognises the importance of metrology and, in 2010, a Memorandum of Understanding was established between the World Meteorological Organization (WMO) and the Bureau International des Poids et Mesures (BIPM), to promote metrology into environmental observation.

The accuracy requirements specified by GOOS for the EOVs are, in many cases, difficult to achieve even in a laboratory and need to be carried out also in environmental conditions. To provide robust, interoperable and long-term data records of EOVs, GOOS must be underpinned by all the core metrological principles. At present, robust metrological methods are not routinely applied to many EOV observations, but there is a growing recognition by the observation communities in the value that metrology can provide in this field.

The marine communities already collaborate with European and international organisations, usually covering several EOVs. However, this integrated landscape is lacking a multidisciplinary and coordinated approach to providing metrological traceability, comparison and uncertainty evaluation to the EOV observations.

III. THE EUROPEAN METROLOGY NETWORK FOR CLIMATE AND OCEAN OBSERVATION

The Memorandum of Understanding of ClimOcNet was signed in May 2019. The new established EMN held its first meeting in June 2019. The EMN is structured in three technical sections: Atmosphere, Ocean, Land and Earth. The thematic areas broadly correspond to the divisions of the GCOS ECVs and principal observational techniques.

A. Atmosphere

The Atmosphere Observation Section supports *in situ* surface, upper air and composition measurements of the GCOS Atmospheric ECVs. These include measurements of gases, aerosols, water vapour and properties of clouds, together with physical ECVs such as temperature, pressure, wind speed and direction.

B. Ocean

The Ocean Observation Section covers the metrological contribution to support *in situ* measurements of GCOS Oceanic ECVs along with the broader GOOS EOVs. These include physical (e.g. temperature, salinity, currents, ice), biogeochemical (e.g. dissolved gases and nutrients, acidification, particulate matter and tracers) and biological (e.g. phytoplankton, ocean sound) variables. The Ocean Observation Section reflects the broader variety of economic, social, and environmental perspectives relating to the oceans.

C. Land and Earth

The Land and Earth Observation Section covers the metrological contribution for *in situ* measurements of the GCOS terrestrial ECVs (hydrology, cryosphere, biosphere and human resource use), along with the remote sensing observations of ECVs in all three GCOS categories: Land, Ocean and Atmosphere.

IV. EXPECTED OUTPUTS OF THE EMN

European National Metrology Institutes (NMIs) and Designated Institutes (DIs) (i.e. members of EURAMET) can become members of the EMN, while any other interested organisation can become a partner of the EMN.

At present, 20 European NMIs and DIs are involved in ClimOcNet, together with more than five partner institutes. During the first year of EMN, several activities were carried out:

- a stakeholder needs review survey and report, that describes the stakeholder needs for metrology in the observation and use of ECVs and EOVs;
- a first stakeholder workshop in February 2020 (in webinar form); a second workshop is foreseen for 2022;
- a collated set of training material to teach the principles of metrology to the observation communities, and communication material to present the concepts of metrology to different stakeholder communities were prepared.

The establishment of a single point of contact for metrology support for climate and ocean observation with a website that presents European metrological capabilities is ongoing.

Some of the main expected outcomes of the EMN activities are the establishment of metrological principles for *in situ* and space-based measurements, improved SI-traceable measurement techniques and reference standards for *in situ* and satellite observations, development of the skills of a greater number of scientists in both observations and metrology.

V. A FOCUS ON THE OCEAN SECTION

The oceans cover 71 % of the earth's surface. Oceans regulate the earth's climate and have absorbed almost 93 % of the enhanced anthropogenic greenhouse warming so far [6]; in doing this they have also been disproportionately impacted by climate change: sea levels have risen, changing coastlines, the oceans have become warmer, more acidic and with increased ocean stratification. They also serve as a natural sink for carbon emissions, with half of the photosynthetically absorbed emissions and thus a ¼ of those emitted, being locked into the Ocean through phytoplankton and algae or direct diffusion. These changes have altered ecosystems and increased the vulnerability of many marine species. Oceans are also a crucial source of food, water, energy and minerals for human life, and are a medium for transport (90 % of goods are shipped by sea), recreation and commerce. The value of marine activities is about 5 % of the global GDP, expecting to reach around US$ 3 trillion by 2030 through sustainable growth (the value following an unsustainable scenario is smaller) [7]. The European Union's Integrated Maritime Policy focusses on 'Blue Growth' – harnessing the potential of Europe's oceans, seas and coasts to stimulate economic development within the environmental boundaries of the ocean ecosystems that sustain that growth.

To balance environmental, social and commercial concerns, GOOS, a programme executed by the Intergovernmental Oceanographic Commission (IOC) of UNESCO, has established a framework for ocean observing centred on EOVs. The EOVs include all the Essential Climate Variables in the oceanic domain and additional variables that relate to ecosystem, disaster-warning and commercial observational requirements.

The marine communities collaborate in national, European and international organisations, usually covering several EOVs. Generally, the development of measurement systems and observational infrastructures are well coordinated, essentially because these structures are multidisciplinary and interconnected and must deliver data serviceable to every organisation member and to policymakers. However, this integrated landscape is lacking a multidisciplinary and coordinated approach to establish fundamental metrological concepts in EOV observations. Therefore, the ocean section of the EMN aims to support the oceanographic community with improved SI traceability for ocean ECVs and EOVs, quality assurance tools (e.g. reference materials, interlaboratory comparisons, uncertainty calculation, accreditation schemes), as well as training for scientific communities in metrology.

VI. CONCLUSIONS

The establishment of a European Metrology Network for Climate and Ocean Observation aims to provide a single point of contact for European metrology in supporting climate and oceanographic observations.

A long-term sustainable European metrology infrastructure is fundamental to support the global understanding of climate change and the sustainable use of the oceans.

VII. ACKNOWLEDGMENT

This project 18NET04 has received funding from the EMPIR programme co-financed by the Participating States and from the European Union's Horizon 2020 research and innovation programme.

VIII. REFERENCES

[1] www.un.org/sustainabledevelopment/

[2] https://gcos.wmo.int/en/home

[3] https://www.goosocean.org/

[4] https://www.euramet.org/european-metrology-networks/climate-and-ocean-observation/

[5] E. Woolliams, C. Pascale, P. Fisicaro, N. Fox, The European metrology network for climate and ocean observation, Proceedings of 19th International Congress of Metrology, 05001 (2019)

[6] IPCC Climate Change 2013: The Physical Science Basis. Contribution of Working Group I to the Fifth Assessment Report of the Intergovernmental Panel on Climate Change, Cambridge University Press, Cambridge, United Kingdom and New York, NY, USA, 1535 (2013), www.ipcc.ch/report/ar5/wg1/

[7] S. Bojinski, M. Verstraete, T. C. Peterson, C. Richter, A. Simmons, and M. Zemp, The Concept of Essential Climate Variables in Support of Climate Research, Applications, and Policy, Bull. Am. Meteorol. Soc., vol. 95, no. 9, pp. 1431–1443, Sep. 2014.

2020 IMEKO TC-19 International Workshop on
Metrology for the Sea
Naples, Italy, October 5-7, 2020

Analysis of multi-sensor sea level measurements in the Adriatic Sea

Gabriele Nardone[1], Saverio Devoti[1], Arianna Orasi[1], Luca Parlagreco[1], Marco Picone[1]

[1] *ISPRA – Istituto Superiore per la Protezione e la Protezione e la ricerca Ambientale,*
Via Vitaliano Brancati, 48 – Roma, Italy
retemareografica@isprambiente.it

***Abstract* – The aim of this study is a preliminary analysis and comparison of a ten years, multi sensor co-located observations of sea level. Starting from data collected by the Italian tide gauge network, we report the description of recurring errors, some statistics for the compared signals and a comparison between closed stations.**

I. INTRODUCTION

Sea level monitoring networks are necessary for many applications, ranging from shoreline protection and coastal flood control to planning and design civil infrastructure that insist on the coast, from the navigation support to the climate change studies, from the sea safety and circulation to the validation and calibration of forecasting models. Most of these activities require both real-time data and multiannual time series.

The principal applications of sea level observations are: the evaluation of the tidal cycles, the estimation of the effects of meteorological contributions, the study of extreme events, the tides prediction, the validation of forecasting models. Moreover, sea level data are used for determining seiches and can support the identification and characterization of tsunami and storms tides.

ISPRA manages the national tide gauge network “Rete Mareografica Nazionale” (in the following RMN), currently counting 36 stations located along Italian coasts. Each station provides sea level measurements and also main meteorological parameters. Some stations also provide data used for the qualitative characterization of environmentally sensitive marine areas.

During the last decade, sea level data have been fundamental in the evaluation of the effects of climate changes on marine environment, in particular on the study of sea level rise acceleration. In this framework the levelling activities assume the same importance then the sea observation and the correct definition of a reference system is a critical step.

For each measurement station the local reference system is directly linked to the Italian IGM high precision leveling network, built in the years between 1950 and 1971, therefore sea level values are referred to the official altimetric system for the mainland Italy (Genoa 1942).

Nowadays the standard high precision leveling has been replaced by GPS measurements of the vertical displacements of the measurement stations. However, the discrepancies between these two approaches, the discontinuity of these operations, suggest the use of continuous monitoring of the vertical displacements through new technologies (e.g. GNSS).

As many other types of measurements, sea level observations collected by tide-gauges, are affected by different types of error.

The problem of sea level error has been addressed by several authors to estimate the measure uncertainty and determine reliability at studies on sea level changes [1].

Since tide-gauges are isolated instruments no comparisons with other independent records were possible, for this reason all the RMN measurement stations are equipped with two sensors that acquire sea level data simultaneously, a guided radar sensor and a float with encoder.

Following [2] we used the differences between the two collocated sensors to identify and classify errors and bias, particularly in relation to the vertical variation of the tide gauges benchmarks.

The aim of this study is then a preliminary analysis and comparison of a decadal multi sensor observations of sea level measured from two different sensors at six RMN stations Venezia (VE), Ravenna (RA), Ancona (AN), San Benedetto del Tronto (SB), Ortona (OR), Tremiti (TR). These stations are located along the northern and the central sector of the Adriatic basin. The investigated area is representative of 400 km of coastline, consisting of lagoon systems, sandy shorelines and rocky promontories, combining different hydraulic conditions and geographic environments.

II. RMN NETWORK

The RMN is the hugest network of sea level measurement in the Mediterranean Sea (Fig. 1), collecting real time series of sea level and meteorological parameters. Sea level data are collected with the very high frequency of 1 observation per minute and experimentally for some stations with a frequency of 15 seconds. The RMN also provides weather data that integrates the National meteorological system.

Fig. 1. RMN stations.

Data used in this study range from 2010 to 2020, which are priory checked to ensure their highest possible accuracy.

III. METHODS

Standard procedures have been applied to remove errors in the time series of measurements and the resulting differences (Δ) calculated as follows:

$$\Delta = SL_r - SL_f$$

where SL_r is the sea level calculated trough the radar and SL_f is the sea level calculated trough the float.

The Δ differences have been calculated at the six stations, on the entire considered period and yearly, and then analysed respect to the amplitude and pattern.

Therefore, an algorithm for multiple change point analysis have been implemented to detect any possible discontinuity in the time series of Δ. This algorithm uses a dynamic programming and pruning approach [3] and detect a suitable number of change points according to the E-statistic as a goodness-of-fit measure.

Moreover, Van de Casteele test [4] has been implemented to analyse the magnitude of the expected error in the recorded sea levels and to provide a qualitative illustration of the type of error involved. Van de Casteele tests [5,6] allow to easily visualise the differences of recorded tidal levels between a sensor and another selected as reference. Following results of previous studies (e.g. [7,8]) which suggest that the radar sensors appear to have a more stable behaviour respect to the pressure gauges, radar sensors have been used as the reference gauge and the floater with encoder as the sensor under testing. Finally, the spatial variability of sea level measurements obtained by radar sensors has been compared among neighbouring stations during selected time intervals.

IV. RESULTS AND DISCUSSION

In the following, results of described analyses are reported and discussed.

A. Descriptive statistics of Δ

Table 1 contains some descriptive statistics of differences Δ at the six gauges listed in the first column.

The second column of Tab. 1 reports the percentage of Δ values less than 2cm that for all gauges always represent more than 83% of the time series analysed. The number of null data is reported in the third column. The ten-years averaged values of differences (fourth column) vary from 0,001 to 0,008. In Fig. 2 the main representative percentiles of the annual difference's distribution are shown to investigate the occurrence of leveling errors and/or drifts between collocated measures. As highlighted in Fig. 2, the representation of the annual difference's main percentiles allows to point out different behaviour between the 10 years otherwise not noticeable with the same statistics calculated on the entire period.

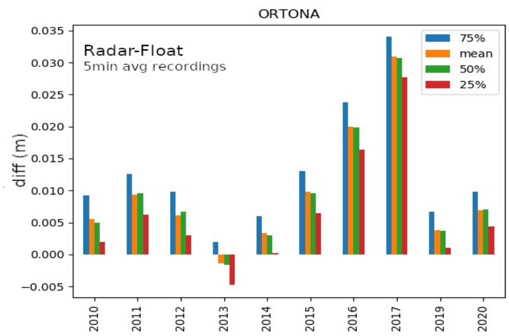

Fig. 2. Annual difference's main percentiles at Ortona station.

Table 1. Descriptive statistics of differences between sensors.

Gauges	% (Δ < 0,02m)	# null data	Avg
VE	91,3	2	0,002
RA	84,7	1018	0,002
AN	98,4	2	0,003
SB	87,1	209	0,007
OR	83,1	780	0,008
TR	99,9	2353	0,001

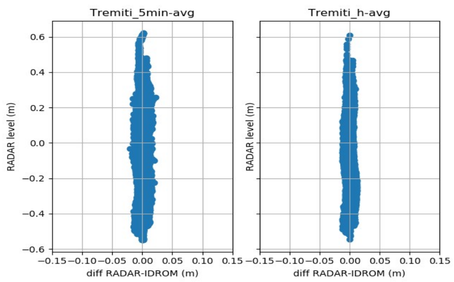

Fig. 3. Van de Casteele plot at Tremiti gauge. On the left 5minutes and on the right hourly averaged time series.

Van de Casteele plots allow to quickly inspect whether time shift errors or instrument and system malfunction affect data during the time period selected. Fig. 3 shows the differences, at Tremiti gauge, respectively averaged with a five minute (on the left) and hour time span (on the right).

B. Type of errors

The differences between sensors at each station fall into one of the proposed categories by [2], with major importance of drifting evidenced by a linear trend (Fig. 4) and sudden 'step' in the recordings (Fig. 5). Sensor or data logging system malfunctions are concentrated in specific stations.

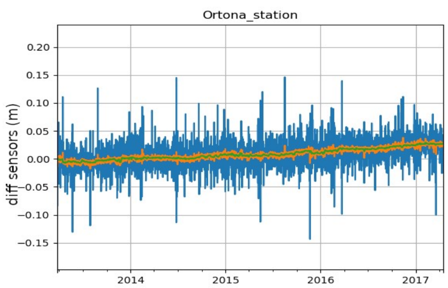

Fig. 4. Drifting of differences. In blue, orange and green respectively the 5minutes, hourly and daily averaged values.

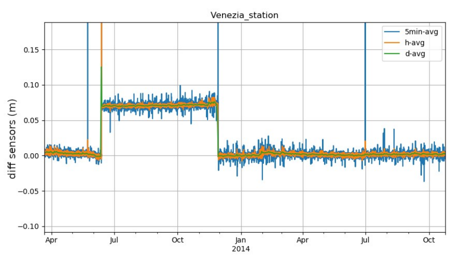

Fig. 5. Sudden change of values.

Table 2 reports some statistics about the amplitude of steps detected through the change points analysis in terms of real value (A) and absolute value (|A|).

C. Spatial analysis of level data

Radar sea level measurements were used to analyse the coherence of the tidal signal in the northern part of the Adriatic Sea. An example of the differences in radar level among Venezia and the other stations is provided in Fig. 6, which highlights the increase of both the median and the deviation from it of the difference values moving away from Venezia, starting from Ravenna (ven-rav) until to Tremiti Islands (ven-trm).

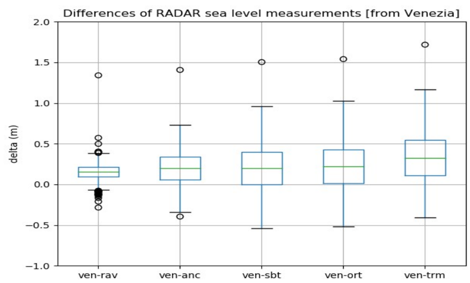

Fig. 6. Distribution of 2014 differences of RADAR recordings relate to Venezia (reference) station.

Table 2. Change points in differences.

Gauges	N	Mean(|A|)	Max(|A|)	Sum(|A|)	Sum(A)
VE	2	0.34	0.61	0.68	0.53
RA	2	0.03	0.03	0.05	-0.05
AN	1	0.01	0.01	0.01	-0.01
SB	0	-	-	-	-
OR	4	0.01	0.03	0.06	-0.04
TR	0	-	-	-	-

V.CONCLUSIONS

All the stations are influenced by a prevalence of positive differences between sensors, indicating that the floater often underestimates.

In order to integrate the tide gauge network of the sector analyzed, GNSS stations will be integrated co-located with some tide gauges, as it has already been done for the Venice station, aimed at discriminating potential altitude reference errors in areas where the subsidence problem is particularly present and then refer the detected level to a global reference datum. This preliminary work is oriented to determine the stations that will be equipped with GPS equipment.

REFERENCES

[1] Woodworth, P. L., and D. E. Smith, 2003: A one year comparison of radar and bubbler tide gauges at Liverpool. Int. Hydrogr. Rev., 4 (3), 2–9.
[2] S. Pytharouli, S. Chaikalis, S.C. Stiros, Uncertainty and bias in electronic tide-gauge records: Evidence from collocated sensors, Measurement 125 (2018) 496–508.
[3] W. Zhang, N. A. James and D. S. Matteson, "Pruning and Nonparametric Multiple Change Point Detection," 2017 IEEE International Conference on Data Mining Workshops (ICDMW), New Orleans, LA, 2017, pp. 288-295.
[4] Miguez, B. M., L. Testut, and G. Wöppelmann, 2008: The Van de Casteele Test Revisited: An Efficient Approach to Tide Gauge Error Characterization. J. Atmos. Oceanic Technol., 25, 1238–1244.
[5] IOC, Manual on Sea Level Measurement and Interpretation, Volume I – Basic Procedures, IOC Manuals and Guides No. 14, vol. III, 1985.
[6] B.M. Miguez, L. Testut, G. Wöppelmann, The Van de Casteele test revisited: an efficient approach to tide-gauge error characterization, J. Atmos. Oceanic Technol. 25 (2008) 1238–1244.
[7] B.M. Míguez, A.P. Gomez, E.A. Fanjul, The ESEAS-RI sea level test station: reliability and accuracy of different tide-gauges, Int. Hydrogr. Rev. 6 (1) (2005) 44–53.
[8] B. Pérez, A. Payo, D. López, P.L. Woodworth, E. Alvarez Fanjul, Overlapping sea level time series measured using different technologies: an example from the REDMAR Spanish network, Nat. Hazards Earth Syst. Sci. 14 (2014) 589–610.

2020 IMEKO TC-19 International Workshop on
Metrology for the Sea
Naples, Italy, October 5-7, 2020

Design and verification of a “Fixed-Point” spar buoy scale model for a “Lab on Sea” unit

D. Alizzio[1], M. Bonfanti[2], N. Donato[1], C. Faraci[1], G. Grasso[2], F. Lo Savio[3], R. Montanini[1], A. Quattrocchi[1]

[1] Dept. of Engineering, University of Messina, Cont.da Di Dio, 98166 Messina, Italy.
[2] Dept. of Electric., Electron., Infor. Eng., Univ. of Catania, Via S. Sofia, 54, 95100 Catania, Italy.
[3] Dept. of Civil Eng. and Arch., University of Catania, Via S. Sofia, 54, 95100 Catania, Italy.
Corresponding Author e-mail: roberto.montanini@unime.it

***Abstract* – The present work is a part of a larger project relative to design of an instrumented spar buoy within the multi-purpose “Lab on Sea” unit equipped with an energy harvesting system for use in marine applications. Such a system will be based on deformable bands integral to the unit to convert the wave motion energy into electricity through piezo patch transducers.**

In this paper, a “fixed-point” spar buoy scale model suitable for tests in a controlled ripples-type wave motion channel was designed, built and tested. The purpose of this model is to verify that it remains fixed maximizing, then, the displacement of the bands under wave motion.

To evaluate its response, the buoy scale model was equipped with a measuring device consisting of a MEMS accelerometer and a gyroscope. Results of acquisitions from on-board sensors revealed a very low susceptibility of the buoy scale model to the wave motion imposed.

I. INTRODUCTION

Nowadays monitoring of the marine habitat is a topic of great relevance [1]. These environments are particularly susceptible to human activity, in terms of industrial and civil development. Therefore, acquiring information on spatial and temporal large enough scales is essential to guarantee effective monitoring in order to produce solutions aimed at reducing the anthropogenic impact on ecosystems. These include monitoring the concentration of pollutants in both natural and artificial reservoirs and near sewage, the detection of microplastics and their concentration in lagoon or open sea waters [2, 3]. In addition, there are also multiple civil protection purposes, including the possibility of detecting anomalous waves or tsunamis that can occur on the coasts [4]. The scientific literature is rich in solutions involving the use of floating devices equipped with a wide range of sensors for environmental monitoring and adequate telecommunication interfaces. The most sophisticated devices employ energy recovery systems for self-maintenance (e.g. energy harvesting) so that they can be used off-shore [5]. Observation platforms include various types: on site, equipped with remote instrumentation, operating on the surface (on board an oceanographic ship [6], surface buoys [7, 8], floating buoys [9, 10], buoys towed by boats [11]), active on the seabed (autonomous underwater vehicles AUV [12], remote control vehicles ROV [13], networks of underwater buoys [14]) and with satellite monitoring [15]. The choice of the type of buoy and the equipment to be adopted is mainly determined by the characteristics of the environment to be investigated (depth of the waters, peculiarities of the waves, etc.) and the required space-time coverage [16].

In this context, the subject of this paper concerns some preparatory operations for the future design of a multi-purpose "Lab on Sea" unit able to perform energy storage automatically from waves and equipped with a communication network able of connecting to any IT infrastructure.

The idea of building a unit equipped with power systems from renewable sources to minimize the implementation and maintenance costs of the entire data collection system and to ensure energy autonomy was deemed convenient. The ultimate purpose of this investigation consists in designing additional elements of the unit able to perform energy harvesting. Thus, the target will be to develop a system with deformable and wave-sensitive bands to convert the mechanical deformation energy into electricity through piezo patch transducers. Since piezoelectric elements are more performing at high frequencies, these bands will be sensitive to ripples-type waves. In order to amplify the input of the transducers, it will be necessary to maximize the deformation by constraining the unit to remain fixed with respect to the wave motion. Hereafter such a condition is named “fixed point” (as in Fig. 1).

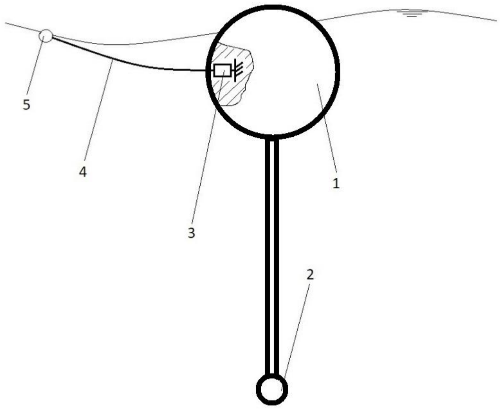

Fig. 1. Scheme of the energy conversion apparatus for the Lab on sea unit: 1. spar buoy; 2. ballast; 3. piezo patch transducer; 4. deformable band; 5. external float.

Consequentially, evaluating if the amount of the energy available through the sea wave motion is enough to recharge the on-board power supplies should be made. In this paper the dynamic behaviour of a spar buoy scale model undergone to a known wave motion was investigated in order to verify that the “fixed point condition” was satisfied.

The scale model can be assimilated to a 2 DOF mass-spring-damper system and, therefore, it was sized to make both vertical and angular oscillations negligible [17].

As known, a mass-spring-damper system of mass m, stiffness k and viscosity β, placed on a vibrating body (such as a fluid subject to wave motion) under an oscillation $x = X_0\sin(\omega t)$ with respect to a fixed reference system, is characterized by the following equation of motion [18]:

$$m\ddot{y} + \beta\dot{y} + ky = m\omega^2 X_0 \sin(\omega t) \tag{1}$$

The ratio between the amplitudes of the response (Y_0) and the forced excitation (X_0) depends on the pulsation of the excitation (ω), the pulsation of the system ($\omega_0 = (k/m)^{1/2}$), the viscosity (β) and the critical value viscosity ($\beta_{cr} = 2(k{\cdot}m)^{1/2}$):

$$\frac{Y_0}{X_0} = \frac{\lambda^2}{\sqrt{(1-\lambda^2)^2 + 4\tau^2\lambda^2}} \tag{2}$$

where $\lambda = \omega/\omega_0$ and $\tau = \beta/\beta_{cr}$. The aim is creating a system with high values of λ, so that the ratio between the amplitudes tends to 1 and the phase angle (φ) to π regardless of τ. This leads to a response having an amplitude equal to that of the excitation but in the counter-phase (i.e. the buoy is integral with the wave motion but in the opposite direction). Furthermore, since for high values of λ the effect of viscosity is almost negligible, the verification of angular oscillations can be traced back to the study of the harmonic motion of a simple pendulum having length L and natural frequency $\omega_n = (g/L)^{1/2}$.

II. MATERIALS AND METHODS

The spar buoy scale model designed in the present paper consists of a spherical buoy with a central through hole where a rigid rod is inserted. The rod has the dual purpose of supporting a stabilizing counterweight (ballast) in its immersed part, and accommodating the sensors and mechanical connection for the dynamic measuring instrumentation on the top (Fig. 2).

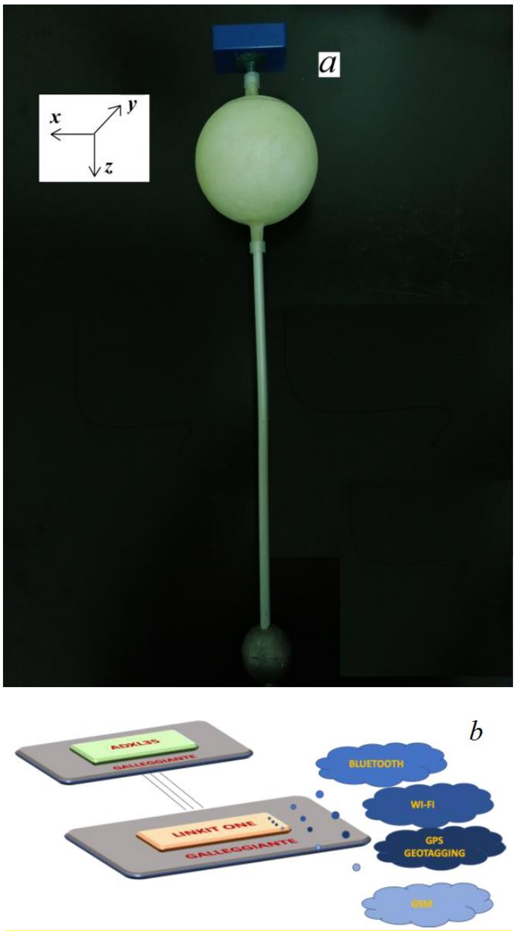

Fig. 2. (a) Spar buoy scale model; (b) block diagram of the data acquisition system.

First of all a preliminary study on both sea and tank tests was carried out for measuring the fundamental characteristics of the wave motion (amplitude and frequency). Indeed, the knowledge of wave frequencies is fundamental to rightly design the spar buoy, above all in compliance with the required "fixed point" condition.

It was found that the trend of the measured acceleration appears to be sufficiently repeatable in both conditions. Furthermore, frequency distributions are comparable despite the different way to excitate. The most representative frequency values found for ripples-type waves ranged from 1 to 3 Hz. Fig. 3 shows the comparison between the vertical accelerations measured at sea (near the shore in the coastal area) and under controlled conditions (artificial canal), and the comparison between their respective signals in frequency domain (DFT). From a preliminary analysis of the comparison between the measurements at sea and within an artificial canal, it was analytically found that the geometric dimensions allowing the unit, subjected to the forced excitations, to satisfy the fixed point condition are shown in Tab. 1.

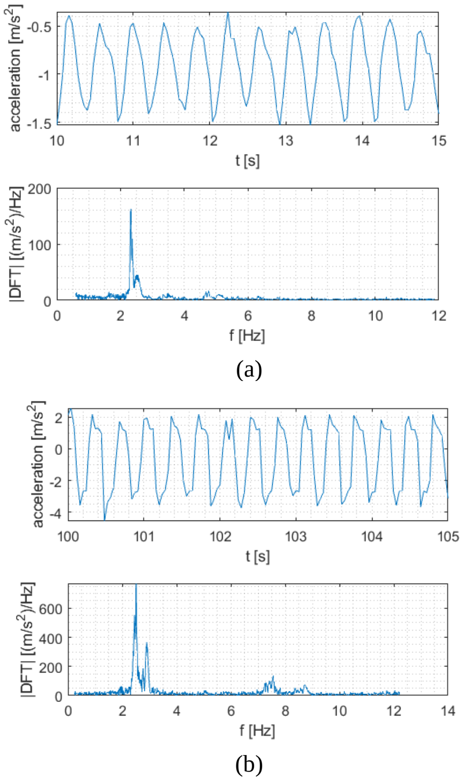

Fig. 3. Comparison between acceleration and DFT at sea (a) and in artificial canal (b)

d	*S*	*B*	H_e	*M*	*L*	λ_{vert}	λ_{ang}
[mm]	*[mm]*	*[N]*	*[mm]*	*[kg]*	*[mm]*		
600	*500*	*1052.5*	*100*	*57.5*	*2000*	*10.62*	*5.67*

Tab. 1. Summary on the buoy unit sizing.

However, in order to experimentally verify that the Lab on sea unity will be capable of satisfying the required "fixed point" condition, a scale model was created because it is best suited to tank tests. Indeed, the water measurement system available consisted of a channel for the production of an established wave motion, having a wet section of 600x600 mm and a length of 10 m. It was equipped with an air system for the generation of ripples-type waves and a measuring device for real-time reading of the wave height and frequency.

Tab. 2 shows the geometric and mechanical scale data for the buoy model and its counterweight. Having imposed a value of 100 mm for the diameter *d* of the buoy model (linear scale factor of 1/6), the choice of values useful for sinking *S* was made so as to fall within the linear section of the relative "buoyancy-sinking" curve. In particular, the value of 86 mm was chosen for *S*, which corresponds to a buoyancy *B* of nearly 3.98 N, and the value of 14 mm was set for the emerged height of the spherical cap H_e. The ballast, also spherical in shape and made of lead (density of 11.34 kg/dm^3), provided a counterweight of mass *M* equal to 0.45 kg and was placed from the buoy centre at a barycentric distance L= 370 mm.

Considering 2.5 Hz as the most representative average value found for the oscillation frequency, the sizing of the buoy model provided sufficiently high values of λ (see section I) both as regards vertical oscillations (λ_{vert} = 12.73) than the angular ones (λ_{ang} = 14.69).

d	*S*	*B*	H_e	*M*	*L*	λ_{vert}	λ_{ang}
[mm]	*[mm]*	*[N]*	*[mm]*	*[kg]*	*[mm]*		
100	*86*	*3.98*	*14*	*0.45*	*370*	*12.73*	*14.69*

Tab. 2. Summary on the buoy model sizing.

The model of the buoy built consists of a polystyrene sphere coated by deposition of polyester thermosetting epoxy powder.

The counterweight was made of lead by means of a casting process on a special plaster mould. The rigid rod for connecting the counterweight to the buoy consists of a cylindrical aluminium tubular with external diameter of 10 mm and thickness of 1 mm. On the top of the rod, a cylindrical seat accommodating a displacement sensor (iNEMO inertial module included in ST SensorTile.box) was obtained. This sensor consisted of a triaxial gyroscope and a triaxial accelerometer. The gyroscope has a RMS rate noise value of 0.075 deg/s. The accelerometer RMS accuracy is 0.01962 m/s^2 in low energy mode. Furthermore, it was internally power supplied and it allowed an easy reading of the measured quantities via Bluetooth communication and data logging on internal SD card.

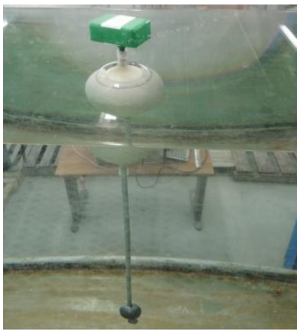

Fig. 4. spar buoy scale model test

A dynamic buoyancy test of the scale model in the above-mentioned controlled water channel was performed (Fig. 4). The ripples-type waves were monitored via image acquisition and post-processed. For the acquisition, a camera Basler acA1300-30 gm GigE with a CCD sensor (Sony ICX445, resolution of 1296 px. 966 px), a 35 mm lens (C23-3520-2 M F2.0) was used. A motion reconstruction of the ripples-type waves was computed through NI Image Acquisition module on LabView environment. As shown in Fig. 5, the average value found for the imposed oscillation frequency was of 2.63 Hz, in line with the most representative frequency values of ripples-type waves.

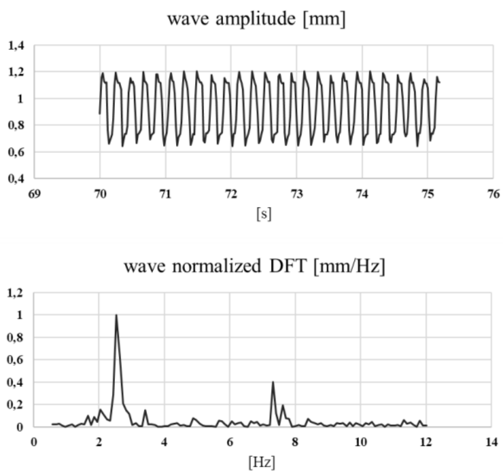

Fig. 5. Amplitude and DFT in controlled water channel.

Acquisitions from both on-board accelerometer and gyroscope was performed at 104 Hz. The ST SensorTile.box mounted on the scale buoy returned values confirming the accomplishment of the required “fixed point condition”. As expected, the Z-signal from the accelerometer of ST remained constant for the whole test and equal to nearly -9.73 m/s^2 (Fig. 6 and Tab. 3), and it means that the scale buoy remained integral to the vertical wave motion. The 3-axis gyroscope also did not detect appreciable variations in angular oscillations returning mean values about 0.40 deg/s around X-axis and -0.63 deg/s around Y-axis.

	max	*min*	*main value*	*st. deviation*
	[m/s^2]	*[m/s^2]*	*[m/s^2]*	*[m/s^2]*
X axis	*0,28449*	*-0,13734*	*0,07633*	*0,065729*
Y axis	*0,04905*	*-0,53955*	*-0,2377*	*0,075556*
Z axis	*-9,59418*	*-9,83943*	*-9,73372*	*0,029311*

Tab. 3. Data from 3-axial accelerometer in iNEMO inertial module

	max	*min*	*main value*	*st. deviation*
	[deg/s]	*[deg/s]*	*[deg/s]*	*[deg/s]*
X axis	*1,9*	*-1,6*	*0,401346*	*0,569683*
Y axis	*0,9*	*-1,9*	*-0,62611*	*0,472373*
Z axis	*9,5*	*-9*	*-0,3975*	*3,103408*

Tab. 4. Data from 3-axial gyroscope in iNEMO inertial module

III. CONCLUSIONS

As expected, the low values found for both vertical and angular oscillations confirm compliance with the "fixed point" condition required. In particular, the average value of vertical oscillations along the Z-axis direction equals to -9.73 m/s^2, meaning that the scale buoy is invariant respect to the vertical wave motion. Moreover, the average values of both angular oscillations around the X-axis and Y-axis are equal to 0.40 deg/s and -0.63 deg/s respectively, as a confirmation of maintaining horizontal position with respect the free surface of the water.

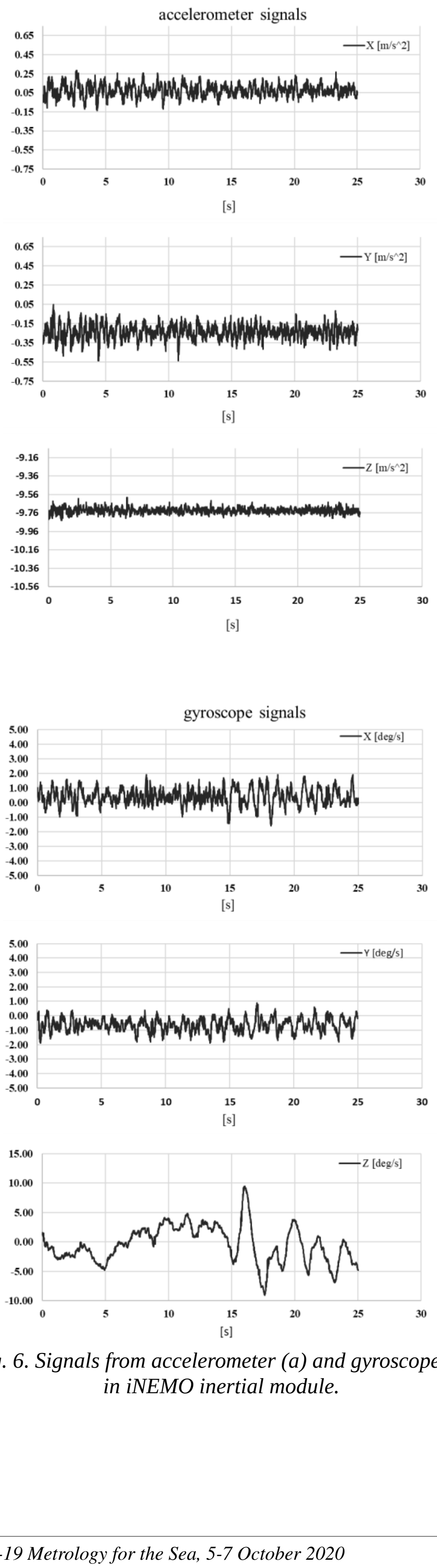

Fig. 6. Signals from accelerometer (a) and gyroscope (b) in iNEMO inertial module.

REFERENCES

[1] C. Albaladejo, F. Soto, R. Torres, P. Sánchez, J.A. López, A Low-Cost Sensor Buoy System for Monitoring Shallow Marine Environments, Sensors 2012, 12, 9613-9634; doi:10.3390/s120709613.

[2] G.F. Schirinzi, M. Llorca, R. Serò, E. Moyano, D. Barcelò, E. Abad, M. Farrè, Trace analysis of polystyrene microplastics in natural water, Chemosphere 2019, 236, doi.org/10.1016/j.chemosphere.2019.07.052.

[3] S. Savoca, G. Capillo, M. Mancuso, C. Faggio, G. Panarello, R. Crupi, M. Bonsignore, L. D'Urso, G. Compagnini, F. Neri, E. Fazio, T. Romeo, T. Bottari, N. Spanò, Detection of artificial cellulose microfibers in Boops boops from the northern coasts of Sicily (Central Mediterranean), Science of the Total Enviroment 2019, Vol. 691, 455-465.

[4] X. Roset, E. Trullos, C. Artero-Delgado, J. Prat, J. Del Rio, I. Massana, M. Carbonell, G. Barco de la Torre, D. Mihai Toma, Real-Time Seismic Data from the Bottom Sea, Sensors 2018, 18, doi: 10.3390/s18041132.

[5] Dong Yeong Kima, Hyun Soo Kima, Dae Sol Konga, Moonkang Choib, Hak Bum Kima, Jae-Hyoung Leec, Gonzalo Murillod, Minbaek Leeb, Sang Sub Kimc, Jong Hoon Junga, Floating buoy-based triboelectric nanogenerator for an effective vibrational energy harvesting from irregular and random water waves in wild sea, Nano Energy 45 (2018) 247-254, http://dx.doi.org/10.1016/j.nanoen.2017.12.052.

[6] C.A Balfour, M.J. Howarth, M.J. Smithson, D.S. Jones, J. Pugh, The Use of Ships of Opportunity for Irish Sea Based Oceanographic Measurements, In Proceedings of the IEEE Conference OCEANS, Vancouver, BC, Canada, 29 September–4 October 2007, 1–6.

[7] Z. Chenbing, W. Xinpeng, L. Xiyao, Z. Suoping, W. Haitao, A small buoy for flux measurement in air-sea boundary layer, In Proceedings of the ICEMI 2017, doi: 10.1109/ICEMI.2017.8265999.

[8] U.M. Cella, N. Shuley, R. Johnstone, Wireless Sensor Networks in Coastal Marine Environments: A Study Case Outcome, In Proceedings of V International Workshop on UnderWater Networks 2019, 1-8.

[9] L. Emery, R. Smith, D. McNeal, B. Hughes, W. Swick, J. MacMahan, Autonomous Collection of River Parameters Using Drifting Buoys, In Proceedings of the IEEE Conference OCEANS, Seattle, WA, USA, 20–23 September 2010, 1–7.

[10] A. Kwok, S. Martinez, Deployment of Drifters in a Piecewise-constant Flow Environment, In Proceedings of the 49th IEEE Conference on Decision and Control (CDC), Atlanta, GA, USA, 15–17 September 2010, 6584–6589.

[11] J.K. Choi, T. Shiraishi, T. Tanaka, H. Kondo, Safe

operation of an autonomous underwater towed vehicle: Towed force monitoring and control, Autom. Constr. 2011, 20, 1012–1019.

[12] I. Masmitja, G. Masmitja, J. Gonzalez, S. Shariat-Panahi, S. Gomariz, Development of a control system for an Autonomous Underwater Vehicle, In Proceedings of the 2010 IEEE/OES Autonomous Underwater Vehicles (AUV), Monterey, CA, USA, 1–3 September 2010, doi: 10.1109/AUV.2010.5779647.

[13] D.B. Duraibabu, S. Poeggel, E. Omerdic, R. Capocci, E. Lewis, T. Newe, G. Leen, D. Toal, G. Dooly, An Optical Fibre Depth (Pressure) Sensor for Remote Operated Vehicles in Underwater Applications, Sensors 2017, 17(2), 406, doi: 10.3390/s17020406.

[14] I.F. Akyildiz, D. Pompili, T. Melodia, Underwater acoustic sensor networks: Research challenges, Ad Hoc Networks 2005, 3, 257–279, doi: 10.1016/j.adhoc.2005.01.004.

[15] S. Calmant, F. Seyler, J.F. Cretaux, Monitoring Continental Surface Waters by Satellite Altimetry, Surveys in Geophysics 2009, 4-5, 247-269.

[16] D. Prandle Operational oceanography—A view ahead, Coast. Eng. 2000, 41, 353–359.

[17] M.E. McCormick, Ocean Engineering Mechanics: With Applications, Cambridge University 2010

[18] G. Diana, F. Cheli, Dinamica dei sistemi meccanici, Polipress 2010, vol. 1, 146-157.

2020 IMEKO TC-19 International Workshop on
Metrology for the Sea
Naples, Italy, October 5-7, 2020

Critical marine environment observation: measurement problems, technological solutions and procedural methods

Ferretti R.[1,3], Bibuli M.[1], Bruzzone G.[1], Caccia M.[1], Odetti A.[1], Cimenti E.[2], Demarte M.[2], Marro M.[2], Nardini R.[2], Ivaldi R.[2], Saroni A[3]., Coltorti M.[3]

[1] CNR – INstitute of Marine engineering, via de Marini 6, 16149, Genoa, IT
[2] Italian Hydrographic Institute, Passo dell'Osservatorio 4, 16134 Genoa, IT
[3] Department of Physics and Earth Sciences, UniFe, Via Saragat 1, 44122, Ferrara, IT

***Abstract* – This paper focus on the observation of critical marine environments, pointing out the difficulties that these kinds of dynamic, sensitive and fragile environments creates for monitoring operations. The technological solutions adopted, through the use of robotic vehicles, and the operating procedures implemented are also described. The data acquired in two particular critical environments, the front of tidewater glaciers in Svalbard and an area in the northern Tyrrhenian Sea affected by submarine gas emissions allow us to identify and characterise phenomena strongly localised and requiring very high resolutions, both in space and time. This result can be useful to obtain environmental indicators that can be used as hazard precursors and, eventually, to implement alarm procedures.**

I. INTRODUCTION

This paper focus on the development of methodologies and procedures to carry out observing operations of critical marine environments through the use of autonomous robotic platforms for the acquisition of biogeochemical parameters and for the seabed characterization.

The use of autonomous vehicles is spreading in a wide variety of marine geoscience studies, originally focused on seafloor mapping but more recently expanding into water column physical, biogeochemical and dynamic measurements, favored by the increase of the quality and accuracy of the data collected thanks to the ability of autonomous vehicles to execute fully autonomous and very precise motion over a predefined area of interest [1], [2].

The particularity of the work consists in adapting the observing methodologies, based on robotic platforms, according to the marine environment being studied in order to obtain results that are reliable, reproducible and comparable with those obtained through the classic monitoring methodologies. The environments in which the tests were executed are particularly dynamic, sensitive and fragile areas where it is necessary to study and apply particular methodologies to observe phenomena strongly localised in space and requiring very high resolutions, in time. Moreover, the critical conditions may present some risks not only for the data acquisition but also for the instrumentation and the operators.

Polar marine areas and marine areas characterised by seabed degassing activities are examples of these environments where it is difficult to acquire data using traditional methods and it is advantageous to apply monitoring methods using robotic platforms.

II. OBJECTIVES

These marine environments can be considered critical from different points of view:

- because they are difficult or impossible to reach (such as the area in front of the glacier front);
- because the instrumentation must operate in extreme conditions (very low temperatures at the pole, very high in the case of submarine emissions of volcanic origin);
- because the event to be observed is not repeatable and not completely predictable.

For all these reasons, it is necessary to implement observation solutions that are adapted to the particular operating environment in order to acquire data that can be interpreted both instantaneously, possibly for alert purposes in the event of a hazard, and inserted in a more general context of time series, to derive long-term trends. Two case studies are described below, in which there are different critical issues and for which different technological solutions and procedural methods were implemented.

A. Observation of tidewater glacier fronts in Svalbard

The first study case concerns different campaigns carried out in the Svalbard Archipelago by the Institute of Marine engineering (CNR-INM). The goal of the campaigns was to perform repetitive sampling of water in the surface and to characterise the bio-chemical-physical parameters of the water and air column close to the front of tidewater glaciers in the Kongsfjorden. From these data acquisition campaigns, valuable scientific data were obtained, as well as important operative indications on the procedures to be followed to observe this critical environment [3].

B. Observation of seabed gas emissions in the northern Tyrrhenian Sea

The second study case concerns the campaign for the identification, localisation and characterisation of gas emission (mainly methane) from the seabed in the area surrounding the Scoglio d'Affrica, Tuscan archipelago, in the northern Tyrrhenian Sea. The scientific campaign was carried out by Italian Navy Hydrographic Office (IIM), the National Institute of Geophysics and Volcanology (INGV), the Institute of Marine Engineering (INM) Genoa of the CNR, University of Ferrara (UniFe) and University La Sapienza (Roma1) [4]. The survey has highlighted the presence on the bottom of numerous emission points, sometimes intermittent, located on different depths. The purpose of the investigation by ROV was the collection of video images of the gaseous emissions from the seabed to be integrated with the acoustic morphological survey done with a multibeam sonar.

III. METHODS

The environmental constraints and the specific outputs to be obtained in term of temporal and spatial resolutions, are the leading factors towards the definition of technological tools and monitoring procedure. Hence, autonomous operations in hardly accessible areas, such as Polar Regions or gaseous emissive seabeds, require specific designs and ad-hoc studied solutions.

To perform the measurements in the Svalbard campaigns, the unmanned vehicle named PROTEUS (Portable RObotic TEchnology for Unmanned Surveys) was developed and used as USSV (Unmanned Semi-Submersible Vehicle) with remote control. As the purpose of the Svalbard campaigns was to capture bio-chemical- physical parameter variations with respect to the distance of tidewater glacier front, PROTEUS was equipped with different sensons (CTD, turbidimeter, fluorimeter, etc...) and all the data collected were integrated in real-time with PROTEUS telemetry (for having all data synchronised and geolocalised). The acquisitions were performed in the stretch of sea facing different glaciers of the Kongsfjorden (i.e. Blomstrandbreen, Kongsbreen, Kronebreen, and Conwaybreen), with the robot moving away from the glacier along paths almost perpendicular to the glacier fronts.

For the Scoglio d'Affrica campaign, the ROV e-URoPe (e-Underwater Robotic Pet) has been embarked on the Magnaghi ship of the IIM, and was used to investigate shallow water areas, which couldn't be reached by the ship itself. e-URoPe instrumentation included sensors needed for underwater vehicle navigation (attitude and orientation, velocimeter, heading, CTD, altimeter) and also three analog cameras, mounted to frame the environment from different points of view, and an Ethernet camera, mounted vertically under the vehicle.

Data acquisition was divided in classic hydro-oceanographic mapping of the whole area of interest using the high resolution multibeam mounted on the Magnaghi ship and video inspections of a sub-set of the area with the e-URoPe ROV. The use of the ROV allowed the observation of the underwater sites of gaseous emissions and demonstrated the possibility of carrying out long-lasting missions, considerably longer than those performed by divers.

IV. DATA ANALYSIS

In the following subsections examples of the data collected during the campaigns at Svalbard and Scoglio d'Affrica are shown.

A. Water mass stratification near the Kongsbreen glacier

The execution of the measures following "data-driven" procedures allowed to collect useful data for the characterization of the environment from physical, chemical, biological point of view, coping with the hostile working conditions typical of the areas close to the fronts of tidewater glaciers.

Data were collected not only on the surface but also along the water column, in order to detect effects due both to currents and to the introduction of substances by the water coming from the glacial ice melting.

The graph in Fig. 1 characterises the area near the front of the Kongsbreen glacier (Kongsfjorden) from a physical point of view: Temperature (°C) and Salinity (PSU) are plotted as a function of the distance from the glacier front (m). The presence of a water mass characterised by lower values of temperature and salinity at about 200-300 meters from the front of the glacier is evident (green/light blue dots). This can be an indicator of the presence of a plume of meltwater coming from the glacier which has physical characteristics different from the surrounding water mass and which, thanks to the lower density, is going up the water column towards the surface to then disperse and mix with the water of the fjord. This is an example of temperature and salinity gradients used as indicators of water mass stratification produced by glacier melting.

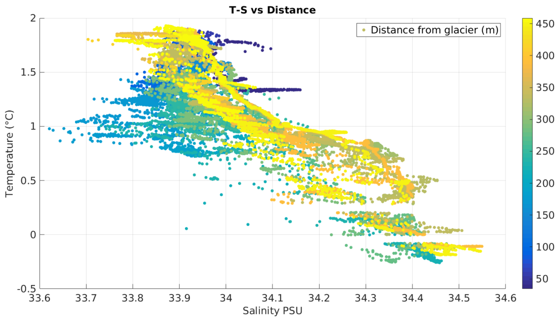

Fig. 1. T-S diagram: temperature (°C, y-axis) is plotted versus salinity (PSU, x-axis). The color scale is proportional to distance from the glacier front (m): yellow = far; blue = near.

B. Mapping of seabed gas emission points near the Scoglio d'Affrica

The data collected using the e-URoPe ROV were acquired in a sub-area of the area investigated by the Magnaghi ship (IIM), for which high-resolution multibeam acoustic data are available. The ROV collected video images of the gaseous emissions from the seabed (methane gas) that were integrated with the acoustic morphological survey (multibeam).

During the operations, e-URoPe was used with the surface console installed on the Magnaghi ship and, due to the configuration of the ship, it was not possible to mount the system for underwater acoustic positioning and therefore a localization of the ROV with respect to the ship was not available during the underwater phases. However, during the post-processing of the data, using the available GPS data, together with the set-up and speed data of the ROV, we reconstruct the possible routes followed by the vehicle during the diving phases and then calculate its position. The correctness of the results obtained was verified using the multibeam acoustic data of the seabed and in particular the morphological reconstruction. In this way, the video acquired were georeferenced and a preliminary map of gas emission points was created, as shown in Fig.2.

Moreover, from the video images, it was obseved that the degassing activity is weak with small bubble columns that are emitted intermittently; the emissions are punctual and come out of small chimney of centimetric dimensions; the type of emission depends on both the porosity of the bottom and the amount of gas in the substrate.

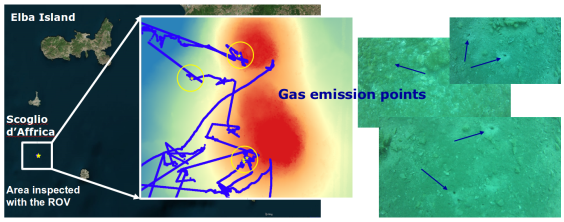

Fig. 2. Preliminary map of gas emission points obtained from the georeferenced video acquired by e-URoPe.

V. DISCUSSION

The complex environmental situations described above are typical examples in which measurements must be made systematically and with high spatial and temporal resolutions otherwise there is a risk of missing to record the event (the plume of freshwater from the glacier or the emission of gas from the seabed) before it ends due to the effect of mixing with the water of the environment. To be able to operate in these conditions and with procedures that ensure the safety of the operators on the one hand and the integrity of the data collected on the other, the use of robotic platforms is necessary. The preliminary results described above are very important because show that, even in situations far from the "ideal operating conditions", it is still possible to obtain indicators that can be interpreted as hazard precursors and, eventually, implement alarm procedures.

REFERENCES

[1] Bellingham, James G., and Kanna Rajan. "Robotics in remote and hostile environments." *Science* 318.5853 (2007): 1098-1102.

[2] Nilssen, Ingunn, et al. "Integrated environmental mapping and monitoring, a methodological approach to optimise knowledge gathering and sampling strategy." *Marine pollution bulletin* 96.1-2 (2015): 374-383.

[3] Bruzzone, G., Odetti, A., Caccia, M., & Ferretti, R. (2020). "Monitoring of Sea-Ice-Atmosphere Interfacein the Proximity of Arctic Tidewater Glaciers: The Contribution of Marine Robotics." *Remote Sensing*, *12*(11), 1707.

[4] Sciarra et al., "A shallow mud volcano in the sedimentary basin off the Island of Elba", EGU *General Assembly Conference Abstracts*, EGU2020, https://doi.org/10.5194/egusphere-egu2020-1336

2020 IMEKO TC-19 International Workshop on
Metrology for the Sea
Naples, Italy, October 5-7, 2020

Reliability and Availability Evaluation of an Autonomous Remote Video Monitoring System for Offshore Sea Farms

David Baldo, Ada Fort, Marco Mugnaini, Giacomo Peruzzi, Alessandro Pozzebon, Valerio Vignoli

Department of Information Engineering and Mathematics,
University of Siena, Via Roma 56, 53100 Siena, Italy
baldo@unisi.it, ada@diism.unisi.it, mugnaini@dii.unisi.it,
peruzzi@diism.unisi.it, alessandro.pozzebon@unisi.it, vignoli@diism.unisi.it

***Abstract* – In this paper, the availability and reliability of a remote video monitoring system for offshore sea farming plants are studied. The scope of the system is to ensure a video surveillance infrastructure so to supervise breeding cages along with the fish inside them in order to contrast undesired phenomena like fish poaching as well as cages damages. The system is supposed to be installed on a cage floating structure. It is mainly composed of an IP camera which is controlled by a Raspberry Pi Zero which is the core of the system. Images are streamed thanks to a 3G/4G dongle while the overall system is powered via two photovoltaic panels charging a backup battery. Simulations are carried out considering two seasonal functioning periods (i.e., winter and summer): each of them is characterized by temperature trends defined according to the average temperatures of the system deployment site, 8 km offshore the city of Piombino, Italy. In order to optimize power consumption without hindering application scenario requirements, the system operates according to a duty cycle of 2 minutes out of 15 (i.e., 8 minutes of operation per hour).**

I. INTRODUCTION

Fish farming has undergone a massive growth for years now, mainly owing to various causes. Primarily, bred seafood could take part within the fight against world hunger without entailing an increase in costs thus proving to be a cheap and valuable alternative for global food supply. Furthermore, bred seafood quality may be easily certified since the complete fish lifetime can be promptly traced throughout the breeding cycle. The upcoming affluence of this sector is also validated by some studies: a prediction on worldwide fishing market in 2030 [1] foresees that 62% of fish for human consumption will be produced via aquaculture by that year. In addition, the Food and Agriculture Organization (FAO) foretold a hopeful situation presuming an aquaculture production expansion up to 58% by 2022 [2]. Concerning Europe, a future discord among fish demand and supply was guessed [3], therefore fostering fish farming may turn to be an advisable initiative. Finally, in Italy aquaculture includes more than 800 companies and the majority of them are situated in the Mediterranean Sea where more than 5000 plants are located.

Offshore sea farms definitely need to rely on surveillance systems so to contrast undesired phenomena like fish poaching as well as breeding cages damages. Therefore, in this paper an autonomous remote video monitoring system for offshore sea farms is presented along with simulations whose outcomes are exploited to study its availability and reliability so to assess its overall effectiveness. The system is designed so to include off-the-shelf components and in order to be energy efficient since it is powered via an energy harvesting system (i.e., two photovoltaic panels and a backup battery). Eventually, the system is supposed to be installed on a cage floating structure.

The rest of this paper is drawn up as follows. Some related works are reported in Section ii. while Section iii. shows the video monitoring system architecture. The reliability configurations on which simulations are carried out are outlined in Section iv. and simulations results are presented in Section v.. Eventually, Section vi. points out remarks and conclusions.

II. RELATED WORKS

Autonomous systems for the monitoring of fish behavior within offshore sea farms during feeding phases was reviewed in [4]: amid sundry enabling technologies and processing techniques, the use of video recordings thorough ad-hoc systems and cameras were pointed out thus showing their feasibility.

Video monitoring systems which are deployed in marine contexts are mainly designed for coastal safeguard so to assess erosion [5, 6, 7] rather than for sea farms surveillance. Such systems make use either of standard IP cameras [5, 6], like the one within the system presented in this paper, or of embedded cameras directly controlled by a single-board computer as Raspberry Pi [7], which is the control unit the system that will be presented in the following Section. However, the literature also comprehends works implementing video monitoring systems which are installed on offshore buoys within breeding plants: in [8], cameras are set up within the fish cages while video streaming is ensured by a radio frequency system which is installed on board of the buoy. Similarly, works reported in [9, 10] extend such a surveillance system. On the other hand, marine video monitoring systems are additionally devised in order to operate underwater so to fulfill submarine investigation and exploration purposes [11] as well as for proper aquaculture ponds characterized by turbid water [12].

Concerning video monitoring systems in a broad sense (i.e., which are employed in diverse contexts with respect to the marine one) that rely on photovoltaic energy harvesting systems and a backup battery, works within [13, 14] confirm the suitability of such a technique thus underlining the potential effectiveness of the solution proposed in this paper.

III. SYSTEM ARCHITECTURE

The block diagram of the video monitoring system is depicted in Fig. 1 and it is composed by 3 main building blocks (i.e., power supply, control and communications and camera).

The power supply block contains 2 photovoltaic panels providing 20 W each, whose task is either to power up the whole system and to recharge a 12 V 25 Ah lead-acid backup battery through a solar charge controller.

The control and communications block is the core of the system since it manages the duty cycling of the camera along with images capturing and transmitting towards a remote server, while minimizing power consumption by the activation of the inner elements only for the minimum amount of time needed. Such a working flow is obtained by the following off-the-shelf components:

- DC-DC converter filters out the power supply coming from the appropriate building block so to correctly power each of the system elements;
- Raspberry Pi Zero is the control unit of the system due to Python scripts managing both the camera and the duty cycling of all of the other components;
- Raspberry Pi relays board contains relay switches that are directly controlled by the Raspberry Pi so to turn on and off the camera and the other system elements whenever they are needed and only for the strictly necessary time in order to limit the overall power consumption;
- 3G/4G dongle provides Internet connectivity which is exploited to send the captured images, along with debug logs so to perform diagnostic, to a remote server;
- Reset switch performs a daily hardware reset of the whole system acting as a sort of long term watchdog timer so to overcome software issues or unexpected behaviours.

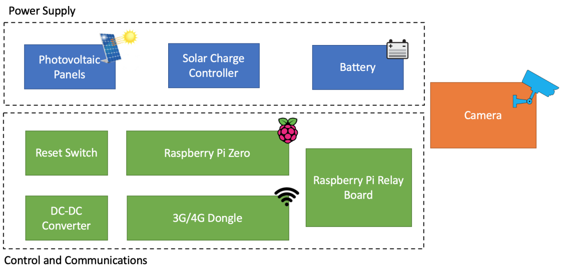

Fig. 1. Video monitoring system block scheme.

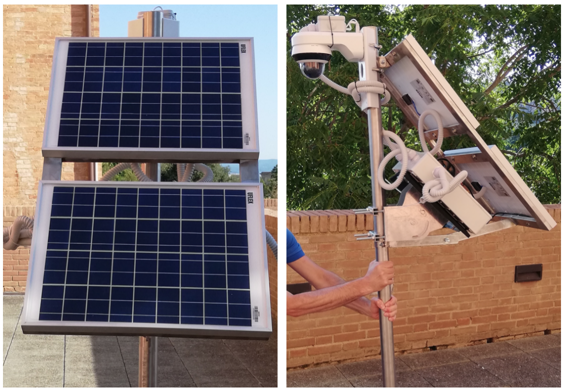

Fig. 2. Realization of the video monitoring system: photovoltaic panels (left) and pole with camera and IP56 box containing the electronics (right).

The camera is an off-the-shelf outdoor IP camera produced by Hikvision, which is especially designed so to resist to marine environments.

All of the elements composing the control and communications block are housed within an IP56 box, while the complete system is mounted on a support pole (see Fig. 2) which will be offshore installed on a breeding cage floating structure.

IV. RELIABILITY CONFIGURATIONS

The application scenario for this video monitoring system does not necessitate of real-time image streaming. In particular, only snapshots on a regular basis (i.e., one every 15 minutes) are required. Therefore, in order to meet functioning requirements the system operates for a time span of 2 minutes every quarter of an hour within which the picture is taken and remotely sent via the Internet. In so doing, only 8 minutes per hour of system activity is experienced (i.e., 172 minutes per day) thus also optimizing power consumption.

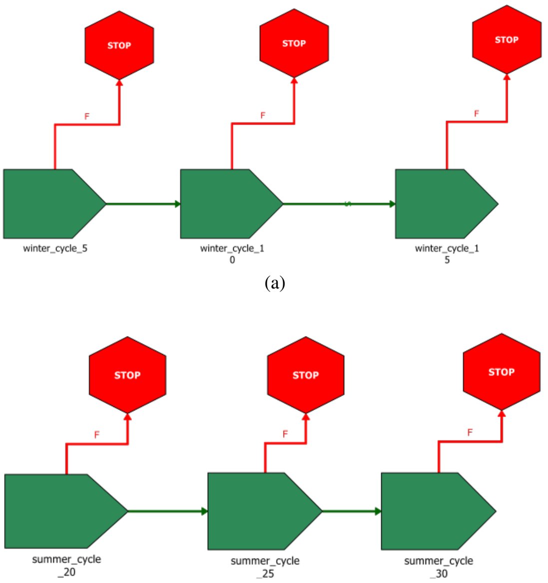

(b)

Fig. 3. Availability and reliability simulation schemes: (a) winter working period and (b) summer working period.

For what concerns weather conditions the system is exposed, two seasonal functioning periods are identified on which availability and reliability simulations are carried out:

- **Winter**, that is made up of 3 8-hours time slots, that are daily repeated, which are in turn characterized by a temperature of $5°C$, $10°C$ and $15°C$;
- **Summer**, which accounts for 3 8-hours time slots, which are daily repeated, that are respectively characterized by a temperature of $20°C$, $25°C$ and $30°C$.

Such temperatures are taken into account because of the future system deployment scenario: $8\,km$ offshore the city of Piombino, Italy.

Availability and reliability simulation schemes are shown in Fig. 3, while simulation parameters are summarized in Fig. 4. MIL HDBK 217F database was selected to evaluate individual component failure rates at different temperatures considering an environment of the kind NU (Naval Unsheltered). Unfortunately, such parameters are usually not available from component producers, therefore a conservative approach given by the mentioned database results in worst condition results was followed.

V. SIMULATIONS RESULTS

As shown in Fig. 5, simulations were performed by means of the BlockSim software (by Reliasoft) on the two scenarios previously described. Fig. 5a reports results connected to the system point availability while Fig. 5b shows the ones related to point reliability. Both prove that the summer period presents a decrease in the final time values with respect to the winter one. Such results are in agreement with what expected by the theory connected to the exploitation of the MIL HDBK 217F database where temperature based degradation, under a fixed environment, takes place. To simulate availability model a fixed $48\,h$ repair time was considered. Of course, due to the very small amount of electronic components and to the low system complexity, the system has to be tested especially for winter time on long periods since the overall MTBF is considerably high at those temperatures. Moreover, either the selected duty cycle for system exploitation and the power consumption reduction limit the internal temperature raise and keep it constant for the system to the environmental one without significant degradation rates apparently induced on individual electronics.

VI. CONCLUSIONS

The aim of this paper was to describe the architecture of an autonomous video monitoring system to be employed for the remote control of offshore breeding cages in aquaculture plants. The proposed solution is characterized by energy self-sufficiency thanks to an energy harvesting system based on the use of photovolatic panel. In order to demonstrate the usability of the system, simulations were carried out in order to validate its reliability and availability. Results prove that the system can be successfully employed in the proposed application scenario for both winter and summer environmental settings.

REFERENCES

[1] M.Kobayashi, S.Msangi, M.Batka, S.Vannuccini, M.M.Dey, J.L.Anderson, “Fish to 2030: the role and opportunity for aquaculture”, Aquac. Econ. Manag., vol.19, No.3, August 2015, pp.282-300.

[2] A.Fredheim, T.Reve, “Future Prospects of Marine Aquaculture”, Proc. of OCEANS 2018 MTS/IEEE Charleston, 2018, pp. 1-8.

[3] L.Angulo Aranda, P.Salamon, M,Banse, M.Van Leeuwen, “Future of Aquaculture in Europe: Prospects under current conditions”, Proc. of XV EAAE Congress, “Towards Sustainable Agri-food Systems: Balancing Between Markets and Society”, 2017.

[4] D.Li, Z.Wang, S.Wu, Z.Miao, L.Du, Y.Duan, “Automatic recognition methods of fish feeding behavior in aquaculture: A review”, Aquaculture, Vol.528, No.15, November 2020.

[5] R.Taborda, A.Silva, “COSMOS: A lightweight coastal video monitoring system”, Comput. and Geosci., Vol.49, December 2012, pp.248-255.

Elements	Characteristics	Model	Temperature [°C] 5	10	15	20	25	30
			MTBF [h]					
Solar Charge Controller	$12 \div 24\,V$ $20\,A$	CMDT-A2420	94000	93000	92000	91000	85000	81000
Reset Switch	$12\,V$	JK11S V1.1	1067577.68	1067577.68	1067577.7	1067577.7	1067577.7	1067577.68
Battery	$12\,V$ $25\,Ah$	Victron Energy AGM12-25	61674757.2	61674757.2	61674757	15059188	11934038	9530309.94
DC-DC Converter	$5 \div 12\,V$	-	6544336.31	5790737.61	5145730.2	4591034.5	4111841.8	3696087.57
Raspberry Pi	-	Zero	9609216.3	9607060.01	9604400.9	9601147.8	9597196.8	9592432.5
3G/4G Dongle	-	Huawei E3372	79365.08	79365.08	79365.08	79365.08	79365.08	79365.08
Raspberry Pi Relay Board	-	-	266894.42	266894.42	266894.42	266894.42	266894.42	266894.42
		Total MTBF [h]	**79336147**	**78579392**	**77930725**	**30756208**	**27141913**	**24313667.2**

Fig. 4. Simulation parameters.

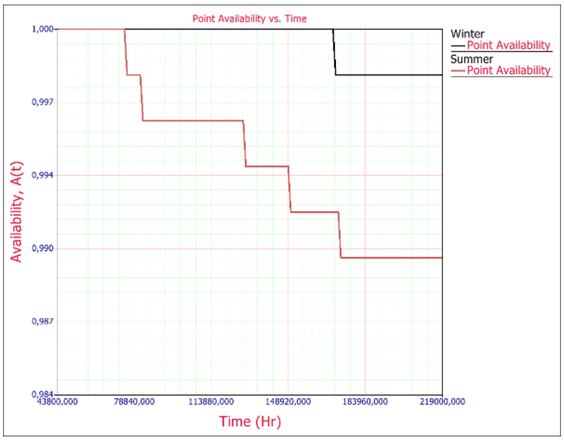

(a)

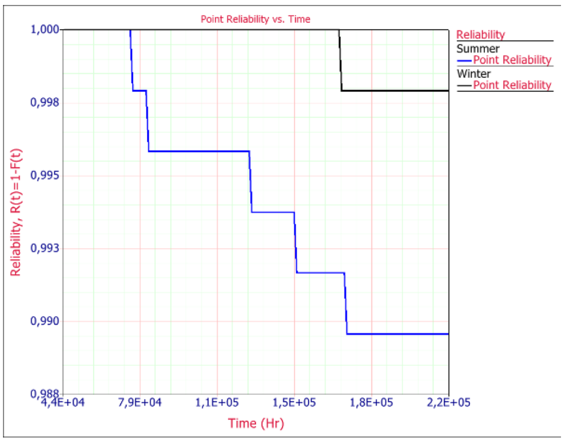

(b)

Fig. 5. Availability and reliability simulation results: (a) availability and (b) reliability during summer and winter working periods.

[6] N.Valentini, A.Saponieri, L.Damiani, “A new video monitoring system in support of Coastal Zone Management at Apulia Region, Italy”, Ocean Coast. Manage., Vol.142, June 2017, pp.122-135.

[7] R.Archetti, M.G.Gaeta, F.Addona, L.Cantelli, C.Romagnoli, F.Sistilli, G.Stanghellini, “COASTAL VULNERABILITY ASSESSMENT THROUGH LOW-COST VIDEO MONITORING: THE CASE OF RICCIONE”, Proc. of SCACR2019 - International Short Course/Conference on Applied Coastal Research, 2019.

[8] B.Fullerton, M.R.Swift, S.Boduch, O.Eroshkin, G.Rice, “Design and analysis of an automated feedbuoy for submerged cages”, Aquacult. Eng., Vol.32, No.1, pp.95-111.

[9] S.J.Boduch, J.D.Irish, “Aquaculture Feed Buoy Control-Part 1: System Controller”, Proc. of OCEANS 2006, 2006.

[10] J.D.Irish, S.J.Boduch, “Aquaculture feed buoy control-Part 2: Telemetry, data handling and shore-based control”, Proc. of OCEANS 2006, 2006.

[11] H.Wang, W.Cai, J.Yang, Q.Chen, “Design of HD video surveillance system for deep-sea biological exploration”, Proc. of 2015 IEEE 16th International Conference on Communication Technology (ICCT), 2015, pp.908-911.

[12] C.C.Hung, S.C.Tsao, K.H.Huang, J.P.Jang, H.K.Chang, F.C.Dobbs, “A highly sensitive underwater video system for use in turbid aquaculture ponds”, Sci. Rep., Vol.6, No1., pp.1-7.

[13] L.Qi-An, L.Peng, F.Gui-zeng, L.Ping, L.Chang-lin, Z.Jun-xiao, “The solar-powered module design of wireless video monitoring system”, Energy Procedia, Vol.17, pp.1416-1424.

[14] K.Abas, K.Obraczka, L.Miller, L., “Solar-powered, wireless smart camera network: An IoT solution for outdoor video monitoring”, Comput. Commun., Vol.118, pp.217-233.

2

Special Session
Underwater Measurement for 3D Characterization of Subsea Objects

Today, underwater scanning techniques are commonly applied in several areas, introducing new ways for monitoring, cataloging and studying submerged objects. Moreover, the use of these technologies allows the marine biology to analize and document morphometric changes due to natural life, pollution of water and to climate change. In this framework, the devices steadily evolving are designed to provide 3D accurate models of targets of interest in subsea environment. In fact, the obtained 3D reliefs aim to perform accurate measurements of volume, chromatic characteristics, surface area and other shape measurements of three-dimensional objects, without the necessity to remove them from the sea.

2020 IMEKO TC-19 International Workshop on
Metrology for the Sea
Naples, Italy, October 5-7, 2020

Uncalibrated Multibeam Echosounder capabilities for fish schools measuring and tracking. An application in the nearby of an Adriatic offshore structure

Annalisa Minelli[1], Anna Nora Tassetti[1], Gianna Fabi[1]

[1] *CNR-IRBIM, Largo Fiera della Pesca 2, 60125 Ancona (Italy), annalisa.minelli@irbim.cnr.it*, annanora.tassetti@cnr.it, gianna.fabi@cnr.it*

***Abstract* – This work aims to investigate the potential capabilities of an uncalibrated Multibeam Echosounder (MBES) in fish school detection, reporting an experience regarding an offshore gas platform in the Adriatic Sea. If, on one hand, the Split-beam Echosounder technology is traditionally used for the purpose of biomass evaluation, on the other hand, recent improvements in Multibeam Echosounder (MBES) technologies and advancing in water column data processing have made possible to detect schools and obtain some relevant metric information, with the advantage that a wide surrounding environment could be quickly surveyed. The possible results that can be obtained with this technology, strength points and weaknesses are presented in this paper. A reflection on other possible usages is given, and a replicable raw-data processing method for schools detection and their metric characterization is presented as well.**

I. INTRODUCTION

The MBES has been historically used with hydrographic purposes, such as submerged obstacle detection, bathymetry and seabed characterization (e. g. [1], [2], [3], [4]). Recently, technological advancements in MBES components and data elaboration have made possible to improve the use of MBES for biological target detection and tracking, and the extraction of some relevant metrics from the collected water column (cfr. [5], [6]). This upgrade allowed eco-biologists to start considering MBES as an attractive technology to be used in new oceanographic studies, to investigate fish behavior and provide additional valuable ecological information (e. g. [7], [8]).

Nevertheless, MBES calibration is a crucial point for the improvement of data quality [9], especially in fish school characterization, where the reference technology has been for long time, and currently it still is, split-beam Echosounder (e. g. [10], [11]).

Since these instruments are often expensive, it is reasonable to recycle such technologies to fully exploit them, taking into account their limitations and potentials. In this context, this research aims to repurpose a hydrographic MBES to investigate an offshore platform and its habitat, quantifying and characterizing at best fish school assemblages and considering expected species in such an environment. Capabilities and limitations of the uncalibrated MBES in fish schools' characterization and measuring are addressed, as well as issues tied to the structure itself (e.g. sound wave reflection and refraction on platforms' poles) and the planning of the survey (i.e. overestimation of the fish presence by detecting the same school more than one time).

Moreover, a replicable MBES survey and data processing is described, and assumptions on targets' classification are made considering expected species in such an environment.

Finally, ongoing research are shortly discussed as well as possibilities of MBES calibration and targets' classification by integrating ground truth information.

II. THE STUDY ZONE

The investigated structure is a three leg gas platform and one of the 130 structures (gas platforms, pipelines and wellheads) constructed in the Adriatic Sea since 1960s. The structure relies in the central Adriatic zone at a distance of 45 km from the coastline far away from Ancona (Marche region, Figure 1), at 76 m depth. It is currently unmanned and the composition of the seabed is mostly muddy. Some of these platforms, just like the one studied here, are subjected to a regular monitoring program with surveys planned and pursued by the CNR-IRBIM from the late 1990s, at monthly rate. The objective of these monitoring plans are multiple, one of all is, for example, the study of the ecological role of these structures on the fish assemblage (cfr. [12], [13]). In this paper, we did not considered a multiannual dataset from the selected platform, since the aim of this work was to explore the capabilities of the MBES analysis. Therefore, only one survey from the 30th of July 2019 was taken as example.

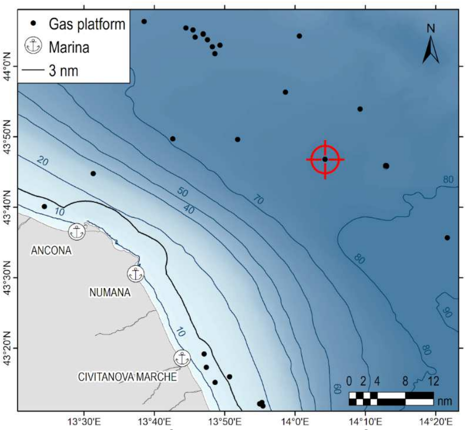

Fig. 1. Position of the investigated platform in the central Adriatic Sea.

III. MATERIALS AND METHODS

Data described here were recorded using a Multibeam Echosounder Simrad Kongsberg EM2040CD. Subsequently, schools were individuated, purged from noise, extracted and measured using Echoview software (Echoview Software Pty Ltd, Hobart, Australia).

For this survey a frequency value of 300 kHz was used, data were recorded on 10 parallel lines (in N-S direction), and Multibeam heads were opened of 80° and 10° outward and inward respectively in order to obtain an almost complete covering for each line (about 150 m width). A total squared area of side 1.5 km and centred on the platform was examined. Before starting the survey, a sound velocity vertical profile was created and integrated into the Seafloor Information System software (SIS, Kongsberg) used to monitor data in real time during their acquisition. A *medium* filter was applied directly while acquiring, since no exceptional peaks or pits were expected on the seabed.

Once data were acquired, a bathymetric map of the sounded zone was extracted and elaborated from the raw data using CARIS software (Teledyne, Canada), while Echoview was used to extract fish schools.

In Echoview Software, two paired lines at a time were examined, and the following semi-automated procedure step by step was applied:

- calculation of Maximum Intensity function for both the heads: this allows to evidence in a 2D echogram where echoes are stronger;
- visual combined examination of echograms coming from the two heads and the Maximum Intensity diagram in order to isolate ping subset where a school is supposed to be located;
- examination of the ping subsets with eventual use of specific filters to cut out noise;
- automated detection of the schools by setting thresholds on schools' dimensions: a spherical minimum target of radius 0.8 m was used;
- visualization of extracted schools on a 3D scene, pruning, basing on shapes, of eventual noise, and extraction of metric variables;
- masking of the ping subset over the identified school and export of each school as 3D point file.

After the extraction of all sounded schools, their position and metrics were visually examined to individuate possible duplicates of the same school, moving during the survey. These duplicates were selected to be inserted in a unique track. Some recent technological advancements on data elaboration allow the tracking of a moving school (called "region") by means of tracking of its mass or geometrical center. In this work the Echoview tool called "3D Region Track" was used, allowing to identify the same school while it was moving.

For each aggregation three elements were considered:

1. position with respect to the center of mass or the geometric center of the region;
2. date/time: mean between a valid start and end time for all pings detecting the 3D region;
3. volume of the 3D region;
4. intensity of the signal: mean of S_v on the 3D region.

Moreover, for the track individuation it is necessary to define: a certain confidence level on position and velocity prediction using two separate constant value parameters that range from 0 (totally unconfident) and 1 (totally confident), and a maximum distance after which the regions are no more considered to be inserted in the same track.

Once tracks were identified, extracted schools were pruned from the duplicates belonging to the same track, and only the last position (the last aggregation) individuated in the schools' group was kept.

The last step of our method implies 3D visualization of the extracted schools. Since MBES is able to capture not only specific targets but also the surrounding environment, from the same survey a 3D points' file of the platform structure was obtained. Platforms' points were imported along with the schools' points and the bathymetric surface in Fledermaus software (QPS, Netherlands) in order to visualize schools' shape, depth, and relative position respect to the platform.

IV. RESULTS AND DISCUSSION

The 30th of July 2019 we started recording data at 10:40 AM (UTC) and we completed the recognition at 12:10 AM (UTC).

After the elaboration of raw data using Echoview software, three schools were automatically individuated as a unique moving school, or track (Figure 2). Position, date-time, recorded intensity (S_v), and velocity were reported for each point composing the track. The last point of the track (Point C) corresponds to the aggregation no. 1, whose position is reported in Figure 3, and metrics in Table 1. The final total number of sounded schools is 13, and their spatial distribution is reported in Figure 3.

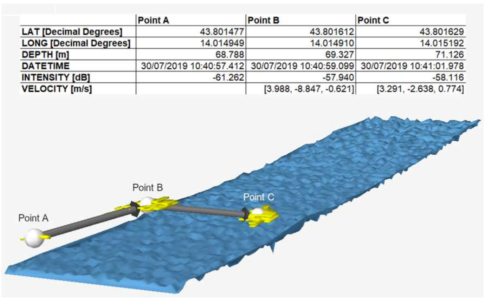

	Point A	Point B	Point C
LAT [Decimal Degrees]	43.801477	43.801612	43.801629
LONG [Decimal Degrees]	14.014949	14.014910	14.015192
DEPTH [m]	68.788	69.327	71.126
DATETIME	30/07/2019 10:40:57.412	30/07/2019 10:40:59.099	30/07/2019 10:41:01.978
INTENSITY [dB]	-61.262	-57.940	-58.116
VELOCITY [m/s]		[3.988, -8.847, -0.621]	[3.291, -2.638, 0.774]

Fig. 2. 3D track visualization in Echoview: schools are in yellow and connecting vectors (with direction) are in grey. The last position of the track is identified by the point C. The table reports the position, time, backscatter intensity, and estimated velocity of the 3 involved schools.

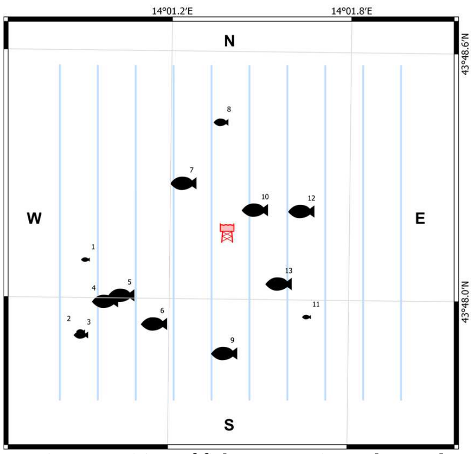

Fig. 3. Position of fish aggregations observed during the survey of the 30th of July 2019. Dimensions of markers is proportional to schools' volume.

From the 3D visualization of the schools in Fledermaus, reported in Figure 4, it is possible to perceive the shape and dimension of the sounded aggregations. Bathymetric map of the entire sounded zone and the point cloud relative to the platforms' structure are also visible.

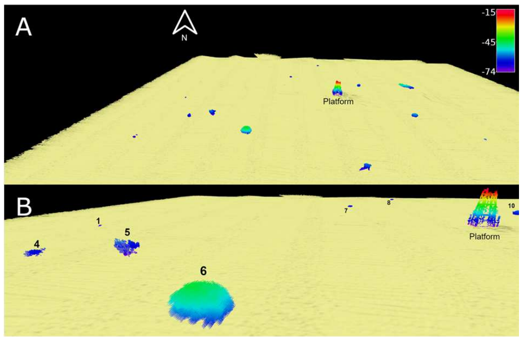

Fig. 4. Fledermaus 3D overview of extracted schools distribution around the gas platform (A), and a close up view of aggregation no. 6, located in the South-West portion of the investigated zone (B).

Detected schools had medium-big dimensions, with mean surface value of 1872.77 m^2 and a mean volume of 1501.62 m^3 (Table 1). Nearly all the schools were recorded in the first 20 m from the seabed, at a mean depth of 63.99 m, which is in line with some fish species expected to populate this geographical zone.

In particular, in the nearby of the platform, it is expected to sound pelagic species like *Trachurus trachurus* or *Boops boops*, tending to aggregate in medium-big schools with relevant height in the surrounding of the platform. It is also expected to encounter nekton-benthic species like *Trisopterus minutus capelanus* and *Pagellus spp* tending to aggregate in small size schools, located in the proximity of the seabed. All these species show a certain affinity and attraction level towards the platform environment (e. g. [14], [12]).

Several studies have attempted to quantify the attractive effect exerted by offshore platforms towards different finfish species, demonstrating as well the tendency of fish to migrate up and downward from the bottom (during the day) to the surface (during the night) of the water column (e. g. [15], [16], [17]).

Table 1. Metrics of extracted schools.

School	Surface (m^2)	Length NS (m)	Length EW (m)	Minimum Depth (m)	Maximum Depth (m)	Height (m)	Volume (m^3)	Geometrical center LAT	Geometrical center LONG	Geometrical center Depth (m)	Roughness (m^{-1})	n. of vacuoles	Tot. V of vacuoles (m^3)
1	53.50	3.46	3.74	65.30	66.93	1.63	12.12	43.796528	14.016786	66.10	4.40	0	0.00
2	408.75	5.59	10.74	45.31	51.38	6.07	158.70	43.808704	14.020122	48.28	2.29	0	0.00
3	1985.21	22.70	16.46	59.48	68.49	9.01	916.72	43.799005	14.022165	64.20	2.15	3	1.85
4	219.70	11.52	8.25	63.53	66.56	3.03	71.23	43.805000	14.026000	65.08	3.08	0	0.00
5	31.32	3.33	5.33	64.39	66.08	1.69	6.20	43.802219	14.028040	65.20	5.05	0	0.00

Table 1. Continuation.

6	584.88	11.29	13.14	59.65	68.69	9.04	330.90	43.803848	14.027231	63.94	1.77	1	0.30
7	1257.82	13.88	15.49	51.89	62.21	10.31	449.53	43.801276	14.028350	57.41	2.80	1	0.21
8	868.93	13.68	13.52	64.72	73.31	8.60	377.34	43.803109	14.025806	69.35	2.30	0	0.00
9	341.89	9.29	10.48	67.38	74.30	6.92	187.38	43.807115	14.028465	71.17	1.83	0	0.00
10	497.81	14.84	19.54	72.33	75.44	3.11	218.84	43.799789	14.029831	74.24	2.28	0	0.00
11	549.21	22.74	16.84	63.78	69.11	5.33	212.60	43.806810	14.031537	66.16	2.58	1	0.46
12	169.24	6.66	22.79	72.86	76.09	3.23	49.18	43.797269	14.031685	74.60	3.44	0	0.00
13	66.37	5.40	6.00	49.95	52.67	2.72	18.67	43.799312	14.031776	51.27	3.56	0	0.00

Being our Multibeam not calibrated, the S_v values must be intended ad S_v uncalibrated values (S_{vu}) and all the measurements strictly related to this variable (e.g. fish school density), cannot be taken in consideration. On the other hand, it is possible to evaluate the presence/absence of the aggregation in the water column, and to measure with a high degree of confidence metric parameters such as area, volume, lengths along main directions (cfr. [18], [19], [20]).

For what concerns a raw evaluation of fish schools' density, even if the S_{vu} values are not reliable, the number of vacuoles can still provide an insight of it, and it is possible to observe from Table 1 that, unless schools no. 6 and 12, there were no or few vacuoles in the sounded aggregations.

V. CONCLUSIONS AND PERSPECTIVES

In this paper we tried to understand what we can and what we cannot do with an uncalibrated MBES in the field of fish school identification and mass evaluation, fish species identification, and schools tracking.

First of all, the metrics of extracted fish schools were perfectly reasonable, since they scarcely depend on the intensity of received signal (S_v), so it is reasonable to advance hypotheses on fish aggregations presence, dimensions, and their position basing on the acquired data. For what concerns mass evaluation, at the present time, the operation is not allowed since sound intensity values are untrustworthy. Similarly, due to the MBES geometry and functioning, it is not possible to perform the single fish tracking inside an aggregation because the point targets composing the aggregations cannot be individually isolated [21]. However, tracking a school as an entire region can easily overcome the issue of considering more times the same aggregation during the survey. Moreover, the MBES itself does not allow species identification, due to the high number of parameters required, or rather, information we can achieve, also from a calibrated MBES is always limited to the shape or particular feature of the specie (e. g swim bladder). So, fish species identification could be quantified with major precision by integrated methods involving more than one technology at a time (cfr. [22],[23]).

Undoubtedly, the calibration of our instrument could be useful in order to advance in interesting tasks still under discussion in the scientific community as the ones mentioned before [9]. Calibration can be done separately for each component of the Multibeam system, knowing the exact efficiency of each component, or the sounder can be calibrated as a unique tool. A very complete review of protocols for standard-target Multibeam calibration is given in [21]. At present, we are planning the calibration of our Multibeam using a standard-target field method in comparison with data coming from a split-beam SBES.

However, the results that we have obtained from our survey are still usable to formulate hypotheses as they gave some interesting information about aggregations and fish behavior.

This information, integrated with those obtained through other sampling methods (e.g, videocameras, catch sampling) could be useful for deployment, maintenance and decommissioning operations of oil and gas platforms, or the monitoring of artificial reefs: fishes often find in these structures shelter and food, and their beneficial effect on aquatic life is evident (e. g. [24], [25], [26]). For what concerns studies on fish aggregations' concentration on natural reefs then, the application on MBES techniques could represent a completely non-invasive approach, useful to preserve natural marine resources. The same workflow and investigation could be applied to artificial reefs as well, if the purpose of the structures is the conservation and repopulation of some fish species.

REFERENCES

[1] B. M. Costa, T. A. Battista, S. J. Pittman, Comparative evaluation of airborne LiDAR and ship-based multibeam SoNAR bathymetry and intensity for mapping coral reef ecosystems. Remote Sensing of Environment, 113(5), 2009, 1082-1100.

[2] J. Best, S. Simmons, D. Parsons, K. Oberg, J. Czuba, C. Malzone, A new methodology for the quantitative visualization of coherent flow structures in alluvial channels using multibeam echo-sounding (MBES). Geophysical Research Letters, 37(6), 2010.

[3] D. M. Kim, E. M. Kim, Processing MBES data to detect changes to seafloor topography. SmartCR, 1(2), 2011, 116-124.

[4] G. Masetti, B., Calder, Remote identification of a shipwreck site from MBES backscatter. Journal of

environmental management, 111, 2012. 44-52.

[5] G. Foster, A. Gleason, B. Costa, T. Battista, T., C. Taylor, Acoustic applications, In Coral Reef Remote Sensing (pp. 221-251), 2013, Springer, Dordrecht.

[6] C. Xu, M. Wu, T. Zhou, J. Li, W. Du, W. Zhang, P. R. White, Optical Flow-Based Detection of Gas Leaks from Pipelines Using Multibeam Water Column Images. Remote Sensing, 2020, 12(1), 119.

[7] K. L. Benoit-Bird, G. L. Lawson, Ecological insights from pelagic habitats acquired using active acoustic techniques. Annual review of marine science, 8, 2016, 463-490.

[8] A. C. G. Schimel, C. J. Brown, D. Ierodiaconou, Automated Filtering of Multibeam Water-Column Data to Detect Relative Abundance of Giant Kelp (Macrocystis pyrifera). Remote Sens. 2020, *12*, 1371.

[9] D. A. Demer, L. Berger, M. Bernasconi, E. Bethke, K. Boswell, D. Chu, R. Domokos, A. Dunford, S. Fassler, S. Gauthier; L. T. Hufnagle, J. M. Jech, N. Bouffant, A. Lebourges-Dhaussy, X. Lurton, G. J. Macaulay, Y. Perrot, T. Ryan, S. Parker-Stretter, S. Stienessen, T. Weber, N. Williamson, Calibration of acoustic instruments. ICES Cooperative Research Report No. 326, 2015, 130pp.

[10] G. Fabi, A. Sala, An assessment of biomass and diel activity of fish at an artificial reef (Adriatic Sea) using stationary hydroacoustic technique. ICES J. Mar. Sci., 59: 411-420, 2002.

[11] A. Sala, G. Fabi, S. Manoukian, Vertical diel dynamic of fish assemblage associated with an artificial reef (Northern Adriatic Sea). Sci. Mar., 71(2): 355-364, 2007.

[12] G. Fabi, F. Grati, A. Lucchetti, L. Trovarelli, Evolution of the fish assemblage around a gas platform in the northern Adriatic Sea. ICES J. Mar. Sci., 59, S309–S315, 2002.

[13] A. Gaetani, A. N. Tassetti, C. Ferrà Vega, G. Pellini, P. Polidori, S. Leoni, G. Fabi, Spatial distribution of fish assemblages around a gas platform, CIESM Congress 2016, Kiel, Conference paper, 2016.

[14] G. Scarcella, F. Grati, G. Fabi, Temporal and Spatial Variation of the Fish Assemblage Around a Gas Platform in the Northern Adriatic Sea, Italy, Turkish Journal of Fisheries and Aquatic Sciences, 11, 2011, 433-444.

[15] K. Tsagarakis, M. Giannoulaki, S. Somarakis, A. Machias, Variability in positional, energetic and morphometric descriptors of European anchovy *Engraulis encrasicolus* schools related to patterns of diurnal vertical migration. Marine Ecology Progress Series 446: 243−258, 2012.

[16] E. Punzo, S. Malaspina, F. Domenichetti, P. Polidori, G. Scarcella, G. Fabi, Fish detection around offshore artificial structures: preliminary results from hydroacoustics and fishing surveys. Journal of Applied Ichthyology 31(S3):48-59, 2015.

[17] A. Gaetani, A. N. Tassetti, S. Guicciardi, C. Ferrà, G. Fabi, How Does Fish Behavior Change during the Day around Gas Platforms? Pages 7-21 in S. A. Bortone, editor. Marine artificial reef research and development: integrating fisheries management objectives. American Fisheries Society, Symposium 86, Bethesda, Maryland. 321 pages, 2018, ISBN: 978-1-934874-51-6, ISSN: 0892-2284

[18] K. Colbo, T. Ross, C. Brown, T. Weber, A review of oceanographic applications of water column data from multibeam echosounders. Estuarine, coastal and shelf science, 145, 2014, 41-56.

[19] M. Kupilik, T. Petersen, Imaging sonar tracking of salmon for size and tail beat frequency. IEEE Signal and Information Processing (GlobalSIP), Atlanta, Georgia, USA, 2014, pp. 1127–1131. I.

[20] K. M. Dunlop, T. Jarvis, K. J. Benoit-Bird, C. M. Waluk, D. W. Caress, H. Thomas, K. L. Smith Jr, Detection and characterisation of deep-sea benthopelagic animals from an autonomous underwater vehicle with a multibeam echosounder: A proof of concept and description of data-processing methods. Deep Sea Research Part I: Oceanographic Research Papers, 134, 2018, 64-79.

[21] Monk, Jaquomo, Ierodiaconou, Daniel, Versace, Vincent L., Bellgrove, Alecia, Harvey, Euan, Rattray, Alex, Laurenson, Laurie and Quinn, Gerry P. 2010, Habitat suitability for marine fishes using presence-only modelling and multibeam sonar, Marine ecology - progress series, vol. 420, pp. 157-174.

[22] Galparsoro, J. G. Rodríguez, I. Menchaca, I. Quincoces, J. M. Garmendia, A. Borja, Benthic habitat mapping on the Basque continental shelf (SE Bay of Biscay) andits application to the European Marine Strategy Framework Directive. J. Sea Res. 100,70–76, 2015.

[23] K. G. Foote, D. Chu, T. R. Hammar, K. C. Baldwin, L. A. Mayer, L. C. Hufnagle, J. M. Jech, Protocols for calibrating multibeam sonar, The Journal of the Acoustical Society of America, vol. 117, no. 4, p. 2013, 2005. http://dx.doi.org/10.1121/1.1869073

[24] T. van der Stap, J. W. Coolen, H. J. Lindeboom, Marine fouling assemblages on offshore gas platforms in the southern North Sea: Effects of depth and distance from shore on biodiversity. PLoS One, 11(1), 2016.

[25] A. B. Paxton, C. H. Peterson, J. C. Taylor, A. M. Adler, E. A. Pickering, B. R. Silliman, Artificial reefs facilitate tropical fish at their range edge. Communications biology, 2(1), 2019, 1-7.

[26] B. Sommer, A. M. Fowler, P. I. Macreadie, D. A. Palandro, A. C. Aziz, D. J. Booth, Decommissioning of offshore oil and gas structures–Environmental opportunities and challenges. Science of the total environment, 658, 2019, 973-981.

3

Special Session
Measurements for improved understanding and forecasting of the ocean dynamics

Ocean and atmospheric measurements play a fundamental role in our understanding of the sea state and its evolution. The aim of this session is to stimulate a discussion on new data processing methodologies aiming at exploiting the information content of current and upcoming sea monitoring technologies, including in situ and remotely sensed. A special attention is given to synergistic and data assimilation approaches and to applications in coastal areas and/or the Mediterranean basin.

2020 IMEKO TC-19 International Workshop on
Metrology for the Sea
Naples, Italy, October 5-7, 2020

New advances in the calibration of Doppler current-meters and current profilers

M. Le Menn[1], S. Morvan [2], A. Lusven [1]

[1] SHOM, 13 rue du Chatellier, CS 92803 29228 Brest Cedex, marc.lemenn@shom.fr
[2] Ecole Nationale Supérieure de d'Électrotechnique, d'Électronique, d'Informatique, d'Hydraulique et des Télécommunications (ENSEEIHT)

***Abstract* – Doppler current profilers are used in oceanography to measure the oceanic circulation but also in hydrology to calculate the flow of rivers. They allow the retrieval in velocity and direction of water masses profiles. The direction is obtained via an electronic compass and tilt sensors, and the velocity by the measurement of Doppler shifts of pulses back scattered by particles located in water cells allocated along the measurement range of the instrument. For current-meters and low range current profilers, calibrations are possible in towing tanks. But, these calibrations are limited in maximum velocity and they are not applicable for long range profilers. In the last years, new techniques were developed to calibrate compass and tilt sensors of current-meters and current profilers in their mooring cages and to obtain in laboratory the deviations in velocity of these instruments. This paper presents the existing methods and the new advances in the metrological mastering of these devices.**

I. INTRODUCTION

Oceans control a big part of earth climate by ocean – atmosphere exchanges, phenomenon’s like El-Niño or great cycles and oceanic currents. Measuring current is essential to build current charts useful for navigation, 3D models of oceanic circulation or more recently, to improve the efficiency of submarine tidal turbines.

Rotor current-meters have been replaced a tenth of years ago by Doppler effect acoustic current-meters. The marine environment being favourable to acoustic wave’s propagation, the arrival time of pulses reflected by particles, allowed the creation of Doppler current profilers. Placed under the hull of oceanographic boats and directed to the seabed, or, placed in cages deposited on the seabed and directed to the surface, velocity profiles of the water column can be obtained. Their range, which depends on their wavelength, extends from a few meters to several hundredths of meters, according to the particles concentrations.

These profiles are cut artificially in cells by the software of the instrument, which gives average velocity values per cell, in relation with the measured Doppler shifts.

Following what was made for rotor current-meters, in the domain of hydrology, quality assurance tests [1], laboratory inter-comparisons [2] or validation by bottom track in towing basins [3-4] have been proposed. In oceanography, Doppler profiler’s ranges often extend from tenth to hundredth of meters, making controls in towing basins impossible. More of that the quantity of stand-alone instruments used in hydrographic and oceanographic centres make this technique difficult to apply. Therefore, in the last years, the calibration or simply the test of these instruments has been an untreated problem.

In Shom, a platform has been built and brought into service in 2012, to calibrate in their instrumental configuration of using, the electronic compasses and the tilt sensors they are equipped with [5-7]. These compasses are used to retrieve the directions of profilers to the magnetic North, their three transducers being used to retrieve the direction of currents in the instrument referential.

It stayed to find a method to calibrate the velocity measurements made by profilers. The solution found was of using an acoustic transducer put down successively on the transducers of the device under test (DUT). Linked to a frequency generator, it allows the simulation of echoes received by the DUT. The exploitation of the Doppler effect formula and of the speeds sensed by the instrument, has allowed the perfecting of a test method of the DUT’s measurement channels [8].

With these last advances, all the quantities measured by current profilers can actually be controlled and calibrated.

II. OPERATING PRINCIPLES OF DOPPLER CURRENT PROFILERS

Current profilers measure velocities (V_1, V_2, V_3) in their beams axes. Their transducers are sloped by 20 °, 25 ° or 30 ° (angle β). Therefore, it is possible to calculate velocities (V_x, V_y, V_z) in their own referential [9]:

$$\begin{bmatrix} V_x \\ V_y \\ V_z \end{bmatrix} = \begin{bmatrix} \frac{2}{3\sin(\beta)} & \frac{-1}{3\sin(\beta)} & \frac{-1}{3\sin(\beta)} \\ 0 & \frac{-1}{\sqrt{2}\sin(\beta)} & \frac{1}{\sqrt{2}\sin(\beta)} \\ \frac{1}{3\cos(\beta)} & \frac{1}{3\cos(\beta)} & \frac{1}{3\cos(\beta)} \end{bmatrix} \begin{bmatrix} V_1 \\ V_2 \\ V_3 \end{bmatrix} \tag{1}$$

They are equipped of ‘flux-gate’ compasses to retrieve the amplitude of components (U, V, W) of currents in reference to the magnetic North (angle Ω), and knowing the magnetic declination, in relation to the true North (2). More of that, their inclination can be corrected thanks to a tilt sensor measuring angles Ψ and θ of roll and pitch (in equation (2), C = cos and S = sin) [10]:

$$\begin{bmatrix} U \\ V \\ W \end{bmatrix} = \begin{bmatrix} C_\psi C_\Omega & (-S_\psi S_\theta C_\Omega + C_\theta S_\Omega) & (S_\psi C_\theta C_\Omega + S_\theta S_\Omega) \\ -C_\psi C_\Omega & (S_\psi S_\theta S_\Omega + C_\theta S_\Omega) & (-S_\psi C_\theta S_\Omega + S_\theta C_\Omega) \\ -S_\psi & -C_\psi S_\theta & C_\psi C_\theta \end{bmatrix} \begin{bmatrix} V_x \\ V_y \\ V_z \end{bmatrix} \quad (2)$$

The speeds (V_1, V_2, V_3) are obtained by measuring the Doppler effect after the detection of echoes resulting of the reflection of pulses on the successive layers of particles. To improve the trueness of measurements, pulses are repeated to a frequency f_r. The maximum measurable speed V_{max} depends on f_r and on the wavelength λ:

$$\pm V_{max} = f_r \lambda / 4 \quad (3)$$

f_r fixes also the maximal profiling range r_{max}, to which a target can be detected without ambiguity on its position:

$$r_{max} = c / 2 f_r \quad (4)$$

c is the speed of sound. Relations (3) and (4) lead to express the ambiguity relation range – velocity [11]:

$$V_{max}\, r_{max} = \pm c \lambda / 8 \quad (5)$$

To overcome the limits imposed by equation (5), different techniques have been found, based on the treatment of emitted and received signals.

Thus, conventional profilers are called ‘incoherent’ or ‘narrowband’ because the received echoes from two different pulses are not correlated. The lower uncertainty that can be obtained on the measurements of (V_1, V_2, V_3) is limited by the variance of the Doppler noise σ_δ, which is inversely proportional to the duration of pulses t_p. This noise is generated by the random displacement of particles. To decrease the uncertainty, it is necessary to multiply the number n of pulses. The uncertainty on V_i’s, $i \in \{1, 2, 3\}$, can be reduced statistically:

$$\sigma_V = \frac{\sigma_\delta}{\sqrt{n}} \quad (6)$$

Another solution rests on the increase of the value of t_p, but it leads a reduction of the spatial resolution. In order to overcome this ambiguity, profilers called ‘pulse-to-pulse coherent’ or ‘pulse coherent’ have been created. Their measurement principle rests on working on series of coherent pulses coded in phase. In order to extract the signal from the noise, an auto-covariance function $R(\tau)$ of these pulses is calculated [12]. To improve the extraction, the auto-covariance is assessed from the reception of M sequences of two pulses and of the average of M functions $R(\tau)$ [13]. Most of time, the average Doppler frequency characterizing the Doppler shift δf, is extracted from the phase $\phi \in [-\pi, +\pi]$ of this average auto-covariance function. Finally, if f_0 is the emitted frequency, the measured radial velocity is obtained by the relation:

$$V_i = \pm \delta f_i\, c / 2 f_0 \quad (7)$$

If t_l is the time corresponding to pulses going there and back, we have $2\pi\delta f = \phi / t_l$. The expression of the velocity becomes:

$$V_i = \pm \phi\, c / 4 \pi f_0 t_l \quad (8)$$

III. THE ‘TRADITIONAL’ CALIBRATION METHODS

For rotor current-meters, this calibration was made in test open channels [14–15] or hydrodynamic channels [16]. The ISO 3455:2007 standard [15] applied in hydrology, specifies the procedure of calibration of current-meters equipped with rotating-element or stationary sensors in straight open tanks.

The DUT is fixed on a mobile trolley. A speed sensor often composed of an optical coded rotation sensor, is mounted on the trolley and is used as a reference to control the speed of the trolley and to calibrate the current-meters. If the DUT is a profiler, it can be used in bottom-track mode or in water-track. In bottom-track, the velocity is obtained over the bed. It is representative of the trolley's speed. The length of basins and the time needed to obtain a constant speed and to slow down, limit the maximum rating carriage to a speed between 1 and 3 m/s.

In the case of hydrodynamic channels, the DUT is in a static position and a turbine allows the variation of the water’s circulation speed in the circular channel. A Laser velocimeter or an electromagnetic flow meter like in ref. [16] gives the reference speed. In this publication, the speed is generated by gravity from a tank and a valve regulates it. A pump allows the reloading of the tank.

These facilities present the advantage to test instruments in hydrodynamic conditions close to using conditions but with some differences [3]: there is no turbulence, the backscatter material is artificial, the bed is smooth, and there are negligible or zero-velocity gradients in the sample volume.

Their measurement uncertainty is limited principally by the time during which the speed can be keep constant to be considered as a reference and by the reading uncertainty of the reference sensor. Acoustic reflections on bed and sidewall can increase also the measurement uncertainty of the DUT, and acoustic interferences can introduce negatives bias [3]. Because of these side effects, when deviations are calculated, it remains

difficult to determine if they come from the instrument or from the experimental bias. The direction of the DUT versus the flow can also leads measurement errors.
These facilities cannot be used in the case of long-range profilers which size of the first measurement cell is superior to the depth of the channel of water. The cleanness of the water is also an obstacle to make measurements with a low noise. Doppler current-meters need particles to detect echoes. The lake of particles increases their measurement uncertainties.
Lastly, these facilities do not allow the calibration of compass and tilt sensors. Generally magnetic interferences lead systematic errors on compass readings and they cannot be used.

IV. THE NEW ADVANCES IN CALIBRATION METHODS

In order to overcome the previous problems and to answer the needs met in oceanography, a calibration platform for compass and tilt sensors and a velocity calibration bed have been built in Shom.

A. The compass calibration platform

References [5] to [7] describe in details the techniques used to built the plateform and the results obtained on a stock of instruments. Compas and tilt sensors are used to retrieve the amplitude and the direction of currents components in relation to the true North, thanks to relation (2). Tilt sensors are necessary also to retrieve the true depth of the cells.

Fig. 1. DORA cage on the calibration platform.

Profilers are often installed in mooring cages equipped with launchers, battery packs, flash lamps or tide recorders. The cage and its components can have a strong influence on the local magnetic field. The mapped magnetic field of the platform allows the measurement of induced errors which can be corrected thanks to polynomial relations. If the DUT is in a amagnetic cage, its instrumental errors can be corrected.

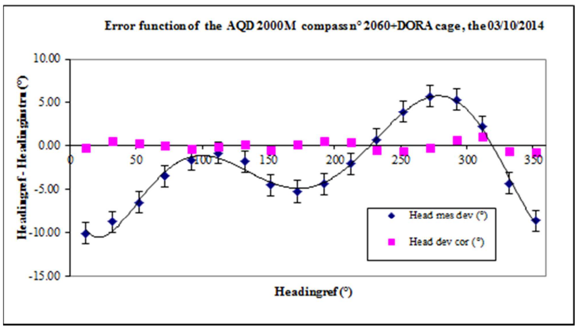

Fig. 2. Error curb of a current-meter's compass installed in a DORA cage.

B. The calibration of transducers

The number of current-meters and current profilers necessary in oceanographic centres (more than 110 units in Shom) make hardly realisable inter-comparisons at sea or calibrations in towing basins.
A method, described in details in ref. [8] has been perfected, based on using of a plane hydrophone put down successively on the transducers of the DUT. This hydrophone is used as a receiver, at first, and connected to a numerical oscilloscope. In order to warrant its stability and accuracy in frequency, it is linked to an external clock Epsilon NTP, synchronised to a GPS signal which is a reference for Time and frequencies [17].
A Fast Fourier Transform (FFT) of the digitized signal allows the accurate measurement of pulses frequencies emitted by the profilers. Thereafter from the relation (7) it is possible to determine a frequency variation range corresponding to its variation range in velocity. It is also possible to determine an increment step δf_s, knowing the resolution in velocity δv of the instrument. A frequency generator is therefore adjusted to transmit a variable sinusoidal frequency $f_0 \pm k\,\delta f_s$, the value of k allowing to explore the velocity range. Therefore, in a second step, the hydrophone is used as a transmitter.
All this equipment is remote controlled by a program developed under the Labview© software. It allows the automation of the test by decoding the messages from different models of profilers, to determine and change their configuration, to extract speed values and to drive the frequency generator.
The calibration consists in calculating a speed deviation δv so that:

$$\delta v = V_{ref} - V_i = \frac{c}{2}\left(\frac{\delta f_{ref} - \delta f_i}{f_0}\right) \qquad (9)$$

with $\delta f_{ref} = k\delta f_s$. δf_i is defined by the relation (7), i being the index of the instrument’s transducer. c is fixed to 1525 m/s to obtain profilers responses in the range ± 6 m/s (except for the Nortek DeepWater where f_r is different). This value is entered in the instrument and in the Labview program to calculate a reference velocity V_{ref}.

As proves of its good working order, this test bed has allowed the detection of defaults on some instruments: noisy transducers, small offsets, small non-linearity's and one with a response completely out of tolerances.

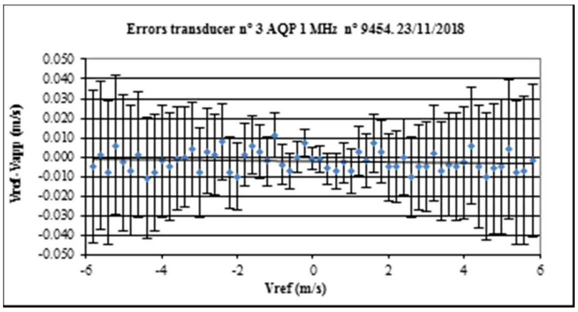

Fig. 3. Example of velocity response curb of a noisy transducer. Error dashes represent the expanded uncertainty of the calibration.

V. CONCLUSION

The new calibration techniques developped for compass, tilt sensors and velocity measurements, allow the test in large number of Doppler current-meter and current profilers. It allows also a calibration in velocity whatever is the range of the instrument. Compared to the 'traditional' calibration techniques, the errors generated by the instrument can be measured and separated of errors in relation with its environment. The uncertainty of the calibration can also be evaluated enough easily.

REFERENCES

[1] Armstrong, B., Fulford, J., and Thibodeaux, K., ‘Quality assurance testing of acoustic Doppler current profiler transform matrices’, 2015 IEEE/OES Eleventh Current, Waves and Turbulence Measurement (CWTM), 2015. DOI: 10.1109/CWTM.2015.7098108.

[2] Le Coz, J., Blanquart, B., Pobanz, K., Dramais, G., Pierrefeu, G., Hauet, A., and Despax, A. ‘Estimating the uncertainty of streamgauging techniques using in situ collaborative interlaboratory experiments’, J. of Hydraul. Eng., 142, 7, 2016. 10.1061/(ASCE)HY.1943-7900.0001109, 04016011.

[3] Oberg, K.A. and Mueller, D.S., ‘Validation of streamflow measurements made with acoustic Doppler current profilers’, J. of Hydraul. Eng., 133(12), 1421-1432, 2007.

[4] Shih, H.H., Payton, C.,Sprenke, J.and Mero T., ‘Towing Basin Speed Calibration of Acoustic Doppler Current Profiling Instruments’, Joint Conference on Water Resource Engineering and Water Resources Planning and Management 2000, July 30-August 2, 2000 | Minneapolis, Minnesota, United States.

[5] M. Le Menn**,** L. Pacaud, ‘Calibration of currentmeters in direction: results obtained on a stock of instruments with a new calibration platform’, Web of Conference et actes, 17th International Congress of Metrology, EDP science, Paris, 2015. DOI: 10.1051/metrology/201501002.

[6] M. Le Menn, A. Lusven, E. Bongiovanni, P. Le Dû, D. Rouxel, S. Lucas, L. Pacaud, ‘Current profilers and currentmeters compass and tilt sensors errors and calibration’, Meas. Sci. Technol., **25,** 2014, 085801 (6pp).

[7] M. Le Menn, M. Le Goff, ‘A method for absolute calibration of compasses’, Meas. Sci. Technol., **18**, 1614-1621, 2007.

[8] Le Menn, M., Morvan, S., 'Calibration of Doppler current profilers in velocity', submitted to Measurement, ref. MEAS-D-20-01633.

[9] Cabrera, R., Huhta, C., Lohrmann, A., ‘A new acoustic Doppler Current Profiler for Shallow Water’, Oceans’95 MTS/IEEE, Conference proceedings, Vol.3, 9-12 Oct. 1995.

[10] Alderson, S. G., and Cunningham, S. A., ‘Velocity errors in acoustic Doppler current profiler measurements due to platform attitude variations and their effect on volume transport estimates’, J. Atmos. Ocean. Technol., 16, 96-106, 1999.

[11] Lhermitte R., Serafin R., ‘Pulse-to-pulse coherent Doppler sonar signal processing techniques’, J. Atmos. Ocean. Technol., **1**, 4, 293-308, 1984.

[12] J. Dillon, L. Zedel, A. E. Hay, ‘Simultaneous Velocity Ambiguity Resolution and Noise Suppression for Multifrequency Coherent Doppler Sonar’, J. Atmos. Ocean. Technol., **29**, 450-463, 2012.

[13] A. Lohrmann, B. Hackett, L. P. Roed, ‘High resolution measurements of turbulence, velocity and stress using a pulse-to-pulse coherent sonar’, J. Atmos. Ocean. Technol., 7, 19-37, 1990.

[14] International Organization for Standardization (ISO). ’Assessment of uncertainty in the calibration and use of flow measurement devices— Part 1: Linear calibration relationship’, ISO 7066-1, Geneva, (1997).

[15] International Organization for Standardization (ISO). ‘Hydrometry—Calibration of current meters in straight open tanks’, ISO **3455**, Geneva, (2007a).

[16] E. Camnasio, E. Orsi, ‘Calibration Method of Current Meters’, Journal of Hydraulic Engineering, **137**, 386-392, (2011). DOI: 10.1061/(ASCE)HY.1943-7900.0000311

[17] M. Le Menn, ‘Instrumentation and Metrology in oceanography, *ISTE – WILEY*, p 38-42, (2012)

4

Special Session
Facing emerging marine environmental challenges using Remote Sensing

The aim of this session is to investigate and analyze the newly developed remote sensing techniques and methodologies specifically developed for facing environmental challenges in marine domain, such as plastic detection and identification, coastal erosion, oil spill detection, ship pollution, etc. A particular attention will be given to methodologies able to exploit ASI and ESA systems, such as Sentinel, Cosmo-SkyMed and the newly launched PRISMA. Moreover, the possibility of jointly exploit multiple sensors will be investigated.

2020 IMEKO TC-19 International Workshop on
Metrology for the Sea
Naples, Italy, October 5-7, 2020

Preserving natural ecosystems: atolls observed by partially polarimetric SAR satellite imagery

Andrea Buono[1], Emanuele Ferrentino[1], Ferdinando Nunziata[1], Maurizio Migliaccio[1]

[1]*Universitá degli Studi di Napoli Parthenope, Dipartimento di Ingegneria,Centro Direzionale isola C4, 80143, Napoli, Italy, andrea.buono@uniparthenope.it*

***Abstract* – In this study, the potential of dual-polarimetric (DP) Synthetic Aperture Radar (SAR) data to observe atolls is addressed. The partial polarimetric information is exploited to both define the coastal profile and to classify the observed area. Experiments are undertaken on a fine resolution DP L-band ALOS PALSAR-2 SAR scene collected under horizontal linear polarization transmission over the Goidhoo Atoll belonging to the Maldivian Baa Atoll, that was selected as test site due its importance for the local ecosystem and the extraordinary value of its biodiversity.**

Preliminary results show that partial polarimetric information can be exploited for atoll observation purposes, including the coastline extraction and the classification of the observed scene.

I. INTRODUCTION

Climate change is an important topic to be addressed but two main issues must be considered. First, is there a simple way to predict climate change ? Second, are economic growth and climate change irredeemably in contrast ? We hereafter focus on the first key question.

In fact, while climatologists agree that the meteorological effects of climate change cannot be adequately predicted for many areas, there is a general consensus that any further global warming will bring with it a further sea-level rise. Since, atolls are among islands with the lowest elevation monitoring and, therefore, atolls are effective proxy of climate change.

An atoll is generally a ring-shaped coral reef, island or series of islets that surrounds a body of water called lagoon. Since reef building corals thrive only in warm waters, atolls are only found at tropical and sub-tropical latitudes, i. e., most of the atolls are located in the Pacific and Indian Oceans. Among the most relevant atolls archipelagos there is the Republic of Maldives, which is made by 26 atolls. It stretches from Ihavandhippolhu Atoll in the north to Addu Atoll in the south. The average ground-level elevation is 1.5 m and the highest natural peak is one of the lowest in the world being 5.1 m. Every Maldivian atoll is formed by a marginal rim surrounding a lagoon commonly 40-60 m deep and interrupted by deep channels, which lead to strong water circulation inside the lagoon, encouraging the development of many patch reefs [1]. Atolls and their associated rim reefs, lagoons and lagoon reefs vary tremendously in their formation, size and physical setting. The atoll rim can be continuous (ribbon reefs) without gaps for tens of kilometers or discontinuous with reefs of different shapes (cuspate, prong, circular, elongated). The Maldivian government has recognized the value of coral reefs and has established 35 marine protected areas since 1995. However, most of the Maldivian atolls are more than 1000 km^2 large, making their in-situ monitoring quite costly. Hence, remote sensing plays a key role for a systematic monitoring. In particular, the Synthetic Aperture Radar (SAR) is a very suitable sensor to observe atolls since it provides routinely images independently of the solar illumination and in almost any weather condition with fine spatial resolution and dense temporal resolution. However, to the best of our knowledge, very few studies focused on the exploitation of SAR data to observe atolls [2, 3].

Hence, in this study, a preliminary investigation on the capability of fine resolution polarimetric SAR imagery to monitor atolls is undertaken, considering the Baa atoll (Republic of Maldives) as a test site. In detail, two issues are addressed in this study: i) the extraction of the atoll's coastline and ii) the atoll classification, with the aim of showing the added-value of partial polarimetric SAR measurements in fulfilling both the tasks.

II. TEST SITE

The Indian Ocean Baa Atoll system (Republic of Maldives) consists of three different natural atolls: Maalhosmadulu Atoll, Fasduthere Atoll and Goidhoo Atoll that, altogether, counts up to 75 islands (see Figure 1). The Baa Atoll, declared as UNESCO heritage and world biosphere reserve due to its biodiversity richness, is 38 km wide and 46 km long, covering an area of approximately 1127 km^2. It includes 105 coral reef ecosystems for a total reef area of 263 km^2 [4]. Most of the atoll is composed by vegetated and sandy inhabited islands whose bathymetry is characterized by atoll rim passages which are usually 35 m - 56 m deep and an average lagoon depth that spans from 30 m up to 50 m [4]. A micro-tidal regime applies with a spring tide range of about 1.2 m [4]. The Baa atoll calls for wind conditions characterized by moderate winds (5.0 m/s, on average) blowing from south- to north-west during summer/autumn and east northeast during winter/spring.

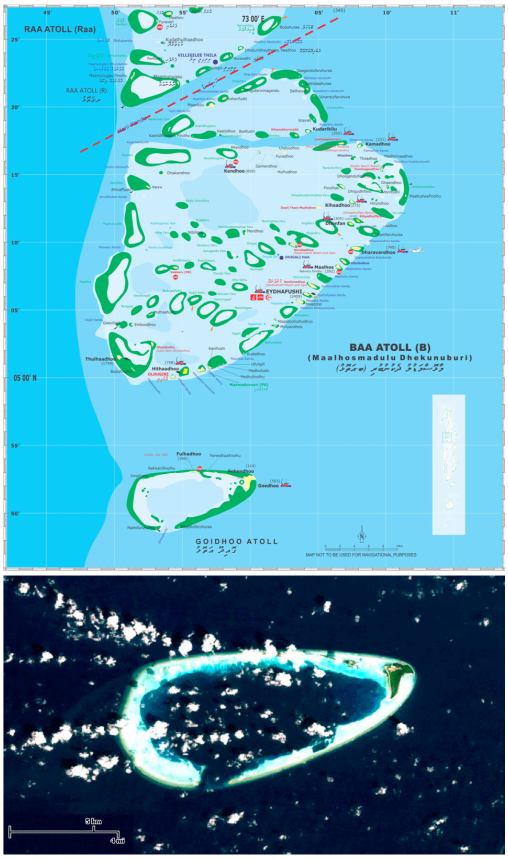

Fig. 1. Maldivian Baa Atoll archipelago. Top: the Baa Atoll system (Photo Credit: Baa Atoll). Down: Landsat 8 satellite optical image of the Goidhoo Atoll.

Due to its location with respect to other atolls, the Baa Atoll is exposed to ocean swell along its western and south-western boundaries [4, 5].
In this study, the Goidhoo Atoll, that consists of Goidhoo, Fehendhoo and Fulhadhoo islands, is observed that belongs to the administrative atoll of Baa [5]. Although on the Goidhoo Atoll there is intensive agriculture activity mainly growing water melon, pumpkin and bilimbi along with a mangrove system [5], the anthropogenic activities have generated no disturbance [6]. Of course, the marine biodiversity is outstanding all over the Maldives although the reef corals were severely impacted by the El Nino southern oscillator event [5]. Associated to the environmental protection the Baa Atoll is also a good example of green/blue economy since the ruled economic activities appear to be sustainable with the ecosystem.

III. METHODOLOGY

In this section, the methodology considered to monitor atolls by means of dual-polarimetric (DP) SAR satellite measurements is briefly revised. It must be underlined how the partial polarimetric information was already successfully exploited for several environmental applications including sea surface observation, inland water body monitoring, and shoreline rotation analysis [7]-[9]
The approach consists of two steps: i) coastline extraction and ii) scene classification.The coastline is extracted according to a two-step approach where the land/sea contrast is first enhanced using a DP parameter that relies on the joint use of co- and cross-polarized channels [7]:

$$r = \langle |S_{xx}||S_{xy}| \rangle \tag{1}$$

where x, y can assume the meaning of horizontal (H) or vertical (V) polarization, while $|\cdot|$ and $\langle\cdot\rangle$ stand for modulus and ensemble average, respectively. In [7] it was already shown that the r parameter is effective and robust to separate land from sea areas, better than single-polarization intensity backscattering signals that, in complex atoll environment (sandy beaches, mangroves, lagoons, etc.) may result in unsatisfactory land/sea discrimination capability. Then, a global-threshold constant false alarm rate (CFAR) approach in combination with an edge detector based on a Sobel kernel is applied to provide a binary image from which the land/sea boundary is detected. The parameter r is assumed to follow a Rayleigh distribution over the sea surface [7].
The scene classification is based on the extra-information provided by DP SAR information from which, at least partly, [10] rough information of the scattering process can be inferred. Among the different polarimetric SAR-based classifiers, the coherent polarimetric decomposition theory is here considered that was shown to be effective even in complex scenarios [11, 12]. In detail, the DP entropy/mean scattering angle classification scheme is adopted which is based on the eigen-decomposition of the 2×2 covariance matrix [10]. Although DP SAR provides partial polarimetric information with respect to full-polarimetric SAR, this DP decomposition can be still exploited to perform a rough classification of the observed scene based on the analysis of the dominant scattering mechanisms, especially when the scattering scene does not call for a large degree of randomness. The classification process is basically based on the pixels partitioning in the 9-zones $H/\bar{\alpha}$ plane according to their mean entropy and mean scattering angle values and in the subsequent clustering performed according to the minimization of the Wishart distance between the classes [10].
Entropy H can be interpreted as a measure of the randomness of the scattering process:

$$H = -\sum_{i=1}^{2} p_i \log_2 p_i \quad , \quad p_i = \frac{\lambda_i}{\sum_{j=1}^{2} \lambda_j} \tag{2}$$

where λ_i is the i-th eigenvalue of the 2×2 covariance matrix.

The mean scattering angle $\bar{\alpha}$ provides information on the average angle from which the signal is backscattered off the target:

$$\bar{\alpha} = p_1\alpha_1 + p_2\alpha_2 \tag{3}$$

where the α_i is the angle corresponding to the i-th eigenvector of covariance matrix. The joint analysis of H-$\bar{\alpha}$ allows extracting rough information on the scattering mechanisms that rules the observed scene and that can be used for classification purposes.

IV. EXPERIMENTS

In this section, experiments undertaken over the Goidhoo Atoll using a DP HH+HV ALOS PALSAR-2 SAR scene are presented to investigate the potential role played by partial polarimetric information in supporting the monitor of atolls from space. The SAR acquisition was collected at L-band on 14 January 2018, in ascending pass, with an incidence angle of about 35° and a very fine spatial resolution of approximately 4 m in both range and azimuth directions.

The HH- and HV polarized intensity images are shown, in dB scale, in Figure 2. It can be noted that the 3 islands of the Goidhoo Atoll call for a larger backscattering in both channels with respect to the surrounding sea. The backscattering intensity over land is very similar in both polarization witnessing the complexity of the scattering scenario, while ocean backscattering, being dominated by Bragg/tilted Bragg mechanisms, calls for co-pol backscattering intensity larger than the cross-pol one. In addition, it can be noted a ring-shaped ocean feature which is likely due to surface waves refraction and shoaling in shallow water near the atoll related to coral reef bathymetry [2]. Results relevant to the coastal profile detection was also shown in Figure 2, where the extracted coastline (a false alarm probability of 10^{-6} was set) is depicted in red and overlaid on the r parameter image. Zoom-in images for Fehendhoo and Goidhoo islands demonstrate the soundness of the proposed methodology, i. e., the extracted coastline well-fits the actual coastal profile very well and it is not severely influenced by false coastlines induced by the presence of the coral reef except for the north-eastern part of the Goidhoo island where a finer tuning of the algorithm should be needed to improve the performance.

Then, the second issue is addressed that consists of classifying the atoll according to the scattering information. Focus is made on the Goidhoo island since it is characterized by a more heterogeneous environments made by buildings, mangroves, sparse vegetation, crops and coral reefs. The classification output is shown in Figure 3, where, according to the conventional $H/\bar{\alpha}$ plane scheme, the following color-code is adopted: dark purple, purple and violet mean a dominant complex structure, dihedral reflector and random surface, respectively; blue, green and light green mean a dominant Bragg surface, anisotropic particles and double reflection, respectively; while gray and yellow mean a dominant dipole and random anisotropic scattering, respectively. Hence, it can be noted that the main scattering classes obtained from the H-$\bar{\alpha}$ decomposition are Bragg and random surfaces over the ocean and double-bounce, complex structures and anisotropic particles over land. By visually inspecting Figure 3, even with the support of optical imagery, it can be noted that the proposed approach is able to at least roughly identify: 1) the ocean/lagoon scattering signature including the coral reef/sea boundary; 2) the presence of sparse vegetation; 3) sandy beaches and small urban settlements.

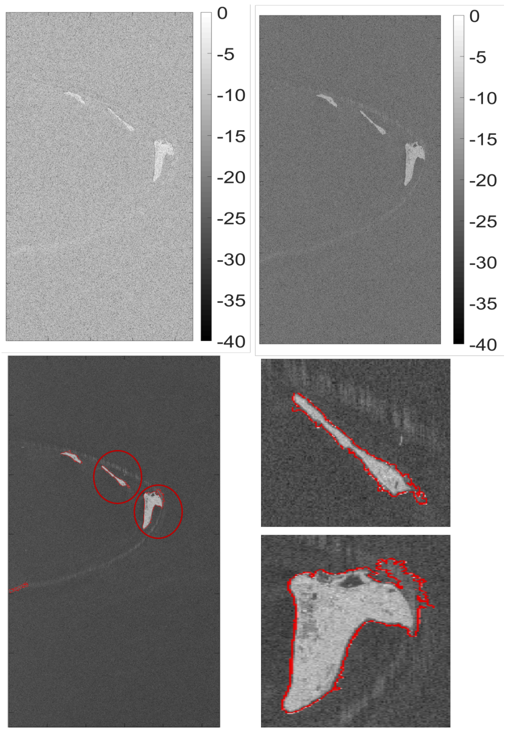

Fig. 2. Coastline extraction results. Top: DP (HH and HV) intensity SAR images (dB) of the Goidhoo Atoll. Down: Extracted coastline, in red, overlaid on the r image, with zoom-in images relevant to the Fehendhoo and Goidhoo islands.

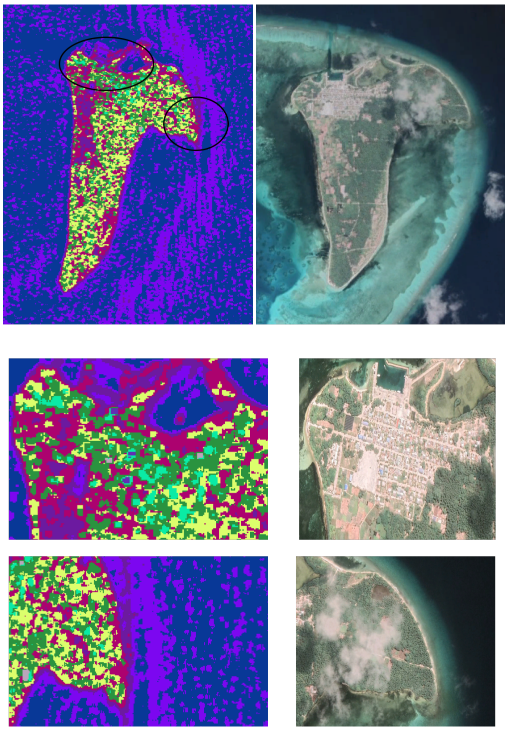

Fig. 3. Classification results. DP H-$\bar{\alpha}$ output over the Goidhoo island with corresponding Google Earth© optical images shown for reference purposes.

V. CONCLUSIONS

In this study, partial (HH+HV) polarimetric SAR information is exploited to observe the Goidhoo Atoll within the Baa Atoll archipelago (Republic of Maldives). Two different algorithms have been applied on an L-band ALOS PALSAR-2 SAR scene to: i) extract the coastal profile according to the r parameter and ii) classify the atoll area according to the $H/\bar{\alpha}$ decomposition.
Preliminary results demonstrate the soundness of the proposed approach, witnessing the potential role played by DP SAR satellites in monitoring atolls. Future work will include the exploitation of available ancillary information and ground truth measurements to support the interpretation of the preliminary results.

REFERENCES

[1] A. Naseer and B. Hatcher, “Inventory of the Maldives’ coral reefs using morphometrics generated from Landsat ETM+ imagery,” Coral Reefs, vol. 23, no. 1, pp. 161- 168, Apr 2004.

[2] M.K. Hsu, A. K. Liu, Y. Zhao *et al.*, “Satellite remote sensing of Spratly Islands using SAR,” Int. J. Remote Sens., vol. 29, no. 21, pp. 6427-6436, 2008.

[3] T. Nair, L. James, C. V. Rao *et al.*, “A study on the delineation of coral reefs in Andaman and Lakshadweep islands using RISAT-1 data,” J. Indian Soc. Remote, vol. 45, no. 5, pp. 873-885, 2017.

[4] P. Kench, “The geomorphology of Baa (South Maalhosmadulu) Atoll and its reef islands,” Atoll Res. Bull., pp. 1-29, 01 2012.

[5] A. V. Bers, “Biodiversity assesment for Maldives Baa Atoll,” 2005.

[6] V. K. E. Duvat and A. K. Magnan, “Rapid human-driven undermining of atoll island capacity to adjust to ocean climate-related pressures,” Sci. Rep., vol. 9, no. 1, pp. 15129, 2019.

[7] D. Di Luccio, G. Benassai, G. Di Paola *et al.*, “Shoreline rotation analysis of embayed beaches by means of in situ and remote surveys” Sustainability, vol. 11, no. 3, 2019.

[8] E. Ferrentino, F. Nunziata, A. Buono *et al.*, “Multi-polarization time-series of Sentinel-1 SAR imagery to analyze variations of reservoirs’ water-body,” IEEE J. Sel. Top. Appl. Earth Obs. Remote Sens., vol. 13, pp. 840-846, 2020.

[9] A. Buono, C. R. de Macedo, F. Nunziata *et al.*, “Analysis on the Effects of SAR Imaging Parameters and Environmental Conditions on the Standard Deviation of the Co-Polarized Phase Difference Measured over Sea Surface,” Remote Sensing, no. 11, pp. 18, 2018.

[10] K. Ji and Y. Wu, “Scattering mechanism extraction by a modified Cloude-Pottier decomposition for dual polarization SAR,” Remote Sens., vol. 7, no. 6, pp. 7447- 7470, 2015.

[11] E. Ferrentino, F. Nunziata and M. Migliaccio, “Full-polarimetric SAR measurements for coastline extraction and coastal area classification,” Int. J. Remote Sens., vol. 38, no. 23, pp. 7405-7421, 2017.

[12] A. Buono, F. Nunziata, M. Migliaccio *et al.*, “Classification of the Yellow River delta area using fully polarimetric SAR measurements,” Int. J. Remote Sens., vol. 38, no. 23, pp. 6714-6734, 2017.

2020 IMEKO TC-19 International Workshop on
Metrology for the Sea
Naples, Italy, October 5-7, 2020

An integrated approach of in-situ data, remote sensing measurements and numerical simulations to study storm events in the Ligurian Sea.

Diana Di Luccio[1], Andrea Buono[2], Valeria Corcione[2], Maurizio Migliaccio[2], Guido Benassai[2]

[1]*University of Naples "Parthenope", Science and Technologies Department, Napoli, Italy*
[2]*University of Naples "Parthenope", Engineering Department, Napoli, Italy*

***Abstract* – Extreme weather events have significant impacts on human activities and related economy in coastal areas. In this scenario, the forecast of sea storms and sea level changes to mitigate the effects of waves on shores, piers and critical coastal infrastructures is a key but challenging goal. The latter can be effectively achieved using a synergistic approach that includes numerical models, in-situ data and remote sensing measurements.**
To this end, we investigated the atmospheric and wave forcing data of the storm event occurred in the Ligurian Sea on 29-31 October 2018, which induced significant damages with coastal defenses collapses, loss of property and infrastructure. The study was carried on using a dataset that consists of atmospheric and sea wave data from RNM stations, sea wind field data from satellite radar and WRF-WW3 model numerical simulations.
The experimental results demonstrate the effectiveness of the proposed integrated approach, showing that in-situ measurements are satisfactory for water level, pressure and waves, while the satellite-based wind speeds better agree with numerical simulations if compared to the in-situ wind observations, which are affected by sheltered position of the weather stations.

I. INTRODUCTION

In order to analyse the reliability of the remote sensing data and in-situ measurements for the validation of wind, wave, sea level and atmospheric pressure numerical simulations, we selected the "Vaia" storm event occurred over the Ligurian Sea on 29-31 October 2018, that produced many damages along the coast of Liguria region. In particular, in the Savona coastal area the storm resulted in the almost complete destruction of the structures and piers of the bathing facilities and the removal of entire stretches of sandy and pebble beaches. Santa Margherita Ligure and Rapallo harbours were particularly affected, with the collapse of the respective breakwaters. Towards Portofino, the storm event caused the entire collapse of a section of provincial road near Paraggi. Hence, in this study, we proposed an integrated approach to analyze this hazardous and destructive storm event.

II. MATERIAL AND METHODS

In this section, the dataset considered for the study of the "Vaia" storm event is presented. It includes in-situ data and spaceborne radar measurements that were both compared with atmospheric and wave numerical models.

A. *Atmospheric and sea wave in-situ observations*

We collected data, with a 1/6 h timestep, available from the RMN stations of Genova (44°24’36.46”N, 08°55’31.86”E), Livorno (43°32’46.63”N, 10°17’57.62”E), and Marina di Campo (42°44’33.48”, 10°14’18.00”), hereafter called P1, P2 and P3, respectively [1]. All the stations provide data on sea level (SL) with millimeter precision since 2010 with a radar coupled with the historical ultrasonic hydrometer sensor equipped since 1998. The stations are also equipped with an anemometer measuring wind speed (WS) and direction (WD) 10 meters above the sea level, a barometer recording the sea level pressure (SLP), an air and water temperature sensor, as well as a relative humidity sensor.
In order to reduce the data spikes in SL measures, we applied a third-order one-dimensional median filter to the whole time-series, while the data gaps were not removed. The sea wave height (H_s), peak period (T_p) and direction (D_p) were recorded by the 140-m deep buoys of Giannutri (42.23°N, 11.04°E) and Gorgona (43.57°N, 09.95°E), hereafter called B1 and B2, respectively, that operate since 1 October 2008 and 6 December 2013, respectively.

B. *Remote sensing observations*

In this study, satellite radar data from ASCAT (Advanced Scatterometer) are exploited for sea wind speed retrieval to support in-situ measurements and numerical modeling. ASCAT is a C-band (5.255 GHz) scatterometer on-board of the EUMETSAT (European Organisation for the Exploitation of Meteorological Satellites) Metop (Meteorological Operational Satellite) satellites. ASCAT measures the VV-polarized normalized radar cross section (NRCS) according to two sets of fan-beams, one on each side of the satellites, covering 550 km-wide swath each

with an incidence angle that spans from 25° to 65°. As a result, an approximately twice global daily coverage at mid-latitudes is achieved due to both ascending and descending swaths and a daily coverage of 65% of the Earth achieving a global coverage after five days [2].
For the purpose of this study, the global wind level-3 ASCAT products consisting of the sea wind field at 10 m above sea level at neutral conditions [3] derived over coastal areas at 12.5 km spatial resolution are considered. They were provided by the Jet Propulsion Laboratory (JPL) through the PODAAC (Physical Oceanography Data Access) web platform (podaac.jpl.nasa.gov/dataaccess). The CMOD7 geophysical model function (GMF) is used to generate the wind field map from the NRCS measurements that results in high accuracy, i. e., ≤ 2 m/s within 12-20 km from the coastline [4, 5]. In this study, three ASCAT-based wind speed maps are provided over the study area during the storm event, from 7:51 UTC of 29 October 2018 to 20:39 UTC of 31 October 2018, in order to provide reliable and spatially-distributed offshore wind speeds.

C. *Numerical models*

A high spatial resolution weather-sea off-line coupled forecasting system was configured using High Performance Computing (HPC) infrastructure to manage and run the open-source model components WRF and WW3 running in cascade [6, 7]. The first workflow component is the atmospheric model WRF-ARW which computes the 10 m wind fields and other atmospheric parameters needed to drive the WW3 offshore wave model. In order to produce the numerical simulations presented in this paper, we configured the WRF model, initialized with the Global Forecast System (GFS) produced by the National Center for Environmental Prediction (NCEP), with two-way nested computational domains: a coarser domain ($d01_{WRF}$) covering the whole Europe and a finer domain ($d02_{WRF}$) covering the Italian peninsula, with about 25 km and 5 km spatial resolution, respectively. A two-way nesting approach was applied also to the WW3 model configuring the spatial domains $d01_{WW3}$, on the Mediterranean Sea, and $d02_{WW3}$, limited to the Italian seas, with a grid spacing with about 5 km and 1 km, respectively. The wind-wave numerical models already supported some studies on coastal dynamics [8], coastal vulnerability assessment [9] and coastal management [10], also in combination with SAR-derived field observations [11, 12].

III. EXPERIMENTAL RESULTS

During the considered storm event, as reported in Di Luccio et al.[1], the comparison between the simulated wind fields and in-situ wind observations at Livorno and Genova ISPRA weather stations show numerical wind speeds higher than 10 m/s coming from W and SW. In addition, numerical and observed pressure data both reported

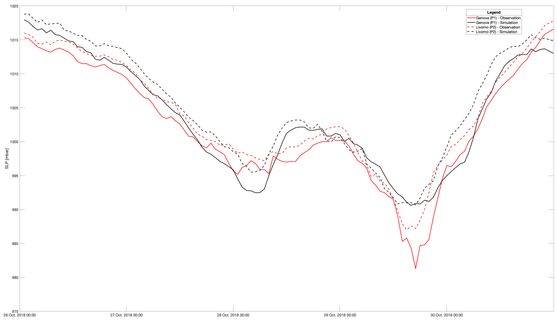

Fig. 1. Comparison between observed and simulated sea level pressure (SLP) during the period 26-30 October 2018 in P1 and P2 locations.

a significant pressure drop, down to 990 mb, see Fig. 1.

Corresponding wind speed maps were derived over the study area from the ASCAT scatterometer measurements, in order to provide reliable offshore information on the storm event. Results are shown in Figure 2, where the subfigure (a) refers to the simulated wind speed from the WRF numerical model and subfigures (b) - (d) refer to ASCAT wind speeds obtained in the mornings of 29 and 30 October, respectively. The comparison suggests that the satellite scatterometers represent a reliable source for offshore wind speed information, since they provide WS values consistent with the storm event, i. e., 20 m/s. In particular, for the reasons will be better explain in the following, the agreement between simulated and in-situ wind observations is much better for the last 30th October 2018.

IV. ACKNOWLEDGMENTS

The authors are grateful to the forecast service of the University of Napoli "*Parthenope*" (`http://meteo.uniparthenope.it`) for the HPC facilities and to CRT Toscana and ISPRA for the data providing.

REFERENCES

[1] D. D. Luccio, G. Benassai, M. de Stefano, and R. Montella, "Evidences of atmospheric pressure drop and sea level alteration in the ligurian sea," in *2019 IMEKO TC19 International Workshop on Metrology for the Sea: Learning to Measure Sea Health Parameters, MetroSea 2019*, pp. 22–27, 2020.

[2] R. D. Lindsley, J. R. Blodgett, and D. G. Long, "Analysis and validation of high-resolution wind from ascat," *IEEE Transactions on Geoscience and Remote Sensing*, vol. 54, no. 10, pp. 5699–5711, 2016.

[3] J. Verspeek, A. Verhoef, and A. Stoffelen, "Ascat-b nwp ocean calibration and validation," *OSI SAF Technical report*, 2013.

[4] A. Verhoef, M. Portabella, and A. Stoffelen, "High-

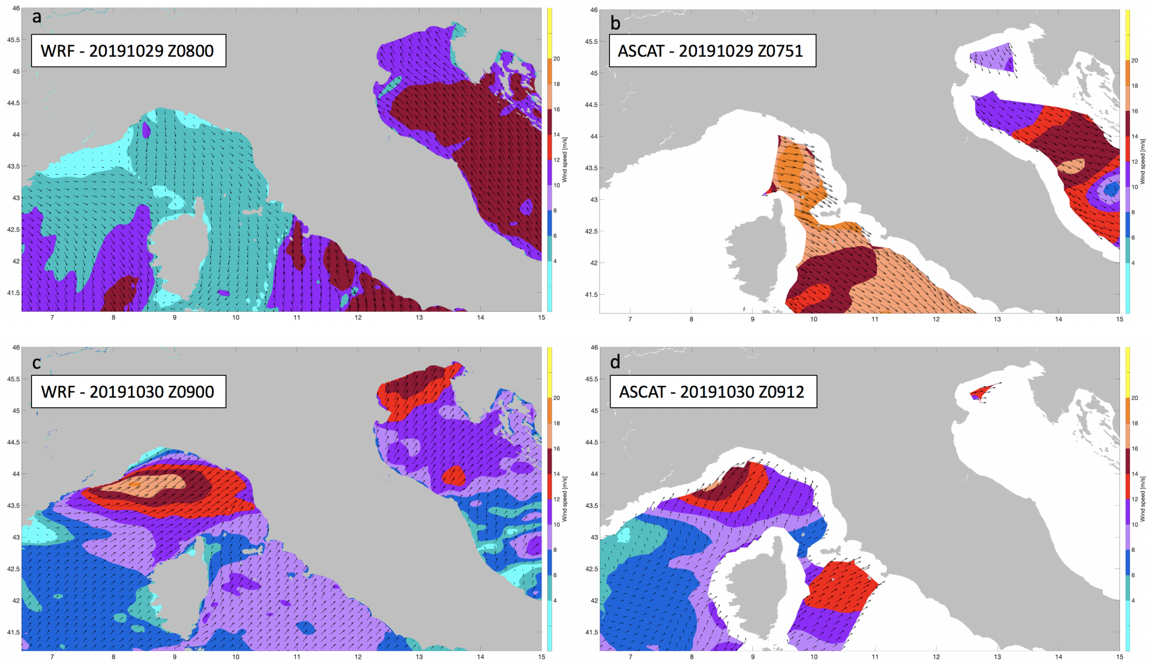

Fig. 2. WRF-based simulations versus ASCAT-based sea wind speed maps obtained over the study area during the storm event. (a) WRF 29 October 2018 at 8:00 UTC; (b) ASCAT 29 October 2018 at 7:51 UTC; (c) WRF 30 October 2018 at 9:00 UTC; (d) ASCAT 30 October 2018 at 9:12 UTC.

resolution ascat scatterometer winds near the coast," *IEEE Transactions on Geoscience and Remote Sensing*, vol. 50, no. 7, pp. 2481–2487, 2012.

[5] C. B. Hasager, "Offshore winds mapped from satellite remote sensing," *Wiley Interdisciplinary Reviews: Energy and Environment*, vol. 3, no. 6, pp. 594–603, 2014.

[6] W. C. Skamarock, J. B. Klemp, and J. Dudhia, "Prototypes for the wrf (weather research and forecasting) model," in *Preprints, Ninth Conf. Mesoscale Processes, J11–J15, Amer. Meteorol. Soc., Fort Lauderdale, FL*, 2001.

[7] H. L. Tolman *et al.*, "User manual and system documentation of wavewatch iii tm version 3.14," *Technical note, MMAB Contribution*, vol. 276, p. 220, 2009.

[8] D. Di Luccio, G. Benassai, G. Budillon, L. Mucerino, R. Montella, and E. Pugliese Carratelli, "Wave run-up prediction and observation in a micro-tidal beach," *Natural Hazards and Earth System Sciences*, vol. 18, no. 11, pp. 2841–2857, 2018.

[9] D. Di Luccio, G. Benassai, G. Di Paola, C. Rosskopf, L. Mucerino, R. Montella, and P. Contestabile, "Monitoring and modelling coastal vulnerability and mitigation proposal for an archaeological site (kaulonia, southern italy)," *Sustainability*, vol. 10, no. 6, p. 2017, 2018.

[10] G. Benassai, M. Migliaccio, and F. Nunziata, "The use of cosmo-skymed© sar data for coastal management," *Journal of Marine Science and Technology*, vol. 20, no. 3, pp. 542–550, 2015.

[11] G. Benassai, A. Montuori, M. Migliaccio, and F. Nunziata, "Sea wave modeling with x-band cosmo-skymed© sar-derived wind field forcing and applications in coastal vulnerability assessment.," *Ocean Science*, vol. 9, no. 2, 2013.

[12] G. Benassai, M. Migliaccio, and A. Montuori, "Sea wave numerical simulations with cosmo-skymed© sar data," *Journal of Coastal Research*, pp. 660–665, 2013.

2020 IMEKO TC-19 International Workshop on
Metrology for the Sea
Naples, Italy, October 5-7, 2020

Exploiting the Deep Learning Potential for Sea Plastic Detection

Sergio Vitale[1], Giampaolo Ferraioli[2], Vito Pascazio[1]

[1]*Università degli Studi di Napoli Parthenope, Dipartimento di Ingegneria*
[2]*Università dedgli Studi di Napoli Parthenope, Dipartimento di Scienze e Tecnologie,*
[sergio.vitale,giampaolo.ferraioli,vito.pascazio]@uniparthenope.it

Abstract – **Plastic debris are one of the most harmful product for the health of the marine ecosystem. Usually, they enter the oceans as macroplastics through river deltas and tend to aggregate with other materials, floating on the sea surface. With the time passing, the macroplastics tend to degrade in microplastic and enter in the marine life because of ingestion. A fast and precise detection of floating plastics is necessary for monitoring and saving the sea ecosystem. Recent studies have demonstrated how remote sensing (an din particular satellite) can be helpful in such detection. Moreover, in the recent years, deep learning (DL) methods have shown great performance particularly in classification and detection. DL methods can help to overcome some pre-processing step that are time consuming and speed-up the detection. The aim of this paper is to exploit the possibility of constructing a large database of satellite images and correspondent mask of detected plastic. Such database will be freely available in order to promote the research on this topic and on the use of DL.**

I. INTRODUCTION

The marine pollution by plastic debris is one of the most critical and emerging global issues that pros a considerable threat to the ecosystems of oceans environments. The plastic pollution is the chemical debris that requires the deeper insight from the scientific community in order to manage and mitigate the consequent threats of their related issues. Plastics are low cost and ease of manufacture synthetic materials that perhaps more than any other material has interred to marine and freshwater ecosystems all around the globe.

Thanks to the great attention moved to the global ecosystem, in the recent years plastic passed from being one of the cheapest and most useful material in the world to the most harmful product for the environment health. Most of the plastics enters the oceans through rivers outlet and starts to float in the coastal waters. The fate of these plastics is either floating in the marine environment moving to open sea or sinking. In both cases, macroplastics tend to fragment and degrade into microplastics and to enter in the marine life through ingestion. Adopting a quick strategy for detecting plastic litter and removing it is fundamental for the health of sea ecosystem.

The issue of marine plastic pollution has been revealed in the 1990s and is currently secured by some universal guidelines [1]. At present, shoreline surveys designed to identify the distributions of plastic litter in oceans and lakes are time-consuming, costly and provide limited areal coverage. Remote sensing technology has the potential to overcome the limitations of open-water and shoreline surveys. Remote sensing has the ability to monitor coastal and open-sea and to detect areas where plastic debris tend to aggregate. Remote sensing sensors mounted on drone, aircraft and satellite give the possibility to easily and rapidly investigate a large areas reducing the human intervention.

Recent studies have demonstrated the ability of optical satellites (like Sentinel-2) in detecting floating litters. The Marine Remote Sensing Group from the University of the Aegean within the Plastic Litter Projects of 2018 and 2019 [2]-[3], have placed standardised plastic objects in coastal waters and have shown the possibility to detect them from Sentinel-2 images. More recently, Bierman et. al have defined a new spectral index FDI that, combined with NDVI, allows the detection of floating debris from Sentinel-2 images after atmospheric correction. In order to validate their method, Biermann at el. have acquired images based on information given by LITTERBASE portal [5] that collects the scientific researches on plastic detection and lists the correspondent study areas.

In order to do such detection a pre-processing step is necessary: first an atmospheric correction, later a mask for removing false alarm on the land are needed.

As in many application, deep learning (DL) solutions have shown great performance in detection, classification and segmentation [6]. In order to speed up the plastic detection and make it faster, using DL technique combined with satellite data could be very useful. The drawback is it needs an huge dataset for the training phase. Thanks to the findings of *Biermann et al.* and the huge information provided by LITTERBASE, the aim of this paper is to exploit the possibility of a database construction suitable for DL based detection of floating litter debris.

Fig. 1. Detection of floating debris with FDI and NDVI: in the top optical image of Accra, Ghana; in the bottom red box zoom: optical image on the left, resulting mask on the right

II. DETECTION OF FLOATING DEBRIS

Among several methods, the most recent has been proposed in [4] where the authors propose the detection and classification of floating litters from optical data acquired by Sentinel-2. To this aim, first an atmospheric correction has been performed on the optical image, cluster of floating material (phising net, plastics, algae, etc...) have been detected by means of spectral indexes and a Naive-Baysian classificator is trained for categorising the detected plastic. They define a new spectral index named Floating Debris Index (FDI) that combined with Normalised Difference Vegetation Index (NDVI) are used for the detection. The FDI is the subtraction of the baseline reflectance of the NIR from the NIR band relying on the high reflectance of the plastic at 700 nm. In such way, the FDI allows the detection of floating materials at subpixel scale. Although, this seems a good indicator, FDI can not be used alone for the detection because it allows us to detect pixel composed of at least 30% of plastic but other materials can be present. At this point, *Biermann et al.*, found the NDVI useful for segregating floating material from others and used a combination of FDI and NDVI for the detection of floating debris composed mostly of plastic. Each material has high reflectance in a certain range of FDI and NDVI, so variation of this range allows the detection of cluster of different floating materials. An example shown in Fig.1 where floating debris where detected in the coastal waters of Accra (Ghana).

For a deeper insight, the reader is invited to refer to [4]. The method proposed by *Biermann et al.* is very useful for the detection of floating material. Anyway, it is well known that DL has reached state-of-art performance in topic such as detection, segmentation and classification of natural images. Recently, many DL algorithms have been proposed for several task such as classification, detection, denoising, super-resolution (and so) on of remote sensed images outperforming model based approach [10],[8],[7],[9]. Naturally, the good performance of DL methods is based on the presence of a good and wide training dataset.

A detection for floating debris based on DL could provide fast and accurate performance avoiding many preprocessing step that are time consuming. Nowadays, a database for detection of plastic floating is not available and its construction could produce a huge investment of the research in this topic. The aim of this paper is to use the FDI and NDVI ranges defined by *Biermann et .al* for the detection of floating debris and construct an accessible database for implementing DL solutions.

III. PROPOSE METHOD

The idea of this paper is to collect Sentinel-2 images in areas characterized by floating materials according to the information provided by the LITTERBASE portal. Once the image is acquired, detection of plastic material is performed applying the method proposed in [4]. The database will be composed of the original Sentinel-2 image and correspondent mask of detected debris. Once a wide dataset is ready, a neural network can be trained for the detection of such materials working directly on the acquired image without any atmospheric correction that is very time consuming for large image (typical of satellites images). Sentinel-2 is an optical satellite that provides thirteen bands images with spatial resolution about 20 m. The idea of using Sentinel-2 is related to two main reason. First, the image are free and so it is possible to access as many images as it is necessary. Second, the great amount of data available allows to train a network and its results can be used for transfer learning to another sensor with higher resolution and/or more bands (e.g WorldView-3 or hyperspectral sensors) but with poorer availability of data. In the final version of the paper processed data and their feasibility for detection by neural network will be shown. The construct dataset will be freely available for future research.

IV. CONCLUSION

In this paper a database construction for floating debris suitable for DL methods has been exploited. Starting from the results of method proposed by *Biermann et al*, several Sentinel-2 images will be acquired in the area indicated by the LITTERBASE portal and detection of plastic by means of the FDI and NDVI will be performed. Such results will be used as ground truth for defining a dataset composed of a satellite images and a reference mask. This dataset will be freely available and an example of neural network trained on such dataset will be provided in the final version in order to exploit the potential of such database.

REFERENCES

[1] (2019, 1-2). U.S. National Oceanic and Atmospheric Administration (NOAA). . Available: https://www.noaa.gov/

[2] Topouzelis, K., Papakonstantinou, A. Garaba, S. P.

"Detection of floating plastics from satellite and unmanned aerial systems (plastic litter project 2018).", International Journal of Applied Earth Observation and Geoinformation 79, 175?183 (2019).

[3] Plastic Litter Project 2019 dataset, Available : *https://mrsg.aegean.gr/?content=&nav=65*

[4] Biermann, L., Clewley, D., Martinez-Vicente, V. et al. "Finding Plastic Patches in Coastal Waters using Optical Satellite Data". Sci Rep 10, 5364 (2020). https://doi.org/10.1038/s41598-020-62298-z.

[5] Alfred-Wegner Institute, LITTERBASE portal, Avialable: *https://litterbase.awi.de/*

[6] Kaiming He, Georgia Gkioxari, Piotr Doll´ar, and Ross B. Girshick, ?Mask R-CNN,? CoRR, vol. abs/1703.06870, 2017

[7] Sergio Vitale and Giampaolo Ferraioli and Vito Pascazio, "Multi-Objective CNN Based Algorithm for SAR Despeckling",arXiv:2006.09050,2020.

[8] A. Budillon, A. C. Johnsy, G. Schirinzi and S. Vitale, "Sar Tomography Based on Deep Learning," IGARSS 2019 - 2019 IEEE International Geoscience and Remote Sensing Symposium, Yokohama, Japan, 2019, pp. 3625-3628, doi: 10.1109/IGARSS.2019.8900616.

[9] Sergio Vitale and Giuseppe Scarpa, ?A detail-preserving crossscale learning strategy for cnn-based pansharpening,? Remote Sensing, vol. 12, no. 3, 2020.

[10] S. Chen, H. Wang, F. Xu and Y.Q. Jin, "Target classification using the deep convolutional networks for SAR images", IEEE Trans. Geosci. Remote Sens., vol. 54, pp. 4806-4817, 2016.

2020 IMEKO TC-19 International Workshop on
Metrology for the Sea
Naples, Italy, October 5-7, 2020

Integrating AIS and SAR to monitor fisheries: a pilot study in the Adriatic Sea

Alessandro Galdelli[1], Adriano Mancini[1], Carmen Ferrà[2], Anna Nora Tassetti[2]

[1]*VRAI Lab, Dipartimento di Ingegneria dell' Informazione, Università Politecnica delle Marche, 60131 Ancona, Italy, a.galdelli@pm.univpm.it, a.mancini@univpm.it*
[2]*CNR-IRBIM, Institute of Marine Biological Resources and Biotechnologies, National Research Council, 60125 Ancona, Italy, annanora.tassetti@cnr.it*

Abstract – **The synergic utilization of data from different sources, either ground-based or spaceborne, can lead to effectively monitor fishing activities in close proximit of managed areas, and help tackle the problem of global overfishing. To this end, the integration of spaceborne Synthetic Aperture Radar (SAR) data and cooperative Automatic Identification System (AIS) information has the appealing potential to provide a better picture of what is happening at sea by detecting vessels that are not reporting their positioning data (intentionally or not) and, on the other side, by validating ships detected in satellite imagery.**

In this context, this paper deals with the investigation of "suspicious" AIS data gap and the integration of SAR-based ship detections by a point-to-point and a point-to-line types of association. Time-filtered and classified AIS transmissions (according to the gear in use) are used to predict SAR positions, with the next step being to search/match corresponding SAR-based targets. A case study is analyzed, in which the method is tested in proximity of managed areas characterized by significant AIS black-outs, using occasional Sentinel-1 images of the central Adriatic Sea and AIS data constantly collected by a proprietary antenna.

I. INTRODUCTION

Improving the Maritime Situational Awareness (MSA) and the sustainable use of oceans, seas and marine resources is nowadays of paramount importance [1] and requires monitoring tools which can provide long-term observations of fish stocks and fishing fleets' activity [2] [3].

The latter can now be monitored by several systems that can be broadly classified as cooperative or non-cooperative. Cooperative systems rely on the ships reporting information about themselves (e.g., identification, position, and speed), as it happens with Automatic Identification System (AIS), Long Range Identification and Tracking (LRIT) and Vessel Monitoring System (VMS). While these systems are powerful tools to track the self-reporting vessels, they only give a partial picture of the situation. Most small vessels do not need to carry AIS or LRIT, and small or even all fishing vessels do not carry VMS depending on the region. Moreover, positions reports can drop out for many reasons, such as weak signals, signal interference in crowded areas or intentionally turning off/tampering when entering port or in close proximity of fishery forbidden areas [4].

On the other hand, non-cooperative systems employ radar and optical sensors (coastal, shipborne, airborne, and spaceborne) to detect the ships from the background sea clutter without relying on their cooperation [5] [6] [7]. Compared with optical remote sensing, satellite Synthetic Aperture Radar (SAR) imaging appears more suited for maritime traffic surveillance in operational contexts, as it allows ship detection over wide swaths without being critically affected by weather conditions and day-night cycles [8] [9] [10] [11].

Obviously, the synergic exploitation of the above mentioned different data sources represents a breakthrough approach to strongly improve maritime situational awareness and effectively monitor of fishing activities [12] [13]. Indeed, ship-related information gathered by both cooperative and non-cooperative systems could result in the quantification and additional mapping of the non-reporting ship traffic, giving a more complete picture of vessels' activity, including Illegal, Unreported and Unregulated (IUU) fishing [14].

Considering the above, this study focuses on AIS black-outs in close-proximity of fishery managed areas, and use open-source Sentinel-1 SAR data to seek and additionally map non reporting ships that could be involved in suspect behaviour.

II. MATERIALS AND METHOD

AIS data are first processed to map transmission gaps, and investigate their overlay with known managed areas, such as the 3 nautical mile zone where the use of towed gears shall be prohibited (as defined by Article 13 of EU Council Regulation 1967/2006).

According to the management measure under investigation and the gear type that is likely to be illegally used, only some AIS report positions are retained (i.e. the ones broadcasted by trawlers) and a distance criteria is applied to match them with ship positions from SAR images. To this end, a classification process is carried out to pre-assign AIS transmissions to specific fishing gears.

A. AIS Data and Processing

AIS data are obtained by a receiver (Comar SLR300N - PHP dispatcher) that is installed on the roof of the Università Politecnica delle Marche, at a height of 205 m above sea level. Data are stored with a poll rate of 2-5 min and cover a reception distance of around 55 nm (Fig. 1).

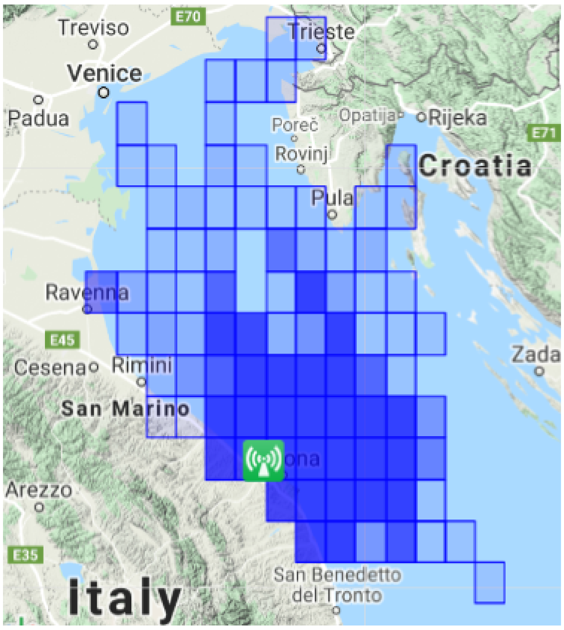

Fig. 1. AIS data coverage.

The Maritime Mobile Service Identity (MMSI) is used to create a tracking layer and values of duration and speed are computed for each segment from the difference between consecutive pings. Tracks with a duration exceeding a predefined threshold of 30 minutes are kept and considered as black-out tracks and gaps in AIS data coverage. Annual black-outs are aggregated intersecting the over mentioned tracks with a 1-km grid, spatial joining each cell with overlapping track portions, and summing relative duration values (hours, Fig. 2)

For each vessel individual trips are first identified, from the time vessels leave ports until they return, and then characterized by a machine learning approach with a boosting algorithm (Fig. 3) that identifies the type of fishing when it occurs, according to pre-defined gear classes: bottom otter trawl, beam trawl, pelagic trawl, purse seine, longline, and other (including cargo and cruise vessels). The Fourier transformation is applied on position and course data and

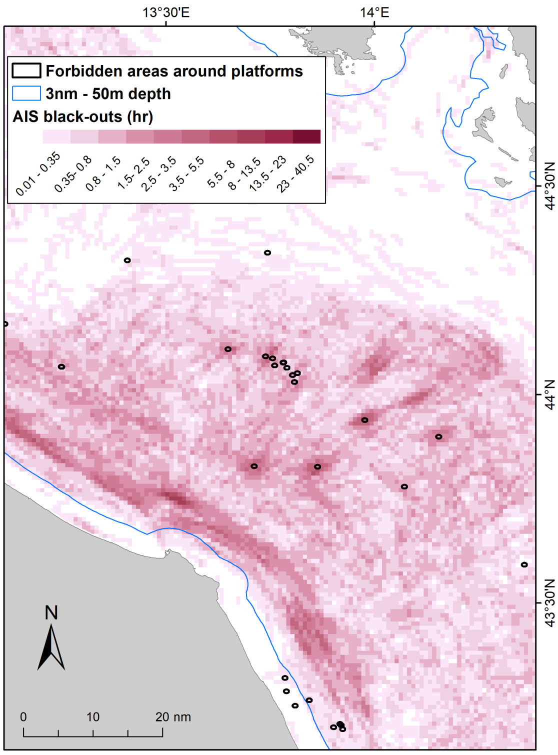

Fig. 2. Aggregated AIS black-outs (1kmx1km grid).

the performance improved by subdividing the spectrum twice into 20 and 100 power sub-bands from which additional features (median, maximum and area) can be extracted.

Trip by trip, the classification algorithm is executed to label single trips according to the gear class showing the highest accuracy index.

B. SAR Data and Processing

The Constant False Alarm Rate (CFAR) approach developed by Mancini et al., 2013 [15] for ship detection and CosmoSkyMed data, is adapted to Sentinel-1 images. The approach is based on the use of integral images and allows to directly manage the presence of masked pixels/invalid data while reducing the computational time. It significantly boosts he performance up to 50x even in case of very high resolution images and large kernels.

The output of the data-processor is a list of georeferenced centroids of the detected ship pixels (Fig. 4), with an estimation of the vessel size. This length estimation is used to filter out targets that are likely too long to be a fishing vessel.

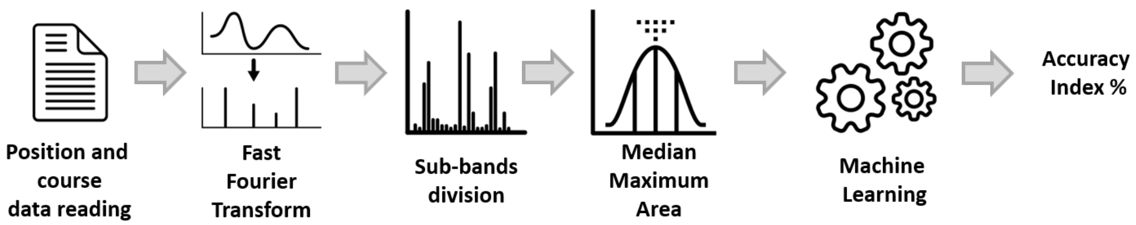

Fig. 3. Classification Vessel Algorithm.

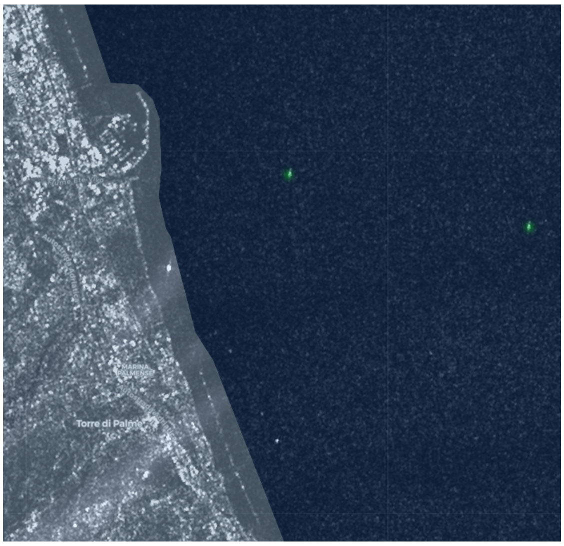

Fig. 4. Example of Sentinel-1 image (Central Adriatic coast, July 2020) and ship detection by CFAR. Land mask is overlaid with stretched SAR amplitude data, while green pixels represent detected ships.

C. AIS-SAR Matching and Data Integration

To integrate AIS and SAR data, a point-to-point type of association is used to assess if a vessel detected by SAR is correlated with an AIS position within a given time-frame, while a point-to-line type of association is attempted in case of AIS black-outs. We identify the following main cases:

- Case #1: the SAR-based estimated vessel location is within a buffer area centered on AIS data. The buffer distance is calculated considering the distance travelled in the time frame of N AIS pings at v speed.
- Case #2: A SAR target is detected but with no AIS report available. This could be caused by a transmission problem or a voluntary switching off. An attempt is done to associate the SAR target to the nearest black track, by drawing an ellipse with the greater axle coinciding with the black track (connecting the ping immediately before the switching off and the one immediately after the power on).
- Case #3: A SAR target is missed even if AIS data is available. It is due to the failure of the vessel detection algorithm.

The values of N is set to 2 (consisting in about 6 minutes), while v is intended, case by case, as the speed of the vessel that is suspected to be fishing (i.e. 2.5-3.5 kn for trawlers).

While Case #1 validates the performance of the SAR-based detection algorithm, Case #2 discriminates collaborative and non-collaborative ships, playing a key-role to detect potential suspect behaviours in a given area.

Of course from a single satellite image is not possible to state that a given fishing vessel is really performing illegal activities. Nevertheless, the positions detected by SAR can be correlated with AIS black-outs to reveal previously unmonitored dark vessels.

III. DISCUSSION

The Boosting algorithm shows a good accuracy of around 95.4%, allowing to assign fishing gears and simplify the AIS-SAR target association by reducing the set of ship positions from AIS data to match. On the other hand, the capability to fast process large remote sensed images and the good performance shown by the SAR-based detection algorithm gives substance to the whole proposed monitoring approach.

Even if the quality of AIS-SAR data matching strongly depends on the density of the ships in the area of interest and on the time lag between AIS and SAR data collection, preliminary results suggest that the proposed approach could help monitor fishing activity and rate the effectiveness of fishery-regulated areas, which is critical in the context of the global overfishing problem.

IV. ACKNOWLEDGEMENTS

Authors would thank the Prof. E. Gambi and Dr. A. De Santis at the Department of Information Engineering of Università Politecnica delle Marche for the AIS data acquisition and pre-processing (http://www.ais.dii.univpm.it).

REFERENCES

[1] United Nation. Transforming our world: The 2030 agenda for sustainable development; resolution adopted by the general assembly. UN: Rome, Italy, 2015.

[2] U. Kanjir, H. Greidanus, and K. Oštir. Vessel detection and classification from spaceborne optical images: A literature survey. *Remote Sensing of Environment*, 207:1–26, March 2018.

[3] N. Kourti, I. Shepherd, H. Greidanus, M. Alvarez, E. Aresu, T. Bauna, J. Chesworth, G. Lemoine, and G. Schwartz. Integrating remote sensing in fisheries control. *Fisheries Management and Ecology*, 12(5):295–307, October 2005.

[4] A.N. Tassetti, C. Ferrà, and G. Fabi. Rating the effectiveness of fishery-regulated areas with ais data. *Ocean and Coastal Management*, 175:90–97, 2019.

[5] C. Dechesne, S. Lefèvre, R. Vadaine, G. Hajduch, and R. Fablet. Ship identification and characterization in sentinel-1 sar images with multi-task deep learning. *Remote Sensing*, 11(24), 2019.

[6] J. Duan, Y. Wu, and J. Luo. Ship classification methods for sentinel-1 sar images. *Lecture Notes in Electrical Engineering*, 571 LNEE:2259–2269, 2020.

[7] H. Greidanus. Satellite Imaging for Maritime Surveillance of the European Seas. In V. Barale and M. Gade, editors, *Remote Sensing of the European Seas*, pages 343–358. Springer Netherlands, Dordrecht, 2008.

[8] A. Grover, S. Kumar, and A. Kumar. Ship detection using sentinel-1 sar data. *ISPRS Annals of Photogrammetry, Remote Sensing and Spatial Information Sciences*, IV-5:317–324, 11 2018.

[9] V. Fernandez Arguedas P. Argentieri M. Alvarez H. Greidanus C. Santamaria, M. Stasolla. Sentinel-1 maritime surveillance. Technical report, European Union, 2015.

[10] C. Santamaria, M. Alvarez, H. Greidanus, V. Syrris, P. Soille, and P. Argentieri. Mass processing of sentinel-1 images for maritime surveillance. *Remote Sensing*, 9:678, 07 2017.

[11] H. Tanveer, T. Balz, and B. Mohamdi. Using convolutional neural network (cnn) approach for ship detection in sentinel-1 sar imagery. 2019.

[12] M. D. Graziano, A. Renga, and A. Moccia. Integration of Automatic Identification System (AIS) Data and Single-Channel Synthetic Aperture Radar (SAR) Images by SAR-Based Ship Velocity Estimation for Maritime Situational Awareness. *Remote Sensing*, 11(19):2196, September 2019.

[13] B. Snapir, T.W. Waine, and L. Biermann. Maritime vessel classification to monitor fisheries with sar: Demonstration in the north sea. *Remote Sensing*, 11(3), 2019.

[14] A. Kurekin, B. Loveday, O. Clements, G. Quartly, P. Miller, G. Wiafe, and K. Agyekum. Use of sentinel-l and sentinel-2 for monitoring illegal fishing off ghana. pages 6875–6878, 07 2018.

[15] A. Mancini, A.N. Tassetti, A. Cinnirella, E. Frontoni, and P. Zingaretti. A novel method for fast processing of large remote sensed image. *Lecture Notes in Computer Science (including subseries Lecture Notes in Artificial Intelligence and Lecture Notes in Bioinformatics)*, 8157 LNCS(PART 2):409–418, 2013.

5

Special Session
Advanced techniques and emerging trends in ecoinformatics applied to data analysis for marine turtles, cetaceans, seahorses and pipefishes

Human activities on pelagic and benthic domains in offshore, coastal and transitional waters have repercussions on different emblematic species as the marine turtles, cetaceans, seahorses and pipefishes which result particularly vulnerable to cumulative impacts. Descriptive, interpretative and predictive models to assess their conservation status need a large amount of biotic and abiotic data extending from biological cycles to habitat use as well as from the incidence of local anthropogenic threats and global changes. To that regard, emerging topics in eco-informatics could highlight enormous benefits from the integration of bio-ecology with the information science and the applied technology, which allows a rapid development of a variety of strategies devoted to maintaining marine biodiversity and ecosystems services. This session is focused on the most advanced and emerging statistical techniques and technology applied to the integration of biological and environmental data oriented to the conservation of marine turtles, cetaceans, seahorses and pipefishes. Contributions with sound methodologies and/or applications are particularly welcomed.

2020 IMEKO TC-19 International Workshop on
Metrology for the Sea
Naples, Italy, October 5-7, 2020

Top-down cascading effects driven by the odontocetes in the Gulf of Taranto (Northern Ionian Sea, Central Mediterranean Sea)

Ricci P.[1,2], Ingrosso M.[1], Cipriano G. [1,2], Fanizza M.[3], Maglietta R.[4], Renò V. [4], Tursi A. [1,2], Carlucci R. [1,2]

[1] *Department of Biology, University of Bari, Via Orabona 4, Bari, Italy, email: pasquale.ricci@uniba.it; m.ingrosso14@studenti.uniba.it; giulia.cipriano@uniba.it; angelo.tursi@uniba.it; roberto.carlucci@uniba.it*
[2] *CoNISMa, Piazzale Flaminio 9, Rome, Italy*
[3] *Jonian Dolphin Conservation, Viale Virgilio,102 - 74121 Taranto, Italy, e-mail: carmelo@joniandolphin.it*
[4] *Institute of Intelligent Industrial Systems and Technologies for Advanced Manufacturing, National Research Council, Via Amendola 122 D/O, Bari, Italy, e-mail: rosalia.maglietta@cnr.it; vito.reno@cnr.it*

***Abstract* – An investigation of the marine food web in the Gulf of Taranto (Northern Ionian Sea, Central Mediterranean Sea) was carried out to explore the top-down cascading effects driven by the Odontocetes. The food web was analysed by a mass-balance model using 51 functional groups and detailing the trophic impacts of the striped and common bottlenose dolphins, the Risso's dolphin and the sperm whale during the period 2010-2014. Odontocetes resulted top-predators with the highest TL estimated for the Risso's dolphin (TL=5.40) and the lowest for the common bottlenose dolphin (TL=4.47). The striped dolphin played the highest top-down controls, which showed cascading effects up to the 3rd TL. The Risso's dolphin and the sperm whale played similar cascading effects, but weaker than the striped dolphin. Understanding pattern and strengthen of trophic controls played by the Odontocetes within the food web could contribute to identify the basal mechanisms involved in the ecosystem functioning.**

I. INTRODUCTION

Predation changes the abundances of prey species influencing their interactions and behaviours in the basal levels of the food web [1]. Thus, the identification of top-down controls and their propagation towards the base of the food web is a critical point to assess the trophic cascades. In marine ecosystems, evidences of cascading effects have been detected in the pelagic domain [2], [3], [4] and the variability in the strength of cascades has been investigated (see [5] and reference therein). However, the investigation of cascading effects in large marine ecosystems remains a critical issue due to the difficulty to apply field experiments, the scarcity of standardized data and the complexity of the food web. Not least, the methodological challenge of assessing ecosystem scale processes is also represented by the need to involve the field of marine ecology, fisheries and oceanography sciences with expert of analytic tools integrating several information [6]. In this contest, the ecological models based on holistic approach resulted more effective to describe the predation and fishing interactions in the trophic cascade process (i.e. [7]). In particular, the mass-balance models allow to estimate indicators of both direct and indirect trophic impacts between the species (or group of species), providing information on the kind of trophic controls and their propagation through trophic levels.

Odontocetes as top predators are firmly recognized for their ecological role in the marine food webs [8]. This condition is generally ensured by their activation of trophic cascades, which are indirect strong top-down cascading effects played by the apex predators on two or more trophic levels [4]. However, the mechanism of such kind of activation and its strength, as well as the impact of fishing competition, the anthropogenic threats and the global change effects on the trophic cascades are still unknown in many marine ecosystems.

In the Gulf of Taranto (Northern Ionian Sea, Central Mediterranean Sea), a significant number of cetacean species coexist with several anthropogenic pressures, such as fishery, industrial discharges, marine traffic and navy exercise areas [9]. In particular, the striped dolphin (*Stenella coeruleoalba,* considered as "Vulnerable" in the IUCN Red List) results the most abundant species [10], followed by the common bottlenose dolphin (*Tursiops truncatus*), the sperm whale (*Physeter macrocephalus*) both listed as "Vulnerable" in the IUCN Red List and the

Risso's dolphin (*Grampus griseus*, considered as "Data Deficient" in the IUCN Red List) [11], [12]. These odontocetes were identified as apex predators and a keystone group in the food web of the North-western Ionian Sea [13], but information on the top-down controls played by each single species are still unknown. The main goal of this study is to explore the cascading effects driven by odontocetes and their top-down controls in the food web of the Gulf of Taranto.

II. MATERIALS AND METHODS

A. Study area

The Gulf of Taranto (GoT) is extended approximately for 14.000 km² in the Northern Ionian Sea (Fig. 1). The area is characterized by a complex geomorphology resulting in a large submarine canyon and sensitive habitats distributed in the shelf and deep zones. Several anthropogenic pressures insist on the basin such as fishery, navy exercises, marine traffic and industrial activities [9]. The food web model of the GoT included an area of about 7745 km^2 from Punta Alice up to S. Maria di Leuca, in a range of 10-800 m of depth.

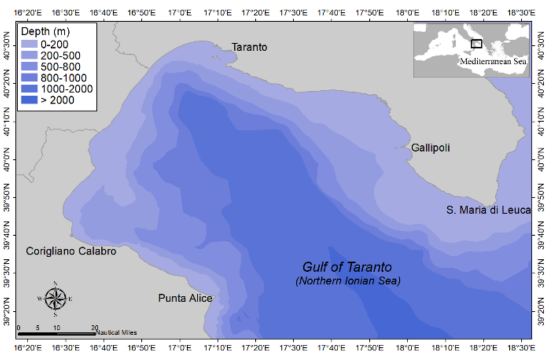

Fig. 1. The Gulf of Taranto in the Northern Ionian Sea.

B. Food-web model approach and data collection

The Ecopath with Ecosim (EwE) modelling approach [14] was used to describe the mass-balance of the food web in the GoT. Food webs are described by means of Functional Groups (FGs), each representing a group of species with similar ecological traits, a single species or a life stage of a species. The FGs can represent consumers, autotrophs and non-living compartments (e.g. organic matter), and links between FGs are formally described by a set of linear equations, one for each FG, representing the balance of energy and matter expressed as:

$$B_i \cdot \left(\frac{P}{B}\right)_i * EE_i - \sum_{j=1}^{n} B_j * \left(\frac{Q}{B}\right)_j * DC_{ij} - Y_i - E_i - BA_i = 0 \quad (1)$$

where Bi is the biomass of group (i), $(P/B)_i$ is the production of (i) per unit of biomass; the consumption i by the other FGs of the food web is then represented through $(Q/B)_j$ the consumption per unit of biomass of all j predators the proportion of (i) in the diet composition of predator (j) in terms of biomass (DC_{ij}); other losses on group i are represented by fishery catches, Y_i, the net migration rate E_i and eventually the biomass accumulation BA_i. The parameter EE_i represents the ecotrophic efficiency, i.e., the proportion of the production of group (i) which is utilized within the system modelled [15]. Energy balance for each group is also ensured by equating its consumption (Q/B_i) with the sum of production (P/B_i), respiration (R/B_i) and unassimilated food ($U/Q*Q/B_i$). The system of equations is solved according to several ecological constrains by providing EwE with diet composition, the unassimilated food, the catches, the exports for each group and three of the basic parameters B_i, $(P/B)_i$, $(Q/B)_i$ and EE_i [14]. The solution provides a snapshot of the trophic flows within the ecosystem (further details on EwE modelling approach can be found in review literature as [15], [16].

A total 51 FGs described the GoT food web detailing the pelagic, demersal, benthic, planktonic domains (or compartments). The striped and common bottlenose dolphins, Risso's dolphin and sperm whale were represented as 4 individual FGs. The demersal and benthopelagic domains are described by a total of 276 sampled species the "MEDiterranean International Trawl Survey" (MEDITS time series 1995-2015, [17]) and, successively, they were aggregated into 29 FGs identified by a reiterative aggregation method, based on similarity in quantitative diet information and the bathymetric distribution of species (see [13] for more details). Moreover, a total of 5 FGs described the planktonic domain (the phytoplankton, the bacterioplankton, the macrozooplankton, the meso-microzooplankton and the gelatinous plankton); 6 FGs the pelagic domain (the fin whale, the loggerhead turtle, the seabirds and the large, medium and small pelagic fishes) and, 4 FGs the benthic domain (the macrobenthic invertebrates, the polychaetes, the suprabenthic crustaceans and the seagrasses and seaweeds). In the last, the non-living matter was represented by 3 groups.

The GoT model was developed for a period of 4 years (2010-2014) using a wide set of input data obtained from several data collections. The diets used for *S. coeruleoalba*, *T. truncatus* and *G. griseus* were mostly derived from the stomach contents analysed in the North Aegean Sea [18]. Starting from these diets used as a baseline, additional food items were also integrated from the literature, when available, to improve the robustness of the input information. In fact, for *T. truncatus* and *G. griseus* food items were added from the Western Mediterranean areas [19], [20], whilst for *S. coeruleoalba* from the Ionian Sea [21]. The diet information for the *P.*

macrocephalus was derived from the Ligurian Sea [22]. The biomass estimates of the 4 investigated odontocetes were derived from abundance data ($N \cdot km^{-2}$) collected during monitoring surveys carried out in the Gulf of Taranto since 2009 (e.g. [10], [23]) and values of mean individual weight [13]. Biomass estimates (in t km^{-2} of wet weight) for many fish species, cephalopods and crustaceans were obtained from the MEDITS trawl surveys carried out during the period 1995-2015 [13]. The biomasses, diet information and productivity and consumption rates of all other FGs were obtained by the previous food web model realized in the area [13].

The fishing activities were described by 5 fishing gears: trawls, long lines, nets, other gears and purse seines. Landings for each gear by species were obtained by the Fisheries and Aquaculture Economic Research for the Ministry of Agricultural Food and Forestry Policies (MIPAAF). Discard was estimated by the available discard rates in literature [24], [25] and using the proportion of commercial and non-commercial discards in MEDITS catches for the no commercial species harvested by the trawl [13].

Balancing steps of the model were carried out to assess the coherence of the input data with the basic thermodynamic laws, rules and principles of ecosystem ecology at the system level [16].

C. Ecological Indicators

The trophic level (TL, [26]) is calculated by the following equation:

$$TLi = 1 + \sum_j (TL_j * DC_{ij}) \qquad (2)$$

TL is a fractional number giving the position of each functional group in its food web, and estimated by Ecopath based on the diet composition (DC) of the group and the TL of its prey items (starting with a TL of 1 assigned to producers and detritus).

The top-down controls and the importance of the odontocetes in the food web were assessed by means the Mixed Trophic Impact analysis (MTI, [27]) and the Keystoness Index (KS). The MTI quantifies the relative impact of biomass change within a component (impacting group) on each of the other components (impacted groups) in the food web. Positive/negative MTI values indicate an increase/decrease in biomass of the group j due to a slight increase in biomass of the impacting group i. Therefore, negative impacts can be associated to prevailing top-down effects and positive ones to bottom-up effects [28]. The MTI provides estimates of the overall effect (ε_i) of the trophic impact component, that together with the relative biomass component (p_i) is used to estimate KS. The overall effect of a group i represents all the direct or indirect trophic impacts of group i on all the other groups in the food web:

$$\varepsilon_i = \sqrt{\sum_{j=1}^{n} m_{ij}^2} \quad (3)$$

where the impact on the group itself (m_{ij} with i=j) is not considered, and ε_i is calculated as a relative value with respect to the maximum [28]. The parameter p_i is the relative biomass of the group in the food web, excluding detritus biomass:

$$p_i = \frac{B_i}{\sum_{k=1}^{n} B_i} \qquad (4)$$

Thus, the KS is expressed as:

$$KS_i = IC_L \times BC_0 \qquad (5)$$

where IC_L (Impact Component) is estimated by means of the ε_i and BC_0 (the Biomass Component) is estimated from p_i, where BC_0 is the biomass in a descending order ranking [29]. In order to assess the cascading effects along the TLs due to the top-down controls of the Odontocetes, the MTI values of each FGs impacted by the Odontocetes (m_{ij} with i=cetaceans and j=all other FGs) was weighted with the proportion of flows of group j belonging to integer TLs calculated by Ecopath’ s routine. In addition, the trophic impacts were assessed at scale of domains: Pelagic, Demersal (Shelf, Shelf- Break and Slope), Benthic and Planktonic. FGs impacted by the odontocetes were aggregated in their own domains. In the end, direct positive impacts on the preys were assessed for each odontocetes, in order to identify the condition of “beneficial predator” [27]. Direct impacts were considered as the impacts on the FGs consumed by the odontocetes (identified by the preys in their diet information).

III. RESULTS

Odontocetes resulted top-predators within the GoT food web, with the highest TLs estimated for the Risso’s dolphin (TL=5.40) and the sperm whale (TL=5.16), followed by the striped dolphin (TL=4.71) and common bottlenose dolphin (TL=4.47).

The striped dolphin showed the highest value among odontocetes (KS=1.31) resulting in the 2nd position of the KS rank. The Risso’s dolphin was in the 4th position (KS=1.13), the sperm whale in the 11th (KS=0.89) and the common bottlenose dolphin in the 15th (KS=0.84). The 1st position in the rank was occupied by the bathyal squids (e.g. *Todarodes sagittatus*, *Histioteuthis* spp.).

The striped dolphin played the highest negative and positive impacts, which showed a clear cascading effect up to the 3rd TL (Fig. 2). The Risso’s dolphin and sperm whale showed similar cascading effects, but with values smaller than the striped dolphin. All these species exerted negative impacts higher than their positives on the FGs placed in the 5th and 4th TLs. On the contrary, the positive impacts on the groups of the 3rd TL resulted higher than the negatives. The common bottlenose dolphin showed negative impacts on the groups of the 3rd TL but without a clear pattern in the cascading effects.

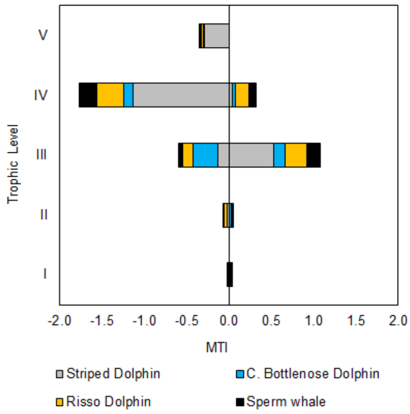

Fig.2. The Mixed Trophic Impact (MTI negative and positive) estimated for the odontocetes with the FGs impacted aggregated by discrete trophic levels.

The striped dolphin showed both the highest negative and positive impacts on the pelagic FGs (< −0.5) and on all demersal FGs (> 0.1), respectively (Fig. 3). High negative impacts were also detected on the shelf-break and slope demersal FGs. *T. truncatus* played negative impacts on all demersal FGs and small positive impacts on all domains, excluding the benthic one. *G. griseus* showed its highest negative and positive impacts on the slope demersal FGs, and positive impacts were detected on both pelagic and the shelf and shelf-break demersal FGs. *P. macrocephalus* played high negative impacts on both the pelagic and slope demersal FGs. Excluding the *T. truncatus*, all odontocetes exerted small negative impacts on the planktonic FGs.

Striped dolphin was the most important beneficial predator, with direct positive impacts on 9 FGs, such as bathyal benthic cephalopods (e.g. Sepiolidae), shelf demersal benthivorous fishes (e.g. *Mullus surmuletus*, *Pagellus acarne*, *Gobius* spp.) and Macrourids.

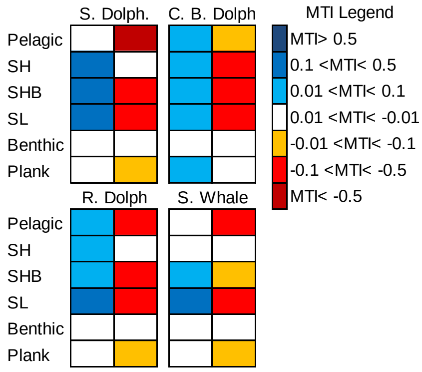

Fig.3. The Mixed Trophic Impact (MTI negative and positive) estimated for the odontocetes with the FGs impacted aggregated in Pelagic, Demersal (Shelf SH, Shelf- Break SHB and Slope SL) Benthic and Planktonic (Plank) domains.

IV. DISCUSSIONS AND CONCLUSIONS

This study represents an attempt to identify top-down controls played by the Odontocetes detailing the pattern and strength of cascading effects induced by their predation activities in the food web of the Gulf of Taranto. The trophic levels estimated for the Odontocetes (TL>4.4) indicated their status of apex predators generally in line with the trophic levels estimated in the Mediterranean areas [30]. The role of striped dolphin in the top-down cascading effects resulted more evident than those estimated for other Odontocetes. Likely, this condition is due to its greater abundance in the study area, where the species performs its entire life cycle [10], [23]. In addition, the feeding preferences and the magnitude of trophic interactions of *S. coeruleoalba* could be another key element. In fact, the striped dolphin plays top-down controls on other keystone species distributed in the middle trophic levels (e.g. mesopelagic fishes and small bathyal squids). Preferential trophic interactions could also explain the cascading effects detected for the Risso's dolphin and sperm whale. In fact, both species are characterized by a specific predation on the bathyal squids, which are the most important keystone species identified in the food web. This strong interaction between large Odontocetes and benthopelagic cephalopods was observed in western Mediterranean Sea by means similar food web models [31]. Moreover, the top-down cascading effect induced by the predation of the sperm whale on the large squids was detected in the Pacific Ocean [32]. Notably, the cascading effects have been detected up to the third trophic level, while below this level the effects seem to be very negligible. This observation was also detected in the analysis on the planktivorous fishes, zooplankton and phytoplankton interactions [3]. Not least, the dominance of bottom-up controls (resource limitation) in the marine systems could be a masking factor of the top-down controls (see [6]). However, in peculiar contexts, where a great decrease of dolphins and overfishing conditions are simultaneous, the strength of this control can be amplified and the cascading effects can also influenced the phytoplankton abundance, as reported in the Black Sea [7]. Although the strength of top-down controls seems to vanish below the 3rd levels, weak negative effects have been detected on the planktonic domain. This observation has been provided by the assessment of the top-down controls aggregating the impacted FGs in the domains. Thus, effects due to the predation activities seems also to propagate in different compartments and along the depth gradient. For instance, even if the striped dolphin feeds on mesopelagic preys distributed on the slope, they determined positive effects even on the shallowest demersal species. However, further investigations are required to better understand the mechanisms of this propagation, which are linked to the degree of connectance among species, the feeding strategies and the changes in the preys' and predators' distribution during the life-cycles [33].

Finally, the condition of beneficial predator identified for the striped dolphin represents a new observation for the food web in the investigated area, highlighting the importance of the predation on the equilibrium dynamic of the trophic structure.

The understanding of the relationships between trophic controls played by the odontocetes and the changes in the species abundance in the food web could contribute to identify the basal mechanisms involved in the ecosystem functioning. The knowledge obtained by such kind of studies seems to be very informative mostly for the implementation of conservation and management plans of marine resources according to the goals for Sustainable Development of the United Nations (Goal 14, Life below water) [34] and the EU Marine Strategy Framework Directive [35].

REFERENCES

[1] J.A.Estes, J.Terborgh, J.S.Brashares, Power, J.Berger, W.J.Bond, S.R.Carpenter, T.E.Essington, R.D.Holt, J.B.C.Jackson, et al., "Trophic downgrading of planet earth", Science, 2011, 333, 301–306.

[2] J.A.Estes, M.T.Tinker, T.M.Williams, D.F.Doak, "Killer whale predation on sea otters linking oceanic and nearshore environments", Science, 1998, 282, 473–476.

[3] F.Micheli, "Eutrophication, fisheries, and consumer-resource dynamics in marine pelagic ecosystems", Science, 1999, 285, 1396–1398.

[4] M.L.Pace, J.J.Cole, S.R.Carpenter, J.F.Kitchell, "Trophic cascades revealed in diverse ecosystems", Trends in Ecology & Evolution, 1999, Volume 14, Issue 12, Pages 483-488. https://doi.org/10.1016/S0169-5347(99)01723-1.

[5] J.B.Shurin, and E.W.Seabloom, "The strength of trophic cascades across ecosystems: predictions from allometry and energetics", Journal of Animal Ecology, 2005, 74: 1029-1038.

[6] J.K.Baum and B.Worm, "Cascading top-down effects of changing oceanic predator abundances", Journal of Animal Ecology, 2009, doi.org/10.1111/j.1365-2656.2009.01531.x.

[7] G.M.Daskalov, A.N.Grishin, S.Rodionov, V.Mihneva, "Trophic cascades triggered by overfishing reveal possible mechanisms of ecosystem regime shifts", Proceedings of the National Academy of Sciences, Jun 2007, 104 (25) 10518-10523; DOI: 10.1073/pnas.0701100104.

[8] N.Hammerschlag, O.Schmitz, A.Flecker, K.Lafferty, A.Sih, T.Atwood, A.Gallagher, D.Irschick, R.Skubel, S.Cooke, "Ecosystem Function and Services of Aquatic Predators in the Anthropocene", Trends in Ecology & Evolution, 2019, 34. 369-383. 10.1016/j.tree.2019.

[9] R.Carlucci, C.Fanizza, G.Cipriano, C.Paoli, T.Russo, P.Vassallo., "Modeling the spatial distribution of the striped dolphin (*Stenella coeruleoalba*) and common bottlenose dolphin (*Tursiops truncatus*) in the Gulf of Taranto (Northern Ionian Sea, Central-eastern Mediterranean Sea)", Ecological Indicators, 2016, 69 707–721.

[10] R.Carlucci, G.Cipriano, C.Paoli, P.Ricci, C.Fanizza, F.Capezzuto, P.Vassallo, "Random Forest population modelling of striped and common-bottlenose dolphins in the Gulf of Taranto (Northern Ionian Sea, Central-eastern Mediterranean Sea), Estuarine, Coastal and Shelf Science, 2018a, Volume 204, Pages 177-192, ISSN 0272-7714, https://doi.org/10.1016/j.ecss.2018.02.034.

[11] R.Carlucci, L.Maglietta, G.Buscaino et al "Review on research studies and monitoring system applied to cetaceans in the Gulf of Taranto (Northern Ionian Sea, Central-Eastern Mediterranean Sea)", Conference: 14th IEEE International Conference on Advanced Video and Signal Based Surveillance (AVSS), Lecce 29 August 01 September 2017. doi: 10.1109/AVSS.2017.8078473.

[12] R.Carlucci, A.A.Baş, P.Liebig, et al., "Residency patterns and site fidelity of *Grampus griseus* (Cuvier, 1812) in the Gulf of Taranto (Northern Ionian Sea, Central-Eastern Mediterranean Sea)", Mammal Research, 2020, https://doi.org/10.1007/s13364-020-00485-z.

[13] P.Ricci, S.Libralato, F.Capezzuto, G.D'Onghia, P.Maiorano, L.Sion, A.Tursi, C.Solidoro, R.Carlucci, "Ecosystem functioning of two marine food webs in the NorthWestern Ionian Sea (Central Mediterranean Sea)", Ecology and Evolution, 2019, 9.

10.1002/ece3.5527.

[14] V.Christensen, C.Walters, D.Pauly, R.Forrest, "Ecopath with Ecosim 6: A user's guide", Vancouver, BC: Fisheries Centre, University of British Columbia, 2008.

[15] V.Christensen and C.Walters, "Ecopath with Ecosim: methods, capabilities and limitations", Ecological Modelling, 2004, 172 (2-4): 109-139.

[16] J.J.Heymans, M.Coll, J.S.Link, S.Mackinson, J.Steenbeek, C.Walters, V.Christensen, "Best practice in Ecopath with Ecosim food‐web models for ecosystem‐based management", Ecological Modelling, 2016, 331, 173‐184. https ://doi.org/10.1016 /j.ecolm odel.2015.12.007.

[17] M.T.Spedicato, E.Massutì, B,Merigot, G.Tserpes, A.Jadaud, G.Relini, "The MEDITS trawl survey specifications in an ecosystem approach to fishery management" Scientia Marina, 2019, 83 S1, 9-20.

[18] C.Milani, A.Vella, P.Vidoris, A.Christidis, E.Koutrakis, A.Frantzis, et al., "Cetacean stranding and diet analyses in the North Aegean Sea (Greece)", Journal of the Marine Biological Association of the UK, 2018, 98, 1011‐1028.

[19] C.Blanco, O.Salomón, J.Raga, "Diet of the bottlenose dolphin (*Tursiops truncatus*) in the Western Mediterranean Sea", Journal of the Marine Biological Association of the UK, 2001, 81. 1053 - 1058. 10.1017/S0025315401005057.

[20] C.Blanco, A.M.Raduán, J.A.Raga, "Diet of Risso's dolphin (*Grampus griseus*) in the western Mediterranean Sea", Scientia Marina, 2006, 70(3):407-411.

[21] G.Bello, "Stomach content of a specimen of *Stenella coeruleoalba* (Cetacea: Delphinidae) from the Ionian Sea", Società Italiana Scienze Naturali Museo Civico di Storia Naturale, 1993, 133:41-48.

[22] F.Garibaldi and M.Podestà, "Stomach contents of a sperm whale (*Physeter macrocephalus*) tranded in Italy (Ligurian Sea, north-western Mediterranean)", Journal of Marine Biology Association UK, 2014, 94(06):1087-1091.

[23] R.Carlucci, P.Ricci, G.Cipriano, C.Fanizza, "Abundance, activity and critical habitat of the striped dolphin *Stenella coeruleoalba* in the Gulf of Taranto (northern Ionian Sea, central Mediterranean Sea)", Aquatic Conservation: Marine and Freshwater Ecosystems, 2018b, 28:324–336.

[24] G.D'Onghia, F.Mastrototaro, A.Matarrese, C.Y.Politou, C.Mytilineou, "Biodiversity of the upper slope demersal community in the eastern Mediterranean: preliminary comparison between two areas with and without trawl fishing", Journal of Northwestern Atlantic Fishery Science, 2003, 31: 263-273.

[25] K.Tsagarakis, A.Palialexis, V.Vassilopoulou, "Mediterranean fishery discards: Review of the existing knowledge", ICES Journal of Marine Science, 2014, 71(5), 1219‐1234. https ://doi.org/10.1093/icesj ms/fst074.

[26] W.E.Odum and E.J.Heald, "The detritus-based food web of an estuarine mangrove community", In: Estuarine research, 1975, pp. 265-286, Ed. by L. E. Cronin, Academic Press, New York, Vol. 1.

[27] R.E.Ulanowicz and C.J.Puccia, "Mixed trophic impacts in ecosystems", Coenoses, 1990, 5: 7-16.

[28] S.Libralato, V.Christensen, D.Pauly, "A method for identifying keystone species in food web models", Ecological Modelling, 2006, 195: 153–171.

[29] A.Valls, M.Coll, V.Christensen, "Keystone species: toward an operational concept for marine biodiversity conservation", Ecological Monographs, 2015, 85: 29-47. doi:10.1890/14-0306.1.

[30] K.Kaschner, K.I.Stergiou, G.Weingartner, S.Kumagai "Trophic levels of marine mammals and overlap in resource utilization between marine mammals and fisheries in the Mediterranean Sea", In: Briand F (ed) Investigating the Role of Cetaceans in Marine Ecosystems. CIESM (Commission Internationale pour l'Exploration Scientifique de la Mer Mediterranee, CIESM Workshop Monographs, 2004, 25, pp 51-58.

[31] X.Corrales, M.Coll, S.Tecchio, J.M.Bellido, A.M.Fernández, I.Palomera, "Ecosystem structure and fishing impacts in the northwestern Mediterranean Sea using a food web model within a comparative approach", Journal of Marine Systems, 2015, 148: 183–199.

[32] T.E.Essington, "Pelagic ecosystem response to a century of commercial fishing and whaling", Whales, Whaling, and Ocean Ecosystems (eds J.A.Estes, D.P. DeMaster, D.F.Doak, T.M.Williams & R.L.Brownell Jr), 2007, pp.38–49. University of California Press, Berkeley, California.

[33] G.A.Polis, D.R.Strong, "Food web complexity and community dynamics", American Naturalist, 1996, 147, 813‐846.

[34] C.M.Duarte, S.Agusti, E.Barbier, et al., "Rebuilding marine life", Nature, 2020, 580: 39–51. https://doi.org/10.1038/s41586-020-2146-7.

[35] M.Authier, F.D.Commanducci, T.Genov, D.Holcer, V.Ridoux, M.Salivas, et al., "Cetacean conservation in the Mediterranean and Black Seas: fostering transboundary collaboration through the European Marine Strategy Framework Directive. Mar. Policy. 2017, 82, 98–103. doi: 10.1016/j.marpol.2017.05.012.

2020 IMEKO TC-19 International Workshop on
Metrology for the Sea
Naples, Italy, October 5-7, 2020

NNPool in SPIR pipeline for Risso's dolphins identification

R. Maglietta[1], V. Renò[1], R. Caccioppoli[2], S. Bellomo[3], FC. Santacesaria[3], G. Cipriano[4], E. Stella[1], K. Hartman[6], C. Fanizza[3], G. Dimauro[2], R. Carlucci[4]

[1]*Institute of Intelligent Industrial Technologies and Systems for Advanced Manufacturing, National Research Council, via Amendola 122, Bari, Italy*
[2]*Department of Computer Science, University of Bari, Via Orabona 4 - 70125 Bari, Italy*
[3]*Jonian Dolphin Conservation, Viale Virgilio 102 - 74121 Taranto, Italy*
[4]*Department of Biology, University of Bari, Via Orabona 4 - 70125 Bari, Italy*
[5]*CoNISMa, Piazzale Flaminio 9 - 00196 Rome, Italy*
[6]*Nova Atlantis Foundation, Risso's Dolphin Research Centre, Rua Dr. A. F. Pimentel 11, 9930-309, Santa Cruz das Ribeiras, Pico, Azores, Portugal*

***Abstract* – Photo-identification is designed to recognize single individuals of a species by exploiting unique and distinctive marks identifiable in one or multiple photographs. The Risso's dolphin's distinctive marks and scars on the dorsal fin proved to be very useful to photo-identify individuals. The aim of this paper is to improve the performances of the photo-identification studies on this species through machine learning techniques. This paper proposes the introduction of *NNpool*, based on Convolutional Neural Networks, in the SPIR pipeline to identify Risso's dolphins in a new photograph.**

I. INTRODUCTION

The Risso's dolphin *Grampus griseus* is one of the least-known cetacean species on a global scale, with Mediterranean subpopulation ranked as Data Deficient by the IUCN Red List [1]. To bridge the gap of understanding this species, a key component is executed through photo-identification (photo-ID) studies, based on the recognition of single individuals thanks to the specific markers on their dorsal fins obtained in photographs. It is their appearance that makes the Risso's dolphins particularly suitable for this kind of research. Generally, adult Risso's dolphins present extensive white scarring on their bodies, (Fig. 1) presumably caused by infraspecific interactions [2], can appear as scratches, stains, or circular marks, and in some animals can cover most of their body surface. As a result, the unique markings on their dorsal fin can be successfully analyzed to identify single individuals.

The state of the art for the photo-identification of Risso's dolphins is the algorithm SPIR (Smart Photo-identification of Risso's dolphin) [3], [4], where Scale Invariant Feature Transform (SIFT) [5] is applied to detect the key-points over the scars on the dorsal fin of Risso's dolphins. The purpose of these photo-ID tool is to match the most similar dolphins, in terms of SIFT features, in a catalogue of *known* and labelled Risso's dolphins. The characteristic of SPIR is that it is a best-matching algorithm, assigning the most similar dolphin in the catalogue to the query image (i.e. the best-matching dolphin) and taking into account the reliability of its identification. In fact, SPIR predicts the identity of the dolphin in the query image as that of the dolphin in the catalogue with the highest number of equally-oriented matched SIFT features with the query image. If this number is less than 4, or if two or more dolphins in the catalogue have the same highest number the system will return a warning to the user. In the pipeline, this step reminds pay attention on the case of *unknown* dolphins, i.e. those individuals that are not part of the reference catalogue, but it does not solve the problem. If we were to have photographs of new fins, for example acquired during a new survey, in order to bring about a more powerful photo-identification, the *unknown* class should be considered among the possible identities for the query dolphin. Machine learning algorithms provide us with strategies able to classify examples never seen before, taking into consideration all desirable classes, and in particular the *unknown* one [6].

Fig. 1. Risso's dolphin Grampus griseus.

The main novelty of this paper is the application of NNpool strategy, recently proposed in [7], in the SPIR pipeline, to manage the *unknown* dolphins class in the Risso's dolphin photo-identification. In particular NNPool consists in a pool of multiple Convolutional Neural Networks, simultaneously queried to photo-identify single individuals, whose outputs are opportunely merged. The DolFin [1] catalogue [3], [7] which collects Risso's dolphins data and photos acquired in the period 2013-2018 in the Northern Ionian Sea (Central-eastern Mediterranean Sea), was used to carry out experiments. To validate experimental results a data set, collecting Risso's dolphins images from Azores, was used. Results show that the combination of this two algorithms improves the performance of the automated Risso's dolphin photo-identification and it is suitable for large data set studies.

II. MATERIALS AND METHODS

A. *Survey area and data collection*

Sighting data of *G. griseus* were collected from July 2013 to August 2018 during vessel-based surveys conducted on board of a 12-m catamaran, investigating an area of about 960 km^2, in the Gulf of Taranto (Northern Ionian Sea, Central-eastern Mediterranean Sea). Date, daytime, sea weather conditions, geographic coordinates, group size (number of specimens), and depth (m) were recorded. In addition, a collection of images for photo-ID were taken using a Nikon D3300 camera with Nikon AF-P Nikkor 70-300 mm, f4,5-6,3G ED lens. 93 different Risso's dolphins were photo-identified using the SPIR algorithm [3], [4] and their photographs are freely accessible using the DolFin 1 platform. The NNPool training set, D_{NN}, consists of 582 images of 24 different dolphins among the 93 collected in DolFin. Since the left and right side of the dolphin's fin are perceived and analyzed independently, as if they belong to separate individuals, there are 28 different models.

To validate the capability of NNPool to recognize and discard *unknown* dolphins and compair it to SPIR on its own, a new data set, D_v, was built. It contains 500 images of Risso's dolphin fins obtained from Azores, specifically off Pico island covering approximately 540 km^2 during May-September 2019. Risso's dolphins were first located from a land based look out (38.4078 N and 28.1880 W) using 25x80 binoculars (Steiner observer) [8], and encountered during ocean based surveys, using a 5.8 meters long zodiac, equipped with a 50 HP outboard engine. This data are unseen and completely new for both, NNPool and SPIR.

B. *NNPool*

NNPool is a methodology, based on Deep Learning [9], a type of machine learning (such as [10]–[13]) in which a model learns how to perform classification tasks directly from images. Through the various levels, then, manages to interpret concepts with a high level of complexity simply by composing concepts of lower complexity, easier to learn. In an image, for example, the first level of a neural network learns the presence or absence of edges and the orientation of the image. The second layer typically identifies the arrangement of edges, regardless of small variations in them. Finally, the third layer can assemble recurring structures into larger combinations that correspond to parts of familiar objects, and subsequent layers will detect objects as combinations of these parts.

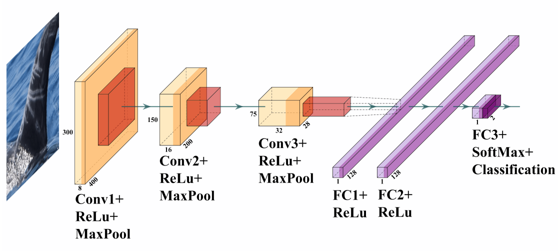

Fig. 2. A graphical representation of the NN build for for each dolphin.

In detail, NNPool uses one of the most popular algorithms for Deep Learning, that is the Convolutional Neural Network (CNN) [14]. A CNN can have dozens or hundreds of layers, each able to learn to detect different features of an image. Like other neural networks, a CNN is composed of an input layer, an output layer, and many hidden layers in between. These layers perform operations that alter the data with the intent of learning features specific to the data. The most common layers are:

- Convolutional (Conv) which puts the input images through a set of convolutional filters, each activating a certain feature from the images.
- Rectified linear unit (ReLu) which allows faster and more effective training by mapping negative values to zero and maintaining positive values, thus adding non-linearity.
- Pooling (MaxPool) which simplifies the output by performing nonlinear downsampling, reducing the number of parameters that the network needs to learn.
- Fully Connected (FC) which multiplies the input by a weight tensor and adds a bias vector. All neurons are connected together and typically these kind of layers are used to actually classify the extracted features from previous layers.
- SoftMax which allows to transform a set of values into probabilities associated to the classes, [15].

[1] http://dolfin.ba.issia.cnr.it/

- Classification which computes the cross entropy loss for multi-class classification problems with mutually exclusive classes.

By mixing these types of layers, we obtain the neural network architecture proposed in this paper. In order to recognize the fin image, we use the following combination of layers for three times: Conv-ReLu-MaxPool, each time doubling the learned filters number on the convolutional layers from 8 to 16 to 32 (Fig. 2).

The image shows an architecture divided into four blocks, in detail:

- Frist block: a convolution layer that preserves the input size, with eight 3x3 size filters, followed by a ReLu type layer used to insert non-linearity. As a last step there is a 3x3 size max pooling layer and stride 2, to reduce the output size of this block.

- Second block: a convolution layer that preserves the input size, with sixteen 3x3 size filters, followed by a ReLu type layer, followed by a 3x3 size max pooling layer and stride 2, to reduce the output size of this block.

- Third block: a convolution layer that preserves the input size, with thirty-two 3x3 size filters, followed by a ReLu type layer, followed by a 3x3 size max pooling layer and stride 2, to reduce the output size of this block.

- Fourth block: a pair of fully connected layers, each with ReLu activation type, with output size 128, and finally another fully connected layer with output size 2, followed this time by a classification layer with softmax activation function.

A CNN model is then trained for each of the 28 models in the D$_{NN}$ data set with a one-vs-all technique and a Crossing Validation strategy with n$_{CV}$ cycles, empirically set to 10.

Class imbalance is managed with a downsampling strategy. Given a dolphin d_i among the 28 dolphins in D$_{NN}$, let n_i be the number of images available for d_i. Then, the *unknown* class is composed of m_i images, where $m_i = 27 \times \kappa^*$ with $\kappa^* = min\{\kappa \in \mathbb{N} \,|\, 27 \times \kappa \geq n_i\}$, i.e. the first multiple of 27 greater than n_i. This way, κ images for each of the remaining 27 individuals are taken into account. The training set is composed of $(n_i + m_i)$ photos. Subsequently, an oversampling technique based on image augmentation is used to increase the number of images in the training set. Two geometric transformations have been applied to every image: random rotation of ±45 degrees (over both y and x axes) and translation of ±20 pixels (over both axes, too).

i	CNN$_i$	p_i	CNN$_i$	p_i
1	FRANGETTA_R	48%	TI_L	90%
2	PREZZEMOLO_L	43%	BLACK_L	50%
3	PINNA_L	41%	PINNA_L	33%
4	TI_L	40%	ZANTE_L	30%
5	BLACK_L	36%	DALMATA_L	27%
6	ZANTE_L	32%	DUBBIO_L	25%
7	CARL_R	30%	CUPIDO_L	12%
8	DELTA_R	28%	PERONI_R	12%
9	DUBBIO_L	24%	TRIS_L	10%
10	ALT_R	20%	FRANGETTA_R	8%
11	PERONI_R	19%	PREZZEMOLO_L	7%
12	CUPIDO_L	18%	PREZZEMOLO_R	6%
13	TRIS_L	10%	SVIRGOLO_L	5%
14	ELE_R	10%	CARL_R	3%
15	PREZZEMOLO_R	6%	DELTA_R	3%
16	SVIRGOLO_L	5%	SVIRGOLO_R	1%
17	DALMATA_L	2%	VITO_R	1%
18	ZANTE_R	2%	ERARD_R	0,8%
19	VITO_R	1%	EMME_R	0,5%
20	JHONATAN_L	1%	ALT_R	0,2%
21	SMILE_R	1%	CUPIDO_R	0,2%
22	ERARD_R	0,5%	JHONATAN_L	0,2%
23	MENO_R	0,1%	MENO_R	0,1%
24	SVIRGOLO_R	0%	ELE_R	0%
25	EMME_R	0%	SMILE_R	0%
26	HUGO_L	0%	JAX_L	0%
27	JAX_L	0%	HUGO_L	0%
28	CUPIDO_R	0%	ZANTE_R	0%
	MODEL WITH p_i>51%	0	MODEL WITH p_i>51%	1
	RESULT LABEL	UNKNOWN	RESULT LABEL	KNOWN

Fig. 3. Example of NNPool output. The NNPool output is a vector P containing p_i values with i = 1, 2, ...,28, where p_i is the probability of the fin in the photo to belong to the dolphin reported to the CNN$_i$ column. On the left (right) a result of the classification of unknown (known) dolphin.

So, NNPool consists of the mixing of the CNN$_i$ networks, with i=1, 2, ..., 28, where CNN$_i$ is made of n$_{CV}$ trained models. NNPool is composed by the (28 × n$_{CV}$) models.

Every CNN$_i$ was built with the following parameters, empirically set:

- Solver Name: *stochastic gradient descent with momentum*, with momentum set to 0.9;

- Inital Learning Rate: set to 0.00001;

- Mini Batch Size: $\frac{1}{4}$ of the Training Set size;

- Max Epochs: 60, shuffling the data at every epoch.

Basically, the pipeline input is a cropped images and, to that regard, an algorithm, devoted to the fin cropping of dolphins photos, has been recently presented in literature [16]. So, every time we want to predict the label of a new photo, it will be first automatically cropped and resized to the dimension required by the input layer of all the CNNs, which is 300x400 pixels. Successively, the photo can be used as NNPool input, giving a P vector as output (as shown in figure 3). If there is only one $p_i \in P > 51\%$, the new photo will be labelled as *known*, otherwise it will be labelled as *unknown*.

III. EXPERIMENTS AND RESULTS

All data are analyzed using Matlab (MathWorks, Natick, MA). The performance of CNN photo-identification, illustrated in [7], was good, with almost all accuracies values above 80%. Moreover it has been proved proved that CNN performance is influenced by the training set size and the images quality. In fact when few images are available for the specimen, CNN sensitivity decreases with images quality, and when the number of images for the specimen increases, good sensitivity values are achieved even if fair or poor quality images are used. In general, CNNs performance is very good both in case of many low quality images as well as in case of few high quality images. Hence, quality of images surely impacts on the algorithm performances and therefore should be taken into account. Several methods to evaluate image quality have been discussed in literature [17], [18]. For NNPool the Perception based Image Quality Evaluator (PIQE scores)[19] was used to evaluate the image quality and was computed for all the images used to train each M_i classifiers. These are no-reference image quality scores, with values in the range $[0, 100]$, inversely correlated to the perceptual quality of an image. A low PIQE score value indicates high perceptual quality and high score value indicates low perceptual quality.

Here we present results of the automated photo-identification of Risso's dolphins captured in photos collected in the datadset D_v, using the combination of NNpool and SPIR. Figure 4 shows the number of False Positive (FP) and True Negative (TN) of NNPool+SPIR and SPIR photo-identification of unknown dolphins. FP represents *unknown* specimens, errouneusly associated to *known* models, TN represents *unknown* specimens, correctly discarded. Among the 500 examples, NNPool+SPIR correctly identifies 392 photos as belonging to *unknown* individuals (i.e TN) and it wrongly classifies 108 examples as *known* (i.e. FP). On the other hand, SPIR correctly identifies 238 images as *unknown* individuals (i.e TN) and wrongly associates to *known* models 262 photo (i.e. FP). Therefore, using NNPool + SPIR the number of False Positives recognized in D_v decreases compared to SPIR, which instead shows comparable FP and TN values. Finally, Table 1 shows a figure of merit ϵ that reflects the ability of recognizing unknown dolphins of the two methodologies on D_v dataset. The ϵ has been calculated as percentage of error made in identification by algorithms, i.e. the percentage of false positives on the total number of photos analyzed. The formula is:

$$\epsilon = \frac{FalsePositive(FP)}{TotalImages} \quad (1)$$

Results highlighted that the combination of NNPool within SPIR pipeline is essential as it can reduce the photo-identification error of unknown individulas.

Table 1. The error, ϵ, in SPIR pipeline with and without NNPool.

	SPIR	NNPool+SPIR
ϵ	0.52	0.22

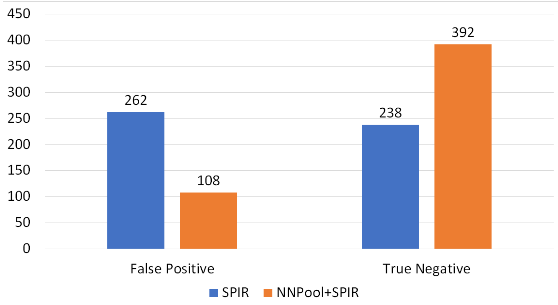

Fig. 4. In orange (blue) the values of FP and TN metrics result from NNPool (SPIR) in photo-identification on D_v.

IV. CONCLUSION AND FUTURE WORKS

Overall, the performance of NNPool+SPIR pipeline appears quite promising, in addition to the fact that this methodology automatically processes large amounts of data with no interaction by the user. When paired with a photo-ID algorithm, such as SPIR [3], the ability of NNPool to identify *unknown* Risso's dolphins, namely those dolphins never encountered during previous surveys, can open new frontiers to photo-identification studies. Combining the advantages and disadvantages of both methodologies to achieve better photo-identification. In fact this double-step processing mechanism is definitely the best approach with as first step a NNPool run, in order to identify the *unknown* dolphins. Subsequently, the *unknown* dolphins should be set apart through a manual photo-identification procedure, while the remaining *known* data set will be analyzed using SPIR algorithm, in order to automatically photo-identify the individuals portrayed in the photographs. This combination of algorithms will provide higher photo-identification performances on novel and larger datasets.

V. REFERENCES

[1] S. Gaspari and A. Natoli, "*Grampus griseus* (Mediterranean subpopulation). The IUCN Red List of Threatened Species," *IUCN*, vol. e.T16378423A16378453, 2012.

[2] K. L. Hartman, "Risso's dolphin: *Grampus griseus*," in *Encyclopedia of Marine Mammals*, Elsevier, 2018, pp. 824–827. DOI: 10.1016/b978-0-12-804327-1.00219-3.

[3] R. Maglietta, V. Reno, G. Cipriano, C. Fanizza, A. Milella, E. Stella, and C. R, "DolFin: an in-

novative digital platform for studying Risso's dolphins in the Northern Ionian Sea (North-eastern Central Mediterranean)," *Scientific Reports*, vol. 8, p. 17 185, 2018.

[4] V. Reno, G. Dimauro, G. Labate, E. Stella, C. Fanizza, G. Cipriano, R. Carlucci, and R. Maglietta, "A SIFT-based software system for the photo-identification of the Risso's dolphin," *Ecological Informatics*, vol. 50, pp. 95–101, 2019.

[5] P. M. Panchal, S. R. Panchal, and S. K. Shah, "A comparison of SIFT and SURF," *International Journal of Innovative Research in Computer and Communication Engineering*, vol. 1, no. 2, pp. 323–327, 2013.

[6] R. Maglietta, A. Bruno, V. Reno, G. Dimauro, E. Stella, C. Fanizza, S. Bellomo, G. Cipriano, A. Tursi, and R. Carlucci, "The promise of machine learning in the Risso's dolphin *Grampus griseus* photo-identification," in *IEEE International Workshop on Metrology for the Sea*, 2018, DOI: 10.1109/MetroSea.2018.8657839.

[7] R. Maglietta, V. Reno, R. Caccioppoli, E. Seller, S. Bellomo, F. C. Santacesaria, R. Colella, G. Cipriano, E. Stella, K. Hartman, C. Fanizza, G. Dimauro, and R. Carlucci, "Convolutional neural networks for risso's dolphins identification," *IEEE Access*, pp. 1–1, 2020. DOI: `10.1109/access.2020.2990427`.

[8] K. Hartman, F. Visser, and A. Hendriks, "Social structure of Risso's dolphins (Grampus griseus) at the Azores: a stratified community based on highly associated social units," *Canadian Journal of Zoology*, vol. 86, pp. 294–306, 2008.

[9] Y. LeCun, Y. Bengio, and G. Hinton, "Deep learning," *Nature*, vol. 521, no. 7553, pp. 436–444, May 2015. DOI: `10.1038/nature14539`.

[10] R. Maglietta, N. Amoroso, M. Boccardi, S. Bruno, A. Chincarini, G. Frisoni, P. Inglese, A. Redolfi, S. Tangaro, A. Tateo, R. Bellotti, and ADNI, "Automated hippocampal segmentation in 3D MRI using random undersampling with boosting algorithm," *Pattern Analysis and Applications*, vol. 19, p. 579, 2016.

[11] R. Maglietta, N. Amoroso, S. Bruno, A. Chincarini, G. Frisoni, P. Inglese, S. Tangaro, A. Tateo, and R. Bellotti, "Random Forest classification for hippocampal segmentation in 3D MR images," in *12th International Conference on Machine Learning and Applications*, 2013, pp. 264–267.

[12] V. Vapnik, "An overview of statistical learning theory," *IEEE Trans on Neural Networks*, vol. 10, no. 5, pp. 988–999, 1999.

[13] L. Breiman, "Random forests," *Machine Learning*, vol. 45, pp. 5–32, 2001.

[14] I. Goodfellow, Y. Bengio, and A. Courville, *Deep Learning*. MIT Press, 2016, `http://www.deeplearningbook.org`.

[15] J. S. Bridle, "Probabilistic interpretation of feed-forward classification network outputs, with relationships to statistical pattern recognition," in *Neurocomputing*, F. F. Soulié and J. Hérault, Eds., Berlin, Heidelberg: Springer Berlin Heidelberg, 1990, pp. 227–236.

[16] V. Renò, G. Losapio, F. Forenza, T. Politi, E. Stella, C. Fanizza, K. Hartman, R. Carlucci, G. Dimauro, and R. Maglietta, "Combined color semantics and deep learning for the automatic detection of dolphin dorsal fins," *Electronics*, vol. 9, no. 5, p. 758, May 2020. DOI: `10.3390/electronics9050758`.

[17] G. Dimauro, "A new image quality metric based on human visual system," in *Proceedings of IEEE International Conference on Virtual Environments Human-Computer Interfaces and Measurement Systems (VECIMS)*, 2012, pp. 69–73.

[18] G. Dimauro, N. Altomare, and M. Scalera, "PQMET: A digital image quality metric based on human visual system," in *Proceedings of 4th International Conference on Image Processing Theory, Tools and Applications (IPTA)*, 2014, pp. 1–6.

[19] N. Venkatanath, D. Praneeth, B. Chandrasekhar, S. Channappayya, and S. Medasani, "Blind image quality evaluation using perception based features," in *Proceedings of the 21st National Conference on Communications (NCC) Piscataway, NJ: IEEE*, 2015.

2020 IMEKO TC-19 International Workshop on
Metrology for the Sea
Naples, Italy, October 5-7, 2020

Head injuries in Loggerheads (*Caretta caretta*): new threat in the Gulf of Taranto?

E. Ottone[1], A. Pisto[1], G. Cirelli[1], F. Catucci[1], V. Aquaro[1], A. Colucci[1], N. Tragni[2], S. Ciccarelli[3], R. Maglietta [4], C. Fanizza[5], R. Carlucci[6]

[1] *Sea Turtle Rescue Center WWF, Piazza Siris, 1, 75025 Policoro (MT) Italy, wwf.poli@gmail.com*
[2] *Italian National Research Council (CNR-IMAA), Tito Scalo (PZ), Italy nicola.tragni@imaa.cnr.it*
[3] Sea Turtle Clinic Departement of Veterinary Medicine, Valenzano (BA) stefano.ciccarelli@uniba.it
[4] Institute of Intelligent Industrial Technologies and Systems for Advanced Manufacturing, National Research Council, Via Amendola 122/D-I, 70126, Bari (BA) Italy, rosalia.maglietta@cnr.it
[5] *Jonian Dolphin Conservation, Viale Virgilio 102, 74121 Taranto (TA) Italy, carmelo@joniandolphin.it*
[6] *Department of Biology University of Bari, Via Orabona 4, 70121 Bari (BA) Italy, roberto.carlucci@uniba.it*

***Abstract* –Among the anthropogenic threats to *Caretta caretta*, fishing is one of the most impactful.**
Boating and fishing can cause traumatic injuries to sea turtles, moreover some fishermen can deliberately injure turtles which are supposed to reduce the catch and damage gear.
The present study synthesizes the skull injuries treatments provided to loggerhead turtles rescued from 2013 to 2019 in the Gulf of Taranto in the Northern Ionian Sea (Central Mediterranean Sea). The type and localization of injury were analyzed in order to evaluated clinical signs, recovery times and healing rates. The timeliness of hospitalization after catch, the application of correct wound treatment and good management practices in the early stages of care have been crucial to increase the chances of clinical recovery and ensure subsequent release to the sea.

I.INTRODUCTION

The loggerhead turtle *Caretta caretta* (Linnaeus, 1758) is the most common sea turtle species in the Mediterranean and worldwide. In the IUCN Red List its global population is considered "Vulnerable"[1], while the Mediterranean sub-population is classified "Least Concern" [2]. Sea turtle rescue centres are acknowledged to reduce mortality in bycatch hotspots, provide a wealth of scientific data, and raise public awareness [3].

One of the major threats for sea turtle conservation is the incidental capture by fishing gears, particularly by bottom trawling [4] and drifting longline [5]. In Italy, the interaction between sea turtles and fisheries were documented in the North Adriatic Sea, the Ionian Sea and surrounding the Straight of Sicily [6,7,8].

Nautical and fishing activities can be associated with traumatic injuries to sea turtles including propeller wounds and blunt force trauma from impact with watercraft or fishing gear. Turtles with boat-strike injuries present severe fractures of the carapace, plastron and skull and flipper lacerations [9]. In addition, reckless fishermen may deliberately traumatize sea turtles presumed to have diminished the fishing catch or damaged gear [10,11]. Among traumatic lesions, those involving the skull, if complicated by brain exposure, are often life-threatening. In these cases, death could be the outcome of direct trauma of the cerebral tissue or of secondary meningoencephalitis [12]. If the sea turtle survives, weakness, disorientation and irreversible deficits may ensue, hindering the turtle’s ability to feed or escape from natural predators [13].

The present study synthesizes the skull injuries treatments provided to loggerhead turtles rescued from 2013 to 2019 in the Gulf of Taranto in the Northern Ionian Sea (Central Mediterranean Sea), in order to warn the management system about a possible new threat to their conservation.

II. MATERIALS AND METHODS

A. *Study area*

The WWF Sea Turtle Rescue Centre located in Policoro (MT), coordinates the Sea Turtles Project in the area of the Gulf of Taranto (from Punta Prosciutto (TA) to Punta Fiume Nicà (CS)), with the collaboration between MATTM, WWF Italy, Sea Turtle Clinic of the Department of Veterinary Medicine of the University of

Bari, Department of Ecology of the University of Calabria and the University of Rome "La Sapienza". As already reported the Gulf of Taranto in the Northern Ionian Sea (Central Mediterranean Sea) represents a suitable habitat for the loggerhead turtle due to eco-physiographic features of the basin [14, 15,16,17].

B. Data collection

Study design was conducted at Sea Turtle Rescue Centre WWF Policoro and (1) the species, (2) type of discovery, (3) the GPS capture coordinates, (4) the reason for hospitalization, (5) the possible presence of epibionts, were assessed, (6) presence of external injuries, fishing lines or hooks have been considered. After clinical, radiographic and other diagnostic investigation methods diagnosis, therapy and prognosis have been reported. Biometric parameters, coordinates of capture, biological samples of sea turtles found stranded dead, were also collected. The alive sea turtles have been carrying to the Policoro Rescue Centre where clinical and neurological examination were performed. Level of consciousness (LOC), flippers movements, and pupillary, eyelid, flippers and cloacal reflexes were evaluated. Each sea turtle was evaluated in the tank to detect any anomalies in the movement of the flippers, diving ability or abnormal buoyancy. The veterinary protocol used belongs to the Sea Turtle Clinic (DVM UniBa) resulting from multiple studies [9,18,19,20,21].

The turtles underwent a total intravenous anesthesia [22] before performing surgical curettage of the skull. Swabs for microbiological evaluation were performed on each wound. The inability to feed on debilitated patients was overcome by inserting an esophagogastric tube feeding [23].

Sea turtles were hospitalized in water at a controlled temperature (ranged from 25 to 28°C), the neurological examination was repeated during hospitalization, healing times and any adverse reactions were monitored [9,24]. Vaseline impregnated gauzes were applied in the depression of the injuries to obtain a waterproof environment and allow the medicament to act without being washed off once the animal was put into the water [9]. Parameters such as the initial wound area and time to heal were recorded.

III.RESULTS

From 2013 to 2019, a total of 335 loggerhead turtles were conferred to the Policoro Rescue Centre, 14 of these with skull injuries, representing 4% of the sea turtle.

Figure 1 shows distribution and the method of discovery of the 14 loggerhead turtles.

All 14 sea turtles analyzed were sub-adults (30 cm <CCL <70) or adults (CCL> 70cm).

Three turtles (n.4, n.7, n.12 see Tab1) were found dead along the Lucanian coast, they were in poor condition, emaciated and malnourished.

At the time of admission, four loggerhead turtles (n.1, n.9, n .13, n.14) presented a recent injury, they did not show an altered level of consciousness (LOC), in two cases (n.1 and n.2) alteration of the ocular reflexes was detected. One turtle (n.14) showed altered reflexes of front flipper and in attitudes of stress and pain, in the tank. No neurological alteration was observed in the sea turtle n.13, that however showed static buoyancy for 15-20 minutes after handling necessary for therapeutic treatment, probably by stress [25]. For these turtles, neurological reflexes returned to normal range after 10-15 days from surgery curettage and topical treatment. After 2 months the turtle n.13 began to make diving attempts and after 3 weeks it was able to swim for long apneas on the bottom of the tank.

The other animals have a not recent injury and neurological examination revealed an alteration of reflexes in all cases, they died after 1-11 days of hospitalization; in two cases (n.5 and n.8) they were hospitalized for 7 and 17 months, but they showed a slight and progressive worsening of neurological symptoms. These two turtles showed slightly extensive lesions without loss of tissues, level of consciousness (LOC) excited and in the tank they showed anomalous attitudes: hyperextension of the anterior limbs and of the neck, crossing of the posterior limbs and immersion inability; it was probably by strong algic symptomatology and by stress [26].

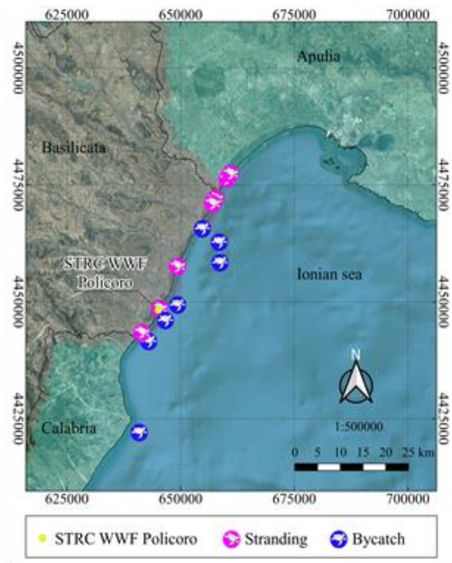

Fig.1. C. caretta with skull injuries recovery map

TABLE 1- Sea turtles with skull injuries both found deceased or hospitalized. LOC is the level of consciousness: ↓ lethargic, ↑ excited. Reflexes were evaluated by assigning a value from 0 to 5: 0 absent, 3 normal, 5 increased. FB (C.caretta n.2) is foreign body.

Caretta caretta (n)	Recovery date	CCL	Days of recovery	Release/ Death	Injury site	LOC	Eyelid, pupillary reflexes	Flippers reflexes	Diving ability
1	15-06-2013	58	137	R	frontoparietal		2	3	
2	02-04-2015	56	3	D	FB in right eye, cranial cavities	↓	1	3	
3	14-07-2015	71	3	D	frontoparietal, supraocular	↓	0 left	3	
4	14-08-2015	47.5							
5	19-08-2015	55	519	D	frontoparietal	↑	1	4	absent
6	04-09-2015	39.5	4	D	frontoparietal, supraocular	↓	0 right	1	
7	12-06-2016	56.5							
8	02-11-2016	50	228	D	frontoparietal	↑	2	4	absent
9	03-06-2017	57	37	R	supraocular		1	3	
10	07-06-2017	71.5	11	D	frontoparietal, supraocular	↓	2	2	
11	13-06-2017	64	1	D	frontoparietal, temporal	↓	1	1	
12	14-06-2017	59							
13	19-06-2019	58	67	R	frontoparietal		3	3	
14	28-10-2019	60	145	R	frontoparietal, prefrontal		3	2	absent

Of the 11 turtles rescued, only 4 turtles (n.1, n.9, n.13, n.14) with recent injury have been reintroduced in nature after long hospitalization period ranging from a minimum of 37days to a maximum of 145 days.

IV.DISCUSSION

In the present study, although the small number of cases, the mortality of sea turtles with skull injuries is high (fig.2). This places attention on the case studies, making it essential to develop clinical and conservation solutions.

Fishing activities in the area under study are attributable to artisanal fishing with the use mostly of set nets. Large sea turtles, are captured by fishing gears typically deployed in neritic area (bottom trawls, set nets, demersal longlines) where large turtles are supposed to spend most of their time [27]. The medium-large sizes of sea turtles with skull injuries confirms that there is a relationship between the traumatic event and artisanal fishing.

In the cases analysed, death was not an immediate consequence of the trauma, confirmed by the state of malnutrition of turtles found deceased and the not recent injuries of hospitalized and subsequently deceased turtles. Probably the reason for death are infections and meningoencephalitis or irreversible deficits that hinder the turtle's ability to feed [12,13]. It is evident that the prognosis is influenced by the rapidity of the rescue [28].

Euthanasia often appears to be the most ethical choice if it is not possible to avoid animal pain, but appropriate treatment can increase life expectancy and may minimize brain injuries [13].

In this study, no relation has been found between prognosis and extent of the lesion (fig.3). The simultaneous presence of altered reflexes both ocular and front flippers, the assumption of abnormal attitudes and inability to swim have been associated with poor prognosis [26,29].

Given the high mortality and the importance of intervening quickly, awareness of the fishermen is necessary.

A compromise is needed between the conservation of protected species and the interests of professional fishing, mitigation devices have become a priority in fishing research [30,31]. In recent years, different approaches have been tried to avoid bycatch in different fishing techniques: for example, a new type of flexible TED, LED lamps and light sticks attached to gillnet float lines and set nets [31,32,33].

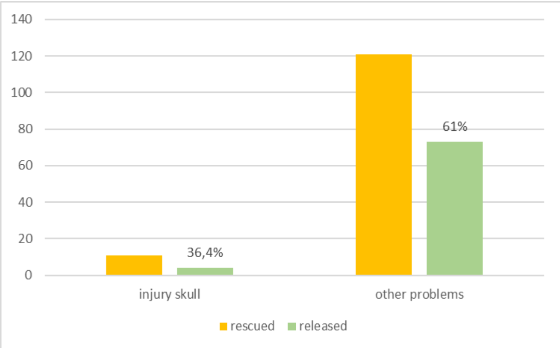

Fig.2 Success rate of recoveries for skull injuries and for other diagnoses (hook ingestion, line constrictions, plastic ingestion, drowning, flipper and carapace injuries).

Fig.3 Loggerhead turtle n.14 at the admission (left) and before release (right) (courtesy of Antonio Di Bello STC).

V. CONCLUSION

Despite the few number of cases analysed, the high mortality of loggerhead turtles with head injuries warning against this threat. Therefore, it is essential to reduce the contact between fishermen and sea turtles by creating new deterrent tools and increasing awareness-raising activities.

VI. REFERENCES

[1]Casale, P. & A.D Tucker. 2017. Caretta caretta. The IUCN Red List of Threatened Species. 2017: e.T3897A119333622.http://dx.doi.org/10.2305/IUCN.UK.2017-2.RLTS.T3897A119333622.en

[2]Casale, P. (Assessor). 2015. Caretta caretta Mediterranean subpopulation. The IUCN Red List of Threatened Species 2015. http://www.iucnredlist.org.

[3]Ullmann J., Stachowitsch M. A critical review of the Mediterranean sea turtle rescue network: a web looking for a weaver Nature Conservation (2015) 10:45-69

[4]Lewison, R.L. and L.B. Crowder. Putting longline bycatch of sea turtles into perspective. Conserv. Biol., (2007) 21(1): 79-86.

[5]Lewison, R.L., S.A. Freeman and L.B. Crowder. – Quantifying the effects of fisheries on threatened species: the impact of pelagic longlines on loggerhead and leatherback sea turtles. Ecol. Lett., (2004) 7: 221-231

[6]Deflorio, M., A. Aprea, A. Corriero, N. Santamaria and G. De Metrio. Incidental captures of sea turtles by swordfish and albacore longlines in the Ionian Sea. Fish. Sci., . (2005). 71: 1010-1018.

[7]Casale, P., L. Cattarino, D. Freggi, M. Rocco and R. Argano. Incidental catch of marine turtles by Italian trawlers and longliners in the central Mediterranean. Aquatic Conserv: Mar. Freshw. Ecosyst., (2007). 17: 686-701

[8]Casale, P., D. Freggi and M. Rocco. Mortality induced by drifting longline hooks and branchlines in loggerhead sea turtles, estimated through observation in captivity. Aquatic Conserv: Mar. Freshw. Ecosyst., (200). 18: 945-954.

[9]Franchini D., Cavaliere L., Valastro C., Carnevali F., Van der Esch A., Lai O., Di Bello A. Management of severe head injury with brain exposure in three loggerhead sea turtles Caretta caretta. Dis Aquat Org, (2016) Vol.119; 145-152,2016.

[10]Lutcavage ME, Plotkin P, Witherington B, Lutz PL. Human impacts on sea turtle survival. In:Lutz PL, Musick JA (eds) The biology of sea turtles, (1997) Vol 1. CRC Press, Boca Raton, FL, p 387− 409

[11]McArthur S, Meyer J, Innis C. Anatomy and physiology. In: McArthur S, Wilkinson R, Meyer J (eds) Medicine and surgery of tortoises and turtles. Blackwell, Oxford, (2004) p 35−71

[12]Naganobu K, Ogawa H, Oyadomari N, Sugimoto M Surgical repair of a depressed fracture in a green sea turtle,Chelonia mydas. J Vet Med Sci (2000) 62: 103−104

[13]Goldberg DW, Adeodato A, Almeida DT, Corrêa LG “Green turtle head trauma with intracerebral hemorrhage: image diagnosis and treatment”, Cienc Rural, (2010), 40: 2402−2405

[14]Pisto A., Cirelli G., Ardolino F., Tragni N., Maglietta R., Renò V., Colucci A. Analysis of bycatch and strandings of sea turtle *Caretta caretta* in the Ionian Sea: understand how the area is used by the species to improve conservation policies In: Ottonello D., Oneto F., Piccardo P., Salvidio S. (Eds). Atti II Congresso Nazionale Testuggini e Tartarughe (Albenga, 11st-13th April 2019): 172-182.

[15]Carlucci R., Bandelj V., Capezzuto F., Sion L., Maiorano P., Tursi A., Solidoro C., Libralato S. 2018. Exploring spatio-temporal changes in the

demersal and benthopelagic assemblages of the northwestern Ionian Sea (central Mediterranean Sea). Marine Ecology Progress Series, 598: 1-19.

[16]Ricci P., Libralato S., Capezzuto F., D'Onghia G., Maiorano P., Sion L., Tursi A., Solidoro C., Carlucci R. 2019. Ecosystem functioning of two marine food webs in the North-Western Ionian Sea (Central Mediterranean Sea). Ecology and Evolution, 9:10198-10212

[17]Cirelli G, Pisto A, Ardolino F, Colucci A, Ottone E, Catucci F, Tragni N, Aquaro V,: Distribuition and causes of sea turtles stranding on the Ionian Coast of Calabria, Apulia 281 and Basilicata. Metrology of the Sea, (2018) Bari.

[18]Camacho M, Quintana MDP, Calabuig P, Luzardo OP, Boada LD, Zumbado M, Orós J. Acid-base and plasma biochemical changes using crystalloid fluids in stranded juvenile loggerhead sea turtles (Caretta caretta). PLoS ONE (2015) 10: e0132217.

[19]Mader DR, Divers SJ (eds) Current therapy in reptile medicine and surgery, 1st edn. Saunders, St. Louis, MO. (2013)

[20]Rinaldi S, Iannaccone M, Magi GE, Costantini E and others. Physical reparative treatment in reptiles. BMC Vet Res (2013) 9: 39

[21]Mitchell MA, Diaz-Figueroa O. Wound management in reptiles. Vet Clin North Am Exot Anim Pract (2004) 7:123−140.

[22]Ciccarelli S, Franchini D, Valastro C, Caprio F, Freggi D, Di Bello A. 2018. Intravenous tramadol for surgical pain relief in general anesthesia with propofol in loggerhead (Caretta caretta). In: Proceedings of the 6th Mediterranean conference on marine turtles. University of Primorska. 15-18th October 2018 Porec, Croatia, p. 141.

[23]Di Bello A, Valastro C, Freggi D, Lai OR, Soloperto S, Crescenzo G. The use of oesophagostomy tube for the force-feeding in sea turtles. In: Jones TT, Wallace BP (compilers) Proc 31st Ann Symp Sea Turtle Biol Conserv. NOAA Tech Mem (2011) NMFS-SEFSC-631, p 187.

[24]Thomas H., Boyer M.D. Turtles, tortoises and Terrapins; section II General husbandry and management. In:Mader DR, Reptile medicine and surgery, 2 edn. Saunders, (2006), p78-99.

[25]Chrisman CL, Walsh M , Meeks JC, Zurawka H, LaRock R., Herbst L., et al. Neurologic examination of sea turtles, J. Am Vet Med Assoc (1997) 211 (8):1043-1047.

[26]Done L., Neurologic disorders. In: Mader DR, Reptile medicine and surgery, 2 edn. Saunders, (2006), p.852-857.

[27] Casale P. Sea Turtle bycatch in the Mediterranean Fish and Fisheries (2011) 12, 299–316

[28]Oertel M, Kelly DF, McArthur D, Boscardin WJ and others (2002) Progressive hemorrhage after head trauma: predictors and consequences of the evolving injury. J Neurosurg 96: 109−116

[29]Werner T, Kraus S, Read A, Zollett EFishing techniques to reduce the bycatch of threatened marine animals. Marine Technology Society Journal . (2006). 40: 50-68.

[30]Lewison, R., Wallace, B., Alfaro Shigueto, J., Mangel, J.C., Maxwell, S.M., Hazen, E.L. Fisheries bycatch of marine turtles: lessons learned from decades of research and conservation. In: In: Wyneken, J., Lohmann, K.J., Musick, J.A. (Eds.), The Biology of Sea Turtles (2013) Volume III. CRC Press, Boca Raton, FL, USA, pp. 329–351.

[31]Lucchetti, A., Punzo, E., and Virgili, M. Flexible turtle excluder device (TED): an effective tool for Mediterranean coastal multispecies bottom trawl fisheries. Aquat. Living Resour. (2016). 29:201. doi: 10.1051/alr/2016016

[32]Wang, J. H., Fisler, S., and Swimmer, Y.. Developing visual deterrents to reduce sea turtle bycatch in gill net fisheries. Mar. Ecol. Prog. Ser. (2010) 408, 241–250

[33]Virgili, M., Vasapollo, C., and Lucchetti, A.Can ultraviolet illumination reduce sea turtle bycatch in Mediterranean set net fisheries? Fish. Res. (2018) 199, 1–7. doi: 10.1016/j.fishres.2017.

2020 IMEKO TC-19 International Workshop on
Metrology for the Sea
Naples, Italy, October 5-7, 2020

Occurrence of zoonotic parasites in free-ranging dolphins and sea turtles in the Gulf of Taranto (Northern Ionian Sea, Central-eastern Mediterranean Sea)

Marianna Marangi[1,2], Piero Carlino[2], Carmelo Fanizza[3], Gianluca Cirelli[4], Annachiara Pisto[4], Rosalia Maglietta[5], Giulia Cipriano[6], Roberto Carlucci[6]

[1]Department of the Science of Agriculture, Food and Environment, University of Foggia, Foggia, Italy, marianna.marangi@unifg.it
[2]Sea Turtle Research, Rescue and Rehabilitation Center, Natural History Museum of Salento, Calimera, Lecce, Italy, piero.carlino@msns.it
[3]Jonian Dolphin Conservation, Taranto, Italy, carmelo@joniandolphin.it
[4]Turtle Rescue Centre Policoro, Italy, wwf.poli@gmail.com
[5]Institute of Intelligent Industrial Systems and Technologies for Advanced Manufacturing, National Research Council, Bari, Italy, rosalia.maglietta@cnr.it
[6]Department of Biology, University of Bari, Bari, Italy, giulia.cipriano@uniba.it; roberto.carlucci@uniba.it

***Abstract* – The occurrence of enteric protozoan parasites *Giardia duodenalis* and *Cryptosporidium* sp. was molecularly investigated in free ranging species of striped (*Stenella coeruleoalba)* and Risso's dolphins (*Grampus griseus*) and loggerhead (*Caretta caretta*) and green (*Chelonia mydas*) sea turtles occurring in the Gulf of Taranto (Mediterranean Sea). Out of forty-two examined faecal samples, 2 samples of striped dolphins were found positive to *G. duodenalis* and 3 of loggerhead sea turtles were found positive to *Cryptosporidium*. Zoonotic *G. duodenalis* assemblage A and *Cryptosporidium parvum* were identified. This is the first report in which the presence of these pathogens have been investigated in free ranging species in this area and the first report of *C. parvum* in loggerhead sea turtles. These results extend the known host range of these water and foodborne parasites and confirm the widespread of zoonotic assemblages/species in the marine environment and their inhabitants probably as a results of an increasing in anthropogenic activities.**

I. INTRODUCTION

Globally, populations of cetaceans and sea turtles have drastically decreased in recent decades, largely due to anthropogenic activities [1]. In fact, according to the International Union for Conservation of the Nature (IUCN) Red List, at least a quarter of the world's cetacean and sea turtle species are classified as *endangered*, although the situation may be worse because the status of many others species is unclear. Their ecological role in the marine food web, global distribution in both coastal and off shore waters, long lifespans as well as prey diversity and migratory pattern [2, 3, 4] makes cetaceans and sea turtles more susceptible to a variety of human-induced risks, including chemical pollutants, emerging and zoonotic pathogens and infectious diseases [5]. Otherwise, often the same bio-ecological traits respond in measurable and interpretable pathway for natural and anthropogenic changes [6, 7, 8]. Consequently, the conservation assessment of their population can be used to indirectly measure marine ecosystem quality and investigate both magnitude and severity of anthropogenic impacts [9, 10]. Moreover, since these species share the coastal environment with humans and feed on overlapped marine resources, they may also serve as effective sentinels even for public health status [11].

Giardia duodenalis and *Cryptosporidium* sp. are emerging water- and foodborne enteric zoonotic pathogens [12], able to infect humans and a wide range of animals, including domestic and wild [13]. *G. duodenalis* cysts and *Cryptosporidium* oocysts may be released into the terrestrial and marine environment through human/animals excreta [13]. Cetaceans and sea turtles may become infected either via contamination of coastal waters by sewage, run-off and agricultural and medical waste or by consumption of infected prey such as fish and shellfish, resulting in increased morbidity and mortality in some populations

[14, 15]. Out of eight Assemblages (A-H) recognized for *G. duodenalis*, the zoonotic assemblages A and B infect both humans and animals, while the others do not infect humans and are mainly host specific [16]. At least thirty species have been recognized in the *Cryptosporidium* genus, with *C. parvum* that exhibits the highest zoonotic potential [12].
The presence of *G. duodenalis* and *Cryptosporidium* sp. cysts/oocysts has been already reported in the faecal samples of bowhead whales (*Balaena mysticetus)* and right whales (*Eubalaena glacialis*) from North Atlantic Sea [17] and *Cryptosporidium* oocysts in some samples of harbor porpoises *(Phocoena phocoena)* from Baltic Seas [18]**.** Moreover**,** zoonotic *G. duodenalis* assemblages and *Cryptosporidium* species have been reported in several species of dead cetaceans such as minke whales *(Balaenoptera acutorostrata)* (*G. duodenalis* Assemblage A), common bottlenose dolphins (*Tursiops truncatus*) *(C. parvum),* striped *(Stenella coeruleoalba)* and short-beaked common dolphins (*Delphinus delphis*) *(G. duodenalis* Assemblage A and *C. parvum),* stranded along the European Atlantic Coast [19, 20].
Within the Mediterranean Sea, the only available studies regard the presence of *G. duodenalis* and *Cryptosporidium* sp. cysts/oocysts in free-ranging bottlenose dolphins (*Tursiops aduncus*) and sperm whales (*Physeter macrocephalus*) inhabiting waters of the Red Sea at Hurghada, Egypt [21] and Balearic Archipelago, Spain [22].
Given the widespread of these emerging pathogens and zoonotic assemblages/species commonly associated with humans in marine ecosystem, the aim of this study is to provide information on *G. duodenalis* and *Cryptosporidium* sp. occurrence in free-ranging individuals of striped dolphin, Risso's dolphin (*Grampus griseus*), loggerhead turtle (*Caretta caretta*) and green turtle (*Chelonia midas*) occurring in the Gulf of Taranto (Northern Ionian Sea, Central-Eastern Mediterranean Sea), where these species are exposed to elevated levels of anthropogenic pressure [23, 24]. The role of these emerging and zoonotic pathogens has been also evaluated.

II. MATERIAL AND METHODS

A. Study area

The Gulf of Taranto (Northern Ionian Sea-Central Mediterranean Sea) extends on about 14000 km^2 from Santa Maria di Leuca to Punta Alice and it is characterized by terraces descending toward a system of submarine canyons that identify the Taranto Valley [25]. This singular morphology involves a complex distribution of water masses with a mixing of surface and dense bottom waters and the occurrence of upwelling currents with high seasonal variability [26]. In the basin, different cetacean and sea turtle species coexist with several anthropogenic pressures, such as fishery, industrial discharges, marine traffic and navy exercise areas [23, 27]. In particular, the striped dolphin is the most frequent and abundant species, followed by the common bottlenose dolphin, the Risso's dolphin and the sperm whale [28, 29, 30, 31]. Concerning the sea turtles, the most frequent species in the basin is the loggerhead sea turtle, followed by the occasionally green and leatherback sea turtle (*Dermochelys coriacea*) [32, 33].

B. Sampling

From August 2018 to August 2019, faecal samples of free-ranging striped and Risso's dolphins were collected during vessel-based surveys aimed to monitoring the cetacean populations carried out in the study area. A total of 17 individual faecal samples were collected, of which 11 samples from striped and 6 from Risso's dolphins. Whenever individual dolphin defecated, floating faces were collected at the water surface by using a fine nylon mesh net, changed between each sample as reported in [34]. During the same sampling period, 25 sea turtles founded stranded along the Ionian Sea coast but still alive, were hospitalized at two Sea Turtle Rescue Centres alongside the Northern Ionian Sea. Out of 25 sea turtles, 23 were loggerhead and 2 green turtle. Once reaching the Rescue Center, each turtle was subjected to the first clinical examination according to the Ministerial Guidelines of the Italian Institute for Environmental Protection and Research, ISPRA [35] and if needed, they received, rehydration with fluidic therapy and vitamin administration. Successively, they were kept in an individual sterilized basin with salt water and faecal sample was collected, as soon as possible, after the first spontaneous faecal voiding from each turtle [36].
Both faecal samples of dolphins and sea turtles were collected in a sterile falcon, individually labelled for identification, refrigerated at 5°C, and delivered to the laboratory analysis within 24h for the analysis.

C. DNA extraction

Genomic DNA was isolated from individual faecal sample by using the Qiagen Stool kit (Qiagen, Germany), according to the manufacturer's instructions. DNA samples were eluted in 50 µl of H_2O, quantified by using a Qubit 2.0 fluorimeter and stored at –20 °C, pending molecular analysis. The individual genomic DNA samples contained approximately from 0.2 to 100 ng µL^{-1}.

D. Giardia duodenalis and Cryptosporidium sp. PCR

For the genetic characterization of *G. duodenalis* and *Cryptosporidium* sp., part of the TPI gene (~530 bp) and of GP60 gene (~358 bp), were amplified following the nested-PCR protocol as described in [37].

All the PCRs were carried out in 25 µL, including 10 µL of Ready Mix REDTaq (Sigma, St. Louis, MO) and 100 pmol of each primer. Approximately 50-100 ng of genomic DNA was incorporated into each reaction and a negative control sample (no-template) and a known positive control sample were included in each PCR run.

D. Sequencing

PCR products were run on 1.2% agarose gel, and positive samples were purified with exonuclease I (EXO I) and thermosensitive alkaline phosphatase (FAST AP) (Fermentas, Whaltham, MA, U.S.A.) enzymes, in accordance with the manufacturer's instructions. PCR fragments obtained were directly sequenced in both directions using the ABI PRIMS BygDye Terminator v. 3.1 Cycle Sequencing Kit (Applied Biosystems, Foster City, CA, U.S.A.) with the same primers as the respective PCR reactions, in accordance with the manufacturer's instructions. The sequences obtained were determined using an ABI PRISM 3130 Genetic Analyser (Applied Biosystems), chromatograms were inspected by eye using FinchTV (https://digitalworldbiology.com/FinchTV) and primer regions plus bad-quality regions were removed. Once the sequences had been cleaned up, to investigate the assemblages and species, each sequence was compared with the *G. duodenalis* and *Cryptosporidium* sp. homologous nucleotide sequences available in GenBank database using the BLAST program (Basic Local Alignment SearchTool; https://blast.ncbi.nlm.nih.gov/Blast.cgi?PROGRAM=blastn&PAGE_TYPE=BlastSearch&LINK_LOC=blasthome). Subsequently the sequences were aligned using the CLUSTALW implementation of BIOEDIT, version 7.0.5 (http://www.mbio.ncsu.edu/BioEdit/bioedit.html).

III. RESULTS

Overall, out of forty-two DNA samples subjected to molecular analysis, 5 (11.9%) were found positive to PCR for *G. duodenalis* or *Cryptosporidium* sp. In particular, 2 samples of striped dolphin were positive to *G. duodenalis* and 3 samples of loggerhead sea turtle were positive to *Cryptosporidium* sp. Risso’s dolphin and green sea turtle samples were found negative to at least one or two protozoan parasites. After sequencing, *G. duodenalis* Assemblage A and *C. parvum* were characterized.

IV. DISCUSSION

This is the first study in which the presence of *G. duodenalis* and *Cryptosporidium* sp. has been molecularly investigated in free-ranging species of striped and Risso’s dolphins as well as in loggerhead and green sea turtles occurring in the Gulf of Taranto, Northern Ionian Sea Central-eastern Mediterranean Sea. Zoonotic *G. duodenalis* assemblage A have been characterized in two individuals of striped dolphins whereas *C. parvum* was found in three of loggerhead sea turtles.

Currently, published data about *G. duodenalis* and *Cryptosporidium* infections in marine animals are limited and they are mainly referred to stranded and dead cetaceans [17, 18, 19, 20]. Few studies investigated the prevalence of *G. duodenalis* and *Cryptosporidium* sp. infections in free-ranging bottlenose dolphins and sperm whales within the Mediterranean Sea [21, 22].

In our study, two individuals of striped dolphins were positive to *G. duodenalis*. Moreover, zoonotic Assemblage A was reported. The finding of a zoonotic assemblage is in line of what reported in the study carried out from [19] in European Atlantic coast, although investigated in dead cetaceans, highlight as anthropogenic activities can be a source of contamination for the marine environment. Contrarily of what reported in the same study [19], striped dolphin samples were founded negative to *Cryptosporidium* sp. Moreover, Risso’s dolphin samples were founded negative to both the parasites. Variations in parasites composition and prevalence might be related to several factors such as dietary differences, the parasite life cycle, the availability of hosts necessary to complete the life cycle, the interactions between parasite species, the host immune response, and the host population density [38]. Moreover, parasites can also spread in different way in marine animals, particularly when they act together with ecological, biological, and anthropogenic factors [39].

In this work, *C. parvum* has been molecularly characterized in three individuals of loggerhead sea turtles while the same sample were found negative to *G. duodenalis*. The green turtles were negative to both the parasites. Parasites prevalence difference may be related to the different diet for the two sea turtle species. Several studies have investigated the presence of *C. parvum* in different species of mussels (*Mytilus galloprovincialis)* [37] and a diet based on mussels can be hypothesized for the loggerhead sea turtles.

To date, no data about the presence of *Giardia* and/or *Cryptosporidium* cysts/oocysts in any sea turtles are available. Oocysts of *Cryptosporidium* and zoonotic species (*C. parvum*) have been reported in several species of terrestrial turtles [40]. Therefore, to the best of our knowledge, this is the first report of *C. parvum* in *C. caretta* and these results extend the known host range of this zoonotic protozoan. The possible role as sea turtles as reservoir of these protozoan need to be further investigated.

The results obtained in the present study confirm the widespread of zoonotic assemblages/species of these protozoan parasites in the marine environment and their inhabitants probably as a result of an increasing in anthropogenic activities. Indeed, different factors have been suggested to influence the prevalence of protozoans in aquatic animals, including proximity to human sewage or agricultural outflow [41].

In the future, zoonotic pathogens prevalence and origin routes establishment, are needed in order to implement management actions and preserve their habitats and, hence, to protect animal and public health.

V. REFERENCES

[1] G. Simmonds, J.E. Wendy, "Climate change and cetaceans: concerns and recent developments", Journal of the Marine Biological, 2009, Vol. 89, pp. 203-210.

[2] IUCN, Marine Mammals and Sea Turtles of the Mediterranean and Black Seas. Gland, Switzerland and Malaga, Spain: IUCN 2012, 32 pages.

[3] G. Notarbartolo di Sciara, "Marine mammals in the Mediterranean Sea: An overview. In: G. Notarbartolo di Sciara, M. Podestà, B.E. Curry (Eds.), Mediterranean Marine Mammals Ecology and Conservation, Advances in Marine Biology, 2016, Vol. 75, pp. 1-36.

[4] N. Marn, M. Jusup, T. Legović, S.A.L.M. Kooijman, T. Klanjšček, "Environmental effects on growth, reproduction, and life-history traits of loggerhead turtles, Ecol. Modell, 2017, Vol. 360, pp. 163-178.

[5] A.A. Aguirre, G.M. Tabor, "Introduction: Marine Vertebrates as Sentinels of Marine Ecosystem Health" Eco Health, 2004, Vol 1, pp. 236-238

[6] M.C. Fossi, S. Casini, I. Caliani, C. Panti, L. Marsili, A. Viarengo, R. Giangreco, G. Notarbartolo di Sciara, F. Serena, A. Ouerghi, M.H. Delpledge, "The role of large marine vertebrates in the assessment of the quality of pelagic marine ecosystems", Marine Environmental Research, 2012, Vol. 77, pp. 156-158.

[7] E.L. Hazen, B. Abrahms, S. Brodie, G. Carroll, M. G. Jacox, M.S. Savoca, K.L. Scales, W.J. Sydeman, S.J. Bograd, "Marine top predators as climate and ecosystem sentinels" Front. Ecol. Environ, 2019, Vol 17, pp. 565-574.

[8] G.D. Bossart, "Marine Mammals as Sentinel Species for Oceans and Human Health", Veterinary Pathology, 2011, Vol. 48, pp. 676-690.

[9] J.F.R.A. Hauser-Davis, L. Lemos, S. Siciliano, "Guiana dolphins as marine ecosystem sentinels: ecotoxicology and emerging diseases" , 2014, Vol. 228, pp. 1-29.

[10] M.C. Fossi, C. Panti, "Sentinel Species of Marine Ecosystems" Interactive Factory, 2017, doi: 10.1093/acrefore/9780199389414.013.110

[11] J.R. Stewart, R.J. Gast, R.S. Fujioka, H.M. Solo-Gabriele, J.S. Meschke, L.A. Amaral-Zettler et al., "The coastal environment and human health: microbial indicators, pathogens, sentinels and reservoirs" Environ Health, 2008, Vol. 7, pp. S3

[12] L. Xiao, Y. Feng, "Molecular epidemiologic tools for waterborne pathogens *Cryptosporidium* spp. and *Giardia duodenalis"*, Food Waterborne Parasitol, 2017, Vol. 29, pp. 14-32.

[13] M. Santin, "*Cryptosporidium* and *Giardia* in Ruminants", Vet Clin North Am Food Anim Pract, 2020, Vol. 36, pp. 223-238.

[14] R. Fayer, J.P. Dubey, D.S. Lindsay, "Zoonotic protozoa: from land to sea", Trends Parasitol, 2004, Vol. 20, pp. 531-536

[15] A.J. Appelbee, R.C. Thompson, M.E. Olson, "*Giardia* and *Cryptosporidium* in mammalian wildlife-current status and future needs", Trends Parasitol, 2005, Vol. 21, pp. 370-376

[16] Y. Feng, L. Xiao, "Zoonotic potential and molecular epidemiology of *Giardia* species and giardiasis", Clin. Microbiol. Rev, 2011, Vol. 24, pp. 110-140.

[17] J.M. Hughes-Hanks, L.G. Rickard, C. Panuska, J.R. Saucier, T.M. O'Hara, L. Dehn, R.M. Rolland, "Prevalence of *Cryptosporidium* spp. and *Giardia* spp. in five marine mammal species", J Parasitol, 2005, Vol. 91, pp. 1225-1228

[18] M.L. Grilo, L. Gomes, P. Wohlsein, L.M. de Carvalho, U. Siebert, K. Lehnert, "*Cryptosporidium* species and *Giardia* species prevalence in marine mammal species present in the German North and Baltic Seas", J Zoo Wildl Med, 2018, Vol. 49, pp. 1002-1006.

[19] A. Reboredo-Fernández, E. Ares-Mazás, J.A. Martínez-Cedeira, R. Romero-Suances, S.M. Cacciò, H. Gómez-Couso. "*Giardia* and *Cryptosporidium* in cetaceans on the European Atlantic coast", Parasitol Res, 2015, Vol. 114, pp. 693-698

[20] A. Reboredo-Fernández, H. Gómez-Couso, J.A. Martínez-Cedeira, S.M. Cacciò, E. Ares-Mazás. "Detection and molecular characterization of *Giardia* and *Cryptosporidium* in common dolphins (*Delphinus delphis*) stranded along the Galician coast (Northwest Spain)", Vet Parasitol, 2014, Vol. 202, pp. 132-137.

[21] S. Kleinertz, C. Hermosilla, A. Ziltener, S.

Kreicker, J. Hirzmann, F. Abdel-Ghaffar, A. Taubert, “Gastrointestinal parasites of free-living Indo-Pacific bottlenose dolphins (*Tursiops aduncus*) in the Northern Red Sea, Egypt” , Parasitol Res, 2014 , Vol. 113, pp. 1405-1415.

[22] C. Hermosilla, J. Hirzmann, L.M.R. Silva, J.M. Brotons, M. Cerdà, E. Prenger-Berninghoff, C. Ewers, A. Taubert, “Occurrence of anthropozoonotic parasitic infections and faecal microbes in free-ranging sperm whales (*Physeter macrocephalus*) from the Mediterranean Sea” , 2018, Parasitol Res, Vol. 117, pp. 2531-2541

[23] R. Carlucci, V. Bandelj, P. Ricci, F. Capezzuto, L. Sion, P. Maiorano, A. Tursi, C. Solidoro, S. Libralato, *“*Exploring spatio-temporal changes in the demersal and benthopelagic assemblages of the northwestern Ionian Sea (central Mediterranean Sea)*”,* Marine Ecology Progress Series, 2018, Vol. 598, pp. 1-19.

[24] P. Ricci, S. Libralato, F. Capezzuto, G. D'Onghia, P. Maiorano, L. Sion, A. Tursi, C. Solidoro, R. Carlucci, “Ecosystem functioning of two marine food webs in the North Western Ionian Sea (Central Mediterranean Sea)”, Ecology and Evolution, 2019, Vol. 9, pp. 10198-10212.

[25] T. Pescatore, M.R. Senatore, “A comparison between a present-day (Taranto Gulf) and a Miocene (Irpinia Basin) foredeep of the southern Apennines (Italy)”. In: Allen, P.A., Homewood, P. (Eds.), Foreland Basins, 8. International Association of Sedimentologists, 1986, pp. 169-182.

[26] A. Bakun, V.N. Agostini, “Seasonal patterns of wind-induced upwelling/downwelling in the Mediterranean Sea”, Sci. Mar, 2001, Vol. 65, pp. 243-257.

[27] G. Cirelli, A. Pisto, F. Ardolino, A. Colucci, E. Ottone, F. Catucci, N. Tragni, V. Aquaro, “Distribution and causes of sea turtles stranding on the Ionian coast of Calabria, Apulia and Basilicata," 2018 IEEE International Workshop on Metrology for the Sea; Learning to Measure Sea Health Parameters (MetroSea), Bari, Italy, 2018, pp. 178-182, doi: 10.1109/MetroSea.2018.8657886.

[28] R. Carlucci, P. Ricci, G. Cipriano, C. Fanizza, “Abundance, activity and critical habitat of the striped dolphin *Stenella coeruleoalba* in the Gulf of Taranto (Northern Ionian Sea, Central Mediterranean Sea)”, Aquat Conserv Mar Freshwat Ecosyst, 2018, Vol. 28, pp. 324-336.

[29] R. Carlucci, G. Cipriano, C. Paoli, P. Ricci, C. Fanizza, F. Capezzuto, P. Vassallo, “Random Forest population modelling of striped and common-bottlenose dolphins in the Gulf of Taranto (Northern Ionian Sea, Central-Eastern Mediterranean Sea)” Estuar Coast Shelf Sci, 2018, Vol. 204, pp. 177-192.

[30] R. Carlucci, A.A. Baş, P. Liebig, V. Renò F.C. Santacesaria, S. Bellomo, C. Fanizza, R. Maglietta, G. Cipriano, “Residency patterns and site fidelity of *Grampus griseus* (Cuvier, 1812) in the Gulf of Taranto (Northern Ionian Sea, Central-Eastern Mediterranean Sea)”, Mammal Research, 2020, https://doi.org/10.1007/s13364-020-00485-z.

[31] R. Maglietta, V. Renò, G. Cipriano, C. Fanizza, A. Milella, E. Stella, R. Carlucci, “DolFin: an innovative digital platform for studying Risso's dolphins in the Northern Ionian Sea (North-eastern Central Mediterranean)”, Sci Rep, 2018, Vol. 8, pp. 17185.

[32] P. Casale, P. Nicolosi, D. Freggi, M. Turchetto, R. Argano, “Leatherback turtles (*Dermochelys coriacea*) in Italy and in the Mediterranean Basin”, Herpetol J, Vol 13, pp. 135-139.

[33] P. Casale, A.C. Broderick, J.A. Camiñas, L. Cardona, C. Carreras, A. Demetropoulos, W.J. Fuller, B.J. Godley, S. Hochscheid, Y. Kaska, B. Lazar, D. Margaritoulis, A. Panagopoulou, A.F. Rees, J. Tomás, Türkozan O, “Mediterranean Sea turtles: current knowledge and priorities for conservation and research”, Endanger. Species Res, 2018, Vol. 36, pp. 229-267.

[34] M. Marangi, S. Airoldi, L. Beneduce, A. Giangaspero, C. Zaccone, “A new multidisciplinary approach to monitor the health status of free living fin and sperm whale in the Pelagos Santuary”, World Marine Mammals Conference, 9-12 December 2019, Barcellona, Spain.

[35] G. Mo, F. Montalto, M.T. Serangeli, E. Duprè, “Linee guida per il recupero, soccorso, affidamento e gestione delle tartarughe marine ai fini della riabilitazione e per la manipolazione a scopi scientifici”, ISPRA, Manuali e Linee Guida , 2013, Vol. 89, pp. 51-53.

[36] M. Marangi, P. Carlino, C. Profico, V. Olivieri, G. Totaro, G. Furii, G. Marzano, R.A. Papini, “First multicenter coprological survey on helminth parasite communities of free-living loggerhead sea turtles *Caretta caretta* (Linnaeus, 1758) from the Adriatic Sea and Northern Ionian Sea”, Int J Parasitol Parasites Wildl, 2020, Vol. 11, pp. 207-212.

[37] A. Giangaspero, R. Papini, M. Marangi, A.V. Koehler, R.B. Gasser,” *Cryptosporidium parvum* genotype IIa and *Giardia duodenalis* assemblage A in *Mytilus galloprovincialis* on sale at local food markets, Int J Food Microbiol, 2014, Vol. 171, pp. 62-67.

[38] A. Pace, L. Rinaldi, D. Ianiello, L. Borrelli, G. Cringoli, A. Fioretti, S. Hochscheid, L. Dipineto,

"Gastrointestinal investigation of parasites and Enterobacteriaceae in loggerhead sea turtles from Italian coasts, BMC Vet. Res, 2019, Vol. 15, pp 370.

[39] M. Kotodziej-Sobocinska, "Factors affecting the spread of parasites in populations of wild European terrestrial mammals", Mammal. Research, 2019, Vol. 64, pp. 301-318

[40] D. Traversa, R. Iorio, D. Otranto, D. Modrý, J. Slapeta, "*Cryptosporidium* from tortoises: Genetic characterisation, phylogeny and zoonotic implications", Mol Cell Probes, 2008, Vol. 22, pp.122-128.

[41] M.A. Miller, I.A. Gardner, C. Kreuder, D.M. Paradies, K.R. Worcester, D.A. Jessup, E. Dodd, M.D. Harris, J.A. Ames, A.E. Packham, P.AS. Conrad. "Coastal freshwater runoff is a risk factor for *Toxoplasma gondii* infection of Southern Sea otters (*Enhydra lutris nereis*)", Int J Parasitol, 2002, Vol. 32, pp. 997-1006.

What goes in, must come out: Evaluation of the DNA metabarcoding approach to analyse diet of threatened seahorses

*Tamara Lazic[1,2], Giuseppe Corriero[1], Bachir Balech[3], Frine Cardone[4], Michele Deflorio[5], Bruno Fosso[3], Carmela Gissi[3,6], Marinella Marzano[3], Graziano Pesole[3,6], Monica Santamaria[3], Michele Gristina[7], Cataldo Pierri[1]

[1] *Department of Biology, University of Bari, Bari, Italy*
[2] *CoNISMa, Rome, Italy*
[3] *National Council of Research (CNR), Institute of Biomembrane, Bioenergetics and Molecular Biotechnology (IBIOM), Bari, Italy*
[4] *Department of Integrated Marine Ecology, Zoological Station Anton Dohrn, Naples, Italy*
[5] *Department of Veterinary Medicine, University of Bari, Bari, Italy*
[6] *Department of Biosciences, Biotechnology and Biopharmaceutics, University of Bari, Bari, Italy*
[7] *National Council of Research (CNR), Institute of Anthropic Impacts and Sustainability in marine environment (IAS), Palermo, Italy*

***Abstract* – Seahorses are considered flagship species of the conservation efforts. Indeed, due to the worldwide decline of local populations during the last decades, all seahorse species were listed on the IUCN Red List and Appendix II of CITES. Because of the threatening status, improving knowledge of their dietary composition, while using a non-invasive approach, might be of great importance. Starting from faecal samples of the European seahorse *Hippocampus guttulatus* collected during feeding trials, we used, for the first time on these fish, metagenomic amplicon-based HTS (High Throughput Sequencing) approach. The findings indicated the reliability of the present molecular approach, allowing the characterization of the effectively ingested prey. Unlike traditional methods on faecal samples, this technique can identify items that might not leave solid remains. As only a small amount of starting faecal material is needed and the sampling procedure is neither invasive nor lethal, DNA metabarcoding appears to be useful in the investigation on threatened seahorse diet and, in future, could help to define management and conservation actions.**

I. INTRODUCTION

The knowledge of the species diet is a keystone to understand the way it exploits the environment and to develop adequate conservation actions both for species and total biodiversity [1]. The dietary composition is traditionally identified through visual morphological analyses of stomach, guts or faecal contents using light microscopy [2]. Although these techniques can be useful, they generally result in a poor resolution of determining taxa, possibly precluding the identification of food items that do not leave behind hard remains and sometimes require the sacrifice of animals [3]. Furthermore, some potential prey species, such as crustaceans, could be morphologically similar to one another [4], making the process taxonomically challenging [5]. In recent years, remarkable progress has been made towards developing accurate and non-invasive DNA metabarcoding strategies using highly degraded samples such as faeces, making it relevant for dietary studies even in threatened species. This strategy involves the amplification of a standard DNA barcode using universal or group-specific primers pairs targeting multiple taxa [6]. This approach, where complex mixtures of DNA are extracted and sequenced by employing Next Generation Sequencing (NGS) technologies, has been successfully applied to faecal dietary studies in many species, including fish, and had promising results [7] [8].

Seahorses (*Hippocampus* spp.) are small predatory fish with an almost worldwide distribution [9]. In the past decades, their populations have gone under severe declines in many areas, which led to the inclusion of all seahorse species, including the European seahorse *Hippocampus guttulatus*, on the International Union for Conservation of Nature (IUCN) Red List of Threatened Species and in Appendix II of the Convention on International Trade in Endangered Species of Wild Fauna and Flora [10]. Seahorses usually rely on their sight to capture prey [11]. They practice “sit-and-wait” predation strategy, which involves an examination of the environment from a hidden place and rapid execution of a surprise attack [12]. By employing morphological examination of gut or stomach contents, stomach flushing or by biochemical means, studies on their diet have shown that seahorses feed mainly on small-sized crustaceans [13]. Despite the sensitive conservation status of seahorses, there have been no published studies demonstrating the use of non-invasive techniques to explore their diet. Indeed, it has been shown that the prey's DNA is recoverable from seahorse faeces [14], suggesting that the dietary DNA metabarcoding could be applied to foraging ecology of these fish.

Therefore, using faecal samples of the European seahorse *H. guttulatus*, the purpose of this study was to validate the effectiveness of DNA metabarcoding to characterize the seahorse diet, while the developed protocol would serve as a reference for the interpretation of diet and feeding behaviour of wild populations. To achieve this, the present study included feeding trials, for which it has been shown to be crucial in validating molecular techniques for prey detection [15]. Importantly, as *H. guttulatus* is a threatened species in the Mediterranean Sea and along the Italian coast [16], it is of value to develop a non-lethal and non-invasive method to study its diet.

II. MATERIALS AND METHODS

A. Sampling and feeding trials

Four adult non-reproductive *H. guttulatus* specimens were collected by diving at Taranto Mar Piccolo (Southern Italy). Specimens were hand-caught and transported to the facilities of agricultural society ''Ittica Caldoli S.r.L.''where they were placed in individual 30 L aquaria. Seawater inside the aquaria was filtered through 0.2 µm pore-size polycarbonate filters. The seawater temperature was maintained at 18 ± 0.5°C, salinity at 36 ± 1‰ and the photoperiod was adapted to the natural day cycle. Except for commercially bought *Artemia* sp., other three prey items (*Gammarus* sp., *Palaemon* sp. and *Nereis* sp.) were collected at Taranto Mar Piccolo and taxonomically classified under the microscope. Before the beginning of the experiment and between successive feeds with different prey, seahorses were starved for 24 h to ensure an empty gut. Seahorses were fed simultaneously on a single prey species added daily at a single dose, according to the following sequence: *Gammarus* sp. at day 1, *Artemia* sp. at day 3, *Palaemon* sp. at day 5, and *Nereis* sp. at day 7. The faeces (n=10; three from the diet with *Artemia* sp., three from *Palaemon* sp., two from Gammarus sp. and two from *Nereis* sp.) produced in aquaria were immediately collected by syphoning, and together with four prey samples (P_ANF - *Gammarus* sp., P_AR - *Artemia* sp., P_PA - *Palaemon* sp., P_PL - *Nereis* sp.) were preserved in 96% ethanol and stored at -20°C. Faecal samples were named according to the individual from which they were collected (FT1-FT4) and diet applied (_ANF, _AR, _PA or _PL). At the end of the trials, all animals were released to the original capture site.

B. DNA extraction

Total genomic DNA was extracted from faecal and prey samples using FastDNA SPIN kit for soil (BIO 101, Carlsbad, Canada). Cell lysis was achieved by bead beating in a FastPrep Instrument (BIO 101) at speed 6 for 40 s. Negative extraction controls were added, and identical molecular analyses were performed upon these to monitor for possible contamination. The quantity and quality of the extracted DNA were assessed spectrophotometrically and by agarose gel (1%) electrophoresis, respectively. A skin filament tissue sample from *H. guttulatus* was processed under the same conditions to minimize host contamination.

C. Cox1 Library preparation and sequencing

An amplicon-based approach was applied to the extracted DNA. The sub-region of Cox1 gene was amplified using primers mlCOIintF and dgHCO2198 [17]. Amplicon libraries were prepared starting from 2 ng of DNA extracted from each sample. RNase/DNase-free Molecular Biology Grade water (Ambion) was used as a negative control of PCR amplification. The adopted strategy is described in details in [18]. Equimolar quantities of the purified amplicons were pooled and subjected to 2 × 250 bp paired-end sequencing on the Illumina MiSeq platform. To increase genetic diversity of the sequenced samples, as required by the MiSeq platform, a phage PhiX genomic DNA library was added to the mix and co-sequenced.

PCR products of two prey samples (*Artemia* sp. and *Palaemon* sp.) and seahorse's skin filament, obtained using the primer pair mlCOIint and dgHCO [17], were subjected to Sanger DNA sequencing by Eurofins Genomics (www.eurofinsgenomics.com). Due to uncertainty that more than one taxa were present in the samples of *Nereis* sp. and *Gammarus* sp., these were processed and sequenced by the Illumina MiSeq platform together with the faecal samples under the conditions described above.

D. Taxonomic analyses

Two Illumina MiSeq runs were performed to achieve an adequate number of Paired-Ends (PE) reads per sample. Given that the expected amplicons length (~400bp) was shorter than the total sequenced PE length (2 x 250bp), most of the generated reads were overlapping and consequently merged into contiguous consensus sequences using PEAR [19]. ASVs (Amplicon Sequence Variants) were defined by applying DADA2 [20]. Chimera removal was performed using the reference-based VSEARCH [21] procedure. The obtained ASV sequences were taxonomically annotated using BioMaS pipeline [22] and mapped on the BOLD-based reference collection using Bowtie2 [23]. Sequences matching, with an identity percentage of at least 97%, were directed to the genera classification [24], while others were classified at higher taxonomic levels. Unassigned sequences were taxonomically investigated

Table 1. Shannon alpha diversity index and Chao1 species richness estimator among analysed samples. Samples: FT1, FT2, FT3 and FT4 refer to one of four individuals used in feeding trials, P refers to the prey sample, while ANF, AR, PA and PL stand for the prey given to seahorses (ANF – Gammarus *sp., AR –* Artemia *sp., PA –* Palaemon *sp., PL –* Nereis *sp.)*

SAMPLE	SHANNON INDEX	CHAO1 INDEX
FT2_ANF	0.354	7.000
FT3_ANF	2.018	19.000
FT1_AR	2.245	16.333
FT2_AR	2.019	35.000
FT3_AR	2.155	24.000
FT2_PA	3.109	78.000
FT3_PA	3.527	34.000
FT4_PA	4.848	113.333
FT2_PL	3.803	164.100
FT4_PL	5.000	104.500

using the BLAST tool [25] [26] against the nucleotide collection at NCBI.

Alpha diversity index (Shannon Index, H Index) and the species richness estimator (Chao1) were calculated using R phyloseq package [27] at the level of ASVs. The diversity among samples' composition (beta diversity) was compared through Principal Coordinate Analysis (PCoA), based on the Bray-Curtis dissimilarity matrix, using Vegan R package [28].

III. RESULTS

Amplicon libraries (from 10 faecal and 2 prey samples) were successfully sequenced on the MiSeq platform using a 2 x 250 bp paired-end sequencing strategy. A total of 4,669,953 paired-end (PE) reads, ranging from 296,279 to 519,847 per sample, were obtained. Approximately 99 % of the PE reads were merged into a consensus sequence, maintaining good quality to pass the quality filtering step. A total of 492 ASVs were identified, ranging from 8 (FT2_ANF) to 224 (FT2_PL) per sample. The values of the Shannon index ranged from 0.354 in sample FT2_ANF to 5.0 in sample FT4_PL (Table 1). Chao1 index varied from 7 in FT2_ANF to 164,1 in FT2_PL (Table 1). Beta diversity assessed from Bray-Curtis distance matrices indicated that the samples were grouped mostly according to the diet applied: samples from the diet with *Gammarus* sp. and *Artemia* sp. were well separated from other samples (*Nereis* sp. and *Palaemon* sp.), while these latter were clustered together (Fig.,1).

The applied approach permitted the identification of one genera in the samples of prey (e.g. *Nereis* sp. and

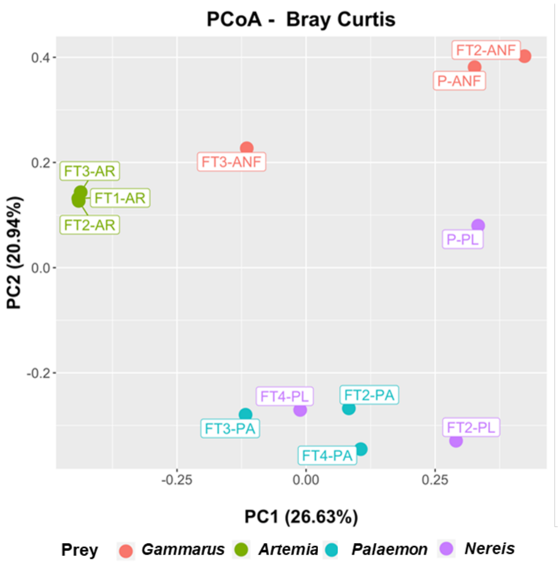

Fig. 1. PCoA obtained using Bray Curtis matrix on ASV. Samples: FT1, FT2, FT3 and FT4 refer to one of four individuals used in feeding trials, P refers to the prey sample, while ANF, AR, PA and PL stand for the prey given to seahorses (ANF – Gammarus *sp., AR –* Artemia *sp., PA –* Palaemon *sp., PL –* Nereis *sp.)*

Gammarus sp.) while in the faecal samples, all prey items (*Gammarus* sp., *Artemia* sp., *Nereis* sp. and *Palaemon* sp.) given to the seahorses during the trials (Fig.,2A, Fig.,2B). Interestingly, *Gammarus* sp. (applied on day 1) DNA was also detected in two samples after feeding with *Artemia* sp. (day 3) and *Palaemon* sp. (day 5). Unknown taxa represented the most abundant group with Phaeophyceae, Hexanauplia and Branchiopoda present at low abundances. Among them, the presence of contaminant taxa has also been observed considering the detection of classes such as Gastropoda and Insecta (Fig.,2A).

IV. DISCUSSION

Using faecal samples of *H. guttulatus* produced during the feeding trials with known ingested prey, the present study represents the first attempt to investigate the diet of seahorses by DNA metabarcoding. The results demonstrated the reproducibility and sensitivity of a developed molecular protocol, based on a metagenomic amplicon-based HTS approach, to systematically detect the ingested prey. Importantly, DNA metabarcoding offered a non-invasive and non-lethal method allowing the identification of soft-bodied prey that might have been difficult or even impossible to detect through morphological analysis of faecal samples, such as *Artemia* sp. and *Nereis* sp.

DNA extraction, preparation and sequencing of amplicon libraries, and sequences analysis were carried

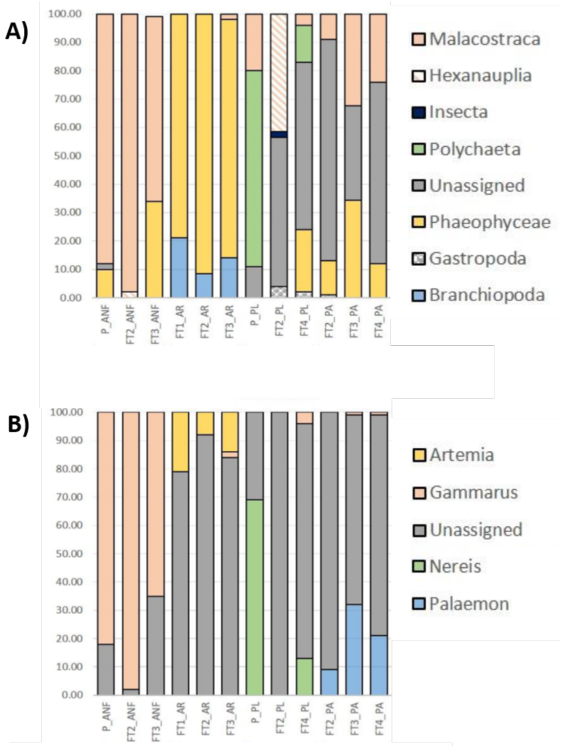

Fig. 2. Taxonomical assignment of ASVs at class (A) and genus (B) levels. Only groups with relative abundances ≥1% are presented. Samples: FT1, FT2, FT3 and FT4 refer to one of four individuals used in feeding trials, P refers to the prey sample, while ANF, AR, PA and PL stand for the prey given to seahorses (ANF – Gammarus *sp., AR –* Artemia *sp., PA –* Palaemon *sp., PL –* Nereis *sp.).*

out according to consolidated procedures [18]. The number of obtained sequences was high enough to cover the diversity of each sample. Chao1 and Shannon indices displayed a similar pattern among faecal samples containing both same and different prey ingested, indicating the efficiency of the applied approach to capture the samples' biodiversity. Beta diversity, based on a Bray–Curtis dissimilarity matrix and calculated via PCoA, revealed that the sample distribution corresponded to the diet applied. Taxonomical assignment of ASVs permitted the identification of all prey items effectively ingested during the trials. The results were in accordance with the morphological analysis on prey samples under the microscope, revealing the same taxa. The presence of remains of *Gammarus* sp. in faeces of seahorses fed with *Artemia* sp. and *Palaemon* sp. might indicate the longer retention of this prey in *H. guttulatus* guts probably due to the poorly digestible chitanaceous exoskeleton. Regarding unassigned sequences, it should be stressed that invertebrates, as main seahorse prey, are a diversified and relatively unstudied group, for which adequate information in reference databases are frequently absent, preventing their full taxonomical annotation. Among taxa detected in seahorse faeces, some of them could presumably result from contamination of different sources, such as aquarium water and prey items. Especially having in mind that most prey items were collected in the wild, detection of taxa such as Phaeophyceae is not surprising given that this alga is consumed by *Artemia* sp. and *Gammarus* sp. Moreover, the incidence of contaminants is even more relevant when analyses are carried out with high-sensitivity techniques, such as Next Generation Sequencing.

This study confirms that DNA metabarcoding on faeces is an effective tool for studying the seahorse diet, following past studies on other fish species [7] [8]. Hence, the technique could be used in further studies of *H. guttulatus* dietary composition in captivity but also in the wild. However, based on sampling experience, it is recommended that only thick faeces should be used, thus increasing the quantity of the extracted DNA and the possibility to detect prey. The results of DNA metabarcoding analysis, associated with the taxonomical classification of prey items under the microscope, showed that the developed molecular protocol ensures correct identification of prey fed to *H. guttulatus*. These findings, together with the advantage of being non-intrusive and especially, non-lethal, make DNA metabarcoding on faecal samples a good candidate to study diet of threatened seahorses in both captivity and wild.

REFERENCES

1. M.E.Soulé, J.A.Estes, J.Berger, C.M.Del Rio, ''Ecological effectiveness: conservation goals for interactive species'', Conserv. Biol., vol.17, No.5, October 2003, pp.1238–1250.
2. L.L.De Sousa, S.Marques Silva, R.Xavier, ''DNA metabarcoding in diet studies: Unveiling ecological aspects in aquatic and terrestrial ecosystems'', Environ. DNA, vol.1, No.3, August 2019, pp.199 – 214.
3. M.A.Forin-Wiart, M.L.Poulle, S.Piry, J.F.Cosson, C.Larose, M.Galan, ''Evaluating metabarcoding to analyse diet composition of species foraging in anthropogenic landscapes using Ion Torrent and Illumina sequencing'', Sci.Rep., vol.8, November 2018, article No.17091.
4. A.E.Radulovici, B.Sainte−Marie, F.Dufresne, ''DNA barcoding of marine crustaceans from the Estuary and Gulf of St Lawrence: A regional−scale approach'', Mol. Ecol. Resour., vol.9, No. s1, May 2009, pp.181–187.
5. T.A.Berry, S.K.Osterrieder, D.C.Murray, M.L.Coghlan, A.J.Richardson, A.K.Grealy, M.Stat, L.Bejder, M.Bunce, ''DNA metabarcoding for diet analysis and biodiversity: A case study using the endangered Australian sea lion (*Neophoca cinerea*)'', Ecol. Evol., vol.7, No.14, July 2017, pp.5435 – 5453.
6. G.K.Zhang, F.J.J.Chain, C.L.Abbott, M.E.Cristescu,

''Metabarcoding using multiplexed markers increases species detection in complex zooplankton communities'' Evol. Appl., vol.11, No.10, December 2018, pp.1901 – 1914.
7. E.Corse, C.Costedoat, R.Chappaz, N.Pech, J.Martin, A.Gilles, ''A PCR-based method for diet analysis in freshwater organisms using 18S rDNA barcoding on faeces'', Mol. Ecol. Resour., vol.10, No.1, January 2010, pp.96–108.
8. T.Taguchi, Y.Miura, D.Krueger, S.Sugiura, ''Utilizing stomach content and faecal DNA analysis techniques to assess the feeding behaviour of largemouth bass *Micropterus salmoides* and bluegill *Lepomis macrochirus*'', J. Fish Biol., vol.84, No.5, May 2014, pp.1271–1288.
9. S.A.Lourie, R.A.Pollom, S.J.Foster, ''A global revision of the seahorses *Hippocampus* Rafinesque 1810 (Actinopterygii: Syngnathiformes): taxonomy and biogeography with recommendations for further research'', Zootaxa, vol.4146, No.1, August 2016, pp.1–66.
10. A.C.J.Vincent, S.J.Foster, H.J.Koldewey, ''Conservation and management of seahorses and other Syngnathidae'', J. Fish Biol., vol.78, No.6, Jun 2011, pp.1681-1724.
11. R.H.Kuiter, ''Seahorses, pipefishes and their relatives: a comprehensive guide to Syngnathiformes'', TMC Publishing, Chorleywood, UK, 2000.
12. K.Tipton, S.S.Bell, ''Foraging patterns of two syngnathid fishes: importance of harpacticoid copepods'', Mar. Ecol. Prog. Ser., vol.47, No.1, July 1988, pp.31-43.
13. F.Ape, G.Corriero, S.Mirto, C.Pierri, T.Lazic, M.Gristina, ''Trophic flexibility and prey selection of the wild long-snouted seahorse *Hippocampus guttulatus* Cuvier, 1829 in three coastal habitats'', Estuar. Coast. Shelf S., vol.224, August 2019, pp.1-10.
14. E.Corse, S.Valladares, M.Planas, A.Chammoro, J.Pintado, ''Analysis of the diet of the long‐snouted seahorse *Hippocampus guttulatus* by 18SrDNA amplification of prey in faeces'', Aquac. Nutr., vol.21, No.5, October 2015, pp.528-540.
15. S.K.Sheppard, K.D.Sunderland, J.Fenlon, D.Skervin, W.O.Symondson, ''Detection of secondary predation byPCR analyses of the gut contents of invertebrate generalist predators'', Mol. Ecol., vol.14, No.14, December 2005, pp.4461–4468.
16. R.Pollom, ''*Hippocampus guttulatus*. The IUCN Red List of Threatened Species 2016: e.T41006A90859949'', available at https://www.iucnredlist.org/species/41006/90859949
17. M.Leray, J.Y.Yang, C.P.Meyer, S.C.Mills, N.Agudelo, V.Ranwez, J.T.Boehm, R.J.Machida, '' A new versatile primer set targeting a short fragment of the mitochondrial COI region for metabarcoding metazoan diversity: application for characterizing coral reef fish gut contents'', Front. Zool., vol.10, No.1, June 2013, pp.34.
18. C.Manzari, B.Fosso, M.Marzano, A.Annese, R.Caprioli, A.M.D'Erchia, C.Gissi, M.Intranuovo, E.Picardi, M.Santamaria, S.Scorrano, G.Sgaramella, L.Stabili, S.Piraino, G.Pesole, ''The influence of invasive jellyfish blooms on the aquatic microbiome in a coastal lagoon (Varano, SE Italy) detected by an Illumina-based deep sequencing strategy'', Biol. Invasions, vol.17, March 2015, pp.923-940.
19. J.Zhang, K.Kobert, T.Flouri, A.Stamatakis, "PEAR: a fast and accurate Illumina Paired-End reAd mergeR", Bioinformatics, vol.30, No.5, March 2014, pp.614–20.
20. S.Weiss, Z.Z.Xu, S.Peddada, A.Amir, K.Bittinger, A.Gonzalez, C.Lozupone, J.R.Zaneveld, Y.Vazquez-Baeza, A.Birmingham, E.R.Hyde, R.Knight, ''Normalization and microbial differential abundance strategies depend upon data characteristics'', Microbiome, vol.5, March 2017, article No.27.
21. T.Rognes, T.Flouri, B.Nichols, C.Quince, F.Mahe, "VSEARCH: a versatile open source tool for metagenomics", PeerJ, October 2018, article No.4:e2584.
22. B.Fosso, M.Santamaria, M.Marzano, D.Alonso-Alemany, G.Valiente, G.Donvito, A.Monaco, P.Notarangelo, G.Pesole, ''BioMaS: a modular pipeline for Bioinformatic analysis of Metagenomic AmpliconS'', BMC Bioinformatics, vol.16, July 2015, article No.203.
23. B.Langmead, S.L.Salzberg, "Fast gapped-read alignment with Bowtie 2", Nat. Methods, vol.9, No.4, March 2012, pp.357–359.
24. D.R.Mende, S.Sunagawa, G.Zeller, P.Bork, "Accurate and universal delineation of prokaryotic species". Nat. Methods, vol.1, July 2013, pp. 881–884.
25. D.W.Mount, "Using the Basic Local Alignment Search Tool (BLAST)", CSH Protoc, July 2007, article No.pdb top17.
26. S.F.Altschul, G.Gish, W.Miller, E.W.Myers, D.J.Lipman, "Basic local alignment search tool". J. Mol. Biol., vol.215, No.3, October 1990, pp.403–410.
27. P.J.McMurdie, S.Holmes, ''phyloseq: An R Package for Reproducible Interactive Analysis and Graphics of Microbiome Census Data'', PloS ONE, vol.8, No.4, April 2013, article No.e61217.
28. J.Oksanen, F.Guilaume Blanchet, R.Kindt, P.Legendre, R.B.O'hara, G.L.Simpson, P.Solymos, M.H.H.Stevens, H.Wagner, ''vegan: Community Ecology Package: R package version 2.5–3'', available at https://CRAN.R-project.org/package=vegan.

2020 IMEKO TC-19 International Workshop on
Metrology for the Sea
Naples, Italy, October 5-7, 2020

Lightweight and efficient convolutional neural networks for recognition of dolphin dorsal fins

Gianvito Losapio[1], Rosalia Maglietta[2], Tiziano Politi[1], Ettore Stella[2], Carmelo Fanizza[3], Karin Hartman[4], Roberto Carlucci[5], Giovanni Dimauro[6], Vito Renò[2]

[1] *Department of Electrical and Information Engineering (DEI), Polytechnic University of Bari, Via Orabona 4, 70125 Bari, Italy; gvlosapio@gmail.com; tiziano.politi@poliba.it*
[2] *Institute of Intelligent Industrial Systems and Technologies for Advanced Manufacturing, National Research Council of Italy (CNR STIIMA), Via Amendola 122 D/O Bari, Italy; rosalia.maglietta@cnr.it; ettore.stella@cnr.it; vito.reno@cnr.it*
[3] *Jonian Dolphin Conservation, Viale Virgilio 102 - 74121 Taranto, Italy; carmelo@joniandolphin.it*
[4] *Nova Atlantis Foundation, Risso's Dolphin Research Centre, Rua Dr. A. F. Pimentel 11, 9930-309, Santa Cruz das Ribeiras, Pico, Azores, Portugal; oceanwatch@gmail.com*
[5] *Department of Biology, University of Bari, Via Orabona 4 - 70125 Bari, Italy; roberto.carlucci@uniba.it*
[6] *Department of Computer Science, University of Bari, Via Orabona 4 - 70125 Bari, Italy; giovanni.dimauro@uniba.it*

***Abstract* – The study of cetaceans is of vital importance to infer biological information useful to drive sustainable action plans aimed at preserving the marine environment and its biodiversity. In a recent study, we developed a novel algorithm for the detection of dorsal fins in the context of a fully automated pipeline for the photo-identification of Risso's dolphins. A lightweight convolutional neural network (CNN) architecture was proposed to recognize fins among cropped images, filtering the inputs for the photo-identification algorithm. In this paper, we compare the performances of that custom CNN to another extremely efficient architecture: Shufflenet. Training an efficient classifier is a key effort to speed up the first part of the photo-identification pipeline, enabling the feasibility of large scale ecological studies. The experiment confirms that both architectures provide a robust feature extraction capability for the problem in hand, even with a significantly smaller number of parameters with respect to other popular state-of-the-art CNNs.**

I. INTRODUCTION

Photo-identification of specimens is arguably one of the best non-invasive methods to estimate several parameters which describe a population of cetaceans: abundance, spatial distribution and site fidelity, to name a few. This knowledge is of vital importance to infer biological information useful to drive sustainable action plans aimed at preserving the marine environment and its biodiversity [1–8].

Risso's dolphin is a particularly well-suited species for the use of photo-identification. Analogously to human fingerprints, sub adult and adult individuals exhibit patterns of scarring and variations in dorsal fin shape as long-lasting identifiable natural marks [9].

Two state-of-the-art algorithms for the automated photo-identification of Risso's dolphins have been recently proposed: SPIR (Smart Photo Identification of Risso's dolphin) [11] and NNPool (Neural Network Pool) [12].

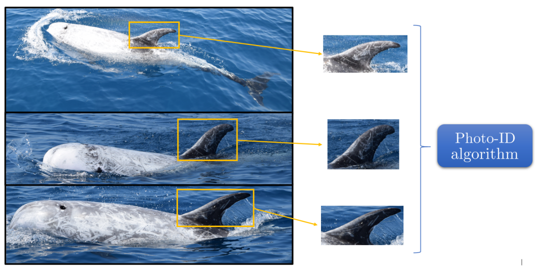

Fig. 1. The crucial role of cropping dorsal fins out of full frame images in the Risso's dolphin photo-identification pipeline.

Similarly to any modern photo-identification algorithm, their effectiveness is guaranteed only if an appropriate area of interest has been designated beforehand in the image. Figure 1 intuitively illustrates such problem. Extracting relevant regions out of full frame images is indeed the main bottleneck in processing data from photographic capture-recapture surveys [13, 14]. For this reason, a novel algorithm has been proposed in our recent work [15] to automatically detect dorsal fins in the context of Risso's dolphin photo-identification.

Particular attention was devoted to the design of a convolutional neural network (CNN) classifier, trained to recognize fins among proposed regions with the objective of filtering the inputs for the photo-identification algorithm. A custom CNN was introduced, with a *lightweight* architecture characterized by a lower number of parameters and a reduced computational demand if compared to the other state-of-the-art architectures [16, 17].

In this paper, a new experiment is conducted in order to compare the performances of that custom CNN to another extremely efficient architecture, which recently gained lots of popularity in the field of convolutional neural networks for mobile devices: Shufflenet [18, 19].

Training an efficient classifier is a key effort to speed up the first part of a more ambitious fully automated Risso's dolphins photo-identification pipeline, enabling the feasibility of large scale ecological studies [15].

II. MATERIALS AND METHODS

A. *Data acquisition*

The data used in this work consist of Risso's dolphins images collected by two private reasearch associations in two different study areas across various time periods:

- $7,881$ pictures taken in the Gulf of Taranto (Northern Ionian Sea) between 2013 and 2018 by marine mammals observers aboard a 40 *ft* catamaran during standardized surveys.
- $2,840$ pictures taken near Pico island (Atlantic Ocean) in 2018 during ocean based surveys, using a 5.8 m long zodiac, equipped with a 50 HP outboard engine.

B. *Methodology*

The image preprocessing algorithm proposed in [15] using *3D polyhedron-based color segmentation* is exploited to create datasets for the deep learning classifier. Given a set of images $(x_i)_{i=1}^n$ cropped according to this procedure, the following classes are created by manually assigning a label to each sample x_i:

- class *Fin*: images x_i containing at least one clearly visible dorsal fin (label $y_i = 1$);
- class *No Fin*: all the remaining images (label $y_i = 0$).

Figure 2 summarizes such dataset creation procedure $\mathcal{D} = (x_i, y_i)_{i=1}^n$.

The considered classifier - in charge of addressing fins recognition among cropped images - is the following regularized cross entropy minimizer

$$\min_{w,b} \sum_{i=1}^{t} \log \left(\frac{e^{f_{y_i}(x_i;w,b)}}{\sum_{j=1}^{2} e^{f_j(x_i;w,b)}} \right) + \lambda \|w\|^2 \qquad (1)$$

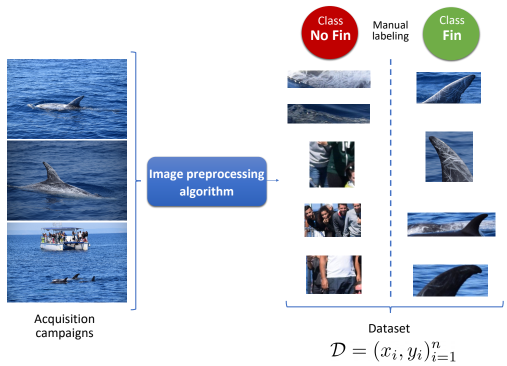

Fig. 2. Dataset creation procedure for the binary classification problem Fin vs No Fin.

where:

- (x_i, y_i) is a sample from the training set $\mathcal{T} \subseteq \mathcal{D}$, $i = 1, \ldots, t$;
- $f(x_i; w, b)$ is the two-dimensional output of a convolutional neural network, x_i being the input and w, b being the weights and the biases considered in the architecture. The subscript f_k is used to denote its k-th entry;
- $\log$ denotes the natural logarithm and its argument represents the softmax function applied to the output layer of the network;
- λ is the L2-regularization parameter used to prevent overfitting.

The minimization problem (1) is solved through an iterative gradient descent algorithm. The canonical binary classification metrics (i.e. accuracy, sensitivity, specificity) are considered to assess performances.

III. EXPERIMENTS AND RESULTS

A. *Datasets*

Three different datasets were created, with the corresponding sizes reported in table 1:

- a random split was performed on the images taken in the Gulf of Taranto: 80% to be used as the training set $\mathcal{T}$ for the problem 1, while the remaining 20% to be used as a test set (later referred as *Taranto test set*). The percentages were balanced upon each class;
- the pictures from Pico island have been used as a second test set (later referred as *Azores test set*).

Table 1. Number of images contained in each dataset.

	Fin	*No Fin*	Total
Training set $\mathcal{T}$	4,302	3,054	7,356
Taranto test set	1,076	764	1,840
Azores test set	2,411	2,383	4,794

B. Custom CNN

Similarly to the other popular convolutional neural networks [16–18], our custom architecture consists of repeated building blocks with the same structure. Dealing with a relatively straightforward binary classification problem, the peculiar design principle is maximum simplicity and clearness, as already proposed in [23].

The total number of layers is 23. There are three blocks of convolutional layers with small 3×3 kernels combined with the rectified linear unit (ReLU) activation function and a max pooling operation which reduces the block size. Later, three fully connected layers are used to get a final binary prediction out of the extracted features. A more detailed analysis of each single layer is presented in table 2.

The third and last max pooling operation (denoted as *MAXPOOL-3*) was designed to perform a more aggressive downsampling of features with respect to the original architecture proposed in [15]. The effect is to reduce the number of parameters required at the next fully connected layer in order to make the total number of parameters of our CNN comparable to ShuffleNet.

C. ShuffleNet

The pre-trained version of ShuffleNet available in Matlab has been used in our experiment [21]. It is composed of 172 layers, similar to the architecture denoted as ShuffleNet $1\times$, $g = 4$ in the original paper [18].

Addressing the binary classification task in hand with ShuffleNet required changing the network output size, from 1000 to 2. This led to a dramatic drop of the number of parameters in the last fully connected layer, from 545,000 to only 1,090 - resulting in a nearly 40% reduction of the total learnable parameters.

Despite a large number of layers, this architecture exploits the potential of a few specific operations - pointwise grouped convolution, channel shuffling and depthwise separable convolution - to greatly reduce both the computation cost and the number of parameters yet maintaining the accuracy.

D. Learning process

Common training options were used for both CNNs: the *stochastic gradient descent with momentum* algorithm, with a minibatch dimension of 30, a total number of epochs (i.e. full pass of the training set) of 30 and constant learning rate of 0.0003. The regularization parameter was fixed to $\lambda = 10^{-4}$. The following settings are instead specific to each architecture:

- the custom CNN was trained from scratch by using the so-called *Glorot initialization* [22];
- the pre-trained ShuffleNet was fine-tuned with transfer learning. A multiplicative factor of 10 was applied to the learning rate associated to the novel bidimensional output layer, in order to speed up the update of parameters in this layer. On the contrary, the learning rate of the first 10 layers was set to zero, *freezing* the initial parameters to keep the same starting features extraction.

The training process took about 39 minutes for the custom CNN and 68 minutes for ShuffleNet, using the *multiple GPUs* mode offered by Matlab on a laptop equipped with Intel Core i7-8750H CPU operating at 2.20 GHz, 8 GB RAM and Nvidia GeForce GTX 1050 Ti with 4GB of memory as graphics card. The quantitative results are reported in table 3, based on the datasets described in section III.A.

The performances on the Taranto test set are very similar for both architectures. A modest difference can be observed on the Azores test set, where ShuffleNet shows slightly better performance as reported in table 3. Considerably, the accuracy value is greater than 90% for both approaches. Designed with an 86% lower number of layers but with a similar number of parameters, the custom CNN reported a 42% speed up in the training time compared to ShuffleNet. This is a remarkable result because, generally speaking, fine-tuning a network with transfer learning should be faster and easier than training a network from scratch with randomly initialized weights (e.g. the gradients of the frozen layers do not need to be computed). However, our custom CNN outperformed ShuffleNet in terms of time required for the training.

Concerning generalization, the experiment confirms that both CNNs provide a robust feature extraction capability for the problem in hand, even with a significantly smaller number of parameters with respect to the other popular state-of-the-art architectures [16, 17].

IV. CONCLUSION AND FUTURE WORKS

A comparison between two lightweight convolutional neural networks was assessed for the task of dorsal fins recognition in the context of a Risso's dolphins photo-identification pipeline: a custom architecture trained from scratch versus a pre-trained ShuffleNet model. Overall, both CNNs achieved good performances, conferming the efficiency of such lightweight architectures for the binary classification task in hand.

Compared to ShuffleNet, the main advantages of the

Table 2. Quantitative details of the custom CNN architecture. A name is assigned to each layer, according to the following conventions: (i) CONV is used for convolutional layers, MAXPOOL for max pooling layers, FC for fully connected layers; (ii) The first index is used to keep track of an increasing order in which same types of layer appear in the architecture; (iii) The second index of the labels CONV represents the number of kernels. Note that Rectified Linear Unit (ReLU) layers placed after every single CONV layer and FC layer complete the architecture (with the exception of a softmax layer after FC-3).

Layer name	Kernel size	Weights	Bias	Output size
Input	-	-	-	224×224×3
CONV1-16	3×3×3×16	432	16	224×224×16
CONV2-16	3×3×16×16	2,304	16	224×224×16
MAXPOOL-1	2×2	-	-	112×112×16
CONV3-32	3×3×16×32	4,608	32	112×112×32
CONV4-32	3×3×32×32	9,216	32	112×112×32
MAXPOOL-2	2×2	-	-	56×56×32
CONV5-64	3×3×32×64	18,432	64	56×56×64
CONV6-64	3×3×64×64	36,864	64	56×56×64
MAXPOOL-3	8×8	-	-	9×9×64
FC-1	128×5184	663,552	128	1×1×128
FC-2	128×128	16,384	128	1×1×128
FC-3	2×128	256	2	1×1×2

Table 3. Quantitative results of the experiment. Acc, Sens, Spec are short versions for Accuracy, Sensitivity and Specificity, respectively.

	Specifications			Taranto test set			Azores test set		
CNN	Layers	Parameters	Training time	Acc	Sens	Spec	Acc	Sens	Spec
Custom	23	752,530	39 m	95.38	95.91	94.63	90.38	86.15	94.67
ShuffleNet	172	862,802	68 m	95.38	96.37	93.98	93.37	90.54	96.22

proposed custom architecture are a significantly lower number of layers - with benefits in the interpretability of its structure - and a faster training time while mantaining similar generalization properties.

Possible future experiments may consist of: (i) comparing our custom CNN to other efficient state-of-the-art architectures designed for low-cost hardware (e.g. MobileNet [24]; (ii) including in our custom architecture the same efficient convolution operations used in ShuffleNet, still preserving a reduced number of layers.

Finally, a benchmark on real hardware shall be considered, i.e. an off-the-shelf ARM-based computing core, with the ultimate goal of deploying the automated photo-identification pipeline on mobile devices with limited computational power. A very interesting use case is indeed real-time identification of individuals during sighting campaigns.

REFERENCES

[1] Carlucci, R.; Fanizza, C.; Cipriano, G.; Paoli, C.; Russo, T.; Vassallo, P. *Modeling the spatial distribution of the striped dolphin (Stenella coeruleoalba) and common bottlenose dolphin (Tursiops truncatus) in the Gulf of Taranto (Northern Ionian Sea, Central-eastern Mediterranean Sea). Ecol. Indicat.* **2016**, *69*, 707–721.

[2] Carlucci, R.; Baş, A.A.; Liebig, P.; Renò, V.; Santacesaria, F.C.; Bellomo, S.; Fanizza, C.; Maglietta, R.; Cipriano, G. *Residency patterns and site fidelity of Grampus griseus (Cuvier, 1812) in the Gulf of Taranto (Northern Ionian Sea, Central-Eastern Mediterranean Sea). Mammal Res.* **2020**, 1–11. doi:10.1007/s13364-020-00485-z.

[3] Azzolin, M.; Arcangeli, A.; Cipriano, G.; Crosti, R.; Maglietta, R.; Pietroluongo, G.; Saintingan, S.; Zampollo, A.; Fanizza, C.; Carlucci, R. *Spatial distribution modelling of striped dolphin (Stenella coeruleoalba) at different geographical scales within the EU Adriatic and Ionian Sea Region, central-eastern Mediterranean Sea. Aquatic Conserv. Mar. Freshw. Ecosyst.* **2020**. doi:10.1002/aqc.3314.

[4] Azzellino, A.; Fossi, M.C.; Gaspari, S.; Lanfredi, C.; Lauriano, G.; Marsili, L.; Panigada, S.; Podesta, M. *An index based on the biodiversity of cetacean species*

to assess the environmental status of marine ecosystems. Mar. Environ. Res. **2014**, *100*, 94–111.

[5] Pace, D.; Tizzi, R.; Mussi, B. *Cetaceans value and conservation in the Mediterranean Sea. J. Biodiv. Endang. Spec.* **2015**, *2015*. doi:10.4172/2332-2543.S1-004.

[6] Arcangeli, A.; Campana, I.; Bologna, M.A. *Influence of seasonality on cetacean diversity, abundance, distribution and habitat use in the western Mediterranean Sea: implications for conservation. Aquatic Conserv. Mar. Freshw. Ecosyst.* **2017**, *27*, 995–1010.

[7] Nowacek, D.P.; Christiansen, F.; Bejder, L.; Goldbogen, J.A.; Friedlaender, A.S. *Studying cetacean behaviour: new technological approaches and conservation applications. Anim. Behav.* **2016**, *120*, 235–244.

[8] Baş, A.A.; Öztürk, B.; Öztürk, A.A. *Encounter rate, residency pattern and site fidelity of bottlenose dolphins (Tursiops truncatus) within the Istanbul Strait, Turkey. J. Mar. Biol. Assoc. UK* **2019**, *99*, 1009–1016.

[9] Hartman, K.L. *Risso's Dolphin: Grampus griseus.* In *Encyclopedia of Marine Mammals*; Elsevier: 2018; pp. 824–827.

[10] Maglietta, R.; Renò, V.; Cipriano, G.; Fanizza, C.; Milella, A.; Stella, E.; Carlucci, R. *DolFin: An innovative digital platform for studying Risso's dolphins in the Northern Ionian Sea (North-eastern Central Mediterranean). Sci. Rep.* **2018**, *8*, 17185. doi:10.1038/s41598-018-35492-3.

[11] Renò, V.; Dimauro, G.; Labate, G.; Stella, E.; Fanizza, C.; Cipriano, G.; Carlucci, R.; Maglietta, R. *A SIFT-based software system for the photo-identification of the Risso's dolphin. Ecol. Inform.* **2019**, *50*, 95–101. doi:10.1016/j.ecoinf.2019.01.006.

[12] Maglietta, R.; Renò, V.; Caccioppoli, R.; Seller, E.; Bellomo, S.; Santacesaria, F.C.; Colella, R.; Cipriano, G.; Stella, E.; Hartman, K.; et al. *Convolutional Neural Networks for Risso's dolphins identification. IEEE Access* **2020**, 1. doi:10.1109/ACCESS.2020.2990427.

[13] Buehler, P., Carroll, B., Bhatia, A., Gupta, V., & Lee, D.E. (2019). *An automated program to find animals and crop photographs for individual recognition*. Ecol. Informatics, 50, 191-196.

[14] Schofield, D., Nagrani, A., Zisserman, A., Hayashi, M., Matsuzawa, T., Biro, D., Carvalho, S. (2019). *Chimpanzee face recognition from videos in the wild using deep learning*. Science Advances. 5. 10.1126/sciadv.aaw0736.

[15] Renò, V.; Losapio, G.; Forenza, F.; Politi, T.; Stella, E.; Fanizza, C.; Hartman, K.; Carlucci, R.; Dimauro, G.; Maglietta, R. *Combined Color Semantics and Deep Learning for the Automatic Detection of Dolphin Dorsal Fins.*, Electronics 2020, 9, 758. doi:10.3390/electronics9050758.

[16] Szegedy, C., Liu, W., Jia, Y., Sermanet, P., Reed, S., Anguelov, D., Rabinovich, A. (2015). *Going deeper with convolutions*. In Proceedings of the IEEE conference on computer vision and pattern recognition (pp. 1-9).

[17] Krizhevsky, A., Sutskever, I., Hinton, G. E. (2012). *Imagenet classification with deep convolutional neural networks*. In Advances in neural information processing systems (pp. 1097-1105).

[18] Zhang, X., Zhou, X., Lin, M., Sun, J. (2018). *Shufflenet: An extremely efficient convolutional neural network for mobile devices*. In Proceedings of the IEEE conference on computer vision and pattern recognition (pp. 6848-6856).

[19] Ma, N., Zhang, X., Zheng, H. T., Sun, J. (2018). *Shufflenet v2: Practical guidelines for efficient cnn architecture design*. In Proceedings of the European Conference on Computer Vision (ECCV) (pp. 116-131).

[20] Russakovsky, O., Deng, J., Su, H. et al. *ImageNet Large Scale Visual Recognition Challenge*. Int J Comput Vis 115, 211-252 (2015). https://doi.org/10.1007/s11263-015-0816-y

[21] `https://mathworks.com/help/deeplearning/ref/shufflenet.html`, accessed on May 10, 2020.

[22] Glorot, X., Bengio, Y. (2010, March). *Understanding the difficulty of training deep feedforward neural networks*. In Proceedings of the thirteenth international conference on artificial intelligence and statistics (pp. 249-256).

[23] Renò, V.; Mosca, N.; Marani, R.; Nitti, M.; D'Orazio, T.; Stella, E. *Convolutional neural networks based ball detection in tennis games*. In Proceedings of the IEEE Conference on Computer Vision and Pattern Recognition Workshops, Salt Lake City, UT, USA, 18-22 June 2018; pp. 1758-1764. doi:10.1109/CVPRW.2018.00228.

[24] A. G. Howard, M. Zhu, B. Chen, D. Kalenichenko,W.Wang, T. Weyand, M. Andreetto, and H. Adam. Mobilenets: *Efficient convolutional neural networks for mobile vision applications.* arXiv preprint arXiv:1704.04861, 2017.

2020 IMEKO TC-19 International Workshop on
Metrology for the Sea
Naples, Italy, October 5-7, 2020

Occurrence of *Physeter macrocephalus* and *Ziphius cavirostris* in the North Ikaria Basin, Aegean Sea

Patrice Hostetter[1], Alexandra Koroza[1], Thodoris Tsimpidis[1], Guido Pietroluongo[1], Roberto Carlucci[2], Giulia Cipriano[2]

[1] *Archipelagos Institute of Marine Conservation, P.O Box 42, Pythagorio 83 103 Samos, Greece, p.hostetter@archipelago.gr, aleksandra24koroza@gmail.com, t.tsimpidis@archipelago.gr guido.p@archipelago.gr*

[2] *Department of Biology, University of Bari, Via Orabona 4, 70125 Bari, Italy, e-mail: roberto.carlucci@uniba.it; giulia.cipriano@uniba.it*

***Abstract* – The presence of two of the 8 regular cetaceans of the Mediterranean Sea, the sperm whale (*Physeter macrocephalus*) and Cuvier's beaked whale (*Ziphius cavirostris*) is well-documented in the Western and Central Mediterranean Sea. In contrast, little information is available on their distribution in the Eastern Mediterranean, especially in the North Ikaria Basin, an underestimated important habitat for both species. Seasonal opportunistic visual surveys were conducted in this area from 2017 to 2019 to investigate their distribution. Out of 15 surveys, 4 sightings of *P. macrocephalus* and 2 sightings of *Z. cavirostris* were recorded. This is the first confirmed visual record of *Z. cavirostris* in this area. The documentation of both species in this preliminary study represents a significant contribution to consider efficient conservation action in this important area.**

I. INTRODUCTION

The Mediterranean Sea is an incredible hotspot of biodiversity [1,2] with around 25,000 species; out of which more than half are endemic [3]. Among cetacean species regularly occurring in the Mediterranean Sea [4,5], the sperm whale, *Physeter macrocephalus,* and Cuvier's beaked whale, *Ziphius cavirostris* are deep-diving species, that due to their short surface period and long dive time, make difficult their field observation at sea [6,7,8].

The Mediterranean subpopulation of sperm whale is genetically distinct from the Atlantic one [9] and has been classified as Endangered by the IUCN [10]. Though no accurate population estimate exists in the basin, there is an estimated decrease in its population size due to anthropogenic impacts, such as entanglements in fishing nets and ship strikes [10].

Cuvier's beaked whale is the only beaked whale recorded in the Mediterranean [11] and much of the knowledge on its presence and distribution has come from stranding data. Recently, its Mediterranean subpopulation was classified as Vulnerable by IUCN [12] and estimated roughly 5800 individuals occurring in few, high-density areas [13].

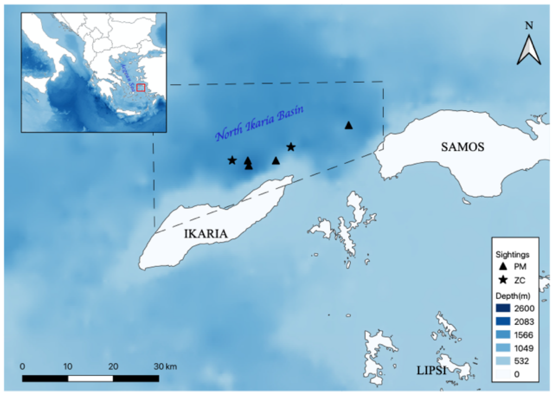

Fig. 1. Sightings of P. macrocephalus *(represented by triangles) and* Z. cavirostris *(represented by stars) in the study area in the North Ikaria Basin, Aegean Sea from 2017 to 2020.*

Although these two odontocete species inhabit both the Western and Eastern Mediterranean basin, knowledge on their distribution is mainly referred to the western region, resulting limited and fragmented in eastern basin especially in the Aegean Sea [13,14,15]. Here, most of the knowledge on *P. macrocephalus* originates especially from acoustic surveys [16,17], followed by sporadic sightings and strandings data [18,19], while information on *Z. cavirostris* derives especially from strandings data and acoustic survey [11,14,16,20]. Therefore, the aim of this study is to provide update information on the presence

2020 IMEKO TC-19 International Workshop on
Metrology for the Sea
Naples, Italy, October 5-7, 2020

of these two deep pelagic species in the North Ikaria Basin, Aegean Sea. In addition, preliminary information on their surface and dive behaviour are provided.

II. METHODS

A. Study Area

The North Ikaria Basin, in the central Aegean Sea, is characterised by an extended plateau with small underwater depressions up to 1000 m in depth [21] and featuring a deep trench that reaches up to 1200 m in depth [22].

B. Data Collection

Sighting data were collected in the North Ikaria Basin during seasonal vessel-based surveys carried out along opportunistic line transects from the islands of Samos and Lipsi to the island of Ikaria from March 2017 to October 2019 (Fig. 1). The sampling effort was set at about 5 h/day along 30 kilometres approximately. Speed was maintained at 6 knots and trips occurred only in favourable sea-weather conditions (Douglas scale $\leqslant$ 3 and Beaufort scale $\leqslant$ 4).

Four trained observers actively searched for cetaceans, using visual techniques by scanning the sea surface 360° around the research vessel, although observers focused the majority of their effort ahead of the vessel at the track line [23]. When a sighting occurred, data including time of first contact, depth (m) and group size (number of individuals) were collected and GPS coordinates were recorded every 3 minutes. In addition, weather conditions, the occurrence of other species or others nearby vessels, was also recorded.

Behavioural data were collected every 3 minutes for at least 30 min or until individuals exhibited negative behaviour, adopting the focal-group method with instantaneous scan sampling [24]. Behavioural variables recorded included distance from boat, speed, aerial displays, and activity [24,25]. When possible, photos were taken using a Canon EOS 1300D with an EF 75-300mm ZOOM Lens and a video recording was taken using a JVC EverioR camcorder.

III. RESULTS

A total of 16 surveys were carried out in the North Ikaria Basin, applying an effort of approximately 54 hrs of observation covering 494 km. Four sightings of *P. macrocephalus* and two sightings of *Z. cavirostris* were recorded during the study period at a depth ranging from 678 to 1465 m (Table 1).

A. Physeter macrocephalus

From March 2017 to October 2019, a total of 7 *P. macrocephalus* were recorded, 2 in 2017 and 5 in 2019 (Table 1). Sightings occurred in a depth range from 678 m

Fig. 2. P. macrocephalus *recorded on 02/09/2019 in the North Ikaria Basin. ©2019 E. Papadopoulou, Archipelagos Institute of Marine Conservation.*

to 1465 m with a mean depth of 1138±362 m and at a distance from shore ranging from 4 to 8 km with a mean of 62±2 km (Table 1). Two sightings occurring in 2017 and 2019 lasted over an hour.

The first occurring on September 13th, 2017 had a duration of 150 minutes in which sperm whales spent approximately 57% of the sighting resting, 37% in short dives (<5 mins) with 2-4 minutes surface interval between each dive and 5% of the time swimming. In addition, 3 breaches and 4 tail out events were observed.

The second sighting occurring on September 2nd, 2019 had a duration of 70 minutes. During the sighting, 2 of the whales dove near the beginning of the sighting and were not re-sighted. The third whale (Fig. 2) spent approximately 62% of the sighting resting and 38% of swimming, approaching and circling the research vessel. A breach event as well as 4 tail outs, a head slap and 2 tail slaps were observed.

Two additional sightings on August 29th, 2019 and October 30th, 2019 lasted less than 5 minutes and therefore no behavioural data was collected.

B. Ziphius cavirostris

In the same study period, a total of 4 individuals of *Z. cavirostris* were recorded, 2 Cuvier's beaked whales for each sighting (Table 1). Sightings occurred at a depth range from 982 to 1206 m with a mean depth of 1094±159 m and at a distance from shore ranging from 6 to 10 km with a mean of 8±3 km (Table 1).

Both sightings lasted less than 10 minutes, in 2017 the sighting had a duration of 9 minutes, while in 2019 both whales dove immediately after being sighted. Unfortunately, no behavioural data was collected.

Table 1. Sampling period, number of surveys, effort (hours and kilometres), depth range of sightings (m), number of sightings and individuals of P. macrocephalus *and* Z. cavirostris *occurred in the North Ikaria Basin, from 2017 to 2020.*

2020 IMEKO TC-19 International Workshop on
Metrology for the Sea
Naples, Italy, October 5-7, 2020

Sampling period	# of survey	Effort		Depth range (m)		# of sightings		# of individuals	
		hours	km	PM	ZC	PM	ZC	PM	ZC
Mar-Oct 2017	5	13:24	187.8	1020	981	1	1	2	2
Mar-Oct 2018	6	20:06	166.6	-	-	-	-	-	-
May-Oct 2019	5	20:48	139.4	678-1465	1206	3	1	5	2
Total	16	54:18	493.8	678-1465	981-1206	4	2	7	4

IV. DISCUSSION

This preliminary study provides reliable evidence of the occurrence of *P. macrocephalus* and *Z. cavirostris* in the North Ikaria Basin and provides an update on current knowledge of their distribution in a data-deficient area [14].

A. Physeter macrocephalus

Until now, the occurrence of *P. macrocephalus* in the North Ikaria Basin resulted in 4 sightings recorded from 2004 to 2012 [13] and by acoustical surveys carried out in 2013 [14]. The addition of 4 sightings of 7 individuals in this area contributes significantly to knowledge base in this data deficient area.

Distribution of *P. macrocephalus* is highly dependent on prey availability, which is found at depths of 500-1000 m [26]. In the Eastern Mediterranean, most records of *P. macrocephalus* occurred at depths ranging from 500-1500 m [14], though some have been recorded at depths as low as 3600 m [16] which is consistent with the sightings in this study. In addition, as with previously recorded sightings [18], sperm whales recorded here in 2017 and 2019 occurred during the fall and winter months. The proximity of the North Ikaria Basin to core habitats [11,15] suggests the hypothesis of migratory routes of the species.

Surface activity of *P. macrocephalus* is thought to have a social function [27,28], even if there are various explanations regarding the purpose of these behaviours [28]. Regardless, the surface behaviour observed here, such as breaching, tail slaps, and tail outs provide a foundation for further research.

B. Ziphius cavirostris

The occurrence of 2 sightings of two individuals of *Z. cavirostris* represents the first published visual record of this species in this area, where it was only detected acoustically [16]. Interestingly, the 2017 sighting is in close proximity to where they were acoustically detected in 2013 [16]. Moreover, the presence of 2 individuals together in both sightings recorded in the study area, provides more discussions about the hypothesis of habitat use and social structure of the species in the study area. This also suggests that the North Ikaria Basin is an important area for *Z. cavirostris*; which is further highlighted by the presence of the steep slope in the sea floor, providing suitable habitat for hunting prey [14,29,30].

V. CONCLUSION

This study provides update occurrence data of *P. macrocephalus* and *Z. cavirostris* in the North Ikaria Basin. Though limited by the lack of regular and dedicated survey effort to this area, it confirms the presence and distribution of these odontocete species in this part of the Aegean Sea providing, in addition, preliminary information on their surface behaviour.

The presence of these top predators is an important factor in maintaining a well-functioning ecosystem [31,32]. Due to their body size, these species can consume hundreds of kilograms of food per day [32,36]. As most of their diet consists of the widely distributed mesopelagic squid [19,30,33-36], the abundance of *P. macrocephalus* and *Z. cavirostris* is an important factor in the management of lower trophic levels.

To better understand their ecological role, it is crucial to understand species distribution in areas like the North Ikaria Basin. In order to fill in these important knowledge gaps that exist for these species, it is necessary to conduct more frequent, dedicated surveys. Areas for future study are the establishment of migratory routes, feeding grounds, as well as seasonal distribution. Furthermore, future management and conservation measures rely on accurate population estimates and distribution. This information is a prerequisite for developing efficient conservation action focused on these species.

VI. REFERENCES

[1] C. N. Bianchi and C. Morri, "Marine biodiversity of the Mediterranean Sea: Situation, problems and prospects for future research", Mar. Pollut. Bull., vol. 40, No. 5, May 2000, pp. 367–376.

[2] M. Coll et al., "The Biodiversity of the Mediterranean Sea: Estimates, patterns, and threats", PLOS ONE, vol. 5, No. 8, August 2010, p. e11842.

[3] A. Cuttelod, N. Garcia, D. A. Malak, H. J. Temple, V. Katariya, "The Mediterranean: a biodiversity hotspot under threat", Wildl. Chang. World- Anal. 2008 IUCN Red List Threat. Species, 2009, pp. 89–101.

[4] G. Notarbartolo di Sciara and A. Birkun, Jr., "Conserving whales, dolphins and porpoises in the Mediterranean and Black Seas: an ACCOBAMS status report", ACCOBAMS, Monaco, 2010.

[5] G. Notarbartolo di Sciara, "Chapter One - Marine Mammals in the Mediterranean Sea: An Overview", in Advances in Marine Biology, vol. 75, G.

2020 IMEKO TC-19 International Workshop on
Metrology for the Sea
Naples, Italy, October 5-7, 2020

Notarbartolo Di Sciara, M. Podestà, and B. E. Curry, Eds. Academic Press, 2016, pp. 1–36.

[6] P.Tepsich, M.Rosso,P.N.Halpin, A.Moulins, “Habitat preferences of two deep-diving cetacean species in the northern Ligurian Sea”. Marine Ecology Progress Series, vol. 508, 2014, pp. 247–260.

[7] H. Whitehead, “Sperm whale: . 2009. In: W.F.Perrin, B.Wursig, J.G.M.Thewissen (Eds.) Encyclopedia of Marine Mammals 2nd ed. Academic Press.

[8] P. L. Tyack, M. Johnson, N. A. Soto, A. Sturlese, P. T. Madsen, "Extreme diving of beaked whales", J. Exp. Biol., vol. 209, No. 21, November 2006, pp. 4238–4253.

[9] V. Dulau et al., "A note on genetic isolation of Mediterranean sperm whales (*Physeter macrocephalus*) suggested by mitochondrial DNA", J. Cetacean Res. Manag., vol. 6, January 2004.

[10] G. Notarbartolo-Di-Sciara, A. Frantzis, G. Bearzi, R. Reeves, "*Physeter macrocephalus*", IUCN Red List Threat. Species, 2012.

[11] M. Podestà et al., "Chapter Four - Cuvier’s Beaked Whale, *Ziphius cavirostris*, Distribution and Occurrence in the Mediterranean Sea: High-Use Areas and Conservation Threats", in Advances in Marine Biology, vol. 75, G. Notarbartolo Di Sciara, M. Podestà, and B. E. Curry, Eds. Academic Press, 2016, pp. 103–140.

[12] A. Cañadas and G. Notarbartolo di Sciara, "*Ziphius cavirostris* (Mediterranean subpopulation)", IUCN Red List Threat. Species 2018, 2018.

[13] A. Cañadas et al., "The challenge of habitat modelling for threatened low density species using heterogeneous data: The case of Cuvier’s beaked whales in the Mediterranean", Ecol. Indic., vol. 85, 2018, pp. 128–136.

[14] A. Frantzis, P. Alexiadou, G. Paximadis, E. Politi, A. Gannier, M. Corsini-Foka, "Current knowledge of the cetacean fauna of the Greek Seas", J. Cetacean Res. Manag., vol. 5, No. 3, 2003.

[15] A. Frantzis, P. Alexiadou, K. C. Gkikopoulou, "Sperm whale occurrence, site fidelity and population structure along the Hellenic Trench (Greece, Mediterranean Sea)", Aquat. Conserv. Mar. Freshw. Ecosyst., vol. 24, No. S1, 2014, pp. 83–102.

[16] C. Ryan et al., "A visual and acoustic survey for marine mammals in the Eastern Mediterranean Sea during Summer 2013", International Fund for Animal Welfare, April 2014.

[17] T. Lewis, O. Boisseau, M. Danbolt, et al.,” Abundance estimates for sperm whales in the Mediterranean Sea from acoustic line-transect surveys”, J. Cetacean Resr. Manage., vol. 18, pp. 103-117.

[18] A. A. Öztürk, A. M. Tonay, A. Ded, "Sperm whale (*Physeter macrocephalus*) sightings in the Aegean and Mediterranean part of Turkish waters", J. Black Sea Mediterr. Environ., vol. 19, No. 2, 2013, pp. 169–177.

[19] T. Katağan, A. Tokaç, Ş. Beşiktepe, B. Öztürk, Eds., "Cetacean in the Aegean Sea", in The Aegean Sea Marine Biodiversity, Fisheries, Conservation and Governance., vol. 41, Turkish Marine Research Foundation, Istanbul, Turkey, 2015, pp. 599–611.

[20] M. Podestà, A. D’Amico, G. Pavan, A. Drougas, A. Komnenou, N. Portunato, "A review of Cuvier’s beaked whale strandings in the Mediterranean Sea", J. Cetacean Res. Manag., vol. 7, 2006, pp. 251–261.

[21] D. Yaşar, "Marine geology of the Aegean Sea", in T. Katağan, A. Tokaç, Ş. Beşiktepe, B. Öztürk, Eds., The Aegean Sea Marine Biodiversity, Fisheries, Conservation and Governance., vol. 41, Turkish Marine Research Foundation, Istanbul, Turkey, 2015, pp. 55–75.

[22] M. Ergün, "General tectonics of the Aegean Sea area and geophysical signatures", in T. Katağan, A. Tokaç, Ş. Beşiktepe, B. Öztürk, Eds., The Aegean Sea Marine Biodiversity, Fisheries, Conservation and Governance., vol. 78–93, Turkish Marine Research Foundation, Istanbul, Turkey, 2015, pp. 55–75.

[23] J. Gordon, S. D. Berrow, E. Rogan, and S. Fennelly, "Acoustic and visual survey of cetaceans off the Mullet Peninsula, Co Mayo", Ir. Nat. J., vol. 26, No. 7/8, 1999, pp. 251–259.

[24] J. Mann, "Unraveling the dynamics of social life." Cetacean societies: field studies of dolphins and whales. University of Chicago Press, Chicago, Illinois, USA, 2000, pp. 45-64.

[25] S. Shane, "Behavior and ecology of the bottlenose dolphin at Sanibel Island, Florida", Bottlenose Dolphin, 1990, pp. 245–265

[26] E. Praca, A. Gannier, K. Das, S. Laran, "Modelling the habitat suitability of cetaceans: Example of the sperm whale in the northwestern Mediterranean Sea", Deep Sea Res. Part Oceanogr. Res. Pap., vol. 56, No. 4, Apr. 2009, pp. 648–657.

[27] B. Würsig and H. Whitehead, ‘Aerial behavior’, in Encyclopedia of Marine Mammals (Second Edition), W. F. Perrin, B. Würsig, and J. G. M. Thewissen, Eds. London: Academic Press, 2009, pp. 5–11.

[28] S. Waters and H. Whitehead, “Aerial behaviour in sperm whales”, *Can. J. Zool.*, vol. 68, No. 10, Oct. 1990, pp. 2076–2082.

[29] A. Gannier and J. Epinat, "Cuvier’s beaked whale distribution in the Mediterranean Sea: results from small boat surveys 1996–2007", J. Mar. Biol. Assoc. U. K., vol. 88, No. 6, September 2008, pp. 1245–1251.

2020 IMEKO TC-19 International Workshop on
Metrology for the Sea
Naples, Italy, October 5-7, 2020

[30] C. D. MacLeod, M. B. Santos, G. J. Pierce, "Review of data on diets of beaked whales: Evidence of niche separation and geographic segregation", J. Mar. Biol. Assoc. U. K., vol. 83, No. 3, June 2003, pp. 651–665.

[31] W. D. Bowen, "Role of marine mammals in aquatic ecosystems", Mar. Ecol. Prog. Ser., vol. 158, November 1997, pp. 267–274.

[32] S. Laran, C. Joiris, A. Gennier, R. Kenney, "Seasonal estimates of densities and predation rates of cetaceans in the Ligurian Sea, northwestern Mediterranean Sea: An initial examination", J. Cetacean Res. Manag., vol. 11, March 2010, pp. 31–40.

[33] F. Garibaldi and M. Podestà, "Stomach contents of a sperm whale (*Physeter macrocephalus*) stranded in Italy (Ligurian Sea, north-western Mediterranean)", J. Mar. Biol. Assoc. U. K., vol. 94, No. 6, September 2014, pp. 1087–1091.

[34] I. Foskolos, A. Alberini, P. Alexiadou, A. Frantzis, "Feeding habits of sperm whales (*Physeter macrocephalus*) in the Greek Seas, Eastern Mediterranean," in 30th Annual Conference of the European Cetacean Society, Funchal, Madeira, March 2016.

[35] I. Foskolos, N. Koutouzi, L. Polychronidis, P. Alexiadou, A. Frantzis, "A taste for squid: the diet of sperm whales stranded in Greece, Eastern Mediterranean", Deep Sea Res. Part Oceanogr. Res. Pap., vol. 155, January 2020, p. 103164.

[36] M. B. Santos et al., "Feeding ecology of Cuvier’s beaked whale (*Ziphius cavirostris*): a review with new information on the diet of this species", J. Mar. Biol. Assoc. U. K., vol. 81, No. 4, 2001, pp. 687–694.

Evaluation of environmental stressors in a population of long-snouted seahorses *Hippocampus guttulatus* through an innovative Citizen Science approach

Michele Gristina1, Tamara Lazic2*, Federico Quattrocchi3, Giuseppe Corriero4, Cataldo Pierri5

1 National Council of Research (CNR), Institute of Anthropic Impacts and Sustainability in marine environment (IAS), michele.gristina@cnr.it

2 Department of Biology, University of Bari Aldo Moro, Bari, Italy, tamaralazic90@yahoo.com

3 National Research Council (CNR), Institute for Marine Biological Resources and Biotechnologies (IRBIM), quattrocchi.federico@gmail.com

4 Department of Biology, University of Bari Aldo Moro, Bari, Italy, giuseppe.corriero@uniba.it

5 Department of Biology, University of Bari Aldo Moro, Bari, Italy, cataldo.pierri@uniba.it

Abstract – The present study describes **the sudden decline in *Hippocampus guttulatus* population at Mar Piccolo di Taranto (MPT) (Southeastern Italy) under the combined effects of fishing activities and illegal trade. Until recently, MPT hosted one of the most interesting and largest populations of long-snouted seahorses in the Mediterranean Sea. Disclosure and online report on the seahorse trafficking from Italy to China (https://veraleaks.org) in February 2019 prompted us to conduct interviews with the main stakeholders operating at MPT in order to evaluate the local population awareness, the extent of the phenomenon and the potential effects on seahorse's population.**

I. INTRODUCTION

According to many documents and scientific papers, Illegal, Unreported and Unregulated (IUU) fishing and Illegal Wildlife Trade (IWT) are among the most serious threats for sustainable fisheries and aquatic animal conservation worldwide [1,2]. To date, following habitat loss and degradation, illegal trade is considered the most damaging hazard to the wildlife [3] and a fundamental driver of biodiversity loss in both aquatic and terrestrial habitats [4,2]. Seahorses (47 species of *Hippocampus* spp. genus) are particularly threatened by IWT and were the first marine bony fish subjected to the trade regulation on a global scale [5]. Seahorses are mainly traded in a dried form for their use in Traditional Chinese Medicine (TCM), but also for curios and aquarium display [5], at a level that probably threatens the sustainability of many populations [6]. In this context [7], it was estimated that the global catches count for approximately 37 million individuals per year, mainly sourced from bycatch and non-selective fisheries [6, 8]. In this paper, we describe the sudden decline in *Hippocampus guttulatus* population at Mar Piccolo di Taranto (Southeastern Italy) (hereafter called MPT) under the combined effects of illegal fishing and trade. MPT hosts one of the largest and most interesting populations of long-snouted seahorses in the Mediterranean Sea [9]. Disclosure and publishing of an online report on the trafficking of seahorses from Italy to China (https://veraleaks.org) in February 2019 triggered to carry out the interviews with the main stakeholders operating at MPT. Due to the difficulties that arise when dealing with the illegal market and its extent, the indirect investigation is often the only possibility. Therefore, by taking advantage of the knowledge of those who attend MPT for various reasons, this study included the distribution of online questionnaires among operators and users of MPT to reconstruct seahorse history by investigating the population status, its trend in the last nine years and the main stressors that could have caused the population decline.

II. MATERIAL AND METHODS

Following the first report on illegal trafficking of seahorses at MPT, in conjunction with the observed decline in population density during a series of experiments on seahorses' home range (10), a questionnaire was prepared and used to assess the extent of the seahorse harvesting. From February to April 2020, the questionnaire was distributed among the main categories operating at MPT (for both professional and recreative purposes). In particular, interviews were carried out with the scientific institutions (local University and National Council of Research of Taranto), environmental associations (WWF, Legambiente, Marevivo), press agency, military and governmental institutions (Coast Guard, Italian Military Navy, Italian Air force), artisanal fishermen and mussel farmers (Tab. 1). The survey sought information on five key topics: 1) General interviewers' information (employment, activities carried out at MPT, number of diving hours/year, the average number of seahorse sighted/hour); 2) Temporal trends of seahorse population (increasing, declining, starting year); 3) Main causes of the population density changes (fishing activities, natural causes, pollution); 4) Features of the legal and illegal fishing activities (gear, season, area, N° of vessels, N° days/year); 5) Eventual presence of the seahorse-targeted fisheries (number of vessels, commercial value). The answer consistency was assessed in the sequence of questions in questionnaires, and only congruent interviews were used for further analysis.

III. RESULTS

A total of 59 questionnaires have been filled by stakeholders operating at MPT. Eight questionnaires that showed inconsistent responses were eliminated and not considered in subsequent analysis. A total of seven operators' categories were consulted, although the participation of categories potentially involved in the activities that could threaten seahorses population (artisanal fishermen, mussel farmers) were very rare and scanty (Table 1).

Table 1 - List of interviewed categories and number of respondents by category.

	Number of respondent per category
Government Official	4
Local NGO	2
Photosub Divers	22
Mussel Farmers	2
Fishermen	1
Academic (Biologist, Reseracher	5
Ricreative Divers	12
n.r.	3

Figure 1 shows that more than 64 % of respondents reported a decline in seahorse density, while the main stressor influencing seahorse population was represented by fishing activities carried out at MPT (Figure 2).

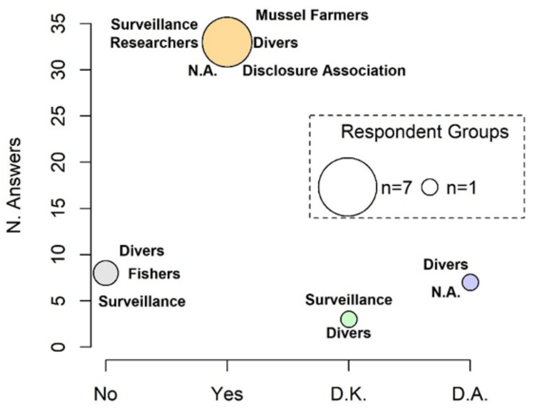

Figure 1 – Perception of density decline in *H. guttulatus* population. The size of the circle is proportional to the number of responding categories. D. K. = doesn't know; D.A. = doesn't answer.

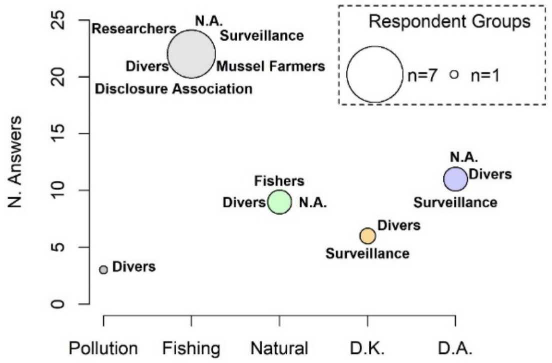

Figure 2 – The mainly responsible causes for the density decline in *H. guttulatus* population. The size of the circle is proportional to the number of responding categories. D. K. = doesn't know; D.A. = doesn't answer.

Fishing activities were conducted with different traditional techniques (using trammel nets, small purse seine, small skid gears (called "firrchjar") or directly by divers (aiming *Sepia* spp. juveniles fishing)), but these mainly reported seahorses as a bycatch. However, only 19,4 % of the respondents underlined that seahorse specimens, caught by professional fishermen, are retained as a curio or are used for the illegal market sale. However, the decline in seahorse density seems to have started in 2016 and continued until 2019.

Conducted interviews only partially confirmed fishing activities that specifically targeted seahorses. 41,1 % of respondents have never directly witnessed this activity, while 39,2 % of respondents confirmed its common practice at MPT (Figure 3). Among the latter, 35 % stated that the fleet is composed of 3/5 boats, 20 % of 2 boats and 10 % of 5/8 boats, while the remaining 30 % of respondents did not provide any number. Only 9 out of 51 questionnaires supplied information on the commercial value of seahorses in the illegal market, ranging from 1 to 20 €/individual or from 500 to 600 €/Kg.

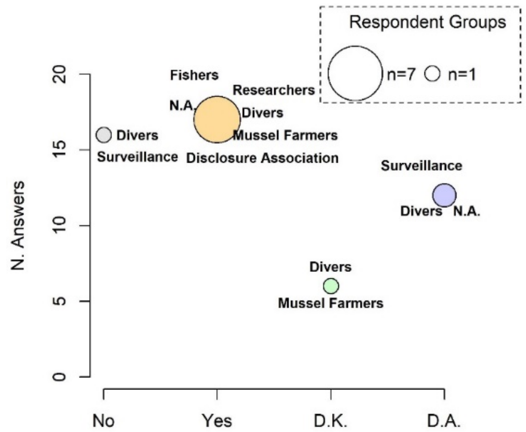

Figure 3 – Presence of *H. guttulatus*-targeted fisheries. The size of the circle is proportional to the number of responding categories. D. K. = doesn't know; D.A. = doesn't answer.

IV. DISCUSSION

Until 2015, the population of long-snouted seahorses at MPT was one of the largest throughout the entire Mediterranean and European waters [8, 11]. The abundance of *H. guttulatus* in this semi-enclosed marine area was comparable to those recorded at Ria Formosa (Portugal), (0.073 seahorses/m2) [12] and Mar Menor (Spain) (www.asociacionhippocampus.com). On a wide time scale, great density fluctuations have been described in some of these populations and were positively correlated with habitat changes, related availability of holdfasts [13] and eutrophication processes (www.asociacionhippocampus.com). From Autumn 2015 to Spring 2016, the density (individuals/m^2) of *H. guttulatus* in some parts of MPT declined dramatically by approximately 90%. Nevertheless, in the investigated period, no apparent changes have been recorded neither in the spatial distribution of habitats nor in the holdfast availability; indeed, analysis of the temperature time series did not reveal any particular anomaly. However, interviews carried out with the main stakeholders allowed the description of increasing fishing activities at MPT. Although interviews underlined that fishermen usually release most of the captured seahorses, we believe that the combined effects of the fishing gears on seabed and displacement of a substantial number of captured individuals (due to their release in different locations and habitats respect to the capture site) may have had an important impact on the population. As suggested by [13], the ability of seahorses to return to the original capture site is rather weak and strongly affected by conditions in the new environment. Due to the illegal and clandestine nature of this activity, however, it appears very difficult to identify its beginning. Notwithstanding, the conducted interviews allowed to highlight that international trafficking, started in early 2016, has a considerable effect on the long-snouted seahorse's population and the perspectives for its conservation. Until recently, fishing along the Italian coasts was generally considered as a negligible danger to seahorse populations, which were rather threatened by degradation and fragmentation of coastal habitats [14]. Nevertheless, as described in this paper, the combination of increasing fishing pressures and renewed market's demand poses a new threat to seahorse populations. There is a need to register a new trade route of the illegal wildlife trafficking in which the Mediterranean is the source while Asia is the final market. In accordance with [15], the present study highlighted these trade routes as a part of the dynamic network. Indeed, not long ago, Europe was considered as an end market and transit hub for illegal wildlife trade, with European seas and airports commonly used for smuggling of the illicit wildlife products from Africa to Asia (www.traffic.org).

This paper contributes to shedding light on a new scenario characterised by a constant demand for seahorses by eastern countries in strong economic expansion and a renewed offer from western countries that, in the recent past, were subjected to an evident economic recession. This unexpected and unpredictable condition represents a new and alarming threat to seahorse populations in the Mediterranean Sea. Therefore, more intense and effective actions to prevent and combat illegal processes, as well as continuous and close monitoring to assess the state of the populations, seem urgently needed.

REFERENCES

[1] FAO, The State of World Fisheries and Aquaculture, 2016. ⟨http://dx.doi.org/92-5- 105177-1⟩.

[2] Margulies JD, Bullough L-A, Hinsley A, et al. Illegal wildlife trade and the persistence of "plant blindness". Plants, People, Planet. 2019;1:173–182. https ://doi.org/10.1002/ppp3.100[53

[3] Zimmerman,M.E.2003.The black market for wildlife: combating transnational organized crime in the illegal wildlife trade. J. Transnat. Law 36: 1657–1689.

[4] Harris, J.B.C., Tingley, M.W., Hua, F., et al. (2016). Measuring the impact of the pet trade on Indonesian birds. Conserv. Biol. DOI: 10.1111/cobi.12729

[5] Sarah J. Foster, Ting-Chun Kuoa, Anita Kar Yan Wan, Amanda C.J. Vincent 2019 - Global seahorse trade defies export bans under CITES action and national legislation. Marine Policy 103, 33–41

[6] Vincent ACJ, Foster SJ, Koldewey HJ. 2011. Conservation and management of seahorses and other Syngnathidae. Journal of Fish Biology 78: 1681–1724.Lawson et al. (2017)

[7] Foster, S.J. (2016). Seahorses (*Hippocampus* spp.) and the CITES Review of Significant Trade. Fisheries Centre Research Reports 24(4): 48 pp.

[8] Gristina M, Cardone F, Carlucci R, Castellano L, Passarelli S, Corriero G. 2015. Abundance, distribution and habitat preference of *Hippocampus guttulatus* and *Hippocampus hippocampus* in a semi-enclosed central Mediterranean marine area. Marine Ecology 36: 57–66.

[9] Curtis JMR, Vincent ACJ. 2005. Distribution of sympatric seahorse species along a gradient of habitat complexity in a seagrass – dominated community. Marine Ecology Progress Series 291: 81-91.

[10] Pierri C, Lazic T, Corriero G, Cardone F, Onen Tarantini S, Desiderato, Mirto, Gristina M (2020) Site fidelity of *Hippocampus guttulatus* Cuvier, 1829 at Mar Piccolo of Taranto (Southern Italy; Ionian sea). Submitted to Environmental Biology of Fishes.

[11] Lazic T, Pierri C, Gristina M, Carlucci R, Cardone F, Colangelo P, Desiderato 508 A, Mercurio M, Bertrandino MS, Longo C, Carbonara P, Corriero G (2018) Distribution and habitat preferences of *Hippocampus* species along the Apulian coast. Aquatic Conservation, Marine and Freshwater Ecosystems 28:1317–1328.

[12] Correia M, Caldwell I, Koldewey H, Andrade JP, Palma J (2015) Seahorse (Hippocampinae) population fluctuations in the Ria Formosa lagoon, South Portugal. J Fish Biol 87:679–690

[13] Caldwell JR, Vincent ACJ. 2012. Revisiting two sympatric European seahorse species: Apparent decline in the absence of exploitation. Aquatic Conservation: Marine and Freshwater Ecosystems 22: 427–435.

[14] Olden J.D., Hogan Z.S., Vander Zanden M.J. (2007) Small fish, big fish, red fish, blue fish: size biased extinction risk of the world's freshwater and marine fishes. Global Ecology Biogeography, 16, 694–701.

[15] Kuo, T.C. and A. Vincent 2018. Assessing the changes in international trade of marine fishes under CITES

regulations – A case study of seahorses. Marine Policy 88 (2018) 48–57

2020 IMEKO TC-19 International Workshop on
Metrology for the Sea
Naples, Italy, October 5-7, 2020

Comparison of acoustic patterns recorded for the sperm whale (*Physeter macrocephalus*) in the Northern Ionian Sea (Central Mediterranean Sea) and in the North-western Levantine Sea (Eastern Mediterranean Sea)

Akkaya. A.[1], Awbery T.[1], Lyne P.[1], Cipriano G.[2], Maglietta R.[3], Renò V.[3], Fanizza C.[4], Carlucci R.[2]

[1] *DMAD-Marine Mammals Research Association, Antalya, Turkey*
2 Department of Biology, University of Bari, Via Orabona 4 - 70125 Bari, Italy.
3 Institute of Intelligent Industrial Technologies and Systems for Advanced Manufacturing, National Research Council, via Amendola 122 - 70126 Bari, Italy.
4 Jonian Dolphin Conservation, Viale Virgilio 102 - 74121 Taranto, Italy

***Abstract* – Sperm whales *Physeter macrocephalus* show a steady population decline, yet despite their threatened status, there remains a dearth of knowledge in the Mediterranean Sea. The current study reports the preliminary results of sperm whales' acoustic patterns within the Gulf of Taranto and the north-western Levantine Sea. "Regular" clicks were recorded in both regions indicating the presence of foraging grounds. "Codas" were also present in the north-western Levantine. The presence of codas and social units emphasises the importance of the north-western Levantine as potential nursery grounds. Further, inter-click intervals were slightly smaller for the Taranto Gulf while recordings from the north-western Levantine Sea showed similarities with the Mediterranean Sea. Lastly, sperm whales were larger in size in the Taranto Gulf compared to the north-western Levantine Sea. The current results depended on data collected on a single date, therefore further research must be implemented to understand the acoustic patterns of sperm whales.**

I. INTRODUCTION

The sperm whale *Physeter macrocephalus* shows a widespread distribution at Mediterranean scale [1] inhabiting offshore and continental slope waters, where mesopelagic cephalopods are most abundant [2,3]. However, since the 1980s, the Mediterranean subpopulation has shown a steady decline and thus, it has been classified as Endangered by the IUCN Red List [4]. Despite an increase in dedicated survey efforts on sperm whale during last decades, the knowledge of its abundance, spatial-temporal distribution, habitat preferences and behavioural patterns tends to be localized mainly to the western and central Mediterranean Sea, with less than a handful of basin-wide research efforts [5,6,7,8]. In addition, only recently a great effort was carried out to investigate the occurrence and abundance of sperm whales in Eastern Mediterranean Sea [5, 9, 10, 11, 12,13,14]. Despite an increase on research effort, the acoustic patterns of Mediterranean subpopulation of sperm whales have been poorly investigated [15,16,17], which can reveal important information from foraging strategies to population structure and cultural transmissions [18]. Sperm whales do not produce whistles, but instead only use broadband pulses or clicks [19]. Typical known vocalization patterns of sperm whales were "regular" clicks, while codas are occasionally produced. The former is identified as extended sequences of loud clicks produced at regular rates of approximately 0.5-2 clicks per second and they generally take place during the long and deep foraging dives and serve to echolocate the prey [20]. The codas are distinctive and short stereotyped sequences of clicks with a time pattern, produced in the presence of multiple individuals and commonly heard during group aggregation, even if they were occasionally produced at the end of a "regular" click sequence of foraging dives [21]. Social groups of females and juveniles produce higher rates of codas at the surface while they are interacting and it was proposed that codas are linked to some types of communication, likely to be learnt within matrilineal social groups [22] and identifiable for the vocal clans [23, 24]. However, individual or group identification does not appear to be the main function of codas and the most plausible primary function of codas is for the maintenance of social bonds, especially following periods of dispersion or separation, such as following foraging events [25]. Although multiple coda repertoires of sperm whales were recorded in Pacific region, the Mediterranean subpopulation showed little variation of coda repertoire

[15]. The Mediterranean subpopulation dominantly produce 3+1 codas, with a duration ranging from 456 to 1280 ms, and an average duration of 908±176 ms [15]. It is important to note that the 3+1 codas in the Mediterranean are dominantly recorded after foraging dives, while in the Pacific Ocean these are recorded in large socializing groups. Further, males tend to have smaller repertoires than females and the recordings in the Central Mediterranean Sea mainly originated from males leaving the potential for greater variation that previously considered [15]. Therefore, considering the different settings, it is likely that even though codas may have similar structures, social structure of the group will affect the codas function.

There is some evidence of variation from the typical 3+1 coda patterns [15]. Nursery groups in the Mediterranean Sea showed 4-, 5- and 7-click codas [26]. Additionally, some groups recorded in the Eastern Mediterranean Sea demonstrated a different coda type, with 2+1 [27] and 3++1 [28] variations. Despite the existing variations on coda patterns, sperm whale tend to show similar codas within the Mediterranean Sea which raised the possibility of sperm whales displaying an "island habitat" [28]. Island populations contain fewer elements in their vocal repertoires but have more variety within the elements [15].

Nevertheless, the scarce number of comprehensive acoustic studies on sperm whales hinders our understanding of the vocal repertoires of sperm whales in the Mediterranean Sea. Studying the variations in vocalization over time and space through acoustic techniques can produce extensive knowledge of the population structure, cultural and genetic evolution, and the presence of local adaptations [29, 30]. The current case study provides information on the variations in vocal behavior of sperm whales occurring in the Northern Ionian Sea (Central Mediterranean Sea) and in the North-western Levantine Sea (Eastern Mediterranean Sea) , contributing, although preliminarily, to the understanding of whether the vocal repertoire varies between these two areas.

II. MATERIAL AND METHODS

Standardized seasonal boat-based surveys with visual and acoustic survey techniques were carried out to monitor the occurrence of cetaceans in the Gulf of Taranto (Northern Ionian Sea, Central Mediterranean Sea) and along the Turkish coasts of the North-western Levantine Sea (Eastern Mediterranean Sea). While a random line transect design was applied in the Gulf of Taranto between February and December 2019, 22 equally spaced transects were followed seasonally in the North-western Levantine Sea between April 2018 and January 2020. A survey effort of approximately five hours per day was completed, along a 65 km line, covering an area of about 960 km2 in the Gulf of Taranto. 24 hour survey effort for an average of five days per season was conducted in the north-western Levantine Sea, consisting of 644 km of track line in each survey, covering an area of 23,438 km².

In both study areas, observations on board were made with the naked eye and 7 × 50 binoculars. When a visual or acoustic detection took place, the focal group was followed, switching to off-effort [31], to collect information such as photo-identification, geographic coordinates of the sighting, time of first contact, depth (m), group size and behavior. Additionally, environmental and anthropogenic (vessel presence, construction, military sonar and hydrocarbon exploration) noises in the area were logged in the north-western Levantine Sea.

A. Acoustic data collection

In the Gulf of Taranto, data were collected using a pre-amplified omnidirectional hydrophone (Colmar GP0190) with a sensitivity of -175±5 dB re 1V/μPa among 5 and 170 kHz, and a flat response of -171 dB re 1V/μPa under 12 kHz up to 1 kHz. The acoustic data were collected only after the engine switched off, to avoid disturbance and noise, and if possible for the entire duration of the sighting.

In the North-western Levantine Sea, a towed hydrophone array was deployed near-continuously during surveys. The hydrophone array (Vanishing Point, UK) consisted of four omni-directional broadband hydrophone elements for high and low frequency monitoring mounted within a streamlined housing and towed on a 200 m strengthened cable. The hydrophone elements were sensitive between 100 Hz and 200 kHz Signals and the hydrophone was amplified and conditioned using a customized hydrophone interface (Magrec HP27) and digitised using a Behringer U-Phoria UMC404HD sound card sampling up to 192 kHz. PAMGuard software ran on a laptop computer making continuous full bandwidth recordings. Additionally, a directional hydrophone was used to localize the sperm whales. In both study area, post-acoustic analyses carried out by PamGuard 2.01.03.

III. RESULTS

In the Gulf of Taranto, during February-December 2019, a total effort of 148 daily surveys was applied accounting for approximately 740 hours of observations and 9600 km covered. A total of 6 visual sightings of sperm whale with a group size ranging from 1 to 5 individuals, occurred in a depth range from 560 and 1050 m in depth. Acoustic data were collected during one sighting. Five possible sperm whales were identified (despite only four being visually confirmed) from 20 recordings lasting 1 hour and 3 minutes recorded on the 17th August 2019. The recordings contained impulsive clicks with well-defined click trains with Inter click interval (ICI) ranging from 0.3 to 1 second. The recorded center frequency has ranged between 8 and 12 kHz and the peak frequency was between 11 to 16 kHz. Peak frequencies are typically recorded in a range 12 to 13.5 kHz. The IPI values received were calculated using the suggested algorithm [32], suggesting a body length of 9 to 10.5m calculated.

In the North-western Levantine Sea, a total of 60 days were spent from April 2018 and January 2020, with an effort of approximately 697 hours of observation and covering 4385 km. 23 sightings of sperm whale were detected in waters with depths between 500 and 2500 m, of which only 4 sightings were visually recorded. A total of 13 acoustic recordings of sperm whales making up 1 hour and 29 minutes on July 15th, 2019 were analysed, revealing the possible presence of 4 or more individuals. This date was chosen for the preliminary analysis due to the presence of clearly distinguishable clicks and possible codas. Sperm whale acoustic recordings revealed the presence of “regular clicks” and “codas”. Regular clicks showed similar characteristics with inter click interval (ICI) values of around 1 second and peak frequencies ranging from 2 to 13 kHz. During one of these recordings, the animals encountered emitted both regular foraging clicks and possible codas or indistinct click trains. Regular clicks emitted during foraging dives started with an ICI of 1.4 seconds and decreased to 0.65 seconds approximately, before decreasing further. The peak frequency of the click also altered from an emphasis on 2 to 4 kHz signals in bimodal clicks with a lower peak at 7.3 to 9.4 kHz. The lower peak frequency reduced on the more frequent clicks presumably at the target being investigated was approached. While some possible codas followed a pattern of a seven click sequence with varying ICI rates alternating from fast to slow to fast. The recorded codas had a range of ICI and frequencies but the peak frequency ranged from 12 to 14.4 kHz and center frequency ranged from 11 to 14 kHz. Inter Pulse Intervals (IPI) suggests body length of 7.8 to 9.3m for four of the whales.

IV. DISCUSSION

The comparison of vocalizations of sperm whales recorded in the Gulf of Taranto and North-western Levantine Sea revealed the occurrence of ‘regular clicks’, indicating both areas hold foraging habitat(s) for sperm whales [18,33]. This hypothesis is supported by the peculiar eco-physiographic features of the Taranto Valley canyon system in the North Ionian Sea and Finike seamounts in the north-western Levantine Sea, both of the location having its energy and biomass exchanges indicating a benthic-pelagic coupling and a rich occurrence of mesopelagic cephalopods [14, 34, 35].

Additionally, in Turkey, the occurrence of coda patterns was indicative of social behaviour [15] thus the area is not only important for the solitary individuals but also for the social, potentially nursery, groups. Hellenic Trench is known to hold one of the most important sperm whale habitats of the Mediterranean Sea with high recording of nursery groups [9,10,11,12]. Therefore, it is highly likely that sperm whales, both the nursery groups and solitary individuals, share the neighbouring waters. The regular foraging clicks recorded in Turkey appear to be similar to the reported acoustic patterns of sperm whales elsewhere. The Inter Click Interval (ICI) of 1.4 seconds decreasing to 0.6 seconds in Turkey is concurrent with sperm whales within the Mediterranean Sea [33] as well as further afield e.g. waters off Norway [36, 37], the Galapagos [38] the Gulf of Mexico [39], who generally have found click intervals of between 0.5 and 2 seconds.

The ICI ranging from 0.3 to 1 second recorded from sperm whales sighted in the Gulf of Taranto is slightly lower than the aforementioned reported values, but it should be noted click interval changes on approach to prey down to as low as 20 ms [37]. Due to variance of the ICI as a function of proximity to prey or target [33] and depth [37], further acoustic studies are needed to confirm whether the ICI recorded in the Gulf of Taranto could be atypical.

The peak frequencies recorded in both study areas were slightly higher than those recorded in the Galapagos [38] but lower than those recorded in the Bahamas [40] and Norway [41]. The center frequencies were comparable to those recorded in Papua New Guinea [42] but they are lower than central frequency recorded in the Gulf of Mexico [39].

Higher frequency clicks observed following dives, in Turkish water, suffer from higher attenuation suggesting that they are more suited to shorter distance investigation [42]. This demonstrates the ability of animals to modulate or change the signal as the target is approached, changing the frequency of the signal to obtain greater resolution of the target. Echolocation clicks are often produced at intervals that are either similar to or slightly longer than the two - way travel time [43] i.e. the time for the sound to reach the prey and return making it a useful proxy for the distance which the animal is directing its attention [44]. Higher frequency signals with shortened ICIs increase the rate of signal return and therefore return more information on the target as it is approached. Thus, considering with a reasonable approximation that speed of sound in the water (valid for water from 100 m to 800 m depth) is 1510±2 m/s [33], with an ICIs of 1.4 and 0.6 second respectively, recorded in Turkish waters, the maximum prey location distances resulted of 1057 m and 491m, respectively. For the Gulf of Taranto, the same method gave maximum prey location distances ranging from 227 m to 755 m for the 0.3 and 1 second ICIs, respectively. Indeed, the target may be closer but it may be that details of the surrounding environment are still of use in orientation and the tracking and capturing prey [33,45].

Preliminary analysis suggested that the coda patterns observed in Turkey were not similar to the typically observed pattern found in the Mediterranean [15] and did not appear to show the 2+1 nor the 3++1 patterns [27,28] in neighboring Greece. However, more recordings of coda clicks would be required in order to reliably determine coda characteristics and associate them reliably to specific social groups.

Two codas recorded in 1995 by the Italian Navy comprise the only other published data on sperm whale acoustics in the Gulf of Taranto, both of which consisted of the typical 3+1 pattern [15]. The body length in this study calculated based on the whale's IPI gave a length of 13.2m [15] which is considerably larger than the range of 9 to 10.5m calculated in this study.

The results presented here are from the first dedicated cetacean seasonal survey carried out in the Turkish waters of the Eastern Mediterranean Sea [14] and to our knowledge, the first recordings analyzed for their acoustic properties. Similarly, the recordings in the Gulf of Taranto are some of the first recordings analyzed. This preliminary analysis provides the scientific baseline of knowledge on the vocalizations of sperm whales in these understudied areas [5]. In turn, results demonstrate the existence of foraging grounds in both the Gulf of Taranto, already suggested as suitable habitat for this and other cetacean species [46] and the Eastern Levantine Sea, where not only solitary individuals but also social units were encountered Acoustic data collected in each case represents recordings in a single day, of a single year while the life of a sperm whales spans approximately 60 years [47] and therefore, these are very limited snapshots into the lives of sperm whales. There is a clear need for further analyses into the recordings collected but the variation observed between the two study areas, even in the preliminary analyses, emphasizes the need for comprehensive data collection in these understudied areas as well as the value of cross-border collaborations in developing our understanding of the ecology of cetaceans that shows long-movement patterns.

V. REFERENCES

[1] L. Rendell, S. Simião, J. M. Brotons, S. Airoldi, D. Fasano, A. Gannier, "Abundance and movements of sperm whales in the western Mediterranean basin". Aquatic Conservation: Marine and Freshwater Ecosystems, 24(S1), 2014, pp. 31-40.

[2] A. Azzellino, S. Gaspari, S. Airoldi, B. Nani.,. "Habitat use and preferences of cetaceans along the continental slope and the adjacent pelagic waters in the western Ligurian Sea." Deep Sea Res. Part I Oceanogr. Res. Pap., vol. 55, No.3, 2008, pp.296-323.

[3] E.Praca, A. Gannier, A., "Ecological niches of three teuthophageous odontocetes in the northwestern Mediterranean Sea.", Ocean Sci., vol.4, February 2008, pp.49–59.

[4] G. Notarbartolo di Sciara, A.Frantzis, G.Bearzi, R.Reeves., Physeter macrocephalus(Mediterranean subpopulation). The IUCN Red List of Threatened Species 2012: e.T16370739A16370477. https://dx.doi.org/10.2305/IUCN.UK.2012-1.RLTS.T16370739A16370477.en. 2012

[5] T.Lewis, O.Boisseau, M.Danbolt, D.Gillespie, C.Lacey, R.Leaper, J.Matthews, R.McLanaghan, A.Moscrop, "Abundance estimates for sperm whales in the Mediterranean Sea from acoustic line-transect survey", J. Cetacean Res. Manag., vol. 18, 2018, pp. 103-117.

[6] A.Gannier, V. Drouot, J. Goold, "Distribution and relative abundance of sperm whales in the Mediterranean Sea.", Mar. Ecol. Prog. Ser., vol. 243, November 2002, pp.281-293.

[7] O.Boisseau, C.Lacey, T.Lewis, A.Moscrop, M.Danbolt, R.McLanaghan, "Encounter rates of cetaceans in the Mediterranean Sea and contiguous Atlantic area.", J. Mar. Biolog. Assoc. U.K. vol. 90, No. 8, December 2010, pp.1589-1599.

[8] C. Lambert, M.Authier, G. Dorémus, S. Laran, S.Panigada, J. Spitz, O.Van Canneyt, V.Ridoux. "Setting the scene for Mediterranean litterscape management: The first basin-scale quantification and mapping of floating marine debris". Environ. Pollut., August 2020, p.114430.

[9] A.Frantzis, P.Alexiadrou, G.,Paximadis, E.Politi, A.Gannier, M.Corsini-Foka, "Current knowledge of the cetacean fauna of the Greek seas." J. Cetacean Res. Manag. vol. 5, No. 3, 2003, pp. 219-232.

[10] A.Frantzis, S.Airoldi, G. Notarbartolo-di-Sciara, C.Johnson, S.Mazzariol, "Inter-basin movements of Mediterranean sperm whales provide insight into their population structure and conservation". Deep Sea Res. Part I Oceanogr. Res. Pap. Vol. 58, No.4, February 2011, pp.454-459.

[11] A.Frantzis, P.Alexiadou, K.Gkikopoulou, "Sperm whale occurrence, site fidelity and population structure along the Hellenic Trench (Greece, Mediterranean Sea)." Aquat. Conserv. vol.24(S1), June 2014, pp.83-102.

[12] A.Frantzis, R.Leaper, P.Alexiadou, A.Prospathopoulos, D.Lekkas, 2019. "Shipping routes through core habitat of endangered sperm whales along the Hellenic Trench, Greece: Can we reduce collision risks?". PloS one, vol. 14, No.2, February 2019, e0212016.

[13] A.Öztürk, A.Tonay, A.Dede, A. Sperm whale (Physeter macrocephalus) sightings in the Aegean and Mediterranean part of Turkish waters. J. Black Sea/Med. Env. vol 19, No. 2, May 2013, pp. 169-177.

[14] A.Akkaya, P.Lyne, X.Schulz, T.Awbery, S.Capitain, B.Rosell, B.Yıldırım, C.İlkılınç, J.Relva, H.Clark, L.Van Walsum., "Preliminary results of cetacean sightings in the eastern Mediterranean Sea of Turkey"., vol. 26, No. 1, April 2020. pp. 26-47

[15] Pavan, G., Hayward, T.V., Borsani, J.F., Priano, M., Manghi, M., Fossati, C. and Gordon, J., "Time patterns of sperm whale codas recorded in the Mediterranean Sea 1985–1996. The Journal of the Acoustical Society of America", vol.107, No. 6, May 2000, pp.3487-3495

[16] V.Drouot, A.Gannier, J.Goold, "Diving and feeding

behaviour of sperm whales (Physeter macrocephalus) in the northwestern Mediterranean Sea." Aquat mamm. Vol. 30, No.3, December 2004, pp.419-426.

[17] V.Teloni, "Patterns of sound production in diving sperm whales in the northwestern Mediterranean." Mar. Mamm. Sci., vol. 21, No. 3. July 2005, pp.446-457

[18] N.Jaquet, S. Dawson, L.Douglas, L., "Vocal behavior of male sperm whales: Why do they click?". J. Accous. Soc. Am., vol. 109, No.5, May 2001, pp.2254-2259.

[19] L.Herman, W.Tavolga, "The communication systems of cetaceans. In Cetacean behavior." Edited by. L. M. Herman. John Wiley & Sons, New York. pp. 149-209. 1990

[20] L.Weilgart, H.Whitehead, "Coda communication by sperm whales (Physeter macrocephalus) off the Galapagos Islands." Can. J. Zoo. vol. 71, No.4, April 1993, pp.744-752.

[21] W.Watkins, W. Schevill, "Sperm whale codas". J. Accous. Soc. Am., vol. 62, No.6, December 1977, pp.1485-1490.

[22] L.Weilgart, H.Whitehead, "Group-specific dialects and geographical variation in coda repertoire in South Pacific sperm whales". Behav. Ecol. Sociobiol., vol. 40, No.5, May 1997, pp.277-285.

[23] K. Moore, W.Watkins, P. Tyack, Pattern similarity in shared codas from sperm whales (Physeter catodon). Mar. Mamm. Sci, vol 9, No.1, January 1993, pp.1-9.

[24] L.Rendell, H.Whitehead, "Vocal clans in sperm whales (Physeter macrocephalus)". Proc. R. Soc. Lond. B., vol. 270, February 2003, pp. 225–231

[25] H.Whitehead, L.Weilgart, S.Waters. "Seasonality of sperm whales off the Galapagos Islands, Ecuador." Reports of the International Whaling Commission, 39,1985, pp.207-210.

[26] V.Drouot, and A.Gannier, "New sperm whale vocalizations recorded in the Mediterranean Sea", European Research on Cetaceans–13. Proc. 13th Ann. Conf. ECS, 1999, Valencia, Spain, pp.5-8.

[27] A.Frantzis, R.Swift, D.Gillespie, C.Menhennett, J.Gordon and S.Gialinakis, "Sperm whale presence off southwest Crete, Greece, eastern Mediterranean" Eur Res Cet, April 1999, vol.13, pp.214-217.

[28] L.Rendell, V.Alexiadou, B.Mussi, A.Miragliuolo and A.Frantzis, "Coda diversity in Mediterranean sperm whales", In Abstract book: 21st Annual Conference of the European Cetacean Society, 2007, pp.23-25.

[29] K.N.Laland, "A theoretical investigation of the role of social transmission in evolution", Ethol. Sociobiol., vol.13, No.2, March 1992, pp.87-113.

[30] L.Rendell and H.Whitehead 2004. "Do sperm whales share coda vocalizations? Insights into coda usage from acoustic size measurement". Anim. Behav., vol.67, No.5, May 2004, pp.865-874.

[31] S.T.Buckland, D.R.Anderson, K.P.Burnham, J.L.Laake, D.L.Borchers and L.Thomas, "Advanced Distance Sampling", Oxford University Press, Oxford, U.K., 2004.

[32] W.A.Beslin, H.Whitehead and S.Gero, "Automatic acoustic estimation of sperm whale size distributions achieved through machine recognition of on-axis clicks", J. Acoust. Soc. Am., vol.144, No.6, Dec 2018, pp.3485-3495.

[33] W.M.Zimmer, M.P.Johnson, A.D'Amico and P.L.Tyack, "Combining data from a multisensor tag and passive sonar to determine the diving behavior of a sperm whale (Physeter macrocephalus)", IEEE J. Oceanic. Eng., vol. 28, No.1, April 2003, pp.13-28.

[34] R.Carlucci, V.Bandelj, F.Capezzuto, L.Sion, P.Maiorano, A.Tursi, C.Solidoro and S.Libralato, "Exploring spatio-temporal changes in the demersal and benthopelagic assemblages of the northwestern Ionian Sea (central Mediterranean Sea)", Mar. Ecol. Prog. Ser., vol.598, June 2018, pp.1-19.

[35] P.Ricci, S.Libralato, F.Capezzuto, G.D'Onghia, P.Maiorano, L.Sion, A.Tursi, C.Solidoro and R.Carlucci, "Ecosystem functioning of two marine food webs in the North-Western Ionian Sea (Central Mediterranean Sea)", Ecol Evol, vol.9, No.18, Sep 2019, pp.10198-10212.

[36] M.Wahlberg, "The acoustic behaviour of diving sperm whales observed with a hydrophone array", J. Exp. Mar. Biol. Ecol., vol.281, No.1-2, Dec 2002, pp.53-62.

[37] A.Fais, N.A.Soto, M.Johnson, C.Pérez-González, P.J.O.Miller and P.T.Madsen, "Sperm whale echolocation behaviour reveals a directed, prior-based search strategy informed by prey distribution", Behav. Ecol. Sociobiol., vol.69, No. 4, Feb 2015, pp.663-674.

[38] L.S.Weilgart and H.Whitehead, "Distinctive vocalizations from mature male sperm whales (Physeter macrocephalus)", Can. J. Zool., vol.66. No.9, Sep 1998, pp.1931-1937.

[39] A.Thode, D.K.Mellinger, S.Stienessen, A.Martinez and K.Mullin, "Depth-dependent acoustic features of diving sperm whales (Physeter macrocephalus) in the Gulf of Mexico", J. Acoust. Soc. Am., vol.112, No.1, Jul 2002, pp.308-321.

[40] E.M.Nosal and L.N.Frazer, "Sperm whale three-dimensional track, swim orientation, beam pattern, and click levels observed on bottom-mounted hydrophones", J. Acoust. Soc. Am., vol.122, No.4, Oct 2007, pp.1969-1978.

[41] B.Møhl, M.Wahlberg, P.T.Madsen, A.Heerfordt and A.Lund, "The monopulsed nature of sperm whale clicks", J. Acoust. Soc. Am., vol.114, No.2, Aug 2003, pp.1143-1154.

[42] P.T.Madsen and M.Wahlberg, "Recording and quantification of ultrasonic echolocation clicks from free-ranging toothed whales", Deep Sea Res. Part I:

Oceanogr. Res. Pap., vol.54, No.8, Aug 2007, pp.1421-1444.

[43] W. W. L. Au, "The Sonar of Dolphins", 1993, Springer, New York

[44] D,M.Wisniewska, M.Johnson, K.Beedholm, M.Wahlberg and P.T.Madsen, "Acoustic gaze adjustments during active target selection in echolocating porpoises", J. Exp. Biol., vol.215, Dec 2012, pp.4358-4373

[45] M.P.Johnson and P.L.Tyack, "A digital acoustic recording tag for measuring the response of wild marine mammals to sound", IEEE J. Oceanic. Eng., vol.28, No.1, Apr 2003, pp.3-12.

[46] S.Bellomo, F.C.Santacesaria, C.Fanizza, G.Cipriano, V.Renò, R.Carlucci and R.Maglietta, "Photo-identification of Physeter macrocephalus in the Gulf of Taranto (Northern Ionian Sea, Central-eastern Mediterranean Sea)", IMEKO TC-19 International Workshop on Metrology for the Sea, 2019.

[47] D.W.Rice, "Sperm whale, Physeter macrocephalus, Linnaeus, 1758", Handbook of Marine Mammals, Academic Press, London, U.K., 1989.

2020 IMEKO TC-19 International Workshop on
Metrology for the Sea
Naples, Italy, October 5-7, 2020

Satellite tracking of loggerheads sea turtles (*Caretta caretta*) in the Gulf of Taranto (Northern Ionian Sea, Central Mediterranean Sea)

Fanizza C.[1], Colella R.[2], Crugliano R.[1], Cirelli G.[3], A. Colucci[3], Pisto A[3], Cipriano G.[4], Ricci P.[4], Maglietta R. [2], Carlucci R.[4]

[1] *Jonian Dolphin Conservation, Viale Virgilio 102, 74121 Taranto (TA) Italy,* areaprogetti@joniandolphin.it

[2] *Institute of Intelligent Industrial Technologies and Systems for Advanced Manufacturing, National Research Council, Via Amendola 122/D-I, 70126, Bari (BA) Italy, rosalia.maglietta@cnr.it*
[3] *Sea Turtle Rescue Center WWF, Piazza Siris, 1, 75025 Policoro (MT) Italy, wwf.poli@gmail.com*
[4] *Department of Biology, University of Bari, Via E. Orabona 4, 70125 Bari (BA) Italy, roberto.carlucci@uniba.it*

***Abstract* – A detailed knowledge of sea turtle distribution in relation to anthropogenic threats is key to inform conservation measures. The movements of two Mediterranean loggerhead sea turtles (*Caretta caretta*) incidentally caught in the Gulf of Taranto, were tracked via satellite telemetry for between 8 and 118 days. With the caution due to the small sample size, results suggested that turtles might have very small home ranges in the area.**

Moreover, one of the two released loggerhead sea turtle, returning to the site where it has been accidentally captured. It has shown to have a remarkable fidelity to the site. Therefore, if confirmed and further detailed, information about sea turtle migration patterns and routes in the Gulf of Taranto will serve to plan effective conservation strategies for this species.

I.INTRODUCTION

The loggerhead sea turtle (*Caretta caretta)* is widely distributed in warm-temperate and subtropical oceans [1]. In the Mediterranean Sea, although its marine habitats extend throughout the basin, the reproductive habitats are concentrated prevalently in the eastern basin, with few registered nests in the western one [2]. Upon attaining sexual maturity, loggerhead sea turtles undertake breeding migrations between foraging grounds and nesting areas at remigration intervals from one to several years, with a mean interval of 2.5-3 years for females. The migration interval for males would be shorter [1]. According to the current criteria of the IUCN Red List, the sub-population of *C. caretta* in the Mediterranean Sea is listed as Least Concern [1]. This assessment confirms the effectiveness of intense conservation programs in the Mediterranean basin, especially oriented to the conservation of its nesting sites to face human induced threats [1]. Therefore, understanding how *C. caretta* uses its habitat both in space and time is essential to effectively buffer its bio-ecology from exposition to anthropogenic threats. In this light, increase the knowledge about the migration patterns of *C. caretta* from local to a wider spatial scale is essential to develop strategies to ensure its conservation. Unfortunately, the lack of this information in the Mediterranean Sea often raised concerns about the possibility of an effective management of the species mostly in case of the increasing anthropic pressures on coastal and offshore areas.

In particular, concerning the Northern Ionian Sea, the knowledge about the spatio-temporal distribution of *C. caretta* is still scarce and fragmentary. To that regard, this study aims to provide new indications about the loggerhead sea turtle movement pattern in the investigated area, implementing current knowledge with modern technologies such as the use of satellite tracking devices. The use of such tools is a response to many of the concerns that have been raised and reviewed surrounding the biology and conservation of sea turtles [3]. This innovative tracking approach can be crucial to enable progress towards a global understanding of sea turtle ecology away from nesting beaches, and to indicate effective conservation and protection strategies.

II. MATERIALS AND METHODS

A. Study area

The Gulf of Taranto in the Northern Ionian Sea (Central Mediterranean Sea) covers an area of approximately 14.000 km^2 from Santa Maria di Leuca to Punta Alice. A narrow continental shelf with a steep slope and several channels characterize the western sector, while the eastern sector shows descending terraces toward the 'Taranto Valley', a NW–SE submarine canyon with no clear bathymetric connection to a major river system [4,5,6]. In addition, a transitional water system [7], the Mar Piccolo of Taranto, characterizes the northernmost part of the Gulf of Taranto. It covers a total surface of about 20.63 km^2 and consists in a system of two distinct inlets, called 'Primo' and 'Secondo Seno' (first and second inlet), the innermost of which receives an inflow from some small streams. The Mar Piccolo is characterized by low water turnover and water movement. Currents are moderate, anticyclonic, and more intense in the first inlet than in the second one, where they are more appreciable near the narrows, which connect the two inlets [8].

B. Data collection

The movements of two loggerhead sea turtles (*C. caretta*) were monitored during January 2020 through May 2020. The sea turtles were incidentally caught in the set nets, typically deployed in neritic area where large turtles are supposed to spend most of their time [9]. They were kept in captivity at Sea Turtle Rescue Centre WWF Policoro for a maximum of one month prior to release.

Fig.1 Loggerhead sea turtle with SPOT-365 transmitter

Animal tracking is usually done using location trackers built for the particular application. In particular, while most of terrestrial animals can be tracked using Global Positioning System, this is not possible for marine animals due to the time required for a GPS receiver to acquire satellite signals and navigation data, and calculate a position solution (called a fix).

SPOT (Smart Position and Temperature) transmitting tags produced by Wildlife Computers well respond to the requirement of our application, as they exploit Argos satellite telemetry (https://argos-system.cls.fr/) a widely used method to relay data and track the movements of marine animals, which regularly spend time at the surface. These tags were provided in the framework of the SAT-CAL Project "Application of Satellite Transmitters on Sea Turtles in the Ionian Sea".

When the tag's antenna completely clears the surface of the water, wet/dry sensors activate the tracker and messages can be successfully transmitted the low-orbiting Argos satellites, and sent to earth-based receiving stations for location processing (using Doppler shift) and distribution. Collected data include time-at-temperature histograms and wet/dry percentage.

Wildlife tags offer many benefits, the most important are:

- Response time: it needs less than half a second, since the activation, for the first packet to be sent to the satellite.
- Long battery life: when submerged, the tracker goes in a low-consumption mode, maximizing the battery duration. Depending on the particular animal behavior and on the tag model, data can be collected for up to several hundreds of days.
- Data availability: data are made available on the Wildlife Computers Data Portal (https://my.wildlifecomputers.com/data/). Argos accounts are checked for new data every hour. If new Argos data are detected, the portal will begin checking every 15 minutes to ensure the new data are captured in a timely manner. If no new data are detected within a 24-hour period, the portal will resume checking for data every hour. Location data can be downloaded and displayed on a map and user can observe how position changes with time.
- Tags can be widely and easily configured, connecting them to a pc through the Wildlife Computers software (named Tag Agent) or offline, from the Wildlife Computers Data portal, Tags section, storing the settings to be updated later. Settings include the possibility of masking hours of the day to prevent uplink when no satellite passes are expected, reducing power consumption. Time-at-temperature histograms can also be customized.

Drawbacks are the lower accuracy of Argos data (250 m) with respect to GPS, that make them not suitable for small scale analysis and the not complete coverage of the whole daytime with satellite passes: a location-based check of the satellite passes is made available on Argos site as a simulation and needs to be carried out before configuring the hourly mask of the tag.

Argos system algorithm analyzes location data and classifies them into six location classes (LC) of decreasing accuracy (LC 3-1: accuracy <1 km, LC 0, LC A, LC B) plus LC Z, which includes invalid, rejected locations. This allows researches easily filter out data that can be considered unreliable because of a too large error.

In order to attach the transmitter to the turtle's carapace, a custom plastic mount was designed and 3D printed. Then, it was fixed to the carapace with some water-resistant resin after the surface had been cleansed of grease and debris and slightly roughened, so that the resin got a better grip on it.

We used two SPOT-365 transmitters (57 x 48 x 24 mm, 57 g.) that are currently in use and will last for a maximum time of 340 days. Both of them have been configured so that transmission is enabled in the interval 6.00 am – 06.00 pm. The data coming from both of them can be visualized on movebank.org, a free online platform for sharing, managing and analyzing data.

III.RESULTS

The first female (ID 01POLI2020) named "Erasmus" was incidentally captured in the second inlet of the Mar Piccolo of Taranto. The turtle was released from Policoro on 31 January 2020 and is currently monitored. Since its release to May 26th, it first remained in an area of 3.5 km radius around the release point for 24 days, then it spent the next 13 days traveling toward Taranto where it was recorded in the second inlet of the Mar Piccolo and where it remained until 26 May 2020. The 275 location data points related to "Erasmus" have been filtered, keeping only the 59 points that belong to LC_0 -3 location classes.

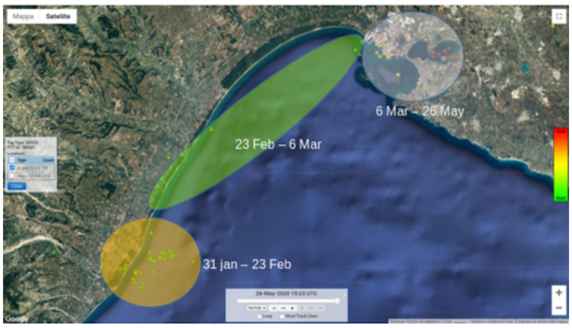

Fig.2 Location points, filtered with respect to data quality, shows that the turtle named "Erasmus" traveled for 13 days from the release zone, where it remained for 23 days, to Mar Piccolo, where it currently is and where it was captured

The second female (ID 04POLI2020) named "Alessandra" was incidentally captured in the coastal area of Policoro. The turtle was released from Policoro on 19 May 2020 and is currently monitored. During these 7 days, the turtle remained in the coastal area of Policoro, moving not more than 3 km away from the release location.

The loggerhead turtles tracked, showed a CCL (Curved carapace length) ranging from 65 to 72 cm, resulting above the minimum size of nesting females in the Mediterranean [10]. Thus, it cannot be excluded that they were adults.

IV.DISCUSSION AND CONCLUSIONS

The present study contributes to the current knowledge of loggerhead sea turtle movements in the Northern Ionian Sea (Central Mediterranean Sea). Particularly interesting is the behavior of the turtle called "Erasmus" who after being released in the coastal waters of Policoro returned to the transitional water in the Mar Piccolo of Taranto. Results suggest that "Erasmus" may have a very small home range. This condition seems to be associated to the local environmental conditions, such as the occurrence of shallow waters with good availability of benthic preys and mostly of extended mussel farms.

"Alessandra" remained in the coastal area of Policoro during the tracking period. This suggests the occurrence of optimal trophic conditions even in the open waters. A longer monitoring period would be needed to identify possible ecological drivers favoring loggerhead turtles.

Present results suggest that turtle occurrence may be higher in shallow waters along the coast, and further investigation may inform conservation actions aimed at reducing the impact of fishing [11]. The use of satellite tracking technology on nesting females can lead us to identify new nesting areas in the Gulf of Taranto. This information could be applied to the conservation and management of the species in order to reduce the interactions between fishermen and sea turtles.

V. ACKNOWLEDGMENTS

We would like to thank Prof. Casale and Dr. Giulia Cerritelli of the Department of Ethology of the University of Pisa, who are committed to assisting and sharing information on the application of satellite transmitters We would also like to express our gratitude to Fondazione con il SUD for funding the purchase of the satellite tracking devices.

VI. REFERENCES

1. P.Casale, "*Caretta caretta* (Mediterranean subpopulation)", The IUCN Red List of Threatened Species, 2015: e.T83644804A83646294. http://dx.doi.org/10.2305/IUCN.UK.20154.RLTS.T83644804A83646294.en.
2. P.Casale, G.Simone, "Seasonal residency of loggerhead turtles *Caretta caretta* tracked from the Gulf of Manfredonia, south Adriatic", Mediterr. Mar. Sci., vol.18, No.1, 2017, pp.4-10. doi:https://doi.org/10.12681/mms.1663.
3. F.Bentivegna, "Intra-Mediterranean migrations of loggerhead sea turtles (*Caretta caretta*) monitored by satellite telemetry", Mar. Biol., vol.141, 2002, pp. 795–800. DOI 10.1007/s00227-002-0856-z
4. R.Carlucci, C.Fanizza, G.Cipriano, C.Paoli, T.Russo, P.Vassallo, "Modeling the spatial distribution of the striped dolphin (*Stenella coeruleoalba*) and common bottlenose dolphin (*Tursiops truncatus*) in the Gulf of Taranto (Northern Ionian Sea, Central-Eastern Mediterranean Sea)", Ecol. Indic. vol.69, 2016, pp.707–721.
5. R.Carlucci, V.Bandelj, F.Capezzuto, L.Sion, P.Maiorano, A.Tursi, C.Solidoro, S.Libralato, "Exploring spatio-temporal changes in the demersal and benthopelagic assemblages of the northwestern Ionian Sea (central Mediterranean Sea)", Mar. Ecol. Prog. Ser., vol.598, 2018, pp.1-19.
6. P.Ricci, S.Libralato, F.Capezzuto, G.D'Onghia, P.Maiorano, L.Sion, A.Tursi, C.Solidoro, R.Carlucci, "Ecosystem functioning of two marine food webs in the North‐Western Ionian Sea (Central Mediterranean Sea)", Ecol. and Evol., vol.9, 2019, pp.10198-10212.
7. E.Cecere, G.Alabiso, R.Carlucci, A.Petrocelli, M.Verlaque, "Fate of two invasive or potentially invasive alien seaweeds in a central Mediterranean transitional water system: failure and success" Botanica Marina, vol.59, 2016, pp.451-462.
8. D. Malcangio, M.Mossa, "Tidal current computation in the Mar Piccolo (Taranto)", G.H.Jirka, W.S.J Uijttewaal, Shallow Flows, (Eds.). The Netherlands, A.A. Balkema, 2004, pp.217-223.
9. P. Casale, "Sea turtle bycatch in the Mediterranean", Fish and Fisheries, vol.12, 2011, pp.299-316.
10. D.Margaritoulis, R.Argano, I.Baran, F.Bentivegna, M.N.Bradai, J.A.Camiñas, P.Casale, G.De Metrio, A.Demetropoulos, G.Gerosa, B.J.Godley, D.A.Haddoud, J.Houghton, L.Laurent, B.Lazar, "Loggerhead turtles in the Mediterranean Sea: present knowledge and conservation perspectives", in: A.B.Bolten (Eds). Loggerhead Sea Turtles, Smithsonian Institution Press, Washington D.C.
11. P.Casale, M.Affronte, D.Scaravelli, B.Lazar, C.Vallini, P.Luschi, "Foraging grounds, movement patterns and habitat connectivity of juvenile loggerhead turtles (*Caretta caretta*) tracked from the Adriatic Sea", Mar. Biol., vol.159, 2012, pp. 1527-1535.

2020 IMEKO TC-19 International Workshop on
Metrology for the Sea
Naples, Italy, October 5-7, 2020

Habitat use of Delphinus delphis (Linnaeus, 1758) in the southern waters of Samos island (Aegean Sea, Greece)

Sebastien Saintignan[1], Matteo Costantino[1], Anastasia Milou[2], Sarah Moscatelli[2], Guido Pietroluongo[2], Marta Azzolin[1]

[1] *Gaia Research Institute Onlus, Turin, Italy, sebastien.saintignan@gmail.com, matteo.costantino91@gmail.com, marta.azzolin@gmail.com*
[2] *Archipelagos Institute of Marine Conservation, Samos, Greece, a.milou@argipelago.gr, s.moscatelli91@gmail.com, guido.p@archipelago.gr*

***Abstract* – The Mediterranean short-beaked common dolphin, *Delphinus delphis* (Linnaeus, 1758) is classified as "Endangered" by the IUCN Red List. Living in coastal waters, *D.delphis* is often exposed to human activities. For that reason, it is important to have a better understanding of the crititcal habitats of the species to implement effective measures of protection. Research activity on D. delphis´distribution and behaviour have been led in the southern waters of Samos Island (Aegean Sea, Greece). Behavioural data concerning dolphin 'activities and boat interactions have been collected. The analysis of distribution and behavioural data allowed to determine the presence of 2 feeding areas, 1 traveling area, and 1 socializing area. The traveling area corresponds to a zone where dolphins move among the other areas. The analysis of dolphin behaviour showed that *D.delphis* interacts positively to boat presence in all areas.**

I. INTRODUCTION

The short-beaked common dolphin, *Delphinus delphis* (Linnaeus, 1758) is classified as "Endangered" in the Mediterranean Sea, by IUCN experts [1]. In the Mediterranean basin, the short-beaked common dolphin occupies coastal and upper slope waters [2]. By this repartition, it often overlaps with human activities. Moreover, it is shown that vessel presence is influencing *D. delphis´* behaviour [3]. For that reason, to investigate the critical habitats of this species in different part of the Mediterranean Sea is essential to implement local protection measures for its effective conservation.

II. METHODS

From February 2017 to November 2018, surveys were realized in the southern waters of Samos Island (Aegean Sea, Greece) with a motor sailing boat, travelling at 5 knots speed. A random line transect method was adopted. Behavioural data were collected every 3 minutes using the focal group method. Information on interactions with boats were also gathered and classified as follow: positive (POS), if the dolphin´s group stop its activity to interact with a boat; neutral (NEU) if the dolphin´s group continue its activity, independently than boat presence; negative (NEG), if the dolphin´s group avoid boat within a 400 m distance.

III. RESULTS AND DISCUSSION

A total of 150 surveys were carried out in an area of 1834 km^2. 84 sightings were realised. Three different type of area were defined by the observed behavioural contexts: 1 traveling zone (300 km^2), 2 feeding zones (11 and 7 km^2), 1 socialising area (37 km^2). Resting behaviour was observed only 3 times.
This study showed that *D. delphis* is more observed in traveling (65%) and feeding (25%), than socialising (5%) and resting (5%). Concerning boat interactions, positive (49%) and neutral (41%) interactions are the most observed, whereas negative interactions are observed just in 10% of the sightings. The analysis of interaction with boats within each area shows that: 1) in the traveling zone, 50% of the interactions are positive, 44% are neutral and 6% are negative; 2) in the feeding zones, 53% of the interactions are positive, 42% are neutral and 5% are negative; 3) in the socialising zone, 100% of the interactions are positive.

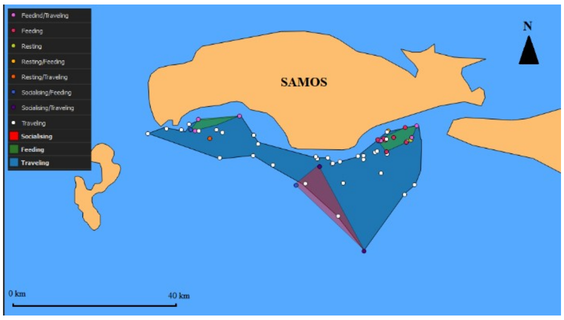

Fig 1. *Habitat use of* D. delphis *in the southern waters of Samos Island (Aegean Sea, Greece).*

IV. CONCLUSIONS

In the study area, traveling activity corresponds to the movement between the two identified feeding areas. In order to have a better understanding of the food preferences of *D. delphis*, it could be interesting to study more in details the environmental characteristics of these feeding areas. Boat presence showed to have a considerable impact on *D. delphis´* behaviour. *D. delphis* are interrupting their behaviour to interact with boats in 49% of the cases. A further study should consider the impact of these interactions on the *D. delphis´* fitness.

V. CITATIONS AND REFERENCES

REFERENCES

[1] Bearzi G. (2012). *Delphinus delphis*, The IUCN Red List of Threatened species.
[2] Bearzi G., Reeves R.R., Notarbartolo Di Sciara G., Politi E., Canadas A., Frantzis A., Mussi B. (2003). Ecology, status and conservation of short- beaked common dolphins (*Delphinus delphis*) in the Mediterranean Sea. Mammal Review, 33(34): 224-252.
[3] Meissner A.M., Christiansen F., Martinez E., Pawley M.D. Orams M.B., Stockin K.A., (2015). Behavioural effects of tourism on oceanic common dolphins, *Delphinus* sp., in New Zealand; the effects of Markov analysis variations and current tour operator compliance with regulations. PloS One. 10(1).

2020 IMEKO TC-19 International Workshop on
Metrology for the Sea
Naples, Italy, October 5-7, 2020

Quantifying the dolphins-fishery competition in the Gulf of Taranto (Northern Ionian Sea, Central Mediterranean Sea)

Ricci P.[1], Ingrosso M.[1], Carlucci R.[1], Fanizza C.[2], Maglietta R.[3], Santacesaria C.[2], Tursi A.[1], Cipriano G.[1]

[1] *Department of Biology, University of Bari, via Orabona 4, 70125, Bari, Italy, e-mail: pasquale.ricci@uniba.it; m.ingrosso14@studenti.uniba.it; roberto.carlucci@uniba.it; angelo.tursi@uniba.it; giulia.cipriano@uniba.it;*
[2] *Jonian Dolphin Conservation, Jonian Dolphin Conservation, viale Virgilio 102, 74121 Taranto, Italy, e mail: carmelo@joniandolphin.it; lia@joniandolphin.it*
[3] *Institute of Intelligent Industrial Systems and Technologies for Advanced Manufacturing, National Research Council, via Amendola 122 D/O, 70126, Bari, Italy, e mail rosalia.maglietta@cnr.it*

***Abstract* - The dolphins-fishery competition in the Gulf of Taranto (Northern Ionian Sea, Central Mediterranean Sea) was investigated during the period 2009-2016. In particular, the biomass removal by the striped and common bottlenose dolphin and the local fishery was estimated by means the food consumption rates of dolphins and landing data of the main fishing gears operating in the area. In addition, an indication on the overlap, in terms of diet/landing composition, occurring between both dolphin species and fishery was discussed.**

I. INTRODUCTION

The competitive interactions between cetaceans and fishery represents a common trait of several harvested marine ecosystems [1]. Although these interactions could cause negative impacts to the fishery due to dolphins' depredation of the fishing gears turning in economic losses [2], the dolphins-fishery conflicts are often dealt with reductive approach overestimating the harmful interactions [3,4]. Moreover, the increase of competition seems to occur in ecosystems overexploited where the fishing activities result unsustainable [5,6], with the risk of a depletion of the cetaceans' food resources [7]. Therefore, potential negative impacts due to the overfishing could affect the cetaceans' populations and the marine ecosystems functioning. Thus, any management actions needed to ensure a sustainable exploitation of the fishing resources requires the adoption of a holistic approach able to integrate ecological and fishing information.

Several studies have demonstrated a scarce competition between dolphin species and fishermen in the Mediterranean areas, especially when the analysis was based on the quantitative comparison between cetaceans food consumptions and fishery catches, as well as the overlapping between dolphins' preys and the landing composition [8,9].

In the marine food web of the Gulf of Taranto, odontocetes species, especially the striped dolphin (*Stenella coeruleoalba*) and the common bottlenose dolphin (*Tursiops truncatus*) have proved to be key species in the trophic controls [10]. However, their interactions with fishing gears and the competition for the harvested resources are scarcely known. Thus, the study aims to provide a preliminary assessment on the dolphins-fishery competition comparing the food consumption rates of the striped and common bottlenose dolphin inhabiting the area with the biomass removal performed by the local fishery. In addition, an indication on the overlap, in terms of diet/ landing composition, occurring between both dolphin species and fishery was discussed.

II. MATERIALS AND METHDOS

A. Study area

The Gulf of Taranto is extended approximately for 14.000 km² from Santa Maria di Leuca to Punta Alice and it is characterized by the system of submarine canyons of Taranto Valley reaching depth of more than 2200 m (Fig. 1) [11]. The basin hosts several habitats identified along the sea floor, such as seagrasses meadows, the Amendolara seamount (Cape Spulico) and the deep-water coral province of Santa Maria di Leuca [12,13]. Moreover, it has been widely recognized as critical area for the day-to-day life of the striped and common bottlenose dolphins [14,15,16,17,18,19], as well as for other cetacean species [20,21,22,23].

The fishing activities occur from coastal waters to about

800 m deep waters and it is characterized by the bottom otter trawls that mainly exploit the shelf break and slope and the small scale fishery operating on the coastal grounds [24]. Thus, the interactions between dolphins and the fishery was assessed for a study area of 7745 km^2 from S. Maria di Leuca to Punta Alice in a range of 10-800 m of depth (Fig. 1).

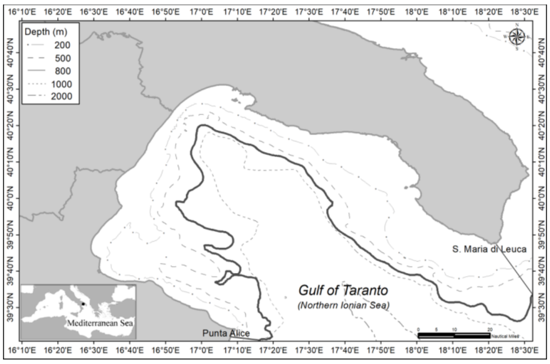

Fig. 1. Map of the Gulf of Taranto in the Northern Ionian Sea (Central Mediterranean Sea). The study area is included in the bold line.

B. Dolphins' food consumption rate

The average value of the daily food consumption, referred to a medium sized dolphin, has been calculated separately for the striped and common bottlenose dolphin, in order to quantify their consumption of annual biomass in the study area. Four different equations have been used for estimating the daily food consumption [8]:

$$IB = 0.123\ M^{0.8} \qquad (1)\ [25]$$

$$IB = 0.482\ M^{0.524} \qquad (2)\ [26,27]$$

$$IB = 0.035\ M \qquad (3)\ [28]$$

$$IB = 0.1\ M^{0.8} \qquad (4)\ [5]$$

where IB is the ingested biomass (kg/day) and M is the body mass of dolphin in kg. The results of these estimates were averaged each other, and the confidence interval (CI) was expressed as two times the standard deviation [8]. Then, IB value, for each dolphin species, has been multiplied for the abundance value estimated in the study area (7745 km^2) (see paragraph C) obtaining the total food consumption (Q expressed as tons).

The value of adult body mass (M) for *T. truncatus* was computed using the following equations:

$$M = 17.261e^{0.0156(L-140)} \qquad (5)\ [29]$$

while, those for *S. coeruleoalba* was computed according the formula:

$$M = 1.38*10^{-4} * L^{2.5177} \qquad (6)\ [30]$$

in both equations, L is the body length expressed in cm.

Body lengths (L) data of several individuals of both dolphin species, coming from the Gulf of Taranto or nearby zones, were gathered from stranding records, ecological studies and the Italian Stranding Network database [31,32,33,34] (Table 1). A total of 74 and 29 measures of body length have been collected for striped dolphins and common bottlenose dolphins, respectively. Body lengths below the value of mean body length minus the standard deviation (i.e. striped dolphins below 119 cm and bottlenose dolphins below 157 cm) were not included in the adult computation, because these values probably referred to young animals including calves [8].

C. Dolphins species abundance estimates

Abundance values used in the calculation of IB were obtained by multiplying the mean values of density estimated for both species in the Gulf of Taranto in the period 2009-2016 [15] for the surface of the study area. These mean values of density were estimated by the application of the Delta approach on Random Forest to sighting data collected in the Gulf of Taranto and they were 0.72±0.26 (individual/km^2) for *S. coeruleoalba* and 0.47±0.09 (individual/km^2) for *T. truncatus*. Consequently, the mean abundances considered in this study were 5576±2014 and 3640±697, for striped and common bottlenose dolphin, respectively.

D. Fishing data

In order to estimate the biomass removed by the local fishery, landing and discard data were considered. The landing data by species were provided from the EU Data Collection Framework reporting the landings during the period 2009-2016 in the sub regions of Puglia and Calabria included in the Geographical Sub Area 19 (GSA 19). The fishing is characterized by trawl (OTB), passive nets (GN), longlines (LL), purse seine (PS) and mixed gears (MG, traps, beach seine and lines) [10]. In addition, discard was estimated applying discard rates by fishing gears available from the literature at local and Mediterranean scale [35 and reference therein].

E. Resource overlap

The overlap between diet composition of the two dolphin species and the landings composition of each fishing gear occurring in the study area has been assessed by means a modified version of Pianka niche overlap index (α) [36]:

$$\alpha = \sum_{i=1}^{n}\left(P_{ji} * P_{ki}\right) / \sqrt{\sum_{i=1}^{n}\left(P_{ji}^{2} * P_{ki}^{2}\right)} \qquad (7)$$

where P_{ji} e P_{ki} are the proportions of the resource *i* exploited by *j* and *k*, respectively.

Diet composition of dolphins in the study area is still not known, therefore dietary preferences were derived from studies conducted in close areas. In particular, diet information for striped dolphin has been obtained from the Ionian Sea [37] and the North Aegean Sea [38], and those for the common bottlenose dolphin has been inferred from the Eastern Ionian Sea [8] and the North Aegean Sea [38].

The average diet of *S. coeruleoalba* was assumed to be composed of 29% Commercial Squids (C Squids, *Illex* spp., *Loligo* spp., *Todaropsis eblanae*), 27% Sparids and

Mullets (SM, *Boops boops*, *Diplodus* spp., *Pagellus* spp., *Mugil* spp.), 21% Other Cephalopds (OC, *Todarodes sagittatus*, *Histioteuthis* spp., *Abralia verany*, *Heteroteuthis dispar*), 17% Other fishes (OF, *Gobius* spp., Myctophidae, *Stomias boa*), 4% Small pelagic fishes (SpelF, Clupeidae, Engraulidae) and 2% Flatfishes (F, *Microchirus* spp.). The average diet of *T. truncatus* was assumed to be composed of 35% Sparids and Mullets, 15% Other Commercial fishes (OCF, *Conger conger*, *Spicara* spp.), 12% Other fishes (OF), 8% Small pelagic fishes (SpelF, Clupeidae, Engraulidae), 9% Hake and Red Mullet (HRM, *Merluccius merluccius* and *Mullus barbatus*), 7% Commercial Squids, 6% Commercial Cephalopods (C Ceph, *Eledone* spp., *Octopus vulgaris*, *Sepia officinalis*), 4% Mackerels (Mack, *Scombrus* spp., *Trachurus* spp.), 3% Other Cephalopods and 1% Medium pelagic fishes (MpelF, *Belone belone*, *Sphyraena sphyraena*).

Table 1. The body length (cm) of stranded individuals of S. coeruleoalba and T. truncatus and stranding area were reported.

Length (cm)	Area	Length (cm)	Area	Length (cm)	Area
Stenella coeruleoalba		*Stenella coeruleoalba*		*Stenella coeruleoalba*	
208	Apulia	186	Calabria	133	Calabria
190	Apulia	185	Calabria	113	Calabria
107	Apulia	184	Calabria	112	Calabria
216	Sicily	182	Calabria	91	Calabria
207	Sicily	181	Calabria	*Tursiops truncatus*	
206	Sicily	181	Calabria	320	Apulia
205	Sicily	181	Calabria	320	Apulia
203	Sicily	180	Calabria	295	Basilicata
202	Sicily	180	Calabria	290	Apulia
199	Sicily	180	Calabria	270	Apulia
98	Sicily	175	Calabria	270	Calabria
95	Sicily	174	Calabria	263	Apulia
91	Sicily	170	Calabria	260	Apulia
90	Sicily	167	Calabria	250	Apulia
90	Sicily	163	Calabria	243	Basilicata
85	Sicily	163	Calabria	240	Apulia
210	Apulia	150	Calabria	236	Apulia
204	Apulia	146	Calabria	224	Calabria
180	Apulia	137	Calabria	206	Apulia
155	Apulia	133	Calabria	200	Apulia
125	Apulia	125	Calabria	200	Apulia
110	Apulia	113	Calabria	195	Apulia
110	Apulia	112	Calabria	188	Apulia
109	Apulia	110	Calabria	185	Apulia
110	Apulia	91	Calabria	182	Basilicata
213	Calabria	74	Calabria	180	Apulia
210	Calabria	193	Calabria	173	Apulia
206	Calabria	206	Calabria	168	Apulia
197	Calabria	186	Calabria	160	Calabria
196	Calabria	185	Calabria	152	Apulia
196	Calabria	184	Calabria	152	Apulia
195	Calabria	181	Calabria	150	Apulia
195	Calabria	180	Calabria	129	Calabria
193	Calabria	180	Calabria	103	Apulia
190	Calabria	137	Calabria		

III. RESULTS

Undersized individuals, such as 19 striped dolphins and 5 common bottlenose dolphins, have been excluded from the average body-length calculation. The mean adult length (L) was 182 cm for the striped dolphins (95% CI=135–229, n=55) and 230 cm for the common bottlenose dolphins (95% CI=131–329, n=24). Thus, the average body mass (M) was of 67 kg for the striped dolphin (CI=47–91) and 130 kg for the common bottlenose (CI=60–283). Average per-capita daily food consumption was therefore, 3.30 (±0.87) kg for striped dolphin (CI=1.56–5.04) and 5.43 (±0.79) kg for bottlenose dolphin (CI=3.85–7.01). The biomass consumed (Q) by the striped dolphin and the common bottlenose dolphin in the study period from 2009 to 2016 was estimated equal to 6712 tons (±1773) and 7219 tons (±206), respectively. The biomass removal by the fishery in the same period was estimated equal to 43310 tons (±246). Thus, on the total of estimated biomass removed from dolphin species and fishery, the biomass removed by dolphin species was 24% whereas those removed by fisheries was 76% (Table 2 and Fig. 2). The overlap of food resources between *T. truncatus* and fisheries (α=0.53) was higher than that *S. coeruleoalba* and fisheries (α=0.24) (Fig. 3). The common bottlenose dolphin showed the highest overlap with the passive nets (α=0.54) and the longline (α=0.47). Differently, the striped dolphin showed overlap values less than or equal to 0.22 for all fishing gears.

Table 2. Code of prey target of dolphins/fishing and estimates of total biomass removed (tons) during the period 2009-2016 reported for each fishing gears, dolphin species (Sc, striped dolphin, Tt, common bottlenose dolphin) and as a total for the overall fleet (OvFleet) and both dolphin species (TotD). Code: Anglers (Ang, Lophius *spp.); Commercial Crustaceans (Crust, Aristeus antennatus, Aristaeomorpha foliacea, Parapenaeus longirostris, Squilla mantis); Sharks and Rays (ShaRay, Galeus melastomus, Raja sp., Squalus acanthias*).

Prey code	OTB	PS	GN	LL	MG	Tt	Sc	OvFleet	TotD	Total
Ang	861	0	135	8	24	0	0	1028	0	1028
SpelF	68	2537	1122	4	305	578	268	4036	846	4882
C Ceph	1896	14	3236	0	365	361	0	5511	361	5872
Crust	7235	0	142	0	150	0	0	7527	0	7527
C Squids	940	25	110	0	66	505	1946	1141	2451	3592
F	4	0	95	2	4	72	134	105	206	311
MpelF	6	296	258	111	63	72	0	734	72	806
HRM	3457	43	2459	911	405	578	0	7275	578	7853
OCF	183	2	294	157	50	1083	0	686	1083	1769
Mack	1949	921	443	83	154	289	0	3550	289	3839
ShaRay	7	0	4	1	1	0	0	13	0	13
SM	1189	314	1592	280	197	2527	1812	3572	4339	7911
OF	0	0	0	0	0	866	1141	0	2007	2007
OC	0	0	0	0	0	217	1410	0	1627	1627
Tot landing (tons	17795	4152	9890	1557	1784	-	-	35178	-	35178
Discard (tons)	6050	228	1761	50	41	72	0	8130	72	8202
Tot catch (tons)	23845	4380	11651	1607	1825	7220	6711	43308	13931	57239
Tot catch (%)	41.7	7.7	20.4	2.8	3.2	12.6	11.7	75.7	24.3	100

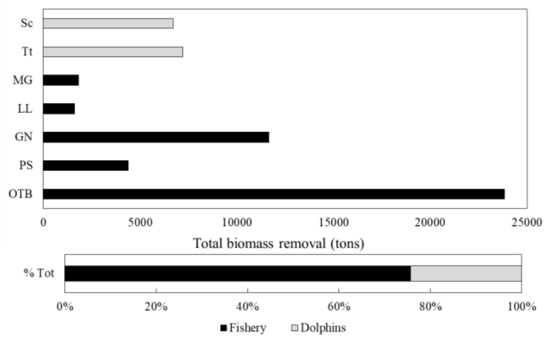

Fig. 2. Estimates of total biomass removed (tons and %) by striped and common bottlenose dolphin and fishing gears in the study area for the period 2009-2016.

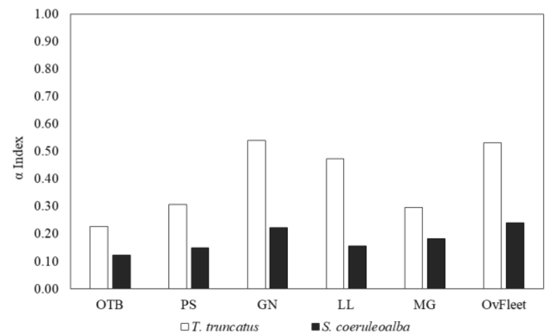

Fig. 3. Overlap index (α) estimated to assess the food resources overlap between the dolphins, the fishing gears and the overall fleet on the basis of the diet/landing composition.

IV. DISCUSSION

The assessment of the dolphins-fishery competition in the Gulf of Taranto has been performed by means of a quantitative analysis estimating the biomass removal and the food resources' overlap in a period of 8 years. The comparison of the biomass removal from dolphin species and fishery highlighted the higher impact of fishery on the local resources, with the trawl and the passive nets as the most important gears in the study area. The value of biomass consumed by dolphin species in the Gulf of Taranto was higher than those reported for the Eastern Ionian Sea [8]. This difference is mainly due to different extension of study areas (Gulf of Taranto 7745 km^2 and Eastern Ionian Sea 1100 km^2, respectively) and to values of estimated abundance. In fact, the mean body length and the average daily consumption of the common bottlenose dolphin calculated in the Gulf of Taranto was lower than those estimated in the Eastern Ionian Sea (243 cm and 6.1 kg/day) [8]. Otherwise, its abundance value estimated in the study area was higher than those reported for the Eastern Ionian Sea, in line with the difference between Ionian and Adriatic Region [15 and reference therein]. Concerning *S. coeruleoalba*, its mean body length was comparable with *D. delphis* considered in [8], but the former species showed a higher abundance value in the study area than those reported for *D. delphis* in Eastern Ionian Sea. The higher total biomass removed by dolphins from the system "Gulf of Taranto" is mainly determined by those conditions.

The striped dolphin showed a very low overlap index than fisheries, stressing the absence of competition with the fishing gears in the study area. This condition is due to its feeding preferences mainly represented by the Myctophidae and bathyal squids distributed in the upper slope of the study area [15]. Differently, the common bottlenose dolphin showed a consistent overlap with passive nets and longlines. In particularly, *T. truncatus* shared the sparids and the mullets with the passive nets and the longlines, the European hake and the red mullet with the trawl and the small pelagic fishes with the passive nets. A similar pattern, in the food resources overlap, between *T. truncatus* and different fishing gears was observed in the Eastern Ionian Sea and in the Thracian Sea [8,9], with the exception of the trawl. In fact, in the Eastern Ionian Sea the overlap index for this species with trawl resulted higher than those calculated for the Gulf of Taranto. This difference could be due to the wider spatial and bathymetric distribution of the trawl fishing effort in the study area. Differently in the Eastern Ionian Sea, a high probability of interactions with the common bottlenose dolphin is due to the exploitation of trawl fishing resources in shallower grounds. The competition by *T. truncatus* with trammel nets and gears belonging to the small-scale fishery has been observed in several Mediterranean areas [39]. However, the results obtained in this study indicated a condition of scarce competition in the Gulf of Taranto confirming the observations reported for the eastern area of the gulf by [40]. This condition could be favoured by a spatial segregation between feeding areas exploited by *T. truncatus*. In particular, a differentiation in the feeding strategy among the common bottlenose dolphin groups could arise reducing the interactions with passive or trawl nets as observed in the Aeolian Archipelago and Ligurian Sea [41,42].

V. CONCLUSIONS

In contexts of the exploited marine ecosystems by fishing activities, the competition between small cetacean species and fishery should be investigated addressing the acquisition of new knowledge useful to quantify the impacts on the resources. In particular, the bio-geographical features, the ecological traits of these species and their consumption rates, as well as the displacement of the fishing effort by different gears and the catches rates, result fundamental elements to understand the level of interactions and competitions between small cetacean species and fishery. The acquisition of these information would allow to implement effective conservation measures of these top-predators, which are keystone species able to control the food web dynamics and to support the processes required by the maintaining of the ecosystem services [43].

REFERENCES

[1] D.Jusufovski, C.Saavedra, A.Kuparinen, "Competition between marine mammals and fisheries in contemporary harvested marine ecosystems", Mar Ecol Progr Series, 2019, 627, 207-232. 10.3354/meps13068.

[2] G.Bearzi, G., "Interactions between cetacean and fisheries in the Mediterranean Sea". In: G.Notarbartolo di Sciara, (Ed.), "Cetaceans of Mediterranean and Black Seas: State of Knowledge and Conservation Strategies", A Report to the ACCOBAMS Secretariat, 2002, Monaco, p. 20 (February, Section 9).

[3] P.R.Reeves, A.J.Read, G.Notarbartolo di Sciara, "Report of the Workshop on Interactions between Dolphins and Fisheries in the Mediterranean: Evaluation of Mitigation Alternatives", ICRAM, 2001, Rome.

[4] G.Bearzi, S.Bonizzoni, S.Agazzi, J.Gonzalvo, "Striped dolphins and short-beaked common dolphins in the Gulf of Corinth, Greece: abundance estimates from dorsal fin photographs", Mar Mammal Sci, 2011a, 27, 165-184.

[5] A.W.Trites, V.Christensen, D.Pauly, "Competition between fisheries and marine mammals for prey and primary production in the Pacific Ocean", J Northwestern Atl Fis Sci, 1997, 22, 173–187.

[6] L.Morissette, V.Christensen, D.Pauly, "Marine Mammal Impacts in Exploited Ecosystems: Would Large Scale Culling Benefit Fisheries?", PLoS One, 2012, 7. e43966. 10.1371/journal.pone.0043966.

[7] G.Bearzi, E.Politi, S.Agazzi, A.Azzellino, "Prey depletion caused by overfishing and the decline of marine megafauna in Eastern Ionian Sea coastal waters (central Mediterranean)", Biol Conserv, 2006, 127, 373–382.

[8] G.Bearzi, S.Agazzi, J.Gonzalvo, S.Bonizzoni, M.Costa, A.Petroselli, "Biomass removal by dolphins and fisheries in a Mediterranean Sea coastal area: do dolphins have an ecological impact on fisheries?", Aquatic Conserv Mar Freshw Ecosyst, 2010, 20: 549-559.

[9] C.Milani, A.Vella, "Interactions between fisheries and cetaceans in the Thracian Sea (Greece) and management proposals", Fish Manag Ecol, 2019, 26. 10.1111/fme.12370.

[10] P.Ricci, S.Libralato, F.Capezzuto, G.D'Onghia, P.Maiorano, L.Sion, A.Tursi, C.Solidoro, R.Carlucci, "Ecosystem functioning of two marine food webs in the North Western Ionian Sea (Central Mediterranean Sea)", Ecol Evol, 2019, 9. 10198-10212.

[11] P.Marin, R.Aguilar, "Mediterranean Submarine Canyons 2012: pending protection". In: M.Würtz (Ed.), "Mediterranean Submarine Canyons: Ecology and Governance", Gland, Switzerland and Málaga, Spain: IUCN, 2012, 191-206.

[12] G.D'Onghia, P.Maiorano, R.Carlucci, F.Capezzuto, A.Carluccio, A.Tursi, L.Sion, "Comparing deep-sea fish fauna between coral and non-coral "megahabitat" in the Santa Maria di Leuca cold-water coral province (Mediterranean Sea)", PLoS ONE, 2012, 7, p. e44509.

[13] R.Carlucci, V.Bandelj, P.Ricci, F.Capezzuto, L.Sion, P.Maiorano, A.Tursi, C.Solidoro, S.Libralato, "Exploring spatio-temporal changes of the demersal and benthopelagic assemblages of the North-western Ionian Sea (Central Mediterranean Sea)", Mar Ecol Progr Ser, 2018a, 598. 10.3354/meps12613.

[14] R.Carlucci, C.Fanizza, G.Cipriano, C.Paoli, T.Russo, P.Vassallo., "Modeling the spatial distribution of the striped dolphin (*Stenella coeruleoalba*) and common bottlenose dolphin (*Tursiops truncatus*) in the Gulf of Taranto (Northern Ionian Sea, Central eastern Mediterranean Sea)", Ecol Indicat, 2016, 69, 707-721.

[15] R.Carlucci, G.Cipriano, C.Paoli, P.Ricci, C.Fanizza, F.Capezzuto, P.Vassallo, "Random Forest population modelling of striped and common-bottlenose dolphins in the Gulf of Taranto (Northern Ionian Sea, Central-eastern Mediterranean Sea)", Est Coast Shelf Sci, 2018b, 204, 177-192.

[16] R.Carlucci, P.Ricci, G.Cipriano, C.Fanizza, "Abundance, activity and critical habitat of the striped dolphin *Stenella coeruleoalba* in the Gulf of Taranto (northern Ionian Sea, central Mediterranean Sea)", Aquat Conserv Mar Freshw Ecosyst, 2018c, 28:324–336.

[17] S.Ciccarese, RCarlucci, E.Ciani, E.Corcella, A.Cosentino, C.Fanizza, G.Linguiti, R.Antonacci, "Cytochrome b marker reveals an independent lineage of *Stenella coeruleoalba* in the Gulf of Taranto", PLoS ONE, 2019, 14(3):e0213826.

[18] F.C.Santacesaria, S.Bellomo, C.Fanizza, R.Maglietta, V.Renò, G.Cipriano, R.Carlucci, "Long-term residency of *Tursiops truncatus* in the Gulf of Taranto (Northern Ionian Sea, Central-eastern Mediterranean Sea)", Proc. IEEE Metrology for the Sea2019 IMEKO TC-19 International Workshop on Metrology for the Sea, Genoa, Italy, 2019, pp.28-32.

[19] M.Azzolin, A.Arcangeli, G.Cipriano, R.Crosti, R.Maglietta, G.Pietroluongo, S.Saintignan, A.Zampollo, C.Fanizza, R.Carlucci, "Spatial distribution modelling of striped dolphin (*Stenella coeruleoalba*) at different geographical scales within the EU Adriatic and Ionian Sea Region, central-eastern Mediterranean Sea", Aquat Conserv Mar Freshw Ecosyst, 2020, 30, 1194-1207.

[20] R.Maglietta, V.Renò, G.Cipriano, C.Fanizza, A.Milella, E.Stella, R.Carlucci, "DolFin: an innovative digital platform for studying Risso's dolphins from the northern Ionian Sea (Central-Eastern Mediterranean)" Sci Rep, 2018, 8:17185.

[21] R.Carlucci, A.Akkaya Baş, R.Maglietta, V.Renò, C.Fanizza, A.Rizzo, R.Crugliano, G.Cipriano "Site fidelity, residency and habitat use of the Risso's dolphin *Grampus griseus* in the Gulf of Taranto (Northern Ionian Sea, Central-eastern Mediterranean Sea) by photo-identification", Proc. IEEE Metrology for the Sea, Bari, Italy, 2018d, pp.173-177.

[22] S.Bellomo, F.C.Santacesaria, C.Fanizza, G.Cipriano, V.Renò, R.Carlucci, R.Maglietta, "Photo-identification of *Physeter macrocephalus* in the Gulf of Taranto (Northern Ionian Sea, Central-eastern Mediterranean Sea)", Proc. IEEE Metrology for the Sea 2019 IMEKO TC-19 International Workshop on Metrology for the Sea, Genoa, Italy, 2019, pp. 33-37.

[23] S.Dimatteo, M.Siniscalchi, L.Esposito, V.Prunella, P.Bondanese, G.Bearzi, A.Quaranta, "Encounters with pelagic and continental slope cetacean species near the northern shore of the Gulf of Taranto, Italy", Ital J Zool, 2011, 78(1):130-132.

[24] T.Russo, E.Bitetto, P.Carbonara, R.Carlucci, L.D'Andrea, M.T.Facchini, G.Lembo, P.Maiorano, L.Sion, M.T.Spedicato, A.Tursi, S.Cataudella, "A holistic approach to fishery management: evidence and insights from a Central Mediterranean case study (Western Ionian Sea)" Front Mar Sci, 2017, 4.

[25] S.Innes, D.M.Lavigne, W.M.Earle, K.M.Kovacs, "Feeding rates of seals and whales", J Animal Ecol, 1987, 56: 115–130.

[26] R.Leaper, D.Lavigne, "Scaling prey consumption to body mass in cetaceans", Paper SC/J02/FW2, International Whaling Commission, Modelling Workshop on Cetacean-Fishery Competition, 2002, La Jolla; 1–12.

[27] K.Kaschner, "Modelling and mapping resource overlap between marine mammals and fisheries on a global scale", PhD thesis, University of British Columbia, 2004, Available at: http: //www.fisheries.ubc.ca/students/graduated.php.

[28] T.Tamura, "Regional assessment of prey consumption and competition by marine cetaceans in the world", In M.Sinclair, G.Valdimarsson (Eds). "Responsible fisheries in Marine Ecosystems", Food and Agricultural Organisation of the United Nations & CABI Publishing, 2003, Wallingford, UK; 143–170.

[29] R.A.Kastelein, N.Vaughan, S.Walton, P.R.Wiepkema, "Food intake and body measurements of Atlantic bottlenose dolphins (*Tursiops truncatus*) in captivity", Mar Environ Res, 2002, 53: 199–218.

[30] J.Andre, A.Boudou, F.Ribeyre, M.Bernhard, Comparative study of mercury accumulation in dolphins (*Stenella coeruleoalba*) from French Atlantic and Mediterranean coasts", Science of The Total Environment, 1991, 104, 191-209.

[31] N.Cardellicchio, S.Giandomenico, P.Ragone, A.Leo, "Tissue distribution of metals in striped dolphins (*Stenella coeruleoalba*) from the Apulian coasts, Southern Italy", Mar Environ Res, 2000, 49, 55-66.

[32] S.Caracappa, R.Puleio, G.Loria, A.Gentile, M.F.Persichetti, G.Caracappa, F.Licitra, M.Arculeo, "Stranding patterns of the striped dolphin (*Stenella coeruleoalba*, Meyen 1833, Delphinidae) along the Sicilian coast (Mediterranean Sea)", Mar Mammal Sci, 2018, 35. 10.1111/mms.12569.

[33] https://geocetus.spaziogis.it/

[34] http://mammiferimarini.unipv.it/index.php

[35] K.Tsagarakis, A.Palialexis, V.Vassilopoulou, "Mediterranean fishery discards: Review of the existing knowledge", ICES J Mar Sci, 2014, 71(5), 1219–1234.

[36] E.R.Pianka, "The Structure of Lizard Communities", Annual Review of Ecology and Systematics, 1973, 4:1, 53-74.

[37] G.Bello, "Stomach content of a specimen of *Stenella coeruleoalba* (Cetacea: Delphinidae) from the Ionian Sea", Soc Ital Sci Nat Museo Civico Storia Nat, 1993, 133:41-48

[38] C.Milani, A.Vella, P.Vidoris, A.Christidis, E.Koutrakis, A.Frantzis, et al., "Cetacean stranding and diet analyses in the North Aegean Sea (Greece)", J Mar Biol Assoc UK, 2018, 98, 1011-1028.

[39] R.T.E.Snape, A.C.Broderick, B.A.Çiçek, et al., "Conflict between dolphins and a data-scarce fishery of the European Union" Hum Ecol, 2018, 46:423–433.

[40] G.Bearzi, S.Bonizzoni, J.Gonzalvo, "Dolphins and coastal fisheries within a marine protected area: mismatch between dolphin occurrence and reported depredation", Aquatic Conserv Mar Freshw Ecosyst, 2011b, 21, 261–267.

[41] M.Bellingeri, F.Fossa, G.Gnone, "Interazione tra *Tursiops truncatus* e pesca a strascico: differente comportamento in due aree limitrofe lungo la costa ligure di levante. Interaction between *Tursiops truncatus* and trawlers: different behaviour in two neighbouring areas along the eastern ligurian sea", Biol Mar Mediterr, 2011, 18, 174-175.

[42] M.Blasi, L.Boitani, "Complex social structure of an endangered population of bottlenose dolphins (*Tursiops truncatus*) in the Aeolian Archipelago (Italy)", PloS One, 2014, 9. e114849.

[43] N.Hammerschlag, O.Schmitz, A.Flecker, K.Lafferty, A.Sih, T.Atwood, A.Gallagher, D.Irschick, R.Skubel, S.Cooke, "Ecosystem Function and Services of Aquatic Predators in the Anthropocene", Trends in Ecology & Evolution, 2019, 34. 369-383. 10.1016/j.tree.2019.

2020 IMEKO TC-19 International Workshop on
Metrology for the Sea
Naples, Italy, October 5-7, 2020

Mediterranean monk seals increased detection in the Gulf of Corinth (Greece) during CoViD-19 lockdown

Marta Azzolin[1,2], Matteo Costantino[1], Sebastien Saintignan[1], Cristina Giacoma[2], Guido Pietroluongo[1]

[1] *Gaia Research Institute Onlus, Turin, Italy and Milokopi, Loutraki, Greece, marta.azzolin@gmail.com; matteo.costantino91@gmail.com, sebastien.saintignan@outlook.com, guido.pietroluongo@gmail.com*
[2] *Life and System Biology Department, University of Turin, Turin, Italy, marta.azzolin@unito.it cristina.giacoma@unito.it,*

***Abstract* – Cryptic endangered species, such as the Mediterranean monk seal, need special conservation measurements for their survival and habitat protection. Globally, CoViD-19 lockdown played as an environmental simulation of protection measurements and practical conservation actions, such as the ban or mitigation of human activities in key habitat for the marine species.**

An analysis of the comparison between historical data and lockdown data about the presence of monk seal in the Alkionides Gulf remarked the evidence of increased sightings of free-ranging individuals, which could have beneficiated of the low anthropogenic impact situation. This area of the Gulf of Corinth could indeed represent an important habitat for this endangered species in Greek waters.

I. INTRODUCTION

The Mediterranean monk seal (*Monachus monachus*, Hermann 1779) is one of the most endangered mammals in the world, classified as "Endangered" by IUCN experts [1].

As the only living representative of the genus Monachus in the Mediterranean Sea, the Mediterranean monk seal represents one of the most endangered mammals in the world [1].

While the species was historically widespread in the Mediterranean Sea, the Black Sea and Eastern Atlantic Ocean [2], the surviving population is now concentrated and fragmented in the Ionian and Aegean waters, the Madeira archipelago, and Cabo Blanco waters in the Eastern Atlantic Ocean [1]. Indeed, the main surviving groups of Mediterranean monk seal are found in Greece and Mauritania. The dramatic decline of the species is addressed to several anthropogenic threats, such as habitat degradation, historical persecution and deliberate killing, negative interaction with fishery as well as natural causes [1].

The Ionian Archipelago features one of the most breeding areas globally for the Endangered Mediterranean monk seal. Therefore, the archipelago is identified as the Ionian Archipelago Important Marine Mammal Area (IMMA) [3].

The erratic behaviour of this elusive species and the similar oceanographic characteristic of the adjacent Gulf of Corinth make this area suitable for the Mediterranean monk seal survival and conservation. Moreover, the Gulf of Corinth is already classified as IMMA. It is included in the Natura 2000 European network of protected areas (Site Code: GR2530007) thanks to its rich biodiversity of marine flora and fauna [4]. A certain number of monk seals sightings are already reported in the Gulf (unpublished data).

A regular land-based and boat-based surveys monitoring activity carried out since June 2009, together with numerous reports provided by local citizens and tourists, confirms the regular presence of the species in the Northern Eastern area of the Gulf of Corinth during the last 11 years. Land-bases monitoring activity carried out during Corona Virus Disease of 2019 (CoViD-2019) lockdown showed an increased presence of monk seals, and for the first time, a couple of individuals were observed in the Gulf.

II. METHODS

A. The area of study: the Gulf of Corinth

The Gulf of Corinth belongs to the north-eastern Ionian Sea and separates the Peloponnesus Region from Northern Greece (Figure 1). On its western portion the Rion Strait, 2km wide and 65m deep, links the Gulf to the

Ionian Sea. On its eastern side, the artificial channel of Corinth leads to the Saronic Gulf and the Aegean Sea. Even if it is a semi-closed basin, the Gulf of Corinth presents a great variety of marine habitats, including pelagic waters, and upwelling currents induced by the wind [5]. In this scenario, the Gulf of Corinth offers the perfect conditions for the survival of many marine species.

B. Data collection

Monk seals presence has been investigated through boat and land surveys focusing on dolphins, starting from summer 2009. Boat surveys were carried out in standard weather conditions (Beaufort ⩽ 3, Douglas ⩽ 3, visibility ⩾ 5 miles), employing a 12m sailing vessel, mainly during the summer season (Figure 1). Land-based surveys were carried out year-round, in the same standard weather condition, from 3 different sites located in the Alkionides Gulf (Northern Eastern): Melangavi Cape, Milokopi, Petrita (Figure 1).

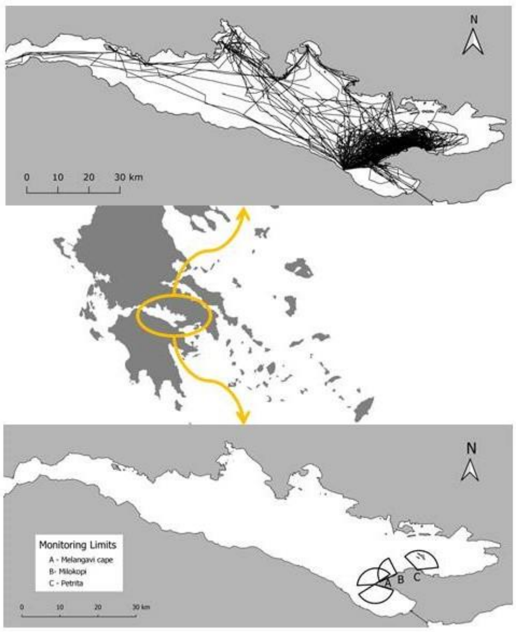

Figure 1: Area of Study. Central: Greece. The yellow oval shows the location of the Gulf of Corinth. Above: effort boat tracks in the Gulf of Corinth. Below: Land-based monitoring sites in the Alkionides Gulf.

III. RESULTS

From June 2009 to June 2020, monk seals have been observed eleven times during dedicated monitoring activity carried out by experienced observer, in an area where the species was not previously reported. Ten sightings belong to the Alkionides Gulf, between Melangavi Cape and Strava, while a single sighting is from the Northern portion of the Gulf of Corinth (Figure 2).

Monk seals have been observed in 2012, 2018, 2020. Latency varies among years. In July 2012, researchers sighted from the research vessel an adult individual in two distinct occasions, with a latency of 20 days, in two different areas, located 5 miles apart: Milokopi bay and the waters between Strava bay and the Alkionides Islands. During spring 2018 (April and May) an individual was sighted from Milokopi cliff with a latency of 16 days. Then, another adult was observed by the sailing vessel close to Pangalos Cape in the Northern portion of the Gulf. In 2020 (April), during the lockdown following the CoViD-19 pandemic, four monk seals sightings were realised from Milokopi cliff, with a latency of just one day. In two of these sightings, for the first time in the Gulf, two adults were observed together.

Individual identification was not possible for all the sightings.

64% of the sightings were realised in the late afternoon, while the remaining 36% refers to the late morning.

In 73% of the cases, monk seals were spotted while doing the land-based surveys, when no boat was around, neither the research vessel. Even the sightings realised at sea were in the absence of boats, except for the research vessel. These results indicate a monk seal preference for quiet areas without boat traffic.

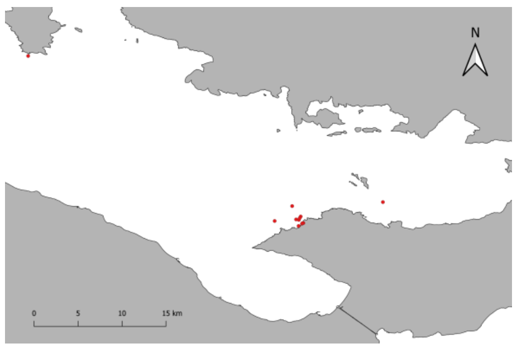

Figure 2: Monk seals sightings.

IV. DISCUSSION

The conservation strategy related to the Mediterranean monk seal aims, on one side, to increase the research effort in the field to gather more information on presence and distribution of this cryptic species and, in parallel, to enforce protection measurements.

The results of the regular monitoring activity carried out by experienced observers in the Gulf of Corinth shows that monk seals are regularly present in the area. Moreover, the distribution of the sighting shows that also some areas, where it was not previously reported, are important for its conservation. Particularly, the area located in the Alkionides Gulf, between Melangavi Cape and Strava, hosting caves and suitable habitats, and just few road accesses for human use, looks valuable for the conservation of the species.

CoViD-19 lockdown represented a singular simulation of protection measurements, such as the ban of human activities in key habitat for the species. The results of this study showed that, while the researchers spotted individuals regularly during the years, the frequency increased during the period of a forced stop of the human activities in the area. Moreover, during this period of low human presence, in the area was recorded for the first time, the presence of two individuals. The stop of fishery activities and heavy marine traffic, the low presence of humans along the coastline and in the potential key habitat for the species, the decrease of underwater ambient noise could have played a role on the increase of sightings recorded. As assessed from the scientific community [6], free-ranging animals, such as Mediterranean monk seals, could have beneficiated of CoViD-19 lockdown to explore or expand their usual habitat range.

IV. CONCLUSION

The results of the present study show that the Alkionides Gulf represents an important area for the conservation of the Mediterranean monk seals.

The global evidence that free-ranging animals could have beneficiated of CoViD-19 lockdown should help the conservation scientists and policymakers to meditate on the role of the practical conservation actions to protect the destiny of species running to extinction such as the Mediterranean monk seal.

REFERENCES

[1] Karamanlidis, A.A.; Dendrinos, P. *Monachus monachus*. IUCN Red List Threat. Species 2015; International Union for Conservation of Nature and Natural Resources: Gland, Switzerland, 2015. [CrossRef]

[2] Karamanlidis, A.A.; Dendrinos, P.; de Larrinoa, P.F.; Gücü, A.C.; Johnson, W.M.; Kiraç, C.O.; Pires, R. The Mediterranean monk seal *Monachus monachus*: Status, biology, threats, and conservation priorities. Mamm. Rev. 2016, 46, 92–105. [CrossRef]

[3] IUCN-MMPATF (2017) Ionian Archipelago IMMA Factsheet. IUCN Joint SSC/WCPA. Marine Mammal Protected Areas Task Force, 2017.

[4] Issaris, Y., Katsanevakis, S., Pantazi, M., Vassilopoulou, V., Panayotidis, P., Kavadas, S., … Karris, G. (2012). Ecological mapping and data quality assessment for the needs of ecosystem-based marine spatial management: Case study Greek Ionian Sea and the adjacent gulfs. Mediterranean Marine Science, 13, 297–311. https://doi.org/10.12681/mms.312

[5] Lascaratos A., Salusti, E, Papageorgaki, G. (1989). Wind-induced upwellings and currents in the gulfs of Patras, Nafpaktos and Korinthos, Western Greece. Oceanonologica Acta 12(3):159 -164.

[6] Rutz, C., Loretto, M., Bates, A.E. et al. COVID-19 lockdown allows researchers to quantify the effects of human activity on wildlife. Nat Ecol Evol (2020). https://doi.org/10.1038/s41559-020-1237-z

6

Special Session
Measurements for past and present sea level changes

Coastal areas are known to be among the most dynamic elements of the physical landscape, strongly influenced by short to long term forcing factors. In the short term, seasonal and catastrophic meteo-marine events and human impacts can directly interfere with the equilibrium of these areas, sometimes producing drastic coastal changes and sea level oscillations. In a longer timescale, GIA, tectonics, volcano activity and climate changes, certainly are the main factors influencing global and local millennial sea-level variations. In this perspective, it is crucial to understand the impact of relative sea level changes on coastal landscape at different geographic scales, to correctly manage the coastal areas and to prepare the coastal communities to face the expected changes driven by global warming. In the last years, the integration between direct measurement and geo-acoustic and/or remote sensing methods allowed acquiring large amounts of four-dimensional -3D points and time high precision data directly related to relative sea-levels variations and/or to rapid changes in coastal morphology, mainly due to extreme events. A multi-proxies approach based on sea level geo indicators and/or sensors based measurements are challenges of great scientific interest, intended to populate specific databases at Mediterranean and global scale, useful to understand and reduce the uncertainty on sea-level changes models and future coastal scenarios. This session welcomes studies from individuals or groups that use multidisciplinary or innovative approaches to measure relative sea levels and coastal changes from the past millennia to present time, to reconstruct geomorphological processes, human impact and system response, as well as issues of landscape resilience and human adaptation. Approaches involving the use of multi-scalar datasets are strongly encouraged.

2020 IMEKO TC-19 International Workshop on
Metrology for the Sea
Naples, Italy, October 5-7, 2020

Estimating RSL changes in the Northern Bay of Cádiz (Spain) during the late Holocene.

C. Caporizzo[1*], P.P.C. Aucelli[1], I. Galán-Ruffoni[2], F.J. Gracia[2], C. Martín-Puertas[3], G. Mattei[1], P. Stocchi[4]

*[1]Dept. of Science and Technology, Universitá degli Studi di Napoli "Parthenope". Centro Direzionale, Isola C4. 80143, Naples, Italy. *e-mail: claudia.caporizzo@uniparthenope.it*

[2]Dept. of Earth Sciences. Facultad de Ciencias del Mar y Ambientales, Universidad de Cádiz, Puerto Real, Spain

[3]Dept. of Geography, Royal Holloway University of London, United Kingdom

[4]Dept. Of Coastal Systems. NIOZ - Royal Netherlands Institute for Sea Research, P.O. Box 59, 1790 AB, Den Burg, Texel, The Netherlands.

***Abstract* – The Bay of Cádiz (SW Spain) is an example of long historical human occupation of a typical estuarine saltmarsh environment affected by notable historical changes that have conditioned the sedimentary evolution of emerged and submerged zones. This study aims to present new data regarding the RSL position during the late Holocene within the Northern bay of Cádiz. Bibliographic data coming from boreholes carried out in the study area were combined with the analysis of a new core. RSL positions, extracted from depositional sea-level index points, were calculated from saltmarshes and tidal deposits dated between 3.0-2.0 ky BP. Comparing these data with the new eustatic sea-level curve of the Bay of Cádiz carried out in this research, we observed that, during the last 3.0 ky BP, the sector has been affected by prevailing subsidence ranging between 0.9 m and 4.3 m.**

I. INTRODUCTION

The Bay of Cádiz, located within the Guadalquivir Tertiary Depression (SW Spain), is made of low-lying coasts that during the Holocene were affected by erosional and progradational episodes, with the development of subsequent beach ridge systems [1, 2, 3, 4].

The Bay, characterized by a mesotidal range of 2.1 m, has an average length and width of 30 km and 15 km respectively and it is mainly made of marshes, extending several kilometers inland and separated from the sea by sand barrier systems.

During the Quaternary, as a result of the N-S convergence between Africa and Eurasia, two main families of strike-slip faults (NE-SW and NW-SE oriented) formed along the southern Iberian coast. [5]

In the Bay of Cádiz such fault system controlled the distribution of emerged and submerged areas and led to the formation of two semi-circular embayments [6, 7].

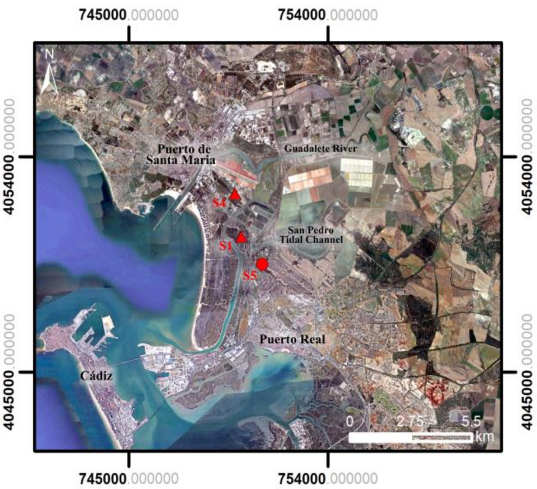

Fig. 1. Location of the study area, the boreholes S1, S4 (Alonso et al.[8]) and the new core S5.

Our study area, located in the northern sector of the Bay of Cádiz, is associated with the estuary of Guadalete River.

During the Pleistocene, the Northern Bay of Cádiz (between Puerto Real and Puerto de Santa Maria, Fig. 1) was affected by significant sedimentary aggradation through the deposition of 30 m of marsh and fluvial sediments. About 6.5 ky BP, the postglacial sea level reached its maximum height in this sector, flooding the former Pleistocene alluvial plains and converting them into a marine bay subject to a still active sedimentary infilling, with sediments mainly supplied by the Guadalete River [2, 3, 9, 10].

II. METHODS

A. Boreholes, stratigraphic analysis and dating

Stratigraphic data from two boreholes (S1 and S4), performed in the study area and published in Alonso et al., 2015, have been revised and combined with those from a new core (S5) carried out in June 2008 and still unpublished. The boreholes are related to a research project elaborated by Gracia and Martín [11]. The obtained continuous cores were stored in appropriate coring-boxes and kept at the laboratories of the University of Cádiz. The description of the cores was carried out in three stages, an initial visual description of the sediments (type, colour, presence of organic remains and organisms), a detailed analysis of the sand fraction using a stereomicroscope, and analysis of the clay fraction on a petrographic microscope. All the detected features were used to define different lithofacies and sedimentary units on which all the boreholes were associated.

Macrofossils such as fragments of shells and roots, as well as bulk sediments where macrofossils were not found, were used for radiocarbon dating at the Centro de Nacional de Aceleradores (CSIC-Spain). Four samples were taken at different depths in boreholes S1, S4 and S5 in levels including rests of skeletons or valves and near the main facies transitions for ^{14}C age determination. Samples were pre-treated with organic solvents and cleaning with AAA. Calibration was made according to curve Marine13 (probability of 95%) [12] by using Calib Rev. 7.0.4 software [13]. A correction had to be made due to the reservoir effect of marine radiocarbon (ΔR), very important in the coasts of the Gulf of Cádiz [14]. In the present work, a weighted value of the reservoir effect of $\Delta R = -108 \pm 31$ ^{14}C years was applied [15].

B. Depositional sea-level proxies

The stratigraphic analysis carried out in this research led to the identification of 4 depositional units, related to specific environments. The recovery of shells fragments inside these layers enabled the dating of different samples characteristic of the Units 3 and 4 and respectively related to saltmarsh and intertidal environments.

According to Vacchi et al. [16], saltmarshes are generally located close to large deltas and coastal lagoon and their samples can be used as sea level index points (SLIPs) by calculating their Indicative Meaning (IM, senu Shennan [17]). We assume for this kind of samples an Indicative Range (IR) ranging from the HAT (sensu Shennan, [17]) to the MSL [16] and a RWL equal to the half of the IR.

The samples collected from intertidal deposits have been used as SLIPs considering an IM with an IR ranging between the MHW and the MLW and a RWL equal to the half of this IR.

Knowing the above-mentioned values, the RSL positions were estimated using the formula proposed by Shennan [17]:

$$RSL = E - RWL \tag{1}$$

Where E is the elevation of the sample (m above MSL).

C. Reconstruction of the RSL curves

The local RSL changes are primarily affected by glacial- and hydro-isostatic adjustment (GIA), which regulates the response of the solid Earth and of the geoid to the melting or accretion of continental ice masses. The GIA-driven RSL changes are described by the gravitationally self-consistent sea level equation (SLE). Solving the SLE for a prescribed ice-sheets chronology and solid earth rheological model [18], yields the regionally varying RSL change over time. The latter strongly depends on the rheological parameters that define the solid Earth model which is assumed to be spherically symmetric, self-gravitating, rotating, radially stratified and characterized by linear Maxwell viscoelastic layers. A suite of RSL curves were produced by using ANICE-SELEN coupled ice-sheet - sea-level model [19]. The sea-level equation (SLE) has been solved for a total of 18 models (6 mantle viscosity profiles x 3 lithosphere thickness). We assumed three values of lithosphere thickness, respectively of 60 km, 90 km and 120 km, and we considered values for the lower, intermediate and mantle viscosity ranging between 2-10, 0.5-1 and 0.2-0.5 Pas, respectively.

III. RESULTS

A. Analysis from the cores

The sedimentological analysis of the cores included in this study reflects the main geomorphological and sedimentary elements presently recognizable in the Bay of Cádiz. In particular:

- S1: This core ,with a maximum depth of 6.5 m, was performed in a tidal plain area, inside a palaeomeander of the ancient Guadalete River. The succession is composed of three different sedimentary units (Table 1). The lower unit (U4) is characterized by sandy facies interpreted as the remains of an estuary channel of the Guadalete River. This hypothesis is in accordance with the interpretation of borehole PSM109 performed in the same location by Dabrio et al. [2]. The upper sedimentary units (U1, U3), made of muddy sands and clays, testify the transition from an estuarine environment to a salt marsh system. Unit 4, interpreted as saltmarsh deposit, was used as a SLIP due to the radiocarbon dating of a shell founded in living position, with an age of 2.8 ky BP.
- S4: This core, located in the inner sand bar of the

old H2 beach ridge [2, 4], has a sedimentary sequence 5 m long and the observation of the stratigraphy led to the identification of 2 sedimentary units (Table 1). The first one (U2, upper 2.4 m), represents a washover deposit, characterized by coarse sands plenty of mollusc bioclasts. The second unit (U3) is mostly constituted by clays, with a major content of organic matter and remains of macrofauna, and interpreted by Alonso et al. [8] as a typical saltmarsh deposit, here used as SLIP. The ^{14}C calibrated dating carried out from shells, founded in living position and located both at the top and the base of U3, established the formation of the salt marsh between 1.88 and 2.8 ky BP.

- S5: The core is located in the tidal plain developed to the south of San Pedro tidal channel and reaches a maximum depth of 6 m. Three different sedimentary units were identified (Table 1). In this case, the deposition of sediments is characterized by a cyclic sequence with the alternation of muddy and sandy facies. The stratigraphic succession is similar to the one of S1, but in S5 a stable establishment of salt marshes has been recorded for a shorter time span. The ^{14}C calibrated dating performed on a shell in living position established the age of 3.1 ky BP for the base of unit U4.

Table 1. Stratigraphical description of the boreholes and environmental interpretation of the deposits

Cores	Unit	Lithofacies	Env. Int.
S1	U1	Dark brown clays with remains of thin roots and amorphous aquatic material. Coarsening upward.	Dried-up saltmarsh
		Yellow sands with remains of roots similar to the upper level. Finning upward.	
		Grey sandy muds with shells remains. Finning upward.	
	U3	Brown muddy sands with no remains of organic matter. Coarsening upward in the first 30 cm and subsequent homogeneity	Active saltmarsh
	U4	Yellow sands similar to the previous level but with a different colour that may represent a transitional period.	Transitional environment
		Coarse-grained sands with visible quartz grains. Abundant shell macro-fragments. Rounded grains of small size at the base, finning upward.	Tidal environment
S4	U2	Brown sands with remains of roots. Low content of water. Present soil.	Washover fan (high energy)
		Yellow fine sands with abundant remains of marine bivalves, gastropods and other organisms.	
	U3	Grey clays with remains of herbal organic matter and foraminifer shells.	Active saltmarsh
	U4	Silty clays with organic remains of amorphous aquatic material and coal.	Tidal plain with fluvial influence
S5	U1	Brown clays with macro-fauna remains (shells). Coarser grains at the base.	Dried-up saltmarsh
		Dark yellow fine sands with shell remains.	Energetic event
	U3	Greyish clays.	Active saltmarsh
		Dark brown muddy sands.	
	U4		Tidal channel

B. *RSLs evaluation*

Using the methodology described in section B of Methods, the related RSLs associated with samples coming from saltmarsh deposits were calculated taking into account that in the Gulf of Cádiz the value of the highest astronomical tide (HAT) is 1.89 m MSL, considering the closest tide gauge to the studied sector [20] (Table 2).

Instead, the RSLs related to samples collected from intertidal deposits were deducted taking into account that in the Gulf of Cádiz the mean high water (MHW) and the mean low water (MLW) are respectively equal to 1.05 m MSL and -0.93 m MSL, considering the closest tide gauge to the study area [20] (Table 2).

Table 2. RSLs from sea-level index points (SLIPs).

Sample	Unit	yr BP	IR	RWL	RSL (m MSL)
S1_a2	U3	2863±134	HAT to MSL	(HAT to MSL)/2	-4.14 ± 0.94
S4_a1	U3	2886±138	HAT to MSL	(HAT to MSL)/2	-2.64 ± 0.94
S4_a2	U3	2005±132	HAT to MSL	(HAT to MSL)/2	-1.14 ± 0.94
S5_a1	U4	3114±212	MHW to MLW	(MHW to MLW)/2	-4.79 ± 0.99

IV. DISCUSSION AND CONCLUSIONS

The RSL positions obtained from the depositional SLIPs (with their specific vertical and horizontal uncertainties) were compared to the eustatic values of the sea-level curve proposed for the area (Fig. 2).

From the comparison of the data, it is possible to affirm that a prevailing subsiding trend affected the Norther Bay of Cádiz during the last 3.1 ky BP.

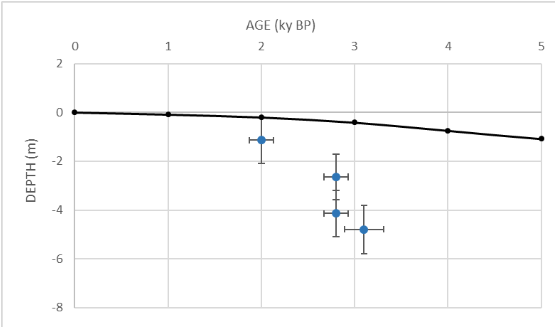

Fig. 2. Graph of the relative sea-level measurements carried out from the depositional SLIPs compared to the GIA model (ANICE-SELEN ice-sheet - sea-level model) proposed for the Gulf of Cádiz.

Such phenomenon progressively reduced its effect as testified by the values of the local vertical displacement (VD) decreasing with time.

In particular, the value of the subsiding rate is 1.4 mm/yr for the SLIP dated at 3.1 ky BP, with a VD of -3.34 m, and 0.47 mm/yr for the younger sea-level marker dated at 2.0 ky BP, with a VD of -0.94 m. In accordance with this trend, the subsiding rate for the SLIPs dated 2.8 ky BP is equal to 1.07 mm/yr, with a mean VD of -3.0 m.

The detected subsiding trend can be interpreted as the main effect of the sediment compaction affecting the more recent deposit of the coastal plain [21, 22, 23, 24].

REFERENCES

[1] F.J.Gracia, J.Rodríguez-Vidal, J.Benavente, L.Cáceres, F.López-Aguayo, F., "Tectónica cuaternaria en la Bahía de Cadiz", In L. Pallí & C. Roqué (Eds.), Avances en el estudio del Cuaternario español, University of Girona, 1999, pp. 67-74.

[2] C.J.Dabrio, C.Zazo, J.L.Goy, F.J.Sierro, F.Borja, J.Lario, J.A.González, J.A.Flores, "Depositional history of estuary infill during the last postglacial transgression (Gulf of Cadiz, Southern Spain)", Marine Geology, 2000, vol.162, pp. 381-404.

[3] O.Arteaga, H.D.Schulz, A.Roos, "Geoarqueología Dialéctica en la Bahía de Cádiz", RAMPAS, 2008, vol.10, pp. 21-116.

[4] C.Alonso, F.Gracia, S.Rodríguez-Polo, "Modelo de evolución histórica de la flecha-barrera de Valdelagrana (Bahía de Cádiz)", XIII Reunión Nacional de Geomorfologia, Cáceres, Geomorfología litoral: Procesos y Formas en las Costas, 2014, pp. 584-587.

[5] P.G.Silva, J.L.Goy, C.Zazo, T.Bardají, J.Lario, L.Somoza, L.Luque, F.M.González-Hernández, "Neotectonic fault mapping at the Gibraltar Strait Tunnel area, Bolonia Bay (South Spain)", Engineering Geology, 2006, vol. 84, pp. 31-47.

[6] Gutiérrez-Mas, J.M., Achab, M., Gracia, F.J., 2004. Structural and physiographic controls on the Holocene marine sedimentation in the Bay of Cadiz (SW Spain). Geodinamica Acta, 17 (2), 47 - 55.

[7] F.J.Gracia, J.Rodríguez-Vidal, G.Belluomini, L.M.Cáceres, J.Benavente, C.Alonso, "Diapiric uplift of an MIS 3 marine deposit in SW Spain. Implications in Late Pleistocene sea level reconstruction and palaeogeography of the Strait of Gibraltar", Quat. Sci. Rev., 2008, vol. 27, pp. 2219-2231.

[8] C. Alonso, F.J.Gracia, S.Rodríguez Polo, C.Martín Puertas, "El registro de eventos energéticos marinos en la Bahía de Cadiz durante épocas históricas", In J. Rodríguez-Vidal (Ed.), Eventos energéticos amarinos históricos y ocupación costera en el Golfo de Cadiz. Cuaternario & Geomorfología, 2015, vol. 29 (1–2), pp. 95-117.

[9] C.Zazo, C.J.Dabrio, J.L.Goy, J.Lario, A.Cabero, P.G.Silva, T.Bardaji, N.Mercier, F.Borjag, E.Roquero, "The coastal archives of the last 15 ka in the Atlantic-Mediterranean Spanish linkage area: Sea level and climate changes". Quaternary International, 2008, vol. 181, pp.72-87.

[10] L.Del Río, J.Benavente, F. J.Gracia, G.Anfuso, M.Aranda, J.B.Montes, M.Puig, L.Talavera, T.A.Plomaritis, "Beaches of Cadiz: Dynamic Processes, Sediments and Management", 2019, 10.1007/978-3-319-93169-2_14.

[11] F.J.Gracia,; C.Martín, "Realización y datación de sondeos en la bahía de Cádiz y las marismas del Barbate", Ministerio de Medio Ambiente y Medio Rural y Marino, 2009, 116 pp.

[12] P.J.Reimer, E.Bard, A.Bayliss, J.W.Beck, P.G.Blackwell, C.Bronk Ramsey,; C.E.Buck, H.Cheng, R.L.Edwards, M.Friedrich, P.M.Grootes, T.P.Guilderson, H.Haflidason, I.Hajdas, C.Hatté, T.J.Heaton, D.L.Hoffmann, A.G.Hogg, K.A.Hughen, K.F.Kaiser, B.Kromer, S.W.Manning, M.Niu, R.W.Reimer, D.A.Richards, E.M.Scott, J.R.Southon, R.A.Staff, C.S.M.Turney, J.van der Plicht, "IntCal13 and Marine13 Radiocarbon Age Calibration Curves, 0-50,000 Years cal BP." Radiocarbon, 2013, vol. 55 (4), pp. 1869-1887.

[13] M.Stuiver, P.Reimer, "Extended 14C data base and revised CALIB 3.0 14C calibration program". Radiocarbon, 2018, vol. 35, pp. 231-237.

[14] A.M.M.Soares, "Datación radiocarbónica de conchas marinas en el golfo de Cádiz: El efecto reservorio marino, su variabilidad durante el Holoceno e inferencias paleoambientales", Cuaternario y Geomorfología, 2015, vol. 29 (1-2), pp. 19-29

[15] J.M.M.Martins, A.M.M.Soares, "Marine Radiocarbon Reservoir Effect in Southern Atlantic Iberian Coast", Radiocarbon, 2013, vol. 55 (2-3), pp. 1123-1134.

[16] M.Vacchi, N.Marriner, C.Morhange, G.Spada, A.Fontana, A.Rovere, "Multiproxy assessment of Holocene relative sea-level changes in the western Mediterranean: Sea-level variability and improvements in the definition of the isostatic signal", Earth-science reviews, 2016, vol. 155, pp. 172-197.

[17] I.Shennan, "Handbook of sea-level research: framing research questions", In: Shennan, I., Long, A. J., Horton, B. P. (Eds.), Handbook of Sea-Level Research, John Wiley & Sons, 2015, Oxford, pp. 3-25.

[18] G.Spada, P.Stocchi, 2007. "SELEN: a Fortran 90 program for solving the "sea-level equation"", Comput. Geosciences, 2007, vol. 33, pp. 538-562.

[19] B.De Boer, L.J.Lourens, R.S.W.Van de Wal, 2014. "Persistent 400,000-year variability of Antarctic ice volume and the carbon cycle is revealed throughout the Plio-Pleistocene" Nat. Commun., 2014, vol.5, 2999 http://dx.doi.org/10.1038/ncomms3999.

[20] RED de MAReógrafos de Puertos del Estado REDMAR, "Resumen de parámetros relacionados con el nivel del mar y la marea que afectan a las condiciones de diseño y explotación portuaria. Puerto de Sevilla-Bonanza", 2019.

[21] V.Amato, P.P.C.Aucelli, A.Cinque, B.D'Argenio,

V.Di Donato, E.Russo Ermolli, P.Petrosino, G.Pappone, C.M.Rosskopf, "Holocene palaeo-geographical evolution of the Sele river coastal plain (Southern Italy): new morpho-sedimentary data from the Paestum area" Il Quaternario, 2011, vol.24, pp.5-7.

[22] G.Pappone, I.Alberico, V.Amato, P.P.C. Aucelli, G.Di Paola, "Recent evolution and the present-day conditions of the Campanian Coastal plains (South Italy): the case history of the Sele River Coastal plain", WIT Trans. Ecol. Environ, 2011, vol.149, pp.15-27.

[23] I.Alberico, V.Amato, P.P.C.Aucelli, G.Di Paola, G.Pappone, C.M.Rosskopf, "Historical and recent changes of the Sele River coastal plain (Southern Italy): natural variations and human pressures. Rendiconti Lincei", 2012. vol.23(1), pp.3-12.

[24] G.Pappone, P.P.C.Aucelli, I.Aberico, V.Amato, F.Antonioli, M.Cesarano, N.Pelosi, Relative sea-level rise and marine erosion and inundation in the Sele river coastal plain (Southern Italy): scenarios for the next century", Rendiconti Lincei, 2012, vol.23(1), pp.121-129.

2020 IMEKO TC-19 International Workshop on
Metrology for the Sea
Naples, Italy, October 5-7, 2020

Risk assessment and management strategies to sea level rise on the Sele River mouth (southern Italy)

Di Paola G.[1], Aucelli P.P.C.[2], Matano F.[3], Rizzo A.[4], Valente E.[5]

[1]*Università degli Studi di Bologna "Alma Mater Studiorum", BiGEA, BOLOGNA, gianluigi.dipaola@unibo.it;*
[2]*Università degli Studi di Napoli "Parthenope", Dipartimento di Scienze e Tecnologie, NAPOLI, pietro.aucelli@uniparthenope.it;*
[3]*Istituto Scienze Marine (ISMAR), CNR, NAPOLI, fabio.matano@cnr.it;*
[4] *REgional Models and geo-Hydrological Impacts (REMHI) Division, Centro Euro-Mediterraneo sui Cambiamenti Climatici, CASERTA, angela.rizzo@cmcc.it;*
[5]*Università degli studi di Napoli "Federico II", DiSTAR, NAPOLI, ettore.valente@unina.it.*

***Abstract* – Rising sea level due to global warming increases the need to analyse coastal risk to conceive management and adaptation strategies aimed at coping with potential marine impacts. In this context, this study presents future scenarios of coastal inundation risk on a strategic area in the Campanian Region (southern Italy): the Sele River mouth. This zone is characterized by low topography and relevant subsidence rates that make it prone to be impacted by sea level rise. Expected local sea level for the year 2065 has been evaluated coupling the global IPCC projection with local subsidence trends. Once the risk has been evaluated as a combination of hazard and exposure, a set of management strategies, which include both Best Management Practises (BMPs) and monitoring actions, have been suggested and applied on the tested area.**

I. INTRODUCTION

Campanian coastal plains are the result of the complex interaction among sedimentary inputs, tectonics and eustatism [1-3]. Among them, the Sele coastal plain (Fig. 1) is characterized by an extended beach-dune ridge system formed by Gromola-S.Cecilia and Arenosola-Aversana paleoridges that dated back to the Last Interglacial period (MIS 5). Based on chrono-altimetric data of the MIS 5 palaeo-sea level, the plain experienced a slight uplift in the last 100–120 ky [4-5]. The back-barrier domains were filled up with marshy and fluvio-palustrine sediments when the sea level rise stopped and aeolian sands finally accumulated on the coastal ridges. Remnants of the back-barrier terrace related to these high-stand phases are preserved in the modern landscape at 11–14 m a.s.l., while the coeval shoreface sediments occur up to 13 m a.s.l. and the dunes up to 23 m a.s.l. [5].

The present coastline (Fig. 1) testifies the evolution of the Holocene barrier-lagoon system [6]. A composite sandy ridge forms a dune system with a mean height of about 3 m a.s.l. currently interrupted by rivers and artificial drainage channels. The large back-ridge depression, rising around 0.50 - 1.5 m a.s.l., hosted palustrine and marshy environments [7], that have been artificially drained and are, today, prone to marine inundation [8].

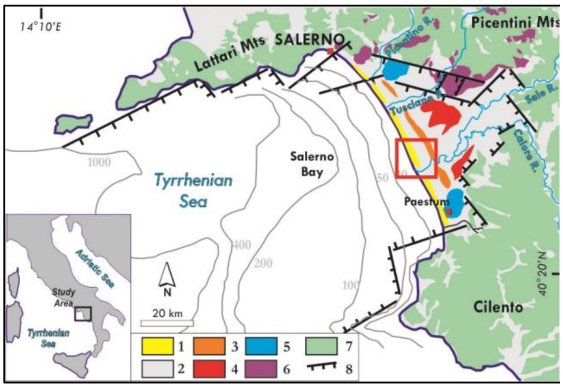

Fig. 1. Schematic geological map of the Sele Plain area (after [5]); the red square indicates the location of the study area, reported in figs. 3 and 4.
Legend: 1) Laura-Sterpina sandy barriers (Holocene); 2) fluvial-marshy and volcano-clastic deposits (Late Pleistocene - Holocene); 3) Gromola-S. Cecilia-Arenosola-Aversana sandy barriers (Late Pleistocene); 4) marine, continental and transitional deposits (Middle-Late Pleistocene);5) travertine deposits (Middle Pleistocene - Holocene); 6) Eboli Conglomerates (Early-Middle Pleistocene); 7) Pre-Quaternary bedrock; 8) Main faults.

The infill of the plain is characterised by several marine to continental lithofacies among which dunal and coastal sands, back-ridge (lagoonal and palustrine) silty clays, palaeosols, and thick peaty layers are the more diffused. Their abundance may promote local subsidence, mainly in sectors where the silty clays and peaty layers are thicker, such as in the back-barrier sectors of the plain [5] (Fig. 1). In this context, the risk assessment procedure applied for the area of the Sele River mouth allows obtaining a zonation that accounts for the dynamic component associated with the local VGD and future SLR projections. Therefore, it enables decision-makers to adapt Best Management Practices (BMPs) to local topographical characteristics and to identify the most suitable adaptation measures suitable to cope with future sea levels with a higher resolution spatial scale.

II. METHODS

In order to assess the future scenario of permanent coastal inundation risk and to identify possible management strategies, a four steps methodology is proposed:

Step 1 - Proneness analysis (H): the low topographic areas are classified in four hazard classes of inundation due to local sea level rise, as proposed in [8-10]. To this aim, the expected relative sea level for the year 2065 is evaluated as a combination of sea level projection proposed in [11] under the RCP8.5 scenario and local vertical displacement rates estimated by MT-InSAR data analysed following the methodological approach proposed in [12].

Step 2 - Exposure analysis (Ex): the anthropic and natural elements located in the areas prone to be impacted by sea level rise as well as the social-vulnerability level are evaluated, and four classes of exposure level are proposed [10].

Step 3 - Risk assessment (R): once the hazard and the exposure classes are identified (Step 1 and Step 2), the risk to sea level rise is calculated by spatially combining these layers. The resulting risk is classified in four classes (ranging from R1- low risk to R4 – very high risk), using the matrix in Table 1, as proposed in [9-10].

Table 1. Coastal risk matrix. The risk is evaluated by combining the coastal Hazard level (H) with the Exposure level (Ex).

Risk		**Exposure**			
		E_x4	**E_x3**	**E_x2**	**E_x1**
Hazard	**H4**	**R4**	**R4**	**R3**	**R2**
	H3	**R4**	**R3**	**R2**	**R1**
	H2	**R3**	**R2**	**R2**	**R1**
	H1	**R2**	**R1**	**R1**	**R1**

Step 4 – Application of coastal risk management measures: a set of suitable planning actions and management strategies are proposed for the management of the coastal areas potentially at risk. According to the "Plan, Do, Check, and Act" (PDCA) Cycle [13-14], different conservation, defence, and recovery actions are proposed:

- PLAN: assessing hazard and risk scenarios;
- DO: defining Best Management Practices (BMPs);
- CHECK: scheduling monitoring actions for the validation of the coastal impact scenarios;
- ACT: planning effective adaptation strategies.

First, BMPs to be undertaken for each specific risk class (R1, R2, R3, R4) are suggested. Then, several checking actions are proposed for monitoring the present trends and validating the future projections provided by models. Finally, once the risk is validated by observational data, several actions are proposed for ensuring the conservation of the natural ecosystems, their related services and the maintenance of human activities by introducing, in addition to BMPs, structural and non-structural adaptation strategies.

III. RESULTS

The results of the quantitative assessment of the subsidence process referred to the studied coastal plain is showed in a 50-m spaced grid maps (Fig. 2A), displaying the average rates of Vertical Ground Deformation (expressed in mm/year) referred to the period 1992-2010. This map shows that the analysed coastal sector on the Sele River plain is characterized by complex subsidence patterns. In detail, the Sele River mouth area is characterized by moderate values of subsidence (-2.5 to -7.5 mm/y) with a hot spot developing 5 km inland. In the northern part of the study area, a continuous coastal strip is characterized by subsidence values ranging between -2.5 to -10 mm/y.

To identify the areas located below the projected future sea levels (evaluated as the sum of eustatic sea level and local vertical ground movements), the GIS topographic model has been processed following the "bathtub approach". The extent of each hazard class has been evaluated for all the investigated coastal plains considering the RCP8.5 scenario for the years 2065 (Table 2). Considering the 2065 projection (Fig. 2B), the extent of H4 class is more than 10%, with an extension of 3.5 km^2, while H3 and H2 classes extend respectively 11% and 15%. Accounting for H1 class, its surface occupies 63% on the investigated area. Regarding the exposure evaluation (Fig. 2C), it has accounted for the current spatial distribution of the vulnerable assets and social vulnerability. Results are shown in Table 1 both in km^2 and as a percentage of the investigated area for each plain. Results show that the more diffused exposure class is the EXP3, with a value of 54% (17 km^2). In order to assess the spatial distribution of the different risk levels along the investigated coastal area, the hazard (Fig. 2B) and the exposure (FIG. 2C) classes have been combined (cf. Step 3 - Table 1). Risk has been classified in four classes and the results are shown as coastal risk map (Fig. 2D). Furthermore, the extent of each class risk is indicated in Table 2, where the results are shown in km^2 and as percentage values. R4 class occupies a considerable area (2.5 km^2) along the study area, while R3 class occupies more than 12% of the area analysed.

Table 2. Coastal inundation scenario, coastal exposure assessment and coastal risk scenario for the Sele River mouth.

H1	**H2**	**H3**	**H4**
(km^2 / %)	**(km^2 / %)**	**(km^2 / %)**	**(km^2 / %)**
19.5 / 62.8	4.6 / 14.7	3.6 / 11.3	3.5 / 11.2
EXP1	**EXP2**	**EXP3**	**EXP4**
(km^2 / %)	**(km^2 / %)**	**(km^2 / %)**	**(km^2 / %)**
0.4 / 1.4	8.9 / 28.5	16.9 / 54.1	5.0 / 16.0
R1	**R2**	**R3**	**R4**
(km^2 / %)	**(km^2 / %)**	**(km^2 / %)**	**(km^2 / %)**
15.8 / 50.3	9.1 / 29.3	3.8 / 12.2	2.5 / 8.2

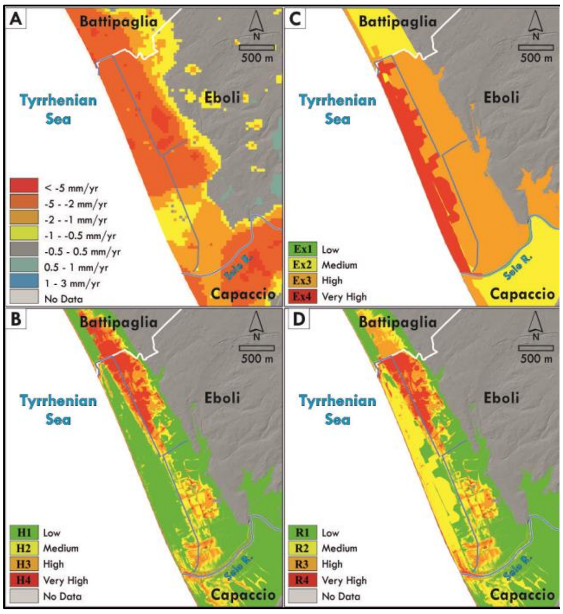

Fig. 2. Subsidence map (A); hazard map (B), exposure map (C) and risk map (D) evaluated for the year 2065 on the Sele River mouth zone

To provide a practical example on how to use the proposed approach for the risk management , a sector of the Sele coastal plain has been considered as a testing site for the identification of the areas suitable for each of the selected actions (Fig. 3). The area is characterized by the presence of a wide range of land use categories, including touristic beaches and wide agricultural zones. Furthermore, the results of the risk analysis have shown that the selected area is characterized by a different distribution of the risk classes (Fig. 2D).

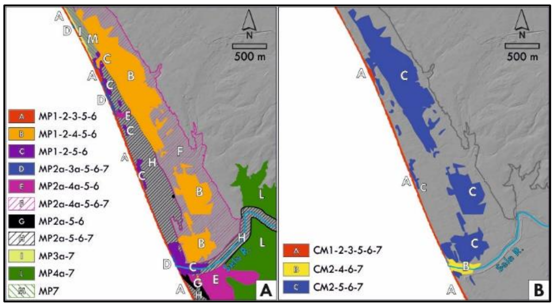

Fig. 3. Application of the actions proposed for the coastal risk management on a tested area of the Sele plain.

Specifically, BMPs and monitoring actions have been classified accounting for the different land use categories, and then localized in the tested area in order to zone the territory according to the practices proposed. The proposed classification is shown in the maps in Fig. 3 (A, B).

Best Management Practices:

- MP1: Introducing land use restrictions;
- MP2: Limiting urban expansion;
- MP2a: Introducing strategies of land use and urban expansion;
- MP3: Avoiding coastal erosion due to human perturbations;
- MP3a: Limiting coastal erosion due to human actions;
- MP4: Avoiding groundwater over-pumping;
- MP4a: Limiting groundwater over-pumping;
- MP5: Promoting specific strategies of civil protection;
- MP6: Enhancing the population's awareness;
- MP7: The management of the territory is regulated by the present-day local management plans of local Basin Authorities.

Monitoring

- CM1: Tide gauge and buoy monitoring system;
- CM2: Weather monitoring system;
- CM3: Beach monitoring system;
- CM4: Hydrological monitoring system;
- CM5: Groundwater and saline wedge monitoring system;
- CM6: Topographic DGPS and UAV surveys;
- CM7: Remote sensing monitoring system.

IV. CONCLUSIONS

The performed analyses allowed evaluating and mapping the potential coastal inundation risk along the Sele coastal plain for the year 2065. The results suggest, in accordance with other studies [8, 15-17], that in the next few decades natural areas, beaches, human infrastructures, and wide portions of agricultural areas located in the study area could be potentially affected by marine impacts (shoreline regression and inundation), with several zones with high hazard level.

In line with the most recent international indications, the here proposed hazard and risk maps represent a valuable tool for increasing effective territorial management aimed at the reduction of future climate-induced risks. Accounting for the proposed management practices, civil protection actions, mainly aimed at improving the local response and at enhancing the population's awareness, should be implemented in all the zones potentially prone to be impacted by future sea levels. Furthermore, specific operative actions, such as limiting the groundwater pumping and avoiding anthropic beach erosion, should be tailored according to the specific land use context.

In conclusion, it is possible to state that the results of this study can effectively address the national and international request of improving the knowledge and raising the awareness of policymakers and local administrators about the potential impacts of climate change to promote and facilitate the definition of effective coastal management regulations and the implementation of suitable adaptation strategies.

REFERENCES

[1] E. Patacca, R. Sartori & P. Scandone "Tyrrhenian basin and Apenninic arcs: kinematic relations since Late Tortonian times". In Memorie Società Geologica Italiana, 45, 425-451 (1990).

[2] M. Sacchi, F. Molisso, A. Pacifico, M. Vigliotti, C. Sabbarese & D. Ruberti. "Late-Holocene to recent evolution of Lake Patria, South Italy: An example of a coastal lagoon within a Mediterranean delta system". In Global and Planetary Change, 117, 9–27 (2014).

[3] E. Valente, A. Ascione, N. Santangelo & A. Santo "The inner sector of the Sarno Plain (southern Apennines, Italy): late Quaternary geomorphological evolution and evidence of post-Campania Ignimbrite (40 ka) fault activity". In Alpine and Mediterranean Quaternary, 32, 185–197 (2019).

[4] P.P.C. Aucelli, V. Amato, F. Budillon, M.R. Senatore, S. Amodio, C. D'Amico, S. Da Prato, L. Ferraro, G. Pappone & E. Russo Ermolli "Evolution of the Sele River coastal plain (southern Italy) during the Late Quaternary by inland and offshore stratigraphical analyses". In Rend. Fis. Acc. Lincei, 23, 81–102 (2012).

[5] V. Amato, P.P.C. Aucelli, G. Corrado, G. Di Paola, F. Matano, G. Pappone & M. Schiattarella "Comparing geological and Persistent Scatterer Interferometry data of the Sele River coastal plain, southern Italy: Implications for recent subsidence trends". In Geomorphology, 351, 106953 (2020).

[6] V. Amato, P.P.C Aucelli, B. D'Argenio, S. Da Prato, L. Ferraro, G. Pappone, P. Petrosino, P. Romano, C.M. Rosskopf & E. Russo Ermolli "Holocene environmental evolution of the costal sector in front of the Poseidonia-Paestum archaeological area (Sele plain, Southern Italy)". In Rend Fis Acc Lincei, 23, 45-59 (2012).

[7] I. Alberico I., V. Amato, P.P.C. Aucelli P.P.C., G. Di Paola, G. Pappone & C.M. Rosskopf "Historical and recent changes of the Sele River coastal plain (Southern Italy): natural variations and human pressures". In Rend Fis Acc Lincei, 23, 3–12 (2012).

[8] G. Di Paola, I. Alberico, P.P.C. Aucelli, F. Matano, A. Rizzo & G. Vilardo "Coastal subsidence detected by Synthetic Aperture Radar interferometry and its effects coupled with future sea-level rise: the case of the Sele Plain (Southern Italy)". In Journal of Flood Risk Management, 11, 191-206 (2018).

[9] P.P.C. Aucelli, G. Di Paola, P. Incontri, A. Rizzo, G. Vilardo, G. Benassai, B. Buonocore & G. Pappone "Coastal inundation risk assessment due to subsidence and sea level rise in a Mediterranean alluvial plain (Volturno coastal plain-southern Italy)". Estuarine, Coastal and Shelf Science, 198, 597–609 (2017).

[10] P.P.C. Aucelli, G. Di Paola, A. Rizzo & C.M. Rosskopf "Present day and future scenarios of coastal erosion and flooding processes along the Italian Adriatic coast: The case of Molise region". In Environmental Earth Sciences, 77, 371 (2018).

[11] IPCC - Intergovernmental Panel on Climate Change. (2014). https://archive.ipcc.ch/report/ar5/syr/

[12] F. Matano "Analysis and Classification of Natural and Human-Induced Ground Deformations at Regional Scale (Campania, Italy) Detected by Satellite Synthetic-Aperture Radar Interferometry Archive Datasets". In Remote Sens., 11, 2822 (2019).

[13] W.E. Deming "Out of the Crisis" Cambridge University Press, Cambridge (1986).

[14] K.N. Dervitsiotis "On Becoming Adaptive: The New Imperative for Survival and Successin the 21st Century. Total Quality Management & Business Excellence", 18, 21–38 (2007).

[15] G. Benassai G., Di Paola G. & Aucelli P. "Coastal risk assessment of a micro-tidal littoral plain in response to sea level rise". In Ocean Coast. Manage., 104, 22–35 (2015).

[16] G. Di Paola, Aucelli P.P.C., Benassai G. & Rodríguez G. "Coastal vulnerability to wave storms of Sele littoral plain (southern Italy)". In Nat. Hazards, 71, 1795–1819 (2014).

[17] G. Pappone, I. Alberico, V. Amato, P. Aucelli & G. Di Paola. "Recent evolution and the present-day conditions of the Campanian Coastal plains (South Italy): the case history of the Sele River coastal plain." In WIT Trans. Ecol. Environ., 149, 15–27 (2011).

2020 IMEKO TC-19 International Workshop on
Metrology for the Sea
Naples, Italy, October 5-7, 2020

Morphological responses to relative sea-level changes along Procida coast (Gulf of Naples, Italy) during the last 6,5 Ky

P.P.C. Aucelli[1], E. Gagliardi[2], G. Mattei[1], F. Napolitano[2], G. Pappone[1], M. Pennetta[2], M.F. Tursi[1]*

[1] *Università degli Studi di Napoli Parthenope – Dipartimento di Scienze e Tecnologie - Centro Direzionale, Isola C4 - 80143 NAPOLI, francesca.tursi@uniparthenope.it*

[2] *Università degli studi di Napoli Federico II- DiSTAR-Complesso Universitario di Monte Sant'Angelo,Edificio 10 -Via Vicinale Cupa Cintia 21- 80126 NAPOLI, pennetta@unina.it*

Abstract –
In this research, the morpho-evolutive trend of sea cliffs placed in the volcanic island of Procida has been investigated. The entire perimeter of the island is bordered by cliffs in some cases connected to narrow shore platforms sloping slightly towards the sea. The presence of different submerged orders of paleo-shore platforms suggests different phases of sea-level stand and related coastal response. Mapping these platforms, together with the interpretation of archaeological and geomorphological markers allowed defining the ancient shoreline of Procida island.
The relative sea-levels deduced from these indicators were compared with the eustatic sea-level curve proposed by Lambeck et. Alii, demonstrating that this area was affected by an overall subsiding trend since the Mid-Holocene, which probably occurred intermittently or with variable intensity over time. By reconstructing the position of the ancient shorelines related to the three orders of platforms, the retreating rates of the cliffs in each area were calculated.

I. INTRODUCTION

Procida Island belongs to the insular part of Campi Flegrei (CF) volcanic area and owes its formation to several explosive eruptions related to the CF volcanic activity started more than 60 ky BP [1]. Campi Flegrei volcanic area, still active today, represents one of the two main hazardous volcanic areas in the Gulf of Naples (Southern Italy) [2-16].
In detail, the island is characterised by steep cliffed coasts and articulated in a succession of headlands and small embayments [17]. The cliffs are generally cut on pyroclastic deposits showing a height of 10/40m and an inclination of over 40°. Small and narrow pocket beaches represent the main tourist attraction of the island such as Ciraccio and Chiaia beaches.
This research aims to reconstruct the coastal response to relative sea-level rise “pressure” since the mid-Holocene, by analysing the emerged and submerged features of the coast [18-21]. Geomorphological and geo-archaeological interpretations obtained from the GIS elaboration of a multi-scale dataset led to evaluate the modification of the coastal landscape in the last 6500 years.

II. METHODS

The coastal sector of the study area has been investigated by using a multi-techniques approach using direct and indirect methods. Several on-site investigations have been integrated with the geomorphological study of aerial photos.

A. Geomorphological and GIS analysis

The 3D elaboration of the topo-bathymetric data followed a specific procedure.
The first step has been the calculation of an onshore-offshore DTM by interpolating the LIDAR (from the Ministry of Environment, 0 – 200 m MSL) and bathymetric data (from the CARG project, 0 – 20 m MSL), with a Topo to Raster interpolator (1 × 1 m grid). The second step has been the slope analysis of the above-mentioned DTM in order to classify the submerged area in sub-horizontal and steep slope sectors.
By integrating the above-mentioned GIS analysis with data deriving from direct surveys, several sub-horizontal submerged surfaces (0-5% of slope) have been detected and interpreted as ancient shore platforms. Consequently, the high-sloping sectors (slope > 20%) adjacent to the sub-horizontal surfaces have been interpreted as related paleo-cliffs.
Finally, the mapped paleo-shore platforms have been reclassified depending on the depth in three orders, and

subsequently dated by overlaying the archaeological evidence from bibliographic sources and our geomorphological interpretations.
The last step has been the morphometric analysis applied to these landforms to evaluate the retreating trends and the vertical ground movements affecting Procida costal sector since the Holocene highstand.

B. Shore Platforms as a sea-level index point

The paleo-shore platforms can be used as indicators of ancient sea levels if their morphology can be reconstructed [22]. While some platforms are incised above sea level, others are incised in intertidal or slightly subtidal areas [23]. According to [24], the outer margin (i.e. the termination point of the platform towards the sea) is the point where active erosion of the bedrock ends. However, the most relevant feature useful for sea-level interpretations certainly is the inner margin, considering that it is located at the same level of the mean higher high water (MHHW- average of the higher high water height of each tidal day observed over a Tidal Datum Epoch) [23]. The RSL associated with this indicator is equal to:

$$SL = E - MHHW \qquad (1)$$

Where E is the present elevation with respect of the mean sea level (MSL) of the platform at issue.

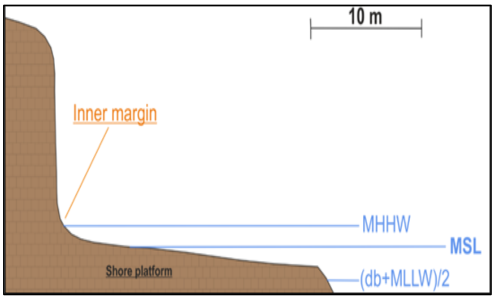

Fig. 1. Shore platforms as sea level index point (modified from Rovere et al. 2016).

III. RESULTS

The sea cliffs bordering the coasts of Procida island have been precisely mapped and classified in two types: sea cliffs with narrow shore platforms sloping slightly towards the sea (type A: sloping shore platform - [25] or near-vertical slope that rise abruptly from the deepwater (plunging cliff: [25]). The presence of different submerged orders of paleo-shore platforms suggests different phases of sea-level stand and related coastal response.
The deepest platforms are positioned at -25/-23 m msl, cutting the volcanic formation of Tufo di Solchiaro [26] emplaced during the last most important eruptive phase of Procida (22 ky BP). Therefore, these platforms have been modelled after that date. By analysing the eustatic sea-level curve [27] in the considered period, the most favourable morphogenetic conditions for their formation started about 6.5 ky BP, when the decrease of the rate of sea-level rise was compatible with platforms formation and related sea cliff retreat. Anyway, the age of these platforms can be comprised between about 6.5 ky and the age of the second order of platforms. The RSL here calculated has been positioned at -23m msl.

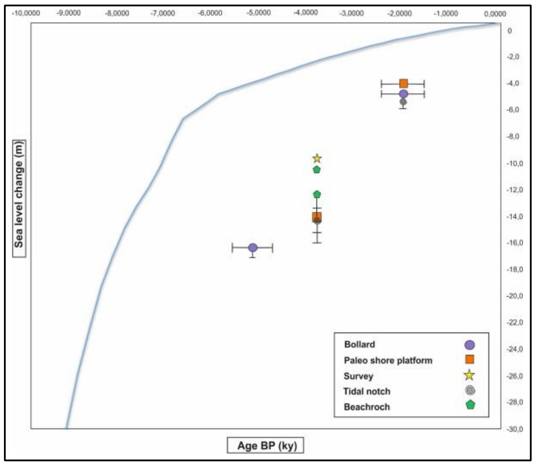

Fig. 2. Eustatic curve where the archaeological and geomorphological indicators found in the perimeter area of Procida are placed. They are represented with the relative uncertainty bars (modified by Lambeck 2011).

The second-order (-20/-11 m msl) has been dated at 3.5 ky BP through coring data carried out in the Genito Gulf, where abundant fragments of archaeological finds have been identified and dated by [28] at 3.5 ky BP. The RSL calculated in this time-span has been positioned at -11m msl.
The third-order (-10/-4 msl) has been dated through ring bollards, detected at a depth of -4.5 m msl and dated in a timespan between 2000 and 1000 years ago [28-29]. The RSL calculated has been positioned at -4.5 m msl.
The former relative sea-levels deduced from these indicators were compared with the eustatic sea-level curve proposed by Lambeck [30] (*Fig. 2.*) demonstrating that this area has been affected by an overall subsiding trend since the Mid-Holocene, which probably occurred intermittently or with variable intensity over the time. By subtracting the RSLs data to the eustatic values, the vertical displacements for each coastal sector have been evaluated.
By reconstructing the position of the ancient shorelines related to the inner margin of the three orders of platforms, the cliff retreating rates in each area has been evaluated.
In particular, in the Ciraccio-Cirracciello sector, a

retreating trend of 0,14 m/y in the last 3.5 ky BP has been calculated, together with a rate of subsidence of 0.002 m/y. In the same sector, the RSL at -4.5 dated at 2.0 ky BP allowed calculating a subsidence rate of about 0.001 m/y. In the Chiaia coastal sector, a retreating trend of 0.12 m/y in the last 3.5 ky BP has been evaluated by measuring the extension of the second-order of shore platform. Instead, by analysing the historical platform dated at 2.0 ky BP a retreating trend of about 0.16 m/y and a related subsiding trend of about 0.001 m/y were respectively measured.

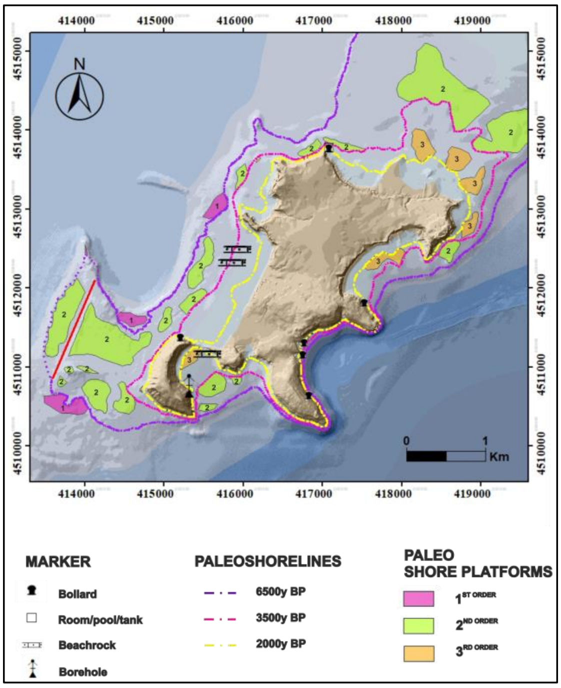

Fig. 3. Map of the three orders of submerged paleo-shore platforms here studied

IV. CONCLUSIONS

In this research, the morpho-evolutive trends of Procida coastal area have been evaluated since the mid-Holocene. For this purpose, three orders of paleo-shore platforms have been used as a witness of ancient sea-level stands, together with other geomorphological and archaeological sea-level markers.

The geomorphological interpretation of these ancient landforms provided the reconstruction of as many ancient shorelines, respectively dated to about 6.5 ky BP, 3.5 ky BP and a third-order positioned in a time range between 2.0 ky BP and 1.0 ky BP. Consequently, the retreating rates along Cirraccio-Cirracciello and Chiaia sectors have been evaluated over the last 6500 years.

However, the precise mapping of these ancient platforms at various depths allowed establishing that an overall subsidence has certainly contributed to the Holocene coastal polyphasic evolution of the island, interrupted by three main phases of relative sea-level standing (or strong decreasing in the rate of sea-level rise) during the last 7 ky.

A volcano-tectonic origin, related to the activity of Campi Flegrei volcanic area, can be assumed as the main cause of this subsidence, even if the analysis of remote sensing data demonstrates that the island is nowadays stable.

REFERENCES

[1] P.Aucelli, L.Brancaccio, A.Cinque "Vesuvius and Campi Flegrei volcanoes. Activity, landforms and impact on settlements", In: Soldati M., Marchetti M. (Eds.), Landscapes and Landforms of Italy, 2017, Springer International Publishing, Cham, Switzerland, pp.389-398.

[2] G.Mattei, S.Troisi., P.P.Aucelli, G.Pappone, F. Peluso, & M.Stefanile "Multiscale reconstruction of natural and archaeological underwater landscape by optical and acoustic sensors", In 2018 IEEE International Workshop on Metrology for the Sea; Learning to Measure Sea Health Parameters (MetroSea), pp. 46-49. IEEE.

[3] G.Mattei, S.Troisi, P.Aucelli, G.Pappone, F.Peluso, M.Stefanile "Sensing the Submerged Landscape of Nisida Roman Harbour in the Gulf of Naples from Integrated Measurements on a USV", Water, 2018, 10(11), 1686.

[4] V.Amato, P.P.Aucelli, G.Mattei, M.Pennetta, A.Rizzo, C.M.Rosskopf, & M.Schiattarella "A geodatabase of Late Pleistocene-Holocene palaeo sea-level markers in the Gulf of Naples", Alpine Mediterr. Quat, 2018, vol.31, pp.5-9.

[5] P.P.Aucelli, G.Mattei, C.Caporizzo, A.Cinque, S.Troisi, F.Peluso, & G.Pappone "Ancient Coastal Changes Due to Ground Movements and Human Interventions in the Roman Portus Julius (Pozzuoli Gulf, Italy): Results from Photogrammetric and Direct Surveys", Water, 2020, vol. 12(3), pp. 658.

[6] P.Aucelli, A.Cinque, G.Mattei, G.Pappone, "Historical sea level changes and effects on the coasts of Sorrento Peninsula (Gulf of Naples): New constrains from recent geoarchaeological investigations" in Palaeogeography, Palaeoclimatology, Palaeoe-cology, 2016, vol.463, pp.112-125.

[7] P.Aucelli, A.Cinque, F.Giordano, G.Mattei "A geoarchaeological survey of the marine extension of the Roman archaeological site Villa del Pezzolo, Vico Equense, on the Sorrento Peninsula, Italy", Geoarchaeology, 2016, vol. 31 (3), pp. 244-252.

[8] P.P.C.Aucelli, A. Cinque, G.Mattei, G.Pappone "Late Holocene landscape evolution of the gulf of Naples (Italy) inferred from geoarchaeological data", In Journal of Maps, 2017, vol. 13 (2), pp. 300-310.

[9] P.Aucelli, A.Cinque, G.Mattei, G.Pappone, M.Stefanile "Coastal land-scape evolution of Naples (Southern Italy) since the Roman period from archaeological and geomorphological data at Palazzo degli Spiriti site", In Quaternary International, 2018, pp. 23-38.

[10] P.P.Aucelli, A.Cinque, G.Mattei, G.Pappone & M.Stefanile "First results on the coastal changes related to local sea level variations along the Puteoli sector (Campi Flegrei, Italy) during the historical times", In Alpine and Mediterranean Quaternary, 2018, vol. 31, pp. 13-16.

[11] P.Aucelli, A.Cinque, G.Mattei, G.Pappone & A.Rizzo "Studying relative sea level change and correlative adaptation of coastal structures on submerged Roman time ruins nearby Naples (southern Italy)", In Quaternary international, 2019, vol. 501, pp. 328-348.

[12] P.P.Aucelli, C.Caporizzo, A.Cinque, G.Mattei, G.Pappone & M.Stefanile "New insight on the 1st century BC paleo-sea level and related vertical ground movements along the Baia - Miseno coastal sector (Campi Flegrei, southern Italy)", In IMEKO TC4 International Conference on Metrology for Archaeology and Cultural Heritage, MetroArchaeo 2019, pp. 474-477 (2019).

[13] G.Mattei , S.Troisi, P.Aucelli, G.Pappone, F.Peluso, M.Stefanile "Sensing the Submerged Landscape of Nisida Roman Harbour in the Gulf of Naples from Integrated Measurements on a USV", In Water, 2018, vol. 10(11), 1686.

[14] G.Mattei, A.Rizzo, G.Anfuso, P.P.C.Aucelli & F.J.Gracia "Enhancing the protection of archaeological sites as an integrated coastal management strategy: the case of the Posillipo Hill (Naples, Italy)", In Rendiconti Lincei, 2020, Scienze Fisiche e Naturali, pp. 1-14.

[15] G.Mattei, A.Rizzo, G.Anfuso, P.P.C.Aucelli & F.J.Gracia "A tool for evaluating the archaeological heritage vulnerability to coastal processes: The case study of Naples Gulf (southern Italy)", In Ocean & Coastal Management, 2019, vol. 179, 104876.

[16] G.Pappone, P.P.Aucelli, G.Mattei, F.Peluso, M.Stefanile & A.Carola "A Detailed Reconstruction of the Roman Landscape and the Submerged Archaeological Structure at "Castel dell'Ovo islet"(Naples, Southern Italy)", In Geosciences, 2019, vol.9(4), pp. 170.

[17] M.Pennetta, M.Assante di Panzillo, G.Mattei, A.Rizzo, P.Aucelli " Historical morphoevolution of the high rocky coast in the southern west sector of Procida island", In IGCP Project 639 "Sea-Level Change from Minutes to Millennia", Third Annual Meeting, Crossing Southern Italy. Taranto (Puglia), 16th - 23rd September 2018, 3rd Meeting.

[18] V.Amato, P.P.C. Aucelli, A.Cinque, B.D'Argenio, V. Di Donato, E.Russo Ermolli & C.M.Rosskopf, "Holocene palaeo-geographical evolution of the Sele river coastal plain (Southern Italy): new morpho-sedimentary data from the Paestum area." *Il Quaternario*, 2011, vol. 24, pp. 5-7**.**

[19] G.Pappone, I.Alberico, V.Amato, P.P.C.Aucelli,. & G.Di Paola, "Recent evolution and the present-day conditions of the Campanian Coastal plains (South Italy): the case history of the Sele River Coastal plain". WIT Trans. Ecol. Environ, 2011, vol. 149, pp. 15-27.

[20] G.Pappone, P.P.C.Aucelli, I.Aberico, V.Amato, F.Antonioli, M.Cesarano & N.Pelosi "Relative sea-level rise and marine erosion and inundation in the Sele river coastal plain (Southern Italy): scenarios for the next century", In Rendiconti Lincei, 2012, vol. 23(1), pp. 121-129.

[21] I.Alberico, V.Amato, P.P.C. Aucelli, G.Di Paola, G.Pappone & C.M.Rosskopf "Historical and recent changes of the Sele River coastal plain (Southern Italy): natural variations and human pressures", In Rendiconti Lincei, 2012, vol. 23(1), pp. 3-12.

[22] P.A.Pirazzoli "Sea-Level Changes: The Last 20 000 years", Wiley, 1996, Chichester.

[23] A.Rovere, M.E.Raymo, M.Vacchi, T.Lorscheid, P.Stocchi, L.Gómez-Pujol, D.L.Harris, E.Casella, M.J. O'Leary, P.J.Heartyh "The analysis of Last Interglacial (MIS 5e) relative sea-level indicators: Reconstructing sea-level in a warmer world", In Earth-Science Reviews, 2016, vol. 159, pp. 404–427.

[24] D.M. Kennedy "Where is the seaward edge? A review and definition of shore platform morphology", In Earth Sci. Rev. vol. 147, pp. 99–108. http://dx.doi.org/10.1016/j.earscirev. 2015.05.007.

[25] T.Sunamura "Geomorphology of Rocky Coasts" In Wiley, 1992, Chichester.

[26] M.L.Putignano & M.Schiattarella "Geomorfologia strutturale e domini di frattura dei fondali marini pericostieri dell'Isola di Procida (Campi flegrei insulari, Italia meridionale)", In Il Quaternario, Italian Journal of Quaternary Sciences, 2010, vol. 23 (2 Bis), pp. 229-242.

[27] J.Benjamin, A.Rovere, A.Fontana, S.Furlani, M.Vacchi, R.H.Inglish, E.Galili, F.Antonioli, D.Sivan, S.Miko, N.Mourtzas, I.Felja, M.Meredith-Williams, B.Goodman-Tchernov, E.Kolaiti, M.Anzidei, R.Gehrels "Late Quaternary sea-level changes and early human societies in the central and eastern Mediterranean Basin: An interdisciplinary review",In Quaternary International, 2017, pp. 1-29.

[28] M.L.Putignano, P. E.Orrù, M.Schiattarella "Holocene coastline evolution of Procida Island, Bay of Naples, Italy". In Quaternary International, 2014, vol. 332, pp. 115-125.

[29] M.L.Putignano, A.Cinque, A.Lozej, C.Mocchegiani Carpano "Late Holocene ground movements in the

Phlegrean Volcanic District (Southern Italy): new geoarchaeological evidence from the islands of Vivara and Procida", In Mèditerranèe, 2009, vol. 112, pp. 43-50.

[30] K.Lambeck, F.Antonioli, M.Anzidei, L.Ferranti, G.Leoni, G.Scicchitano, S.Silenzi "Sea level change along the Italian coast during the Holocene and projections for the future", In Quaternary International vol. 232, 2011, pp. 250-257.

2020 IMEKO TC-19 International Workshop on
Metrology for the Sea
Naples, Italy, October 5-7, 2020

Assessment of shoreline detection using UAV

Silvio Del Pizzo[1], Antonio Angrisano[2], Salvatore Gaglione[1], Salvatore Troisi[1]

[1] *University of Naples Parthenope, Centro Direzionale Isola C4 80133 Naples Italy, (silvio.delpizzo;salvatore.gaglione;salvatore.troisi)@uniparthenope.it*
[2] *University of Benevento "G. Fortunato", Benevento, Italy, a.angrisano@unifortunato.eu*

***Abstract* – The shoreline is an important feature of the costal morphology. Several methodologies are used to detect such line. In this paper a photogrammetric approach was employed to achieve both an accurate shoreline detection and a DTM (Digital Terrain Model) of the coast using Structure from Motion (SfM) algorithms. The goal of this method is to extract the shoreline from an accurate three-dimensional model of the coast. The proposed approach was performed using an Unmanned Aerial Vehicle (UAV) equipped with a digital camera. In order to avoid regrettable deformations on the 3D model several Ground Control Points were located on the scene, furthermore a precision assessment was performed using check points. The obtained result was compared with a classic RTK-GNSS survey of the shoreline performed by a skilled operator.**

I. INTRODUCTION

The construction of harbours, water breakers and, in general, all port and marine infrastructures implicates several problems and challenges for the civil marine engineers applied to improve the logistic and the transportation with minimal impact on the surrounding lands, seabed and the marine environment. To predict the impact on the shore, civil marine engineers inspect their projects using several mathematical/hydraulic models; such studies are considered an essential preliminary step before to start to build the structure [1].

When the building is completed, further inspections are conducted to check the structure status and shore alteration. In this framework, the shoreline position is very useful to monitor the costal evolution [2]. Indeed, the inspection of the shoreline retreat provides an important index of the sediment transport through the flow of the water and then the impact of the structure on the shore [3,4]. Moreover, in last years the climate change has had devasting effects on the coastal areas, that had deeply changed the morphological features of the coast [5].

Basically, the monitoring of the shoreline plays a fundamental role for the environment protection.

Several methodologies and strategies are used to detect the shoreline [6], and all of these begin from the definition of it, that can be easily declared as the line that marks the transition between the sea and land [7,8]. Due to the sea waves and the tide effect such line is in constant movement. A rigorous definition of shoreline is therefore necessary, in order to perform repeatable and reliable measurements. In this work, the shoreline is defined as the line of intersection between the ground and the mean sea level surface.

Generally, two different approaches have been employed to survey the shoreline [9]:

- Direct survey way, when the surveyor carries out the measurements along the visible shoreline. Such approach is considered as classical way, and is performed using the total station or GNSS receiver (generally in RTK - Real Time Kinematic mode).
- Remote survey way, when the shoreline is determined using a remote sensing approach, such as LiDAR, satellite and aerial images.

The direct approach allows to limit the survey on a narrow strip of the coast (restricted to the interested area) and to break down the time processing. On the other hand, in some cases the shore is not easy to reach, furthermore the physical shoreline is different from the theoretical one. Indeed, in order to obtain reliable results, the surveyor divides the operations in two steps: the former detects the dry boundary of the shore, where the heights from the mean sea level are surely positive; the second one detects the wet line of the shore before that the terrain slope rapidly changes. Such approach allows to determine the shoreline as spatial linear interpolation between the two surveyed lines [7].

The remote survey approach allows to minimize the on-field operations and to reach no-go areas. On the other hand, the post-processing time cannot be neglected. In this case, several approaches have been developed, depending on the platform employed to derive the shoreline. For instance: the process for satellite images or aerial orthophoto may be based on the use of segmentation and classification (supervised or unsupervised) on digital images to detect the visual separation of coastal features [10,11]. On the other hand, the LiDAR data allows to obtain a DTM of the coast and to extract the shoreline as contour line [12]; furthermore if the LiDAR is equipped with a bathymetric laser the DTM obtained can cover the shallow water as well [13]. Finally, the photogrammetric

process is an hybrid solution between the LiDAR and Image-Processing approach since it allows to achieve both a visual distinction water-coast (i.e. using orthophoto) and estimate a DTM of the shore [14,15].
In this work a photogrammetric workflow was developed involving a UAV (Unmanned Aerial Vehicle) equipped with a low-cost digital camera used to acquire nadiral images of a little beach located on Sorrento coast.
Actually, this platform is very flexible, low cost and it can be adapted to different surveys scenario. The flight planning, handling and control are totally automatic, assuring a completed coverage of the survey area and minimizing the time consuming.

II. METHODOLOGY

Photogrammetry is the science and technology of obtaining metric information about physical environment from images, with a focus on several applications such as mapping, surveying and high precise metrology. The aim of photogrammetry is to provide procedures for these engineering tasks with emphasis on a specified measurements accuracy and reliability [16].
In this case study the developed procedure is based on automated photogrammetric techniques known as Structure from Motion algorithms, allowing to carry out automatically the classical photogrammetric workflow. The images were acquired with a UAV system equipped with a 3-axis gimbal stabilizer for built-in low-cost camera.

Figure 1-Image classification result

The post-processing workflow adopted in this study is the following:

1. Every acquired image is segmented and classified in two areas, in order to detect the sea and the coast zones (Fig. 1);
2. The image orientation process, using SfM algorithms, is performed cutting the image areas recognized as "sea" in the previous step;
3. A DSM (Digital Surface Model) of the shore is then carried out by a classical image-matching approach keeping a multiplicity factor on image block higher than 3 (Fig. 2);
4. Estimation of a DTM using a linear interpolator is then carried out;
5. Shore line is then detected from a contour line extraction.

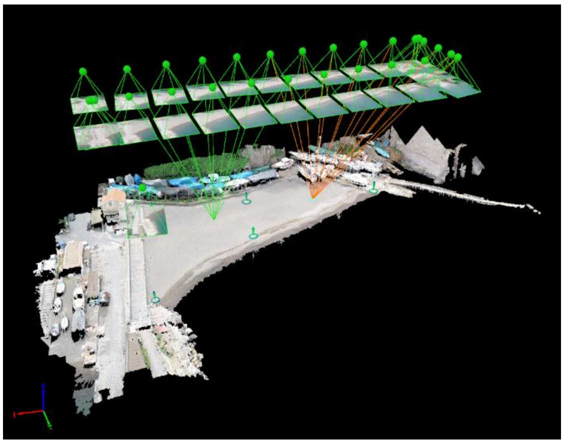

Figure 2- DSM and Image block configuration acquired by UAV- model Phantom 4

The shore offers several challenges and specific problems to the surveyor. Due to the tapered shape, that constrains an image acquisition along a linear axis, the image block configuration could be extremely trick, and it often leads to a bended 3D model (such result is known as "bowl effect") (Fig. 3) [17,18].

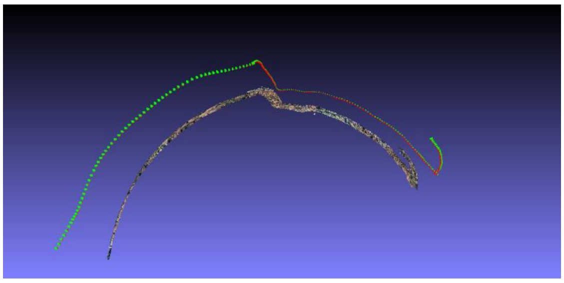

Figure 3-Blow effect due to camera calibration bad estimation of internal camera parameters

A less accurate camera self-calibration could yield a deformation effect on the orientation of image block and then on the final 3D model, this effect can be avoided adding Ground Control Points in the bundle adjustment computation. Indeed, GCPs play a fundamental role to limit this outcome.
In this work a multi constellation GNSS receiver, set in RTK mode, was used to determine the geographic coordinates of six targets located on the scene. All of them can be automatically detected and marked during the elaboration process. Four of them were used as ground

control points (GCPs) allowing to obtain the final DTM correctly scaled and georeferenced according to the chosen datum. The other two points were used as Check Points in order to assess the absolute accuracy of the three-dimensional model.

III. RESULTS

The image dataset was acquired with a quadcopter drone, model "DJI Phantom 4 – pro" equipped with a digital camera optimized for aerial acquisitions. The camera has the following characteristics: CMOS sensor with a pixel size of 2.4 µm and wide-angle lens (equivalent focal length of 24 mm). During the flight 28 nadiral images were acquired at an altitude of 50 metres, assuring a mean GSD (Ground Sample Distance) of 1.5 cm/pixel.

The Bundle Block Adjustment was performed using 4 GCPs as constrain, while 2 CPs were used as check points. All points coordinates were measured using a GNSS survey in RTK mode with an estimated position accuracy of 0.05 metres. The survey was linked to the ETRF-2000 using the Leica permanent network station named ITALPOS, the nearest station is located at a distance of 1 km from the survey site. The transformation between ellipsoidal height to the orthometric one was performed using the geoid ITALGEO2005.

The obtained results by the bundle block adjustment are reported in table 1. These results provide a potential accuracy of the photogrammetric model, especially the RMSE of check points, that complies with the accuracy magnitude of the RTK survey.

Table 1. Accuracy results of the photogrammetric 3D model.

Type		Error in meters		
		X axis	Y axis	Z axis
GCPs	Mean	-0.001	0.000	0.001
	RMSE	0.017	0.006	0.002
CPs	Mean	-0.002	-0.010	0.022
	RMSE	0.020	0.011	0.023

The densification procedure was conducted using multiscale approach with half image geometric resolution. To avoid false matches, a point must be detected on 3 images at least. The final result provided a dense point cloud of about 9.5 millions of points (Figure 2).

The DSM (Digital Surface Model) was extracted from the dense point cloud setting a cell size of 2 cm and employing a linear interpolator. The shoreline was then extracted as a contour line (figure 4, red line).

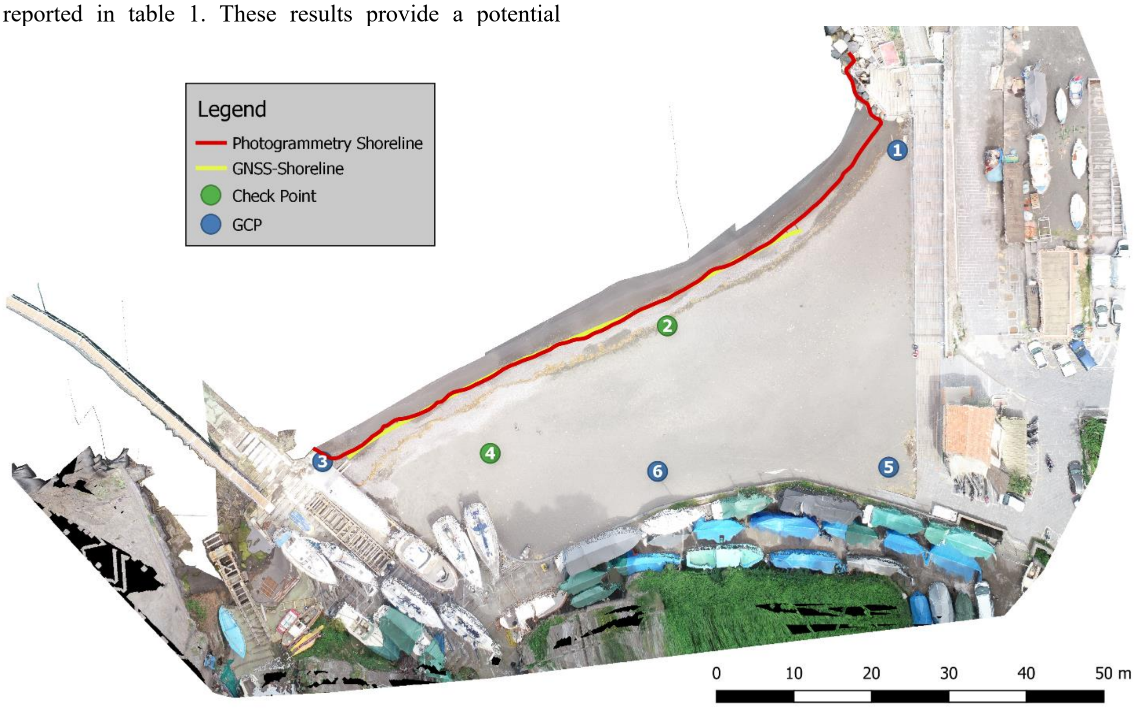

Figure 4 – Orthomosaic of the scene, where is reported the position of the GCPs (blue dot), CPs (green dots) and the shoreline detected by the proposed approach (red line) and the classical RTK-GNSS survey (yellow line)

Moreover, an assessment analysis was performed comparing the obtained result with an independent direct survey based on GNSS-RTK method (Figure 4). A former inspection was conducted on the vertex number obtained from the two different approaches as reported in Table 2.

Table 2. Comparison between GNSS based shoreline and Photogrammetry one.

Survey Type	Vertex Number
GNSS	83
Photogrammetry	179

Further inspection was conducted about the planimetric distance between the two lines. Specifically, each distance between a single vertex of the GNSS surveyed shoreline and the nearest segment of the shoreline detected by the photogrammetry is computed; furthermore an arbitrary sign was assigned to distance in according to the relative position between the two polylines (Figure 5). Such analysis provided a mean deviation of 0.03 meters with an RMSE of 0.230 meters.

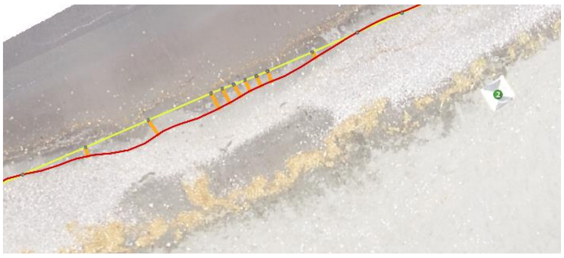

Figure 5 – Calculated distance (in orange) between the GNSS shoreline and the photogrammetric one.

IV. CONCLUSIONS AND FUTURE DEVELOPMENTS

In this paper a method to detect the shoreline based on photogrammetric survey is presented. The obtained results show that the proposed approach allows to obtain a shoreline with comparable accuracy with a direct method and to achieve a polyline with high density vertexes in according to the DSM cell size. Furthermore, the 3D model allows to extract section or additional morphological features.

The data acquisition for the presented case study was realized in low tide condition and with calm sea. A further development of this approach can be achieved in any tide condition. Indeed, performing a resample image in according with the approach illustrated by Maas [19] it is possible to determine the bathymetry DTM in shallow water using the image acquired by UAV, with sufficient accuracy [20]. Such improvement allows to achieve a complete and continue DTM of the dry and wet shore using the same acquisition low-cost platform and the same images. Furthermore, the survey zone could be extended in order to extract several cross sections of the coast and the shallow water seabed with continuity, in order to inspect the evolution of the coast.

REFERENCES

[1] Dentale, Fabio; Donnarumma, Giovanna; Carratelli, Eugenio Pugliese. Simulation of flow within armour blocks in a breakwater. Journal of coastal research, 2014, 30.3: 528-536.

[2] Mole, M. A., Davidson, M. A., Turner, I. L., Splinter, K. D., Goodwin, I. D., & Short, A. D.. Modelling multi-decadal shoreline variability and evolution. In 33rd International Conference on Coastal Engineering 2012, ICCE 2012 (pp. 1-10). Coastal Engineering Research Council. 2012.

[3] Ranasinghe, R.; Larson, Magnus; Savioli, J. Shoreline response to a single shore-parallel submerged breakwater. Coastal Engineering, 2010, 57.11-12: 1006-1017.

[4] Iskander, M. M., Frihy, O. E., El Ansary, A. E., Abd El Mooty, M. M., & Nagy, H. M. Beach impacts of shore-parallel breakwaters backing offshore submerged ridges, Western Mediterranean Coast of Egypt. Journal of environmental management, 85(4), 1109-1119, 2007.

[5] Enríquez, A. R., Marcos, M., Álvarez-Ellacuría, A., Orfila, A., & Gomis, D. Changes in beach shoreline due to sea level rise and waves under climate change scenarios: application to the Balearic Islands (western Mediterranean). Natural Hazards And Earth System Sciences, 2017, vol. 17, num. 7, p. 1075-1089.

[6] Toure, S., Diop, O., Kpalma, K., & Maiga, A. S. Shoreline detection using optical remote sensing: a review. ISPRS International Journal of Geo-Information, 8(2), 75, 2019.

[7] Milli, Manuela; Surace, Luciano. Le linee della costa: Definizioni, riferimenti altimetrici e modalita di acquisizione dei dati. Alinea Editrice, 2011.

[8] Boak, Elizabeth H.; Turner, Ian L. Shoreline definition and detection: a review. Journal of coastal research, 2005, 21.4 (214): 688-703.

[9] Pugliano, G., Robustelli, U., Di Luccio, D., Mucerino, L., Benassai, G., & Montella, R. Statistical Deviations in Shoreline Detection Obtained with Direct and Remote Observations. Journal of Marine Science and Engineering, 7(5), 137, 2019.

[10] Aedla, R., Dwarakish, G. S., & Reddy, D. V. Automatic shoreline detection and change detection analysis of netravati-gurpurrivermouth using histogram equalization and adaptive thresholding techniques. Aquatic Procedia, 4(0), 563-570, 2015.

[11] Maglione, Pasquale; Parente, Claudio; Vallario, Andrea. Coastline extraction using high resolution

WorldView-2 satellite imagery. European Journal of Remote Sensing, 2014, 47.1: 685-699.

[12] Stockdonf, H. F., Sallenger Jr, A. H., List, J. H., & Holman, R. A.. Estimation of shoreline position and change using airborne topographic lidar data. Journal of Coastal Research, 502-513, 2002.

[13] Kim, Hyunsuk; Lee, Suk Bae; Min, Kwan Sik. Shoreline change analysis using airborne LiDAR bathymetry for coastal monitoring. Journal of Coastal Research, 2017, 79: 269-273.

[14] Ahn, Yushin; Shin, Bumshick; Kim, Kyu-Han. Shoreline change monitoring using high resolution digital photogrammetric technique. Journal of Coastal Research, 2017, 79: 204-208.

[15] Varela, M. R., Patrício, A. R., Anderson, K., Broderick, A. C., DeBell, L., Hawkes, L. A., ... & Godley, B. J. Assessing climate change associated sea‐level rise impacts on sea turtle nesting beaches using drones, photogrammetry and a novel GPS system. Global change biology, 25(2), 753-762, 2019.

[16] Förstner, Wolfgang; Wrobel, Bernhard P. Photogrammetric computer vision. Springer International Publishing Switzerland, 2016.

[17] Alessandri, L., Baiocchi, V., Del Pizzo, S., Rolfo, M. F., & Troisi, S. . Photogrammetric survey with fisheye lens for the characterization of the la sassa cave. International Archives of the Photogrammetry, Remote Sensing & Spatial Information Sciences, 2019.

[18] Alessandri, L., Baiocchi, V., Del Pizzo, S., Di Ciaccio, F., Onori, M., Rolfo, M. F., & Troisi, S. A flexible and swift approach for 3D image–based survey in a cave. Applied Geomatics In press.

[19] Maas, Hans-Gerd. On the accuracy potential in underwater/multimedia photogrammetry. Sensors, 2015, 15.8: 18140-18152.

[20] Skarlatos, Dimitrios; Agrafiotis, Panagiotis. A novel iterative water refraction correction algorithm for use in structure from motion photogrammetric pipeline. Journal of Marine Science and Engineering, 2018, 6.3: 77

2020 IMEKO TC-19 International Workshop on
Metrology for the Sea
Naples, Italy, October 5-7, 2020

Reconstructing past sea level through notches: Orosei Gulf

Nikos Georgiou[1], Paolo Stocchi[2], Alessio Rovere[3], Elisa Casella[4]

[1] University of Patras, University Campus 265 04 Rio Patras, Greece, ngeorgiou@upatras.gr
[2] NIOZ - Royal Netherlands Institute for Sea Research, Coastal Systems (TX), Utrecht University, P.O. Box 59, 1790 AB Den Burg, Texel, the Netherlands, Paolo.Stocchi@nioz.nl
[3]Leibniz Centre for Tropical Marine Research (ZMT), Fahrenheitstraße 6, 28359 Bremen, Germany University of Bremen, Center for Marine Environmental Sciences (MARUM), Leobener Straße 8, 28359 Bremen, Germany, arovere@marum.de
[4] Leibniz Centre for Tropical Marine Research (ZMT), Fahrenheitstraße 6, 28359 Bremen, Germany, elisa.casella@leibniz-zmt.de

I. INTRODUCTION

Physical, chemical and biological processes are responsible for the erosion of the carbonate rocky coasts of the Mediterranean Sea. These erosional processes have always been leaving imprints such as tidal notches, especially in the Mediterranean and the Tropics [1],[2]. The Mediterranean Sea constitutes one of the most ideal study areas due to the microtidal regime and the low wave energy which allow the formation of very precise paleo-sea level and tectonic activity indicators [3]. Relative sea level is the result of eustatic, isostatic and tectonic processes, hence in tectonically stable sites the shape of tidal notches keep record of the eustatic and isostatic contribution [4]. Orosei Gulf in Sardinia is considered an almost tectonically stable site and is characterised by the presence of a continuous, lateral, 60km tidal notch [5], [6]. Orosei tidal "fossil" notch is an imprint carved during the MIS 5e, when the sea level was higher that the present one, while it constitutes a double, smoothed notch that reaches a maximum elevation of 10.5m [5], [7]. It is believed that preservation of this imprint is owed to its burial by talus deposits during MIS4-2 glacial periods [8].

II. MOTIVATION

This unique geological phenomenon is one of the best-preserved, tectonic-free, past sea level testimonies from the last time when the sea level was at a higher level than today. Hence, detailed 3D reconstruction of the Orosei site by using advanced mapping methods is considered essential for the preservation of this finding but also for the analysis of the morphological characteristics. This couold give the possibility to scientists to reconstruct possible sea level curves during the notch formation (~110-130 ka BP) through modelling.

Fig. 1 Photo of Orosei notch (diver: Paolo Stocchi)

III. METHODOLOGY

A cost-effective method of 3D reconstructing Orosei site, which is generally an inaccessible area and approachable only by boat, is photogrammetry. A local GPS-fixed station was set and a GPS receiver was placed on the camera used for the photogrammetry in order to georeference the 3D model. The photoshooting was operated by boat at a specific distance from the cliff while scales where placed manually on the notch. The 3D model acquired by the photogrammetry was then interpreted in visualization software and was resampled to 1m cell size on the x axis and 0.1m on the y axis. Vertical sections of the notch were then extracted at a 1m interval. These sections were used as input for the notch reconstruction model.

The notch modeling algorithm generates a random Sea Level Curve (SLC) within a pre-selected time interval, using the Monte-Carlo simulation. This SLC is used as one of the inputs in a quadric polynomial equation [9]:

$$d(z)= az^2 + bz + Er*dt \qquad (1)$$

that calculates the indentation depth d(z) of the notch on the cliff at different elevations. It also uses the parameters of erosion rate, tidal range, bedrock slope and tectonics rate as inputs.

The modeled notch that is produced from the random SLC is then compared to the original notch measured with the use of photogrammetry, and generates the percentage deviation. In case the modeled notch is reaching the desired deviation, the model saves the random SLC. This process is repeated until a user-defined limit.

IV. RESULTS & DISCUSSION

First results showed that the modeled notches that matched more than 80% with the original notch, originated from modeled SLCs that presented similar characteristics. The most successful modeled SLCs were bimodal and presented the higher peak (~9m) either at the begining of the notch formation or in the end, for a very short period. The sea level during the lower peak was rising at a low rate in both cases.

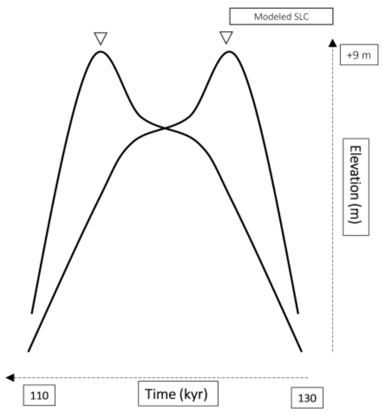

Fig. 2 Successful modeled Sea Level Curves

Photogrammetry and modeling of notches proved to be a successful methodology of reconstructing past sea level. Orosei Gulf is a very promising site which is expected to give to the scientific community an insight to the last period when the sea level was higher than today. Finally, it will give the possibility to compare present conditions with those of the past and also to make estimates about future sea level fluctuation.

REFERENCES

[1] F. Antonioli *et al.*, “Tidal notches in Mediterranean Sea : A comprehensive analysis Tidal notches in Mediterranean Sea : a comprehensive analysis,” no. July, 2015.

[2] A. S. Trenhaile, “Earth-Science Reviews Coastal notches : Their morphology , formation , and function,” *Earth Sci. Rev.*, vol. 150, pp. 285–304, 2015.

[3] P. A. Pirazzoli and N. Evelpidou, “Tidal notches: A sea-level indicator of uncertain archival trustworthiness,” *Palaeogeogr. Palaeoclimatol. Palaeoecol.*, vol. 369, pp. 377–384, 2013.

[4] A. Trenhaile, “Earth-Science Reviews Rocky coasts — their role as depositional environments,” *Earth Sci. Rev.*, vol. 159, pp. 1–13, 2016.

[5] F. Antonioli, L. Ferranti, and S. Kershaw, “A glacial isostatic adjustment origin for double MIS 5 . 5 and Holocene marine notches in the coastline of Italy,” vol. 146, pp. 19–29, 2006.

[6] F. Antonioli, S. Silenzi, E. Vittori, and C. Villani, “Sea level changes and tectonic mobility: Precise measurements in three coastlines of Italy considered stable during the last 125 ky,” *Phys. Chem. Earth, Part A Solid Earth Geod.*, vol. 24, no. 4, pp. 337–342, 1999.

[7] M. Siddall *et al.*, “Sea-level fluctuations during the last glacial cycle,” *Nature*, vol. 423, no. 6942, pp. 853–858, 2003.

[8] Antonioli F., Ferranti, L., 1992. Geomorfologia costiera e subacquea e considerazioni paleoclimatiche sul settore compreso tra s.m. in navarrese e punta goloritze (Golfo di Orosei, sardegna). Il Giornale di Geologia 54 (2), 65–89.

[9] S. J. B. Schneiderwind, “Journal of Geophysical Research : Earth Surface,” pp. 1154–1181, 2017.

2020 IMEKO TC-19 International Workshop on
Metrology for the Sea
Naples, Italy, October 5-7, 2020

Sea-Level Variability in the Gulf of Naples and the "Acqua Alta" Episodes in Ischia from Tide-Gauge Observations in the Period 2002–2019

Berardino Buonocore, Yuri Cotroneo, Vincenzo Capozzi, Giuseppe Aulicino, Giovanni Zambardino and Giorgio Budillon

Università degli Studi di Napoli "Parthenope", yuri.cotroneo@uniparthenope.it

Abstract **– This work presents an 18-year-long (2002–2019) tide-gauge dataset collected on the Island of Ischia (Gulf of Naples, Southern Tyrrhenian Sea) that can contribute to the analysis of the basic features of sea-level variability in this region. Analysis of tidal constituents shows that the Gulf of Naples is characterized by the absence of any amphidromic system. In this area, sea-level changes due to the astronomical component of the tide are generally limited to □20 cm with respect to the mean sea level, but the impact of this variability is enhanced by global sea-level increase and the effect of regional atmospheric perturbations that might also triple sea-level variations. The effects of these events, whose frequency has increased in recent decades, has been dramatic in coastal areas where intense social and economic activity occurs, e.g., in Ischia. On interannual time scales, the results indicate that the relative sea-level rise in Ischia has a magnitude of 3.9 mm/year. Special attention is dedicated to the "acqua alta" episodes and to their linkage with long-term sea-level trends and atmospheric forcing.**

7

Special Session
Improved geomatic and ship motion measurements to enhance the safety of navigation

The safety of ship and navigation, as well as of all sea coastal activities, mainly depends on the accuracy and reliability of the information about the sea state conditions. Measurements are fundamental to effectively support decisions and their quality reduces the decisional risk. In this respect, measurement obtained from onboard GNSS systems, inertial devices or gyroscopes, as well as from SAR or optical images and ground-based devices, could be useful to improve the safety of navigation and coast environments and detect in almost real time the main sea state parameters. The session focuses on recent developments in the field of measurement systems and techniques to deliver more accurate information about the surveyed environment.

2020 IMEKO TC-19 International Workshop on
Metrology for the Sea
Naples, Italy, October 5-7, 2020

Developing a low-cost GNSS/IMU data fusion platform for boat navigation

Matteo Cutugno[1], Giovanni Pugliano[1], Umberto Robustelli[1]

[1]*Department of Engineering, Parthenope University of Naples, 80133 Naples, Italy, (matteo.cutugno;umberto.robustelli;giovanni.pugliano)@uniparthenope.it*

***Abstract* – Methods of measuring a vessel's motion involve the use of expensive and complex Inertial Navigation Systems (INS). Cargo ships or passenger transport ships can afford the implementation of such systems while private small boat market has been cut off. The alternatives for small boat INS navigation are few. This paper investigates the potentiality of GNSS/IMU data fusion, experimenting low-cost hardware like Aceinna openIMU 300ZI and a GNSS receiver based on u-blox ZED-F9P module. The final goal is building a low-cost self-powered system and assess the performance in small boats navigation tests. To address this goal the INS shall be light-weight, cost-effective, and easy-to-install.**

I. INTRODUCTION

Inertial Navigation Systems (INS) are made by sensors that comprise accelerometers and gyroscopes that use microcontrollers to analyze collected measurements. Nowadays, inertial navigation technology is used widely for aircraft, ships, and land vehicles motion tracking [1]. Inertial navigation is a self-sufficient navigation technique in which measurements provided by sensors are used to track the position, velocity, and attitude (orientation) of an object relative to a known start position, velocity, and attitude. The INS signal processing chain consists of high-speed sampling of the 9 degree-of-freedom (DOF) sensor cluster (accelerometers, angular-rate sensors, and magnetometers). Since an INS does not rely on any external information sources that can be disturbed or jammed, it is an attractive means of navigation for many applications where 100% coverage and a high continuity-of-service is needed. Further, it also provides a full 9 degree of-freedom navigation solution and generally has a high update rate ($\geq$ 100 Hz). However, an INS suffers from integration drift, which means that small errors in the accelerometers and gyroscopes accumulate over time and the position error will increase without bound. To overcome this problem, the navigation information provided by a low-cost INS is frequently fused with the navigation information provided by a GNSS-receiver. On the other hand, a stand-alone GNSS receiver can be affected by signal outages due to the presence of buildings, vegetation, or jamming interference. An INS suitable for sea navigation has to provide a position accuracy as a GNSS-receiver and a full 6 degrees-of-freedom navigation solution at high update rate. Moreover, for short periods it can provide a suitable navigation solution even during GNSS signals outages [2]. This paper wants to investigate the potentiality of a low-cost INS navigation technique within the open-source software scenario. IMU/GNSS sensor integration relies on the fusion of estimate absolute positions from GNSS useful to correct the IMU sensor's drift. In this research, to synchronize both sensor sampling and processing, a 1PPS time pulse has been provided to IMU from the GNSS receiver.

II. METHODOLOGY

INS navigation technique is well described in literature [4] and here we made just a brief recall of the key concepts. Remembering that an object position and orientation can only be measured referred to coordinate-frame, inertial sensors permit to calculate attitude and position of the object in a 3-D space related to an "inertial" frame, such as the Earth-Centered, Earth-Fixed frame (ECEF) [3]. The three attitude parameters that describe an object relative to the ECEF frame are direction cosine matrices, quaternion elements, and euler angles. The navigation solution obtained is based on a Kalman Filter (KF) that generates estimates of attitude, position, and velocity. The KF is an optimal linear estimator when the process noise and the measurement noise can be modeled by white Gaussian noise. In real-life situations, when the problems are nonlinear or the noise that distorts the signals is non-Gaussian, the Kalman filters provide a solution that may be far from optimal. Nonlinear problems can be solved with the extended Kalman Filter (EKF) [5]. KFs work on a predict/update cycle. The system state of the new time-step is predicted from current states plus system measurements, i.e. for attitude is the angular rate-sensor signal while for velocity and position is accelerometer signal. The update stage corrects the state estimates for errors in the measurement signals using measurements of the true values of position, velocity, and attitude.

III. EXPERIMENTAL SETUP

In this research, the author's goal is to test the feasibility and the performances of a low-cost light-weight inertial navigation system made for small boats motion tracking.

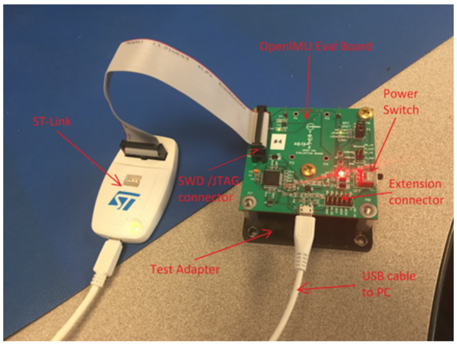

Fig. 1. Aceinna openIMU 300ZI evaluation kit (https://www.aceinna.com/).

A. Hardware setup

The hardware used in the experiment consists of an Aceinna openIMU 300ZI eval kit, a GNSS receiver equipped with u-blox ZED-F9P module [7] [8] and a Raspberry PI3 [9]. The IMU's main features are shown in Table 1. In Figure 1 is shown the Aceinna openIMU 300ZI evaluation kit employed. The configuration consist in the IMU device connected to the ST-link used to compile and upload on the board the customized application. The device is connected to the computing platform via USB 3.0 assuring also power supply. The external GNSS receiver, as shown in Figure 2 is a u-blox receiver relying on ZED-F9P GNSS module. U-blox has been configured to interface the IMU on Serial Peripheral Interface (SPI). Also, Universal Asynchronous Receiver-Transmitter (UART) is available, but the choice has fallen on the former interface for data-rate speed issues. Accelerometer, angular-rate sensor, and magnetometer of the IMU and GNSS sensor are used to obtain the information needed to estimate the position, velocity, and attitude. In particular, the position is obtained by the GNSS sensor while accelerometers provide the signal that is integrated to get velocity information. Then, GNSS provides velocity and supplemental information to the algorithm which is used to estimate the accelerometer bias. Roll and pitch are obtained by angular-rate sensor output where the errors due to integration are corrected with a gravity reference given by accelerometer. Lastly, heading is obtained combining data provided by three sensors: angular-rate sensor for the heading information, magnetometer for the North reference, and GNSS also provides more accurate low-rate heading information value. Finally, in Figure 3, is shown the Raspberry PI3, choosen for its features of portability and computing performances.

Table 1. Main features of Aceinna openIMU 300ZI Evaluation board

Integrated 3-Axis Angular Rate
Integrated 3-Axis Accelerometer
Integrated 3-Axis Magnetic Sensor
168MHz STM32 M4 CPU
SPI / UART Interfaces
Update Rate up to 800Hz
In-System Upgrade
Small Size (24x37x9.5mm)
Drop-in Upgrade for IMU380ZA, IMU381ZA
Wide Temp Range -40 to 85 ° C
High Reliability > 50,000hr MTBF
1kHz time pulse input

Fig. 2. U-blox ZED-F9P GNSS receiver.

Fig. 3. Raspberry PI3.

B. Software setup

On the IMU side, the software used is VisualStudio core with PlatformIO where it's possible to upload different ready-to-go applications provided by the manufacturer as well as build customized application. For GNSS messaging protocol, the choice has fallen on uBlox NAV-PVT protocol because of the few decimal numbers of NMEA protocol. In particular, *gpsBaudRate* parameter has been set to 115200, while *gpsProtocol* parameter to *UBLOX_BINARY*. On the GNSS receiver side, the software used to set up the u-blox to output proper navigation messages is u-center. Using *UBLOX_BINARY* as protocol, u-blox receiver has been configured to output NAV PVT message at 1 Hz making sure that other messages are disabled. Additionally, a python live plotting tool has been created in order to visualize in real-time navigation information and log on the computing platform data recorded.

IV. FUTURE WORKS

The next future work will be making the INS portable and self-powered to assess the performances of this system in terms of feasibility, reliability, and solution accuracy when stressed in a long time real-life tests. Sea navigation tests will be carried out employing a commercial high-grade IMU to compare openIMU 300ZI performances.

V. REFERENCE

VI. *

References

[1] Noureldin, A., Karamat, T. B., Georgy, J. (2013). Fundamentals of inertial navigation, satellite-based positioning and their integration (1st ed.). Berlin: Springer.

[2] Groves, P. D. (2015). Navigation using inertial sensors [Tutorial]. IEEE Areospace and Electronic Systems Magazine, 30(2), 42-69.

[3] Mehdi, J. (2017). Quaternions Algebra and Its Applications: An Overview. International Journal of Theoretical and Applied Mathematics. 2. 79-85. 10.11648/j.ijtam.20160202.18.

[4] Salychev, O.S. Voronov, V.V. Cannon, M. E. Lachapelle, G. "Low cost INS/GPS integration: concepts and testing". Proceeding of the Institute of Navigation National Technical Meeting. 2000.

[5] Montella, C. (2011). The Kalman Filter and Related Algorithms: A Literature Review.

[6] Aceinna website. https://openimu.readthedocs.io/en/latest/. Accessed on 10/04/2020.

[7] Cutugno, M. Robustelli, U. Pugliano, G. (2019). Testing a GNSS software receiver for end-user utilization.

[8] Cutugno, M. Robustelli, U. Pugliano, G. (2020). Low-Cost GNSS Software Receiver Performance Assessment. Geosciences 2020, 10, 79.

[9] Raspberry website. https://www.raspberrypi.org/documentation/. Accessed on 11/04/2020

2020 IMEKO TC-19 International Workshop on
Metrology for the Sea
Naples, Italy, October 5-7, 2020

Performance assessment of GNSS single point positioning with recent smartphones

Jacek Paziewski[1], Giovanni Pugliano[2], Umberto Robustelli[2]

[1]*Department of Geodesy, Faculty of Geoengineering, University of Warmia and Mazury in Olsztyn, Oczapowskiego 1, 10-719 Olsztyn, jacek.paziewski@uwm.edu.pl*
[2]*Department of Engineering, Parthenope University of Naples, 80133 Naples, Italy, (giovanni.pugliano;umberto.robustelli)@uniparthenope.it*

***Abstract* – The new generation of Android smartphones are equipped with high performance Global Navigation Satellite System (GNSS) chips. The new chips are capable of tracking dual frequency multi constellation data. Moreover, starting from version 9 of Android users can disable the duty cycle power saving option, thus it is feasible to acquire good quality raw data. In this work we assessed the performance of GPS+Galileo single point positioning of three recent smartphones, namely Xiaomi Mi8, Xiaomi Mi9 and Huawei P30. The best positioning accuracy, in terms of horizontal root mean square error (DRMS), was obtained by Huawei P30 with a DRMS of 4.46 m. Xiaomi MI8 shows very similar performance (4.56 m of DRMS) but these results were subject to outliers. Finally Xiaomi Mi9 shows a DRMS of 7.26 m.**

I. INTRODUCTION

As reported by GSA [1], smartphones are nowadays dominating the installed base of devices equipped with GNSS (Global Navigation Satellite System) chipsets. The ubiquity and current positioning performance of recent smartphones have expanded their initial applications such as personal navigation and social networking and therefore opened the door to novel areas of market, industry and science [6]. Recently a great deal of effort has been made in the development of the processing algorithms which address the specific limitations of smartphone GNSS observations. As a result, several researchers have proved the feasibility of precise positioning with such observations under the specific conditions ([8], [9], [10]). Nevertheless, there is still a need to evaluate the accuracy which may be reached with current smart devices in a standard positioning service based on code pseudoranges, since even now there are few smartphones which support continuous phase observations. In a view of these expectations, this paper aims at the characterisation of the positioning performance level which may be reached with the selected most recent smartphones. This evaluation was preceded by the analysis of the GNSS observations in terms of signal power.

II. EXPERIMENT DESIGN AND RESULTS

A. *Data collection*

The smartphone GNSS observation analysis as well as single point positioning performance assessment take advantage of GNSS data collected by selected most recent Android smartphones, namely Huawei P30, Xiaomi Mi 8 and Xiaomi Mi 9. All receivers are capable of collecting dual frequency multi constellation signals. The last smartphone collects only code pseudoranges, whereas Huawei P30, Xiaomi Mi 8 allow also the acquisition of phase observables. Phase observables are however not employed in a standard navigational solution with the single point positioning (SPP) approach, therefore were not used in this case study. The observations were collected on December 11, 2019 over a timespan of about 5 hours (approx. 8-13 UTC) using Geo++ RINEX Logger ver. 2.1.6 application running on Android system. The applied smartphones were collocated and centred over temporal site using tribrachs and tripods as showed in figure 1. The coordinates of the temporal geodetic sites were determined be the means of static relative positioning using high-grade receivers.

B. *Observation analysis*

The discussion of the results of the single point positioning is preceded by an assessment of GNSS observation derived from the employed smart devices. As recent studies show, smartphone GNSS observations are not only the subject of several unwanted effects but also suffer from significant observation noise and low suppression to multipath effect ([3], [5], [7]). Hence this subsection examines selected characteristics of GNSS observations and verifies with regard to recent smartphones the common presumption that smartphone GNSS signals are of lower quality with respect to geodetic grade receivers.

We have used the Carrier-to-noise density ratio (C/N0) as the parameter which characterises the GNSS signal power. Figure 2 shows the skyplots of the C/N0 of the GPS signals collected by the applied smartphones. Taking advantage of the presentation of C/N0 in the function of signal azimuth and elevation, we may easily verify the

Fig. 1. Huawei P30, Xiaomi Mi 8 and Xiaomi Mi 9 during data collection.

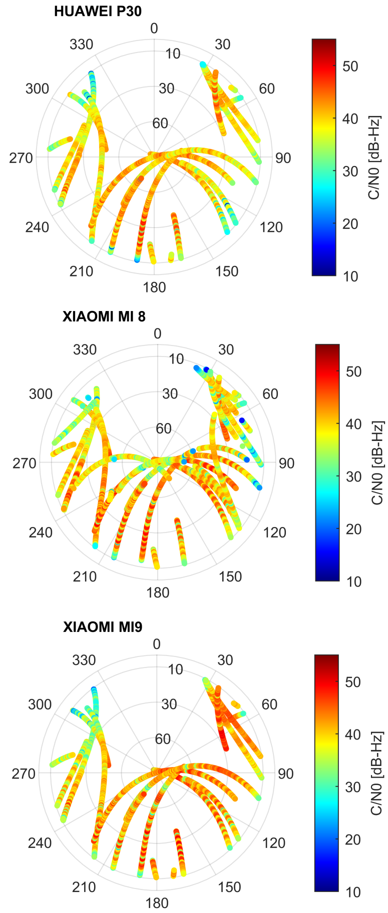

Fig. 2. Skyplots of smartphone C/N0.

presumption of high dependency of C/N0 on signal elevation, which was proved for high grade receivers. However, looking at the plots in figure 2, we may learn that this statement does not hold true with regard to GNSS observations collected by the smartphones. Such results may suggest the application of other than commonly used elevation dependant weighting functions ([4], [7]).

In figure 3 we present the time series of C/N0 of GNSS signals collected by applied smart devices. As we may read from the plots, the maximal power of acquired signals does not exceed 50 dB-Hz. This is a significantly lower value with respect to geodetic grade receivers which allow acquisition of signals with power reaching up to 60 dB-Hz ([2], [11]). In general the applied smartphones show similar performance in this term, however we can easily detect a higher number of outliers characterised by ultra-low values of C/N0 for Xiaomi Mi 8. This may be connected with higher susceptibility to multipath effect or worse elimination of outlying observations by Xiaomi Mi 9 with respect to other, analysed in this case study, smartphones.

C. Assessment of Single Point Positioning

Three selected post processing scenarios were applied for each smartphone; in the first one we used only GPS constellation, the second one took advantage of Galileo system and in the last both constellations were used. Tables 1, 2 and 3 demonstrate detailed results of single point positioning performance assessment achieved with the application of Xiaomi MI9, Xiaomi MI8 and Huawei P30 smartphones, respectively. As expected, the results clearly proved the benefit from multi-constellation signals over single system solution. Here, for the sake of brevity, only the most interesting results will be described in detail.

Figure 4 shows the scatter plot of single point positioning with three selected smartphones. Blue, red and yellow markers represent errors obtained using Xiaomi Mi 9, Xiaomi Mi 8 and Huawei P30 multi constellation measurements (both GPS and Galileo) respectively. In this figure the outliers detected in Mi 8 dataset (described in previous section) have been eliminated. The horizontal accuracy expressed in terms of DRMS (horizontal root mean square error) is of 7.26 m, 4.56 m and 4.46 m for Xiaomi Mi 9, Xiaomi Mi 8 and Huawei P30 respectively. With regard to vertical accuracy, the results confirmed the best performance of the Huawei P30 with a RMS of the vertical component of 7.46 meters compared to the 8.56 m and

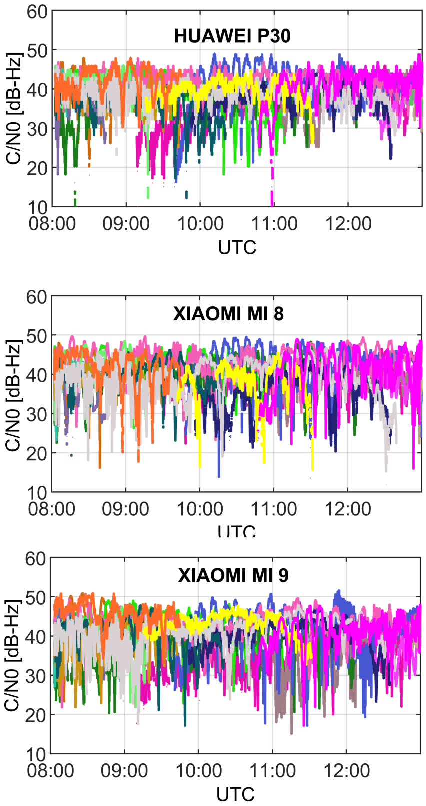

Fig. 3. Time series of C/N0 collected by smartphones.

11.49 m of the Mi8 and Mi9, respectively.

Figure 5 depicts the time series of East (top panel), North (middle panel) and Up (bottom panel) error components obtained with Xiaomi Mi 9 (in blue), Xiaomi Mi 8 (in red) and Huawei P30 (in yellow) in multi constellation scenario. We can read from the figure that the best performances are provided by the P30 in the GPS-Galileo configuration. In reality, the performance of the MI8 is also very similar after outliers cut.

Table 1. Xiaomi Mi9 coordinate statistics.

	GAL	GPS	GPS+GAL
DRMS [m]	9.64	11.77	7.26
RMS East [m]	5.31	5.63	4.02
RMS North [m]	8.05	10.33	6.05
RMS Up [m]	15.86	16.98	11.49
#Pos	18196	18196	18196

In figure 6 are presented the time series of East (top panel), North (middle panel) and Up (bottom panel) error components obtained with Xiaomi Mi 9 (in blue) and

Table 2. Xiaomi Mi8 coordinate statistics.

	GAL	GPS	GPS+GAL
DRMS [m]	12.45	6.01	4.56
RMS East [m]	3.93	2.95	2.38
RMS North [m]	11.81	5.24	3.89
RMS Up [m]	19.42	10.63	8.56
#Pos	9284	17300	17300

Table 3. Huawei P30 coordinate statistics.

	GAL	GPS	GPS+GAL
DRMS [m]	-	5.49	4.46
RMS East [m]	-	2.59	2.33
RMS North [m]	-	4.83	3.81
RMS Up [m]	-	7.90	7.46
#Pos	0	18218	18221

Xiaomi Mi 8 (in red) using only the signals of Galileo constellation. In this analysis P30 is not represented since no solution was obtained using only the Galileo measurements. The figure clearly shows that with Mi8 smartphone measurements it was feasible to obtain about a half of the expected epoch solutions. This was not the case for Mi9 which provided the position during entire time span. A poor availability of Mi8 positioning was caused by a low number of tracked Galileo satellites during the experiment.

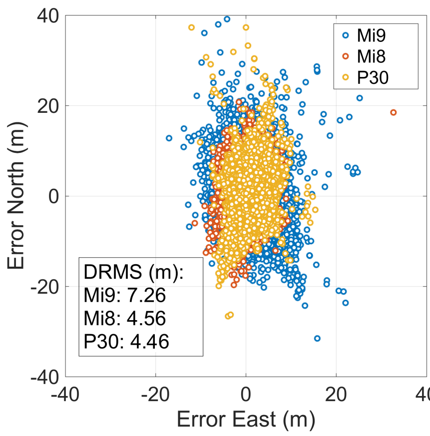

Fig. 4. Horizontal error scatter plot: blue, red and yellow circles correspond to MI9, Mi8 and P30 solution, respectively.

III. CONCLUSIONS

In this work we assessed the performance of single point positioning with recent Android smartphones, namely Xiaomi Mi8, Xiaomi Mi9 and Huawei P30. Detailed results

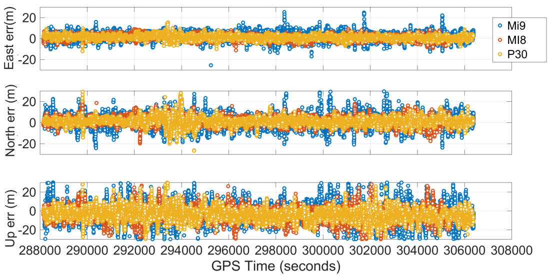

Fig. 5. Time series of coordinate error for Xiaomi MI 9 (in blue), Xiaomi MI 8 (in red) and Huawei P30 point (in yellow) SPP solution obtained using both GPS and Galileo observables. Top, middle and bottom subplots show East, North and Up components, respectively.

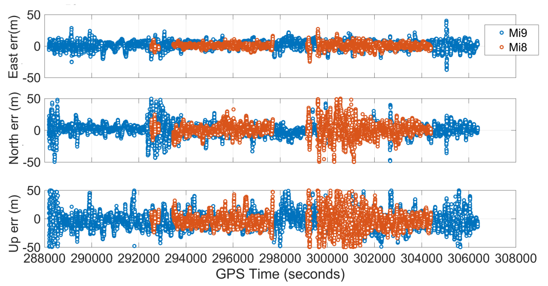

Fig. 6. Time series of coordinate error for Xiaomi MI 9 (in blue), Xiaomi MI 8 (in red) SPP solution obtained using only Galileo observables. Top, middle and bottom subplots show East, North and Up components, respectively.

revealed a better horizontal accuracy for Huawei P30 and Xiaomi Mi8 (4.46 m and 4.56 m of DRMS, respectively) with respect to Xiaomi Mi9 with a DRMS of 7.26 m. With regard to vertical accuracy, the results confirmed the best performance of Huawei P30 with a RMS of the vertical component of 7.46 meters compared to the 8.56 m and 11.49 m of Mi8 and Mi9 smartphones, respectively. The results proved a high impact of the outliers on SPP positioning with smartphones, hence this issue should be further investigated.

REFERENCES

[1] GSA GNSS Market Report Issue 6. Accessed: 2020-03-30.

[2] M. Gill, S. Bisnath, J. Aggrey, and G. Seepersad. Precise point positioning (PPP) using low-cost and ultra-low-cost GNSS receivers. In *Proceedings of the ION GNSS*, pages 226–236, 2017.

[3] T.E. Humphreys, M. Murrian, F. van Diggelen, S. Podshivalov, and K.M. Pesyna. On the feasibility of cm-accurate positioning via a smartphone's antenna and GNSS chip. In *2016 IEEE/ION Position, Location and Navigation Symposium (PLANS)*, pages 232–242. IEEE, 2016.

[4] W. Liu, X. Shi, F. Zhu, X. Tao, and F. Wang. Quality analysis of multi-GNSS raw observations and a velocity-aided positioning approach based on smartphones. *Advances in Space Research*, 63(8):2358–2377, 2019.

[5] M. Navarro-Gallardo, N. Bernhardt, M. Kirchner, J. Redenkiewicz Musial, and M. Sunkevic. Assessing Galileo readiness in Android devices using raw measurements. In *Proceedings of the ION GNSS*, pages 85–100, 2017.

[6] J. Paziewski. Recent advances and perspectives for positioning and applications with smartphone GNSS observations. *Measurement Science and Technology*, in print, https://doi.org/10.1088/1361-6501/ab8a7d, 2020.

[7] J. Paziewski, R. Sieradzki, and R. Baryla. Signal characterization and assessment of code GNSS positioning with low-power consumption smartphones. *GPS Solutions*, 23(4):98, 2019.

[8] U. Robustelli, V. Baiocchi, and G. Pugliano. Assessment of dual frequency GNSS observations from a Xiaomi Mi 8 Android smartphone and positioning performance analysis. *Electronics*, 8(1), 2019.

[9] L. Wanninger and A. Heßelbarth. GNSS code and carrier phase observations of a Huawei P30 smartphone: quality assessment and centimeter-accurate positioning. *GPS Solutions*, 24, 2020.

[10] Q. Wen, J. Geng, G. Li, and J. Guo. Precise Point Positioning with ambiguity resolution using an external survey-grade antenna enhanced dual-frequency Android GNSS data. *Measurement*, 157, 2020.

[11] X. Zhang, X. Tao, F. Zhu, X. Shi, and F. Wang. Quality assessment of GNSS observations from an Android N smartphone and positioning performance analysis using time-differenced filtering approach. *GPS Solutions*, 22(3):70, 2018.

2020 IMEKO TC-19 International Workshop on
Metrology for the Sea
Naples, Italy, October 5-7, 2020

Sea state monitoring based on ship motion measurements onboard an icebreaker in the Antarctic waters

Silvia Pennino[1], Antonio Angrisano[2], Salvatore Gaglione[1], Anna Innac[1], Vincenzo Piscopo[1], Antonio Scamardella[1]

[1] *Department of Science and Technology, University of Naples "Parthenope", Centro Direzionale Isola C4, 80143 Naples, Italy; silvia.pennino@uniparthenope.it; salvatore.gaglione@uniparthenope.it; anna.innac@uniparthenope.it; vincenzo.piscopo@uniparthenope.it; antonio.scamardella@uniparthenope.it*
[2] *University of Benevento "G. Fortunato", a.angrisano@unifortunato.eu*

***Abstract* – A new wave spectrum resembling procedure is applied to detect the sea state parameters, namely the wave peak period and the significant wave height based on the analysis of heave and pitch motion time series, obtained by on board measurements. The outlined procedure is applied to Laura Bassi oceanographic ship, assumed as reference vessel. Heave and pitch motion time histories are evaluated from the survey of the amplitudes of the vessel motions, starting from different sensors measures collected by a smartphone located on board the vessel. The obtained results were compared with the weather forecast data provided by the global-WAM (GWAM) model.**

I. INTRODUCTION

The real-time knowledge of the sea state conditions, encountered by the ship in the course of its route, is of fundamental importance for different aspects ranging from the safety of navigation to the comfort on board. In particular, the assessment of the weather conditions is useful to minimize the risks of navigation and reduce the costs, as it provides a decision support system to avoid potential dangerous phenomena in following and quartering seas, and, in order to detect the optimal route, the evaluation of the environmental conditions is also required when the ship voyage is planned by weather routing methods. Additional advantages coming from the knowledge of sea state parameters, are connected to the safety of crew and the assessment of the on-board comfort level. Finally, the continuous monitoring of sea state conditions is helpful to improve the statistics of long-term wave data, providing additional information where the weather buoys are very scattered.

The ship system can be considered as a mobile laboratory capable of carrying out in situ measurements for the estimation of ship motions and, subsequently, to derive the characteristics of the incident wave. The determination of the sea spectrum starting from the survey and analysis of vessel motions can lead to the onset of problems mainly related to the Doppler shift between the absolute and encounter wave frequencies. Heave and pitch motions are evaluated from the survey of the amplitudes of the ship vertical motions and pitch acceleration, the response spectra are evaluated and knowing the ship complex transfer functions, the sea spectrum generating the motions is determined. Finally, from the spectral distribution of the sea in the absolute frequency domain, the characteristic parameters are obtained.

II. LITERATURE REVIEW

Since the mid-70s a variety of research activities were carried out to explore the possible analogy between ships and wave buoys. In 1973 Takekuma and Takahashi [1] presented the first pioneering work on wave spectrum resembling, based on ship motion measurements, without forward speed. In the following years, Isobe et al. [2] and Kobune et al. [3] have carried out several attempts to include the Doppler shift for ships advancing in head and bow seas and, subsequently, in quartering and following seas by Iseki and Ohtsu [4]. Following these works, in the last two decades a variety of research activities was performed with the aim to apply a reverse analysis technique to obtain the wave spectra with sufficient accuracy, especially for ships advancing in following seas, considering that in this case the encounter frequency has a non-bijective relation with the absolute wave one (Iseki and Terada [5]; Nielsen [6]; Nielsen et al. [7], Montazeri et al. [8]). Brodtkorb et al. [9] developed a signal-based algorithm, to detect the wave spectrum by iteratively solving a set of linear equations, based on heave, pitch and roll motion measurements. Nielsen and Diez [10] analysed the motion measurements of a containership, focusing on the incidence of the advance speed and performed a comparative analysis between sea state estimates obtained by motion measurements and a hindicast study. Nielsen [11] provides an account of the available techniques for shipboard sea state estimation in both frequency and time-domain. As concerns the application of time-domain techniques, only few works, mainly based on Kalman filtering, applied to convert the ship motion measurements into the wave elevation time history, are available in literature (Pascoal and Soares, [12]; Pascoal et al. [13]), due to the high numerical effort required to resemble the unknown sea state parameters.

Piscopo et al. [14] presented a new wave spectrum resembling procedure, consisting of two subsequent steps and based on the analysis of heave and pitch motions. The significant wave height, the wave peak period and the wave spectrum shape parameter are obtained from the analysis of heave and pitch time-domain simulations but which can be obtained by onboard measurements. The incidence of time duration on resembled sea state parameters has been investigated, the statistics of errors on wave peak periods and significant wave heights have been analysed to select the proper time duration of onboard measurements that allows balancing the reliability of resembled data with the need of an almost real-time sea state monitoring.

III. SEA STATE MONITORING ALGORITHM

A. Ship motion measurements

Heave and pitch motions are evaluated from the survey of the amplitudes of the vessel motions, starting from different sensors measures collected by a smartphone located on board the vessel. Most smartphone devices have built-in sensors able to collect measures of motion, orientation, and various environmental conditions. These sensors provide raw data with high sample-rate, and are useful to monitor three-dimensional device motion or positioning. The sensors embedded into the smartphone belong to three major groups:

- Motion sensors, including accelerometers, gravity sensors, gyroscopes, and rotational vector sensors to measure device motion.
- Environmental sensors, such as ambient air temperature and pressure, illumination, and humidity using barometers, photometers (light sensors), and thermometers used to collect measurements of various environmental conditions,
- Position sensors, including magnetometers (geomagnetic field sensors) and proximity sensors, to provide information about the physical position of the device.

The acceleration, angular velocity, magnetic field, and orientation sensors log data referred to the smartphone coordinate system shown in Fig. 1. The coordinate origin is at the center of the touch screen, x-axis points to the right direction, y-axis the front and z-axis the top. When the smartphone moves, the accelerometer and gyros provide three-axis accelerations and angular velocities components. The orientation sensor can output azimuth angle, defined as the angle between the projection of the y-axis on horizontal plane and the north direction.

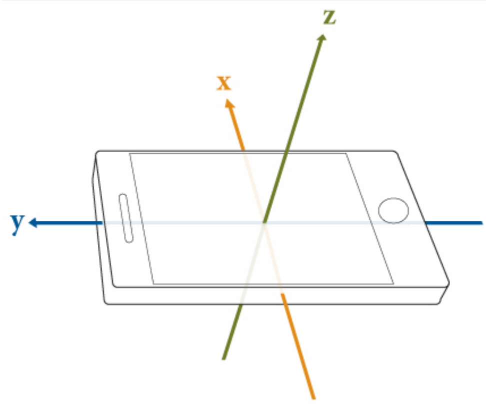

Fig. 1. System coordinates of the device (https://se.mathworks.com/help/supportpkg/mobilesensor/ug/phoneorv2.gif)

Smartphones are also equipped with a GNSS receiver which can computes the position and velocity in a global framework. The adopted Android smartphone is Xiaomi Mi 8 located approximately in the centre of mass of the vessel and MATLAB® Mobile™ is used to collect the desired measures. MATLAB support Android devices to obtain data of the built-in sensors, acquiring sensor data locally on an Android™ device, with or without a network connection. This is especially useful if the users want to collect sensor data while the device does not have a network connection. For the aim of the work, orientation and position sensors are used to collect, respectively, the temporal variations of the device pitch angle (defined as the angle between a plane parallel to the device's screen and a plane parallel to the ground) and of altitude (U). Specifically, the ship vertical motions between consecutive epochs (k) is computed as:

$$\Delta U_k = U_k - U_{k-1} \qquad (1)$$

So, heave and pitch variations obtained from the smartphone are used as input parameters for the sea spectrum determination. In addition, the velocity and the course of the device are collected from position sensors using MATLAB Mobile, in order to evaluate the encounter frequencies.

B. Ship motion analysis and wave spectrum resembling

The modulus of heave and pitch motion transfer functions have been derived after solving the heave/pitch motion equations in the encounter wave frequency-domain [14], both for swell and wind waves, the zero-speed added mass and radiation damping values are determined by the open source code NEMOH and subsequently corrected to account for the forward speed using the corrective factors provided by Salvesen et al. [15]. The heading angle between the vessel route and the prevailing wave direction is assumed to be known, the weather forecast data from GRIB file are used. Based on relevant time histories, recorded by the onboard equipment, the encounter spectra of heave and pitch motions, are assessed. The wave spectrum resembling procedure consists of two subsequent steps, the procedure belongs to the class of parametric methods. At the first step the wave peak period and the spectrum shape parameter are iteratively varied and determined by a best-fit parametric procedure. The best-fit iterative procedure leads to the assessment of the two unknown variables or to the detection of the only wave peak period, if the shape parameter is preliminarily known, as it occurs for fully developed seas (γ=1). The number of tentative peak periods and shape parameters, to be embodied in the iterative procedure, needs to be selected in order to obtain an accurate assessment of the two variables, paying attention to not excessively increase the time effort amount required to perform the calculations. At the end of Step I the wave peak period and the shape parameter of the JONSWAP spectrum are obtained. Subsequently, the significant wave height is assessed, based on single or combined heave/pitch motion analysis, at the end of Step II the significant wave height is assessed, so resembling all sea state parameters. All the procedure is in detailed reported in Piscopo et al. [14].

IV. MAIN DATA OF REFERENCE SHIP

The Laura Bassi oceanographic ship, used for scientific activity and logistical support for Italian Antarctic explorations, is assumed as reference vessel in the case study performed in the following. The main dimensions are listed in Table 1, while in Fig. 2 are reported the pitch and heave RAOs separating the response operator due to wind waves and swell.

Table 1. Main particulars of Laura Bassi

Length overall	80.00	m
Length between perpendiculars	72.40	m
Beam on WL	17.00	m
Design draught	6.15	m
Displacement	4736	t
Waterplane area	1074	m^2
Block coefficient	0.599	

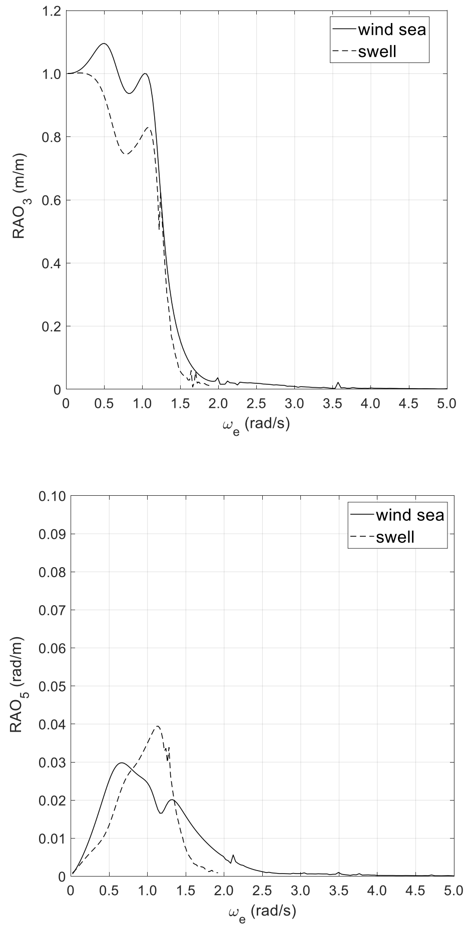

Fig. 2. Heave and Pitch RAOs

V. ONBOARD SHIP MOTION MEASUREMENTS

A. Data collections

To assess the capabilities of smartphones to provide measurements to be used for the wave spectrum resembling, the tests are carried out using real data collected by the smartphone Xiaomi Mi 8 located on board the Laura Bassi oceanographic ship. In detail, a data collection of one hour is chosen on 14th of February 2020 starting from 13:21 (local time) and with a sample rate of 1 Hz. The selected route falls in Antarctic Ocean and has (60.15°S, 167.08°E) departure and (59.96°S, 167.19°E) arrival coordinates.

B. Reference weather data

The performance of the results obtained by the proposed wave spectrum resembling procedure are compared to the sea state conditions based on weather forecast data provided by Global Wave Model (GWAM) and collected in GRIB (GRIdded Binary) file.

For the aim of the work, the GRIB file is downloaded for the 14th of February 2020, with 3-hour forecast interval and 0.25° x 0.25° grid spacing and the weather forecast data are extrapolated for the considered route and temporal period. The model outputs, used as reference, are the significant wave height, the mean wave period and direction of both wind and swell components.

C. Sea state resembling

The wave spectrum resembling procedure is tested against a sea state conditions characterized by a combination of swell and wind waves, both by separating the two contributions and considering them together by evaluating a total component of significant wave height and peak period. The peak periods of swell and wind wave spectra are generally quite different, so as it is possible to separate the spectral components due to swell and wind waves, located up to and beyond the so-called separation frequency respectively, the separation frequency can be efficiently detected based on the only heave motion encounter spectrum. In Fig. 3 are shown the heave and pitch motion amplitude encounter spectrum, in black the same applying the smooth, as it is possible to see from the figure the separation frequency is too high, theoretically it is approximately zero. The high value of the separation frequency is clearly attributable to the values of the wave period very similar for swell and wind waves, also the prevailing sea state directions do not belong to very different ranges and consequently the Doppler effect does not intervene for a clear separation between encounter frequencies. In Fig. 4 are reported the significant height, the peak period and the angle between the ship route and the prevailing direction of swell and wind wave provided by the global-WAM (GWAM) model. The high value of the separation frequency makes the clear separation of the components limited meaning, the sea spectrum is a single-mode spectrum and there is no effective separation between the two peaks. In Fig. 5 and in Table 2 it has been reported only the results relative the reconstruction of the sea spectrum considering the two contributions together. The results shown a difference for the combined spectrum on the significant height of about 2% and on the peak period of 3 seconds.

Table 2. Parameters of rebuilt spectrum for a combined sea spectrum

	H_S (m)	T_P (s)
Data from WWIII	4.441	9.001
Resembled combined sea spectrum	4.346	9.300

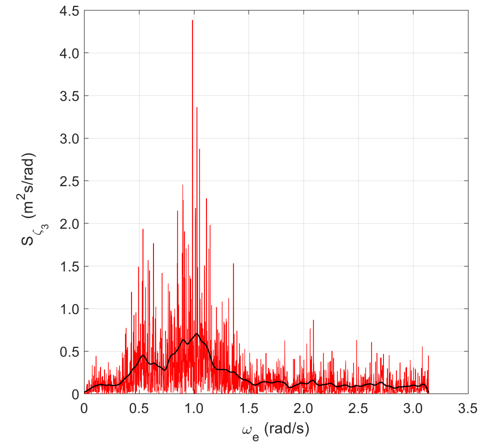

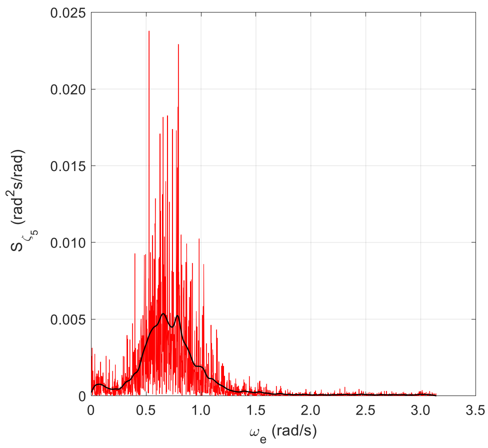

Fig. 3. Heave and Pitch motion amplitude encounter spectrum

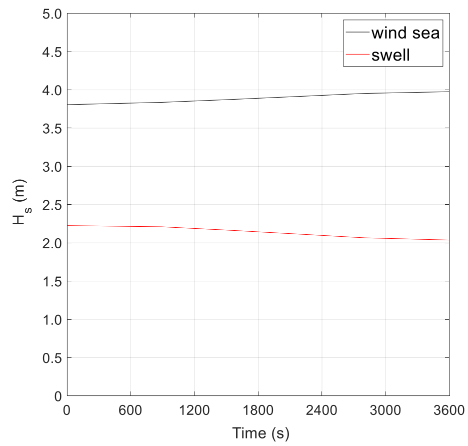

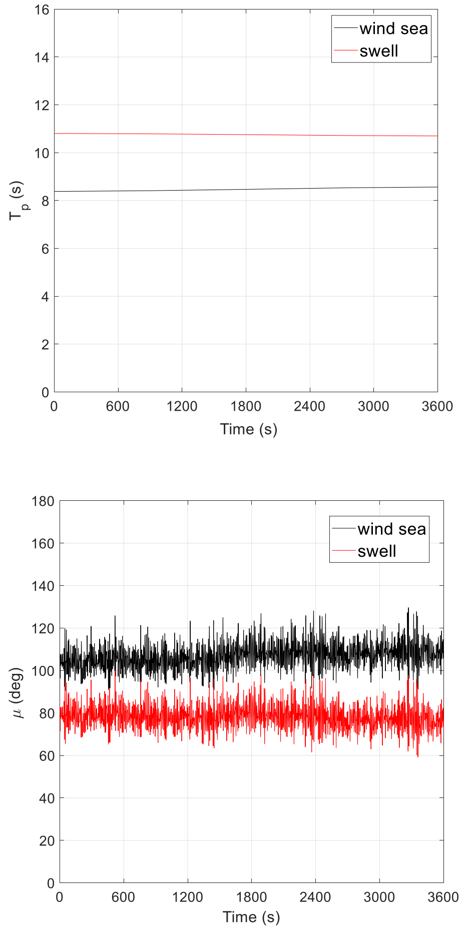

Fig. 4. Characteristics of swell and wind wave

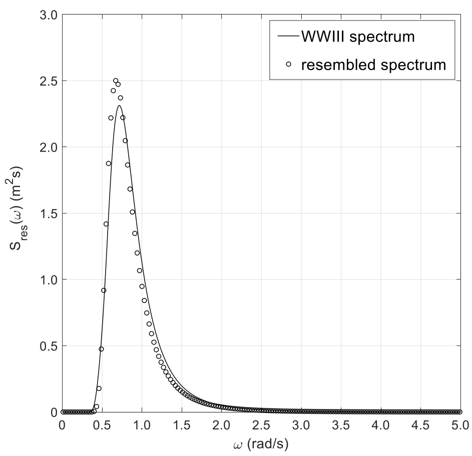

Fig. 5. Resembled combined sea spectrum

VI. CONCLUSIONS

A new wave spectrum resembling procedure based on the analysis of heave and pitch motion time series, presented in detail in [14], has been applied to assess the sea state parameters. The Laura Bassi oceanographic ship was the reference vessel and the procedure was tested using real onboard measurements for heave, pitch, velocity and ship course. The sea state parameters have been compared with weather forecast data showing a good agreement, furthermore, it stands to reason a further improvement in the results for sea states with a more distinct separation between swell and wind waves. Current outcomes seem to be promising for further developments, mainly devoted to investigate the possible employment of windowing functions in the Fourier analysis of ship motions and the incidence of time duration on resembled sea state parameters.

ACKNOWLEDGMENTS

The work was supported by “DORA - Deployable Optics for Remote sensing Applications DORA” (ARS01_00653), a project funded by MIUR - PON “Research & Innovation”/PNR 2015-2020.
The authors special thank to Dr. Riccardo Scipinotti (Agenzia nazionale per le nuove tecnologie, l’energia e lo sviluppo economico sostenibile - ENEA) and Dr. Franco Coren (Istituto Nazionale di Oceanografia e di Geofisica Sperimentale - OGS) for the data and all technical information on Laura Bassi vessel provided.

REFERENCES

[1] K. Takekuma, T. Takahashi, “On the Evaluation of Sea Spectra Based on the Measured Ship Motions”, Transactions of the West-Japan Society of Naval Architects 45, 1973, pp. 51-57.

[2] M. Isobe, K. Kondo, K. Horikawa, “Extension of MLM for Estimating Direction Wave Spectrum” Proceedings of the Symposium on Description and Modeling of Direction Seas, 1984, volume A-6.

[3] K. Kobune, N. Hashimoto, “Estimation of Directional Spectra from the Maximum Entropy Principle”, Proceedings of the 5th International Offshore Mechanics and Arctic Engineering (OMAE) Symposium, 1986, pp. 80-85, Tokyo, Japan.

[4] T. Iseki, K. Ohtsu., “Bayesian estimation of directional wave spectra based on ship motions”, Control Engineering Practice 8, 2000, pp. 215-219.

[5] T. Iseki, D. Terada, “Bayesian estimation of direction wave spectra for ship guidance systems”, International journal of Offshore and Polar Engineering 12, 2002, pp. 25-30.

[6] U.D. Nielsen, “Estimations of on-site direction wave spectra from measured ship responses” Marine

Structures 19, 2006, pp. 33-69.

[7] U.D. Nielsen, I.M.V. Andersen, J. Koning, “Comparisons of means for estimating sea states from an advancing large containership”, Proceedings of the 12th PRADS, Changwon, South Korea, 2013.

[8] N. Montazeri, U.D. Nielsen, J.J. Jensen, “Estimation of wind sea and swell using shipboard measurements – A refined parametric modelling approach” Applied Ocean Research 54, 2016, pp. 73-86.

[9] A.H. Brodtkorb, U.D. Nielsen, A. Sørensen, “Online wave estimation using vessel motion measurements” Proceedings of the 11th IFAC Conference on Control Applications in Marine Systems, Robotics, and Vehicles CAMS 2018, Opatija, Croatia, pp. 10–12.

[10] U.D. Nielsen, J. Diez, “Ocean wave spectrum estimation using measured vessel motions from an in-service containership”, Marine Structures 69, 102682, 2020.

[11] U.D. Nielsen “A concise account of techniques available for shipboard sea state estimation”, Ocean Engineering 129, 2017, pp. 352-362.

[12] R. Pascoal, C. Guedes Soares, “Kalman filtering of vessel motions for ocean wave directional spectrum estimation”, Ocean Engineering 36, 2009, pp. 477-488.

[13] R. Pascoal, L.P. Perera, C. Guedes Soares, “Estimation of directional spectra from ship motions sea trials”, Ocean Engineering 132, 2017, pp. 126-137.

[14] V. Piscopo, S. Gaglione, A. Scamardella, “A new wave spectrum resembling procedure based on ship motion analysis”, Ocean Engineering 201, 2020.

[15] N. Salvesen, E.O. Tuck, O. Faltinsen, “Ship motions and sea loads”, SNAME Transactions 6, 1970, pp. 1-30.

2020 IMEKO TC-19 International Workshop on
Metrology for the Sea
Naples, Italy, October 5-7, 2020

Data processing for the accurate evaluation of combined wind sea and swell spectra

Giovanni Battista Rossi [1], Francesco Crenna [1], Marta Berardengo [1],

Vincenzo Piscopo [2], Antonio Scamardella [2]

[1] *University of Genova, DIME, Via Opera Pia 15A, 16145 Genova, Italy.*
[g.b.rossi, francesco.crenna, marta.berardengo]@unige.it
[2] *University of Naples "Parthenope", Department of Science and Technology, Naples, Italy,*
[vincenzo.piscopo, antonio.scamardella]@uniparthenope.it

Abstract **– The reliable monitoring of sea state parameters is a key factor for weather forecasting, as well as to ensure the safety of ship and navigation. In current analysis different spectrum estimation techniques are applied to random wave signals, generated from a theoretical wave spectrum obtained by combining both wind sea and swell components, with different significant wave heights and peak periods. Hence, the proposed spectrum resembling methods are applied in order to compare the relevant performances, with reference to both short and long-time durations of the considered wave signal.**

I. INTRODUCTION

The assessment of wave spectra from the analysis of random wave elevations has been a widely investigated topic since the works of Mansard and Funke [1-2] and Battjes and val Vledder [3], since it is a key factor to detect the sea state conditions and ensure the safety of ship and navigation [4-6]. Really, the assessment of the wave spectrum parameters, namely the significant wave height, the wave peak period and peak enhancement factor, reveals to be a quite challenging issue, provided that some key factors, such as the selection of the proper spectrum estimation technique, the minimum duration of the wave time signal and the trade-off between spectral resolution and variance of the spectral estimator, represent key factors of the entire data processing procedure. Recently, some advances have been gathered by Rossi et al. [7-8] that compared different spectrum estimation techniques, applied to single peak wave spectra, concluding that the Welch and Thomson methods are the most promising techniques, combined with the Nonlinear Least Square Method (NLSM) for the assessment of sea state parameters, that reveal to be reliable even for short time signals.

Hence, the proposed procedure is now extended to double peak wave spectra, obtained by the superposition of wind sea and swell components, with different significant wave heights and peak periods. A comparative analysis between different spectrum estimation techniques is performed, in order to detect the best method combined with both short and long-time durations.

II. INPUT WAVE SPECTRUM AND RANDOM WAVE GENERATION

Combined wind sea and swell are described by a double peak wave spectrum according to the following equation [9]:

$$S(\omega) = S_{wind}(\omega) + S_{swell}(\omega) \quad (1)$$

where the wind sea and swell components are assumed to be uncorrelated and to follow the JONSWAP spectrum S_J that, in turn, is determined as follows:

$$S_J(\omega) = A_\gamma S_{PM}(\omega)\gamma^{exp\left(-0.5\left(\frac{\omega-\omega p}{\sigma\omega p}\right)\right)} \quad (2)$$

In eq. (2) ω is the wave circular frequency, $\omega_p = 2\pi/T_p$ is the spectral peak frequency depending on the wave peak period T_p, γ is the peak enhancement factor and σ denotes the spectral width parameter, equal to 0.07 if $\omega \leq \omega_p$ and 0.09 otherwise.

In eq. (2) A_γ is a normalizing factor, depending on the peak enhancement factor:

$$A_\gamma = 1 - 0.287ln(\gamma) \quad (3)$$

while S_{PM} denotes the Pierson-Moskowitz spectrum:

$$S_{PM}(\omega) = \frac{5}{16}H_s^2\omega_p^4\omega^{-5}exp\left(-\frac{5}{4}\left(\frac{\omega}{\omega_p}\right)^{-4}\right) \quad (4)$$

that, in turn, depends on the significant wave height H_s and the wave peak frequency ω_p. In absence of additional data, the wave peak period T_p is related to the wave mean period T_m by the following equation which is valid for γ ranging from 1 up to 7:

$$\frac{T_m}{T_p} = a + b\gamma + c\gamma^2 + d\gamma^3 \quad (4)$$

with a=0.7303, b=0.04936, c=-0.006556 and d=0.000361 [9]. After assessing the combined wind sea and swell spectrum, the random wave elevation is determined by the following equation (5), based on the superposition of N wave components, each one with circular frequency ω_i and random phase φ_i:

$$\varsigma(t) = \sum_{i=1}^{N} \sqrt{2S(\omega_i)\Delta\omega_i} cos(\omega_i t + \varphi_i) \quad (5)$$

where $\Delta\omega_i$ denotes the circular frequency interval between two subsequent wave components.

III. SPECTRUM ESTIMATION

Spectrum estimation is one of the most effective and amply used approaches for extracting the useful information from a time-series record, in the experimental investigation of a dynamic phenomenon [10]. Due to its complexity, a considerable literature has been developed along the years on the theoretical aspects of this estimation process [11], and efforts have also been put in addressing its application in specific investigation areas. In the case of sea wave monitoring, based on previous experience [7-8], in this study, two methods have been mainly considered, namely Welch's (averaged modified periodogram) and Thomson's (multi-taper method).

In Welch' method the acquired data record of duration T in segments of duration T_0, with partial overlap, typically from 20% to 50%. Each segment is pre-treated by tapering with a smooth window, to reduce spectral leakage and the periodogram (the square of the Discrete Fourier Transform) is calculated. The final estimate is obtained by averaging over segments. For a given overall duration T, the quality of the result depends upon the choice of the taper (the shape of the time window) and the duration T_0 of the segments. The combination of the window and of T_0 determines the effective bandwidth of the analyser, according to $\Delta f_e = \alpha_w T_0^{-1}$. It should be noticed that the greater Δf_e is, the lower spectral resolution is. On the other hand the variance of the estimate is proportional to the ratio T_0/T. Therefore, a trade-off is required between the conflicting needs of having a good time resolution and a small variance.

The basic idea of Thomson's method is to taper the overall data sequence with different tapers, each able to highlight different features of the signal, also accounting, in a way, to phase information. A typical choice for the taper is the discrete prolate spheroidal sequences, which have optimal properties for preventing spectral leakage. Here the main analysis parameter is usually denoted by W, which constitutes the (semi)bandwidth of the analyser. Again a trade-off is required between spectral resolution, which requires a small W, and variance, which decreases when W increases. Yet for optimal choices of analysis parameters, the results from the two estimators may be different, since the two approaches are quite different.

IV. WAVE SPECTRUM FITTING

The sea state parameters, namely the significant wave height H_s, the wave peak period T_p and the peak enhancement factor γ, are determined by the Nonlinear Least Square Method (NLSM), embodied by Rossi et al. [7-8] and purposely modified to fit double peak wave spectra, obtained by combined wind sea and swell components. The fitted wave spectrum is assessed by a two-step procedure, as detailed in the following:

(i) The peak frequencies, corresponding to the swell and wind wave components, are preliminarily detected, as they correspond to the relative maxima of the smoothed estimated spectrum.

(ii) The remaining spectral parameters, namely the significant wave height and the peak enhancement factor of the two components, are obtained by the NLSM, based on the iterative trust-region-reflective algorithm and the interior-reflective Newton method [12]. Particularly, it allows detecting the unknown parameters by iteratively solving a large set of linear equations by the method of the preconditioned conjugate gradients.

The parameters of the bimodal spectrum can be accurately detected if the peak frequencies of the wind sea and swell components are far enough to assure that the two spectral components are separated for practical purposes.

V. NUMERICAL APPLICATION

The numerical procedure, outlined in Sections IV and V, is applied to random wave elevation time histories obtained by the bimodal spectrum having the main data outlined in Table 1 and depicted in Figure 1. The time series have been obtained using eq. (5) using a circular frequency interval $\Delta\omega_i$ equal to 0.001 rad/s. Besides, two different time durations, are analysed in order to investigate the incidence of the sample length on the reliability of the resembled wave spectra.

TABLE I. INPUT BIMODAL SPECTRUM

Parameter	Method	
	Wind wave	Swell
H_s (m)	3.00	2.00
T_m (s)	12.00	20.00
T_p (s)	15.51	22.77
γ (---)	1.00	7.00

Particularly, two random wave records, having a duration of 600 and 3600 s respectively, have been generated at 10 Hz sampling frequency. The two random wave signals are analysed by the Multi-Taper Thomson (MT) and Welch (W) methods, outlined in Section III. Hence, Figures 2.1 and 2.2 provide the estimated spectrum by the MT method, with reference to the short (600s) and long (3600s) time durations, respectively. Similarly, Figures 3.1 and 3.2

provide the wave spectra estimated by the Welch method. Based on current results, the estimated spectra, based on the short time duration, are slightly poor, while the quality of the resembled spectra, combined with the long-time duration, is very good.

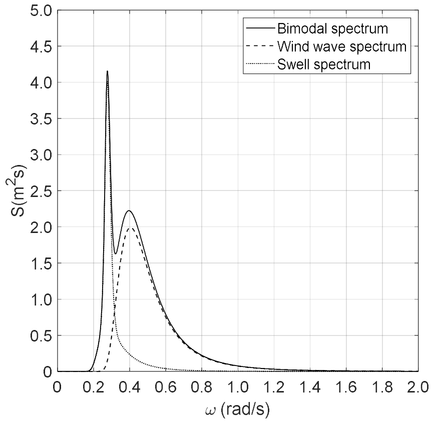

Fig 1. Bimodal wave spectrum

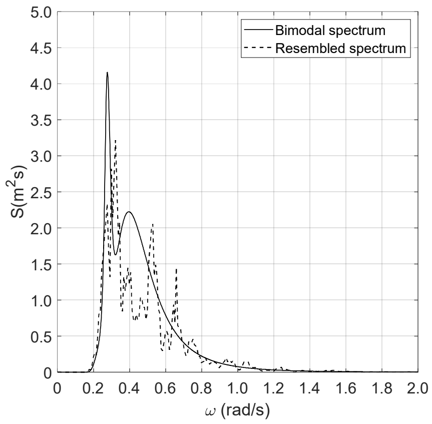

Fig 2.1 Resembled spectrum - MT method – 600 s

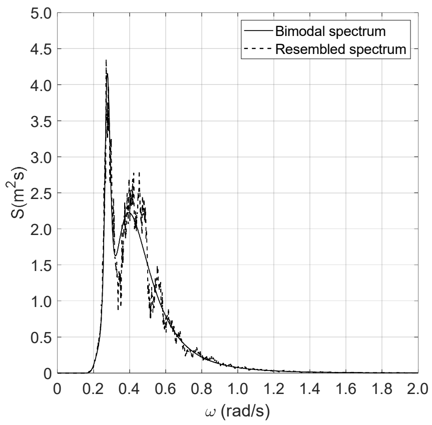

Fig 2.2 Resembled spectrum - MT method – 3600 s

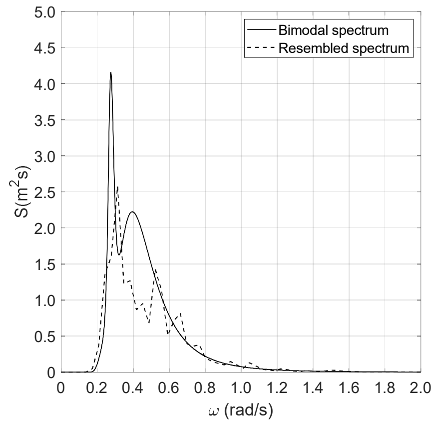

Fig 3.1 Resembled spectrum - W method – 600 s

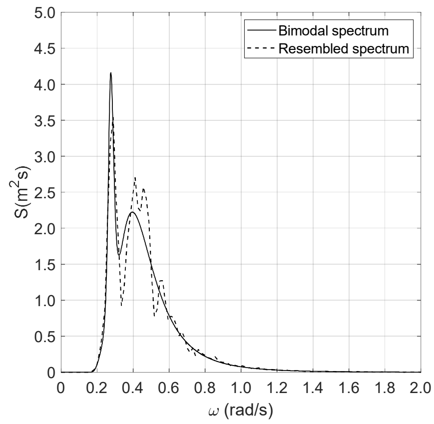

Fig 3.2 Resembled spectrum - W method – 3600 s

The main parameters of the resembled spectra, based on 1-hour wave history, are listed in Tables II and III, while the fitted spectra are plotted in Figures 4.1 and 4.2 in order to carry out a comparative analysis with the reference bimodal spectrum.

TABLE II. FITTED SPECTRUM – MT METHOD – 3600 S

Parameter	Fitted spectrum		% Difference	
	Wind wave	Swell	Wind wave	Swell
H_s (m)	3.01	2.04	0.33	2.00
T_p (s)	15.31	22.52	-1.29	-1.10
γ (---)	1.01	5.35	1.00	-23.57

TABLE III. FITTED SPECTRUM – W METHOD – 3600 S

Parameter	Fitted spectrum		% Difference	
	Wind wave	Swell	Wind wave	Swell
H_s (m)	2.94	2.17	-2.00	8.50
T_p (s)	14.71	21.68	-5.16	-4.79
γ (---)	1.00	4.00	0.00	-42.86

Based on current results, both methods allow efficiently resembling the main parameters of the bimodal spectrum, apart from the peak enhancement factor of the swell component which is in both cases underestimated, probably due to the low range of the swell spectrum. Besides, by the percentage differences between the fitted and reference parameters of the bimdoal spectrum, the MT method seems to be slightly superior if compared with the W one.

VI. CONCLUSIONS

The paper focused on the application of different spectrum estimation methods to resemble the main parameters of a bimodal wave spectrum obtained by the superposition of wind wave and swell components. Two random wave time histories, with 10-min and 1-hour duration, have been

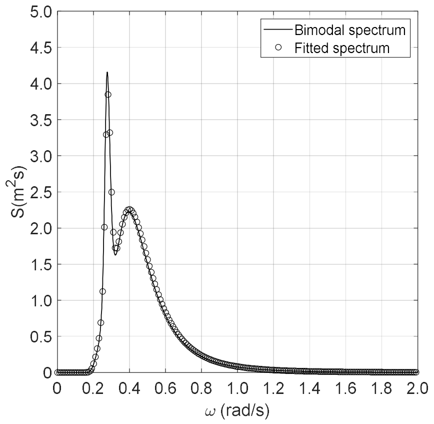

Fig 4.1 Fittied MT spectrum – 3600 s

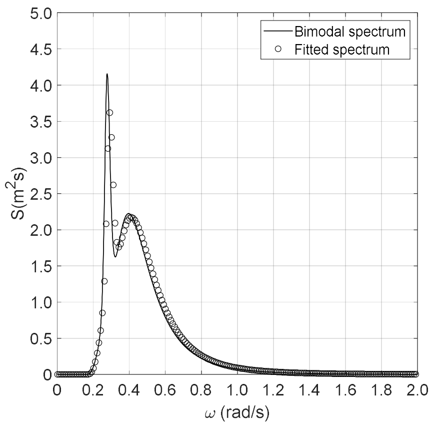

Fig 4.2 Fittied W spectrum – 3600 s

generated from a theoretical bimodal spectrum and subsequently anlyzed by the Multitaper Thomson and Welch methods. Based on current results, it is gathered that the time duration plays a fundamental role in terms of reliability of the resemling procedure. In this respect, the short time duration, corresponding to a 10-min wave time history, is not sufficient to estimate the input wave spectrum with a sufficient accuracy. On the contrary both specturm estimation methods provide a reliabile estimate of the input bimodal spectrum, combined with the 1-hour wave record.

Besides, the two-step fitting procedure, outlined in Section IV and based on the Nonlinear Least Square Method, seems to provide a reliable assessment of the main spectrum parameters, namely the significant wave height, the wave peak period and the peak enhancement factor. In this respect, the Multitaper Thomson method seems to be the most promising technique to estimate and resemble bimodal wave spectra. Nevertheless, this outcome needs to be further investigated by means of parametric study devoted to analyze and combine different wind wave and swell spectra.

REFERENCES

[1] E.P.D. Mansard, E.R. Funke, “On the fitting of JONSWAP spectra to measured sea states”, Proceedings of the 22nd Conference on Coastal Engineering, Delft, The Netherlands, 1990.
[2] E.P.D. Mansard, E.R. Funke, “On the fitting of parametric models to measured wave spectra”, Proceedings of the 2nd International Symposium on Waves and Coastal Engineering, Hannover, Germany, 1988.
[3] J.A. Battjes, G.P. van Vledder, “Verification of Kimura’s theory for wave group statistics”, Proceedings of the 19th International Conference on Coastal Engineering, Houston, USA, 1984.
[4] V. Piscopo, A. Scamardella, “Passenger ship seakeeping optimization by the Overall Motion Sickness Incidence”, Ocean Engineering 76, 2014, pp. 86-97.
[5] S. Pennino, V. Piscopo, A. Scamardella, “Incidence of Fourier transform parameters on sea spectrum resampling from wave time history”, Proceedings of the 2018 IEEE International Workshop on Metrology for the Sea, pp. 227-231.
[6] V. Piscopo, A. Scamardella, S. Gaglione “A new wave spectrum resembling procedure based on ship motion analysis”, Ocean Engineering 201, 2020, 107137
[7] G.B. Rossi, F. Crenna, V. Piscopo, A. Scamardella, “Data processing for the accurate evaluation of sea-wave parameters”, Proceedings of the 2019 IEEE International Workshop on Metrology for the Sea, pp. 75-79.
[8] G.B. Rossi, F. Crenna, V. Piscopo, A. Scamardella, “Comparison of Spectrum Estimation Methods for the Accurate Evaluation of Sea State Parameters”, Sensors 20(5), 2020, pp. 1-15.
[9] Det Norske Veritas, “Environmental conditions and environmental loads”, Recommended Practice DNV-RP-C205, October 2010.

[10] G. B. Rossi, “Toward a unified framework for static and dynamic measurements”, Proc. IEEE Int. Instrum. Meas. Technol. Conf. May, 2015, pp 1516-1521.

[11] D. B. Percival, A. T. Walden, Spectral Analysis for univariate time series, Cambridge University Press, Cambridge, UK, 2020.

[12] T.F. Coleman, Y. Li, “Trust Region Approach for Nonlinear Minimization Subject to Bounds”, SIAM Journal on Optimization 6, 1996, pp. 418-445.

2020 IMEKO TC-19 International Workshop on
Metrology for the Sea
Naples, Italy, October 5-7, 2020

DANAE: a denoising autoencoder for underwater attitude estimation

Paolo Russo[1], Fabiana Di Ciaccio[2], Salvatore Troisi[2]

[1] *University of Rome La Sapienza, via Ariosto 25, paolo.russo@diag.uniroma1.it*
[2] *Parthenope University of Naples, Centro Direzionale Isola C4, (fabiana.diciaccio, salvatore.troisi)@uniparthenope.it*

***Abstract* – One of the main issues for underwater robots navigation is their accurate positioning, which heavily depends on the orientation estimation phase. The systems employed to this scope are affected by different noise typologies, mainly related to the sensors and to the irregular noise of the underwater environment. Filtering algorithms can reduce their effect if opportunely configured, but this process usually requires fine techniques and time. In this paper we propose DANAE, a deep Denoising AutoeNcoder for Attitude Estimation which works on Kalman filter IMU/AHRS data integration with the aim of reducing any kind of noise, independently of its nature. This deep learning-based architecture showed to be robust and reliable, significantly improving the Kalman filter results. Further tests could make this method suitable for real- time applications on navigation tasks.**

I INTRODUCTION

Localization is one of the most important tasks for unmanned robots, especially in underwater environments. Being a highly unstructured and GPS-denied environment, other than characterized by different noise sources and by the absence of man- made landmarks, the underwater setting provides more challenges for the orientation estimation.

In a typical configuration, the Euler angles representing the vehicle attitude (roll, pitch, and yaw) are obtained through the integration of raw data acquired by the sensors embedded into an Inertial Measurement Unit (IMU), or in the more cost-effective Attitude and Heading Reference System (AHRS).

One of the most successful methods to perform this elaboration is based on the Kalman filter [1] (KF) , in its linear and non linear versions [2]. Although known as the perfect estimator under some assumptions, the estimation provided by the KF strongly depends on a good knowledge of the error covariance matrices describing the noise affecting the system. Moreover, the on-line computation of these matrices is often required for anytime-varying or nonlinear system, squaring the number of necessary updating step at each time. Finally, the procedure employed to accurately fine tune the filter parameters is known to be unintuitive,

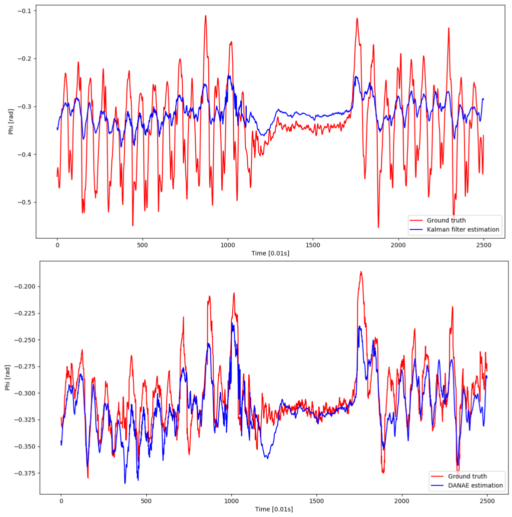

Fig. 1. KF (upside) and DANAE (downside) roll angle estimation compared to the ground truth. This experiment is made on a subsection of the slow walking set of OxIOD.

requiring specific settings for different scenarios [3].

In order to overcome these issues, we propose a deep learning-based approach which aims to attenuate any source of error from the attitude estimation of a KF. The strength of our proposed method stands in the ability of acting as a full-noise compensation model for both noise and bias errors, without the need to separately process each influencing factor.

Extensive tests performed on two different datasets to evaluate Euler angles show the power of our approach, with sensible improvement of both mean squared error and max deviation w.r.t. ground truth data.

The remainder of this study is organized as follows: Section II presents a brief literature review for Kalman-based algorithms and deep learning techniques applied on similar tasks. Section III introduces the concepts of KF and of deep denoising autoencoder, followed by a concise description of our method. In Section IV the datasets used for the experiments are described. Section V illustrates the details of our architecture and the hyper parameters chosen for the training. Section VI analyzes the experiment results through the use of standard metrics, concluding with Section VII which contains some final considerations on the topic, including future possible improvements.

II RELATED WORKS

The use of KF in robotic applications is ubiquitous. [4] proposed an effective Adaptive Kalman Filter (AKF) which is able to exploit low-cost AHRS for efficient attitude estimation under various dynamic conditions, with an interesting underwater application developed by [5].

Non-linear implementations of the filter include for example [6], which gets the robot pose by fusing camera and inertial data with an Extended Kalman Filter (EKF), and [7] where the same task is accomplished using an Unscented Kalman Filter (UKF).

Beside the critical task of sensor fusions, the estimation of biases is also crucial for an effective navigation system [8], as well as the detection of sensor noises [9].

The rise of Deep Learning has radically changed fields like Computer Vision and Natural Language Processing. Convolutional Neural Networks (CNN) produce state of the art accuracy on classification [10] and detection [11] tasks. Autoencoders is another successful deep architecture where the aim is to reconstruct a signal by learning a latent representation from a set of data. Since their introduction [12], denoising autoencoders (DAE) have been used for a broad number of tasks like medical images improvement [13] and speech enhancement [14]. To the best of our knowledge, DANAE is the first application of denoising autoencoder on attitude estimation.

III METHOD

In this section we provide some basic concepts on linear KF and autoencoders followed by a brief overview of our method. However it should be emphasized that DANAE is filter agnostic and can be used seamlessly on non-linear KF (EKF, UKF) as well as any other type of filter able to perform attitude estimation.

A. *Kalman filter*

KF is a widely used algorithm for state estimation of dynamic systems since it is able to minimize the related variance under some perfect model assumptions.

The system behaviour in a discrete time setting can be described by a state equation 1 and a measurement equation 2:

$$x_t = Ax_{t-1} + Bu_{t-1} + v_{t-1} \tag{1}$$

$$y_t = Cx_t + w_t \tag{2}$$

where x_t is the state vector to be predicted, x_{t-1} and u_{t-1} are the state and the input vectors at the previous time step and y_t represents the measurement vector. A and B are the system matrices and C is the measurement matrix. The vectors v_{t-1} and w_t are respectively associated with the additive process noise and the measurement noise, assumed to be zero mean Gaussian processes. The final estimate is obtained by a first prediction step (3, 4) followed by the update phase (5, 6, 7, 8):

$$x'_t = Ax_{t-1} + Bu_{t-1} \tag{3}$$

$$P'_t = AP_{t-1}A^T + Q \tag{4}$$

$$K_t = P'_t C^T (CP'_t C^T + R)^{-1} \tag{5}$$

$$x_t = x'_t + K_t(y_t - Cx'_t) \tag{6}$$

$$P_t = (I - K_t C)P'_t \tag{7}$$

The a-posteriori state estimate x_t is obtained as a linear combination of the a-priori estimate x'_t and a weighted difference between the actual and the predicted measurements called residual (see equation 6); the Kalman gain (K in Eq. 5) minimizes the a-posteriori error covariance (P in Eq. 7), initially set by the user. Finally, Q and R are the covariance matrices of the process and of the measurement noise. Q models the dynamics uncertainty, while R represents the sensors internal noises. These matrices heavily affect the final filter performance, thus a tricky tuning process is necessary to correctly estimate noises statistics. A proper fine-tuning is also important for sensors biases estimation; however, even in this case traditional approaches based on the KF suffer from implementation complexity and require non-intuitive tuning procedures [15].

B. *Denoising autoencoder*

DAE is a deep convolutional model which is able to recover clean, undistorted output starting from partially corrupted data as input. In the original implementation, the input data is intentionally corrupted thorough a stochastic mapping:

$$\tilde{x} \sim q_D(\tilde{x}|x) \tag{8}$$

Then, the corrupted input is mapped into an hidden representation as in the case of a standard autoencoder:

$$h = f_\theta(\tilde{x}) = s(W\tilde{x} + b) \tag{9}$$

Finally, the hidden representation is mapped back to a reconstructed signal:

$$\hat{x} = g_{\theta'}(h) \tag{10}$$

During the training procedure, the output signal is compared with a reference signal in order to minimize the L2 reconstruction error:

$$\mathcal{L}(x - \hat{x}) = ||x - \hat{x}||^2 = ||x - s(W\tilde{x} + b)||^2 \tag{11}$$

In our implementation, DANAE takes as input the noisy angles prediction performed by the KF and as reference signal the ground truth angles provided by the dataset. For this reason, we underline that our method is able to remove both stochastic errors (e.g. electromagnetic- and thermo-mechanical- related ones), and systematic errors (due for example to sensors misalignment).

IV DATASETS

DANAE has been developed and tested on the Oxford Inertial Odometry Dataset (OxIOD) [16] and on the Underwater Caves sonar dataset (to which we will refer as UCS) [17].

OxIOD has been chosen for its accurate ground truth measurements over big heterogeneous settings. Developed for deep learning-based inertial-odometry navigation, OxIOD provides 158 sequences (for a total of 42.587 km) of inertial and magnetic field data acquired from low-cost sensors. Five users made indoor and outdoor acquisitions while normally walking with phone in hand, pocket and handbag and slowly walking, running and performing mixed motion modes. Different smartphones were used to acquire data, but the major part was collected by an iPhone 7 plus equipped with an InvenSense ICM20600. A Vicon motion capture system was used to get the ground truth with a precision down to 0.5 mm.

The UCS dataset is collected by a Sparus AUV navigating in the underwater cave complex "Coves de Cala Viuda" in Spain. The vehicle explored two tunnels, closing a 500m-long path at a depth of approximately 20m. Among the equipped sensors (e.g. DVL, sonar, etc), a standard low cost Xsens MTi AHRS and an Analog Devices ADIS16480 are mounted. The latter is a 10 DOF MEMS which provides more accurate raw sensors measurements and dynamic orientation outputs (obtained by their EKF fusion). The elaboration of images containing six traffic cones placed on the seabed allowed the relative positioning of the vehicle. Unfortunately, the ground truth thus obtained is synchronized with the low-rate camera acquisitions, making the comparison with the high-rate IMU measurements inconsistent. For this reason, we assumed that the orientation directly provided by the AHRS could at first glance substitute the true ground truth. Despite not being a proper solution to the issue, this choice allowed us to understand the ability of DANAE to work in a true underwater scenario with its unique features.

V EXPERIMENTAL SETUP

Some details on the experiments will be given in this section. Both datasets have been split in a training and test set: in the case of OxIOD, for each setting we used the run 1 as test set, leaving all the other sessions as training set. UCS provides instead a single file for each system containing all the measurements stored during the entire survey. We then decided to split the data, using the first 80% to train DANAE and the remaining 20% to test the performance.

Table 1. OxIO Dataset: performance of KF and DANAE vs GT.

KF	ϕ	θ	ψ
Mean dev. $[rad]$	0.0661	0.0483	1.9518
Max dev. $[rad]$	0.2929	0.2134	9.0145
RMSE $[rad]$	0.0815	0.0600	2.4000
DANAE	ϕ	θ	ψ
Mean dev. $[rad]$	0.0224	0.0157	0.7392
Max dev. $[rad]$	0.1382	0.1082	5.7907
RMSE $[rad]$	0.0282	0.0196	1.3194

Three main phases can be distinguished: during the first one, the inertial and magnetic field data are integrated with a linear KF, providing the estimation of the three Euler angles. In the second phase, these outputs are fed to the DANAE module for training, while on the third phase tests are performed using a pipeline of KF and DANAE. All the code has been developed in Python 3.6.9 running on Ubuntu 18.04, with the help of Pytorch framework.

A. *KF initialization*

We implemented the filter in its most basic formulation following the equations from 3 to 7. The covariance matrices P, Q and R have been initialized as identity matrix, and no tuning has been done with relation to both the internal system and the measurements noises. The elaboration of accelerometer and magnetometer raw data provided the measurements vector (see Cx_t in Equation2), while the gyroscope-derived angles have been set as external input (see Bu_{t-1} in Equation1).

B. *Autoencoder settings*

DANAE can work with any input signal length; here, we present the version working with a length of 20. The encoder part of DANAE is made of four *dilated* 1D convolutions which bring the original 20-length signal to an hidden representation made of 128 features. The decoder part transforms this representation back to a 20-length vector by alternating three transposed-dilated 1D convolutions to four standard ones. While the transposed convolution is exploited to increase the input resolution back to the original size, the i_{th} standard convolution is working on the sum of the i_{th} encoder and the i_{th} decoder outputs. This approach, loosely inspired by the WaveNet architecture, is able to enforce additional constrains to the encoder/decoder pipeline, enabling a more faithful signal reconstruction. All these layers have 128 $3x3$ kernels with an appropriate dilation value depending on the layer depth, while stride and padding have been fixed to 1. The Adam optimizer chosen for the training has been set with a fixed learning rate of 0.002 with a batch size of 16. The number of epochs has been set to 100 for UCS and to 1 for each set of OxIOD. Additional experiments performed with different hyper-parameters values did not produce any sensible difference in the final accuracy, demonstrating the robustness of our approach.

VI RESULTS

To numerically evaluate the filters performances, simple estimator as mean deviation, maximum deviation and root mean square error have been calculated with respect to the ground truth values.

For the sake of brevity, we report the results of one of the experiments performed on OxIOD, referring to the full paper for a more detailed analysis. As can be seen from Table 1, DANAE is able to considerably improve the performance on all the estimators, with a mean reduction of the RMSE equal to 63%. Futhermore, even though the strong noise affecting the KF predictions, DANAE exhibits a sensible lowering of the elongations for all the angles. Figure 1 shows the comparison between the KF and DANAE estimations for the angle ϕ w.r.t. the ground truth. A similar behaviour is found also in the UCS experiments: DANAE output faithfully resembles the reference signal for all the estimated angles, with a final mean reduction of the RMSE equal to 54%.

VII CONCLUSIONS

This paper propose DANAE, the first denoising autoencoder model for attitude estimation. Our noise and filter agnostic architecture is able to compensate any kind of error with respect to a reference angle, boosting the KF prediction for both the considered datasets. Further experiments will be performed on non-linear filters (EKF and UKF), and deployments for on-line underwater applications will be investigated.

REFERENCES

[1] R. E. Kalman, "A new approach to linear filtering and prediction problems," *Transactions of the ASME–Journal of Basic Engineering*, vol. 82, no. Series D, pp. 35–45, 1960.

[2] M. St-Pierre and D. Gingras, "Comparison between the unscented kalman filter and the extended kalman filter for the position estimation module of an integrated navigation information system," in *IEEE Intelligent Vehicles Symposium, 2004*, pp. 831–835, IEEE, 2004.

[3] V. M. Tereshkov, "An intuitive approach to inertial sensor bias estimation," *International Journal of Navigation and Observation*, vol. 2013, 2013.

[4] W. Li and J. Wang, "Effective adaptive kalman filter for mems-imu/magnetometers integrated attitude and heading reference systems," *The Journal of Navigation*, vol. 66, no. 1, pp. 99–113, 2013.

[5] B. Allotta, A. Caiti, R. Costanzi, F. Fanelli, D. Fenucci, E. Meli, and A. Ridolfi, "A new auv navigation system exploiting unscented kalman filter," *Ocean Engineering*, vol. 113, pp. 121–132, 2016.

[6] M. B. Alatise and G. P. Hancke, "Pose estimation of a mobile robot based on fusion of imu data and vision data using an extended kalman filter," *Sensors*, vol. 17, no. 10, p. 2164, 2017.

[7] H. G. De Marina, F. J. Pereda, J. M. Giron-Sierra, and F. Espinosa, "Uav attitude estimation using unscented kalman filter and triad," *IEEE Transactions on Industrial Electronics*, vol. 59, no. 11, pp. 4465–4474, 2011.

[8] E. Taghavi, R. Tharmarasa, T. Kirubarajan, Y. Bar-Shalom, and M. Mcdonald, "A practical bias estimation algorithm for multisensor-multitarget tracking," *IEEE Transactions on Aerospace and Electronic Systems*, vol. 52, no. 1, pp. 2–19, 2016.

[9] K. Nirmal, A. Sreejith, J. Mathew, M. Sarpotdar, A. Suresh, A. Prakash, M. Safonova, and J. Murthy, "Noise modeling and analysis of an imu-based attitude sensor: improvement of performance by filtering and sensor fusion," in *Advances in Optical and Mechanical Technologies for Telescopes and Instrumentation II*, vol. 9912, p. 99126W, International Society for Optics and Photonics, 2016.

[10] K. He, X. Zhang, S. Ren, and J. Sun, "Deep residual learning for image recognition," in *Proceedings of the IEEE conference on computer vision and pattern recognition*, pp. 770–778, 2016.

[11] K. He, G. Gkioxari, P. Dollár, and R. Girshick, "Mask r-cnn," in *Proceedings of the IEEE international conference on computer vision*, pp. 2961–2969, 2017.

[12] P. Vincent, H. Larochelle, Y. Bengio, and P.-A. Manzagol, "Extracting and composing robust features with denoising autoencoders," in *Proceedings of the 25th international conference on Machine learning*, pp. 1096–1103, 2008.

[13] L. Gondara, "Medical image denoising using convolutional denoising autoencoders," in *2016 IEEE 16th International Conference on Data Mining Workshops (ICDMW)*, pp. 241–246, IEEE, 2016.

[14] X. Lu, Y. Tsao, S. Matsuda, and C. Hori, "Speech enhancement based on deep denoising autoencoder.," in *Interspeech*, pp. 436–440, 2013.

[15] V. M. Tereshkov, "A simple observer for gyro and accelerometer biases in land navigation systems," *The Journal of Navigation*, vol. 68, no. 4, pp. 635–645, 2015.

[16] C. Chen, P. Zhao, C. X. Lu, W. Wang, A. Markham, and N. Trigoni, "Oxiod: The dataset for deep inertial odometry," *arXiv preprint arXiv:1809.07491*, 2018.

[17] A. Mallios, E. Vidal, R. Campos, and M. Carreras, "Underwater caves sonar data set," *The International Journal of Robotics Research*, vol. 36, no. 12, pp. 1247–1251, 2017.

2020 IMEKO TC-19 International Workshop on
Metrology for the Sea
Naples, Italy, October 5-7, 2020

Kriging interpolation of bathymetric data for 3D model of the Bay of Pozzuoli (Italy)

Emanuele Alcars[1], Claudio Parente[1], Andrea Vallario[1]

[1] *Department of Sciences and Technologies, Centro Direzionale di Napoli, Isola C4, 80143 Naples (Italy), (emanuele.alcaras, claudio.parente, andrea.vallario)@uniparthenope.it*

***Abstract* – Bathymetric data acquired by a single-bam echo-sounder, as well as those derived by a navigational chart, require interpolation procedure to pass from cloud point dataset to continuous tridimensional representation. Among different algorithms available in GIS software, Kriging interpolators are very powerful tools to process bathymetric data. This paper aims to analyze the accuracy levels that can be reached using Kriging. Bathymetric information included in two Electronic Navigational Charts (ENCs) of the Bay of Pozzuoli (nominal scale 1:30.000) is used for digital 3D model of this area. Interpolation processes are performed in GIS environment (software: ArcGIS 10.3.1, including the extension Geostatistical Analyst, by ESRI); the achieved results are analyzed by varying the choice of the mathematic function for semi-variogram. The experiments carried out in this study demonstrate how the careful choice of the semi-variogram model can help to increase the accuracy of the interpolation process.**

I. INTRODUCTION

Hydrographic survey permits to acquire in water depth estimation that is fundamental for many purposes, first of all in ship navigation: by providing possible paths that a vessel can take, it allows to chart safe routes that do not cross any dangerous terrain. Another important purpose of hydrography is in the field of dredging, the activity concerning the removal of weeds, mud, and rocks at the seabed. The knowledge of the seabed is useful in determining shorelines that extend around a coast, suitable to support studies on the effect of water bodies on land and to predict possible flooding zones and to suggest measures to effectively counter this [1].

Hydrographic survey can be carried out by using different techniques. Single beam sonar (SBS) and multi beam sonar (MBS) determine the depth of any waterbody by using sound beams and measuring the time lag between transmitting and receiving a signal that travels through the water, springs back the seafloor, and returns to the sounder [2]. SBS is a less expansive system that MBS, but provides much lower spatial resolution [3]. A good level of information about seabed morphology can be extract by multispectral satellite images, even if only in shallow water (depths less than 20 meters) [4].

The results of bathymetric survey are used for nautical charts that provide seabed morphology through depth points and contours. Available in digital form (raster or vector), nautical charts are legible and manageable by information systems supporting ship navigation, i.e. Electronic Charting System (ECS) and Electronic Chart Display and Information System (ECDIS) [5].

Regardless of the technique with which they are obtained and the source from which they are extracted, data concerning seabed morphology can be used to produce bathymetric model that, according to International Hydrographic Organization (IHO), can be defined, as ‘‘a digital representation of the topography (bathymetry) of the seafloor by coordinates and depths’’ [6].

When a point cloud dataset is available, i.e. single beam data or depth data derived from a nautical chart, an interpolation process is necessary to generate a 3D model: starting from irregular spaced measured points, the depths in unsampled areas must be calculated. Several interpolation methods are available in GIS software, but in many cases, the most performing ones result Kriging interpolators, i.e. Ordinary Kriging, Universal Kriging and Simple Kriging [2]. They are not be applied in automatic way, but require the supervision of the user who sets specific parameters.

The aim of this article is to demonstrate that the level of accuracy that can be achieved depends crucially on the choice of one of these parameters, that is the mathematical model of the semi-variogram, a graphical representation of the spatial correlation between the measurement points.

II. DATA AND METHODS

In order to pursue an empirical study, we have identified the Bay of Pozzuoli as a study area subject to 3D modeling of the seabed. Located in the northwestern end of the Gulf of Naples in the Tyrrhenian Sea, it lies west of Naples and is dominated by the port of Pozzuoli. The study area and its location in the Gulf of Naples are reported in Fig. 1.

Fig. 1. The Bay of Pozzuoli (lower) and its location in the Gulf of Naples (upper).

Depth data are extracted from two Electronic Navigational Charts (ENCs) produced by the by Istituto Idrografico della Marina Militare (IIMM), in scale 1:30.000, identified as n° 129 and n° 130. The original files are formed in accordance to the official standards established by the International Hydrographic Organization (S-57 IHO) [6]. They are transformed in shp for using them in ArcGIS 10.3.1 by ESRI. ENCs are georeferred to WGS84 geodetic datum and for this study are projected in the Universal Transverse of Mercator (UTM)/WGS84 Zone 33 N. ENC depth points and contour lines in the Bay of Pozzuoli and around areas are shown in Fig. 2.

Firstly, we group the vertices of contour lines and the depth points in one shape file; formerly we select from them only ones that fall in the area shown in Fig. 3. This area extends within the following UTM/WGS84 plane coordinates - 33T zone: E_1 = 423,500 m, E_2 = 429,000 m, N_1 = 4,514,000 m, N_2 = 4,518,500 m. Depth values range between -10 m and -115 m. Those points are used as dataset for the application of Kriging interpolation methods available in Geostatistical Analyst [7], an extension included in ArcGIS software [8].

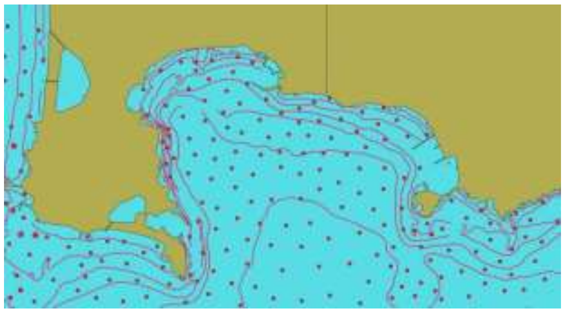

Fig. 2. ENC depth information in the Bay of Pozzuoli and around area.

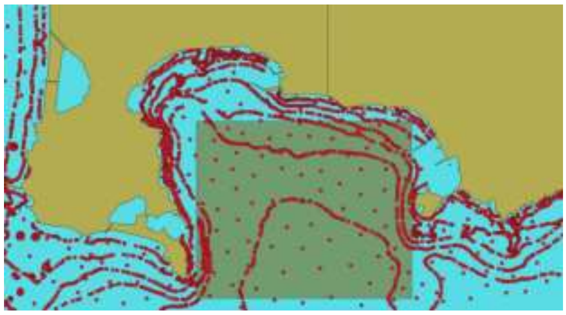

Fig. 3. The selected point dataset (in the green rectangle) submitted to kriging interpolation.

Kriging is founded on the first law of Geography introduced by Waldo R. Tobler's in 1969: "everything is related to everything else, but near things are more related than distant things" [9]. In other words, things closer together are more similar than things further away. Unlike to deterministic methods, Kriging applies the statistical model, which includes the spatial correlation between sampled points, and uses it to estimate the value at an unknown point: the spatial arrangement among the measured points, rather than a presumed model of spatial distribution, is used for interpolation; it also allows estimations of the uncertainty neighbouring each interpolated value [10].

The spatial correlation between the measurement points can be computed using the semi-variance formula:

$$\gamma = \frac{1}{2N(h)} \sum_{i=1}^{N(h)} [Z(u_i) - Z(u_i + h)]^2 \qquad (1)$$

Where:
N(h) is the number of pairs of measurement points with distance h apart;
$z(u_i)$ is the value at location u_i;
$z(u_i+h)$ is the value at location u_i+h.

The semi-variance calculated between each pair of points in the sampled data is plotted against the distance and the resulting graphical representation is called "variogram" or, since half the variance is plotted, "semi-variogram".

To facilitate the procedure and make it faster, the pairs are grouped into lag bins, e.g. the semi-variance is calculated for all pairs of points that present distance between 10 meters and 20 meters.

Mathematical models can be used to substitute the empirical ones, fitting the data in the best way, i.e. linear, gaussian, exponential, stable, etc. This substitution permits to introduce in the kriging process semi-variogram values for lag distances that are not used in the empirical semi-variogram [11].

Cross validation allows t to define the accuracy level of predictive values. Particularly, leave-one-out (LOO) method is currently adopted: each point is removed in turn from the dataset and the other points are used to estimate a value at the location of the removed point; finally, the performance is tested calculating the difference between the known value and estimated value in each removed point [12], [13], [14] .

III. RESULTS AND DISCUSSION

In this study, ordinary Kriging is applied to the chosen dataset, by varying mathematical semi-variogram models available in Geostatistical Analyst. In Fig. 4, two example of semi-variogram generated respectively by the Circular model (upper) and the Gaussian model (lower) tare shown.

LOO cross validation is used for each kriging application The statistical parameters (mininimum, maximum, mean, standard deviation and root mean square error) of all residuals for each semi-variogram mathematical model are calculated. Those parameters are shown in table 1.

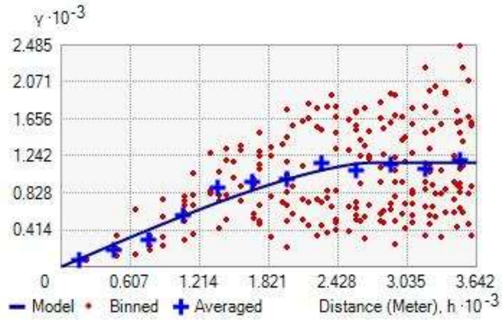

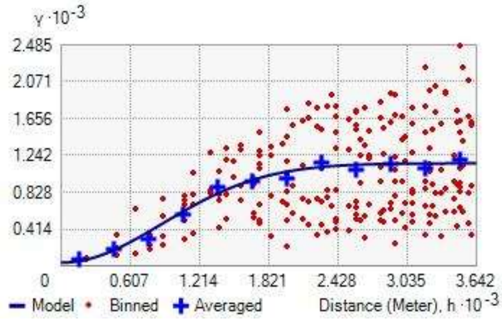

Fig. 4. Examples of semi-variograms applied to the used dataset, generated respectively by the Circular model (upper) and the Gaussian model (lower).

Table 1. Statistical terms of the residuals supplied by Cross validation for the ordinary kriging

model	min (m)	max (m)	mean (m)	s. d. (m)	rmse (m)
Gaussian	-14.72	11.98	-0.03	2.62	2.62
Circular	-18.79	14.43	0.09	2.01	2.01
Gaussian	-14.72	11.98	-0.03	2.62	2.62
Circular	-18.79	14.43	0.09	2.01	2.01
Expon.	-19.76	15.22	0.12	2.12	2.13
Spheric.	-18.82	14.50	0.09	2.01	2.01
Tetras.	-18.83	14.47	0.09	2.01	2.01
Pentas.	-18.86	14.48	0.09	2.01	2.01
Stable	-15.81	13.23	0.01	2.07	2.07
J-Bessel	-15.24	11.75	-0.04	2.72	2.72
K-Bessel	-14.99	13.58	0.00	2.18	2.18
Rational	-14.83	14.36	-0.02	1.84	1.84
Hole	-17.89	12.53	-0.06	3.24	3.24

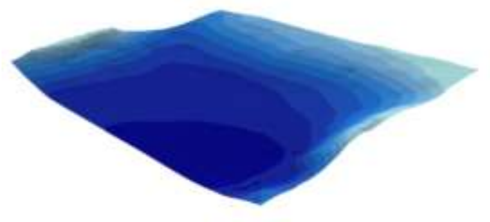

Fig. 5. 3D visualization of the most performing bathymetric model generated by ordinary kriging interpolator).

IV. CONCLUSIONS

Our research remarks the high performance of the Kriging interpolation and demonstrates the relevance of the choice of the mathematical model for the semi-variogram. As tested by using LOO cross validation, different levels of accuracy can be achieved in dependence of the function used to substitute the empirical semi-variogram, fitting the depth data in the best way. By analyzing residuals between measured and interpolated values of bathymetric depths, it is possible to identify the best performing 3D model of seabed in the study area.

REFERENCES

[1] A.Menon, "A Guide to Hydrographic Surveys", Marine Technology, Marine Insight, 2020.

[2] C.Parente, A.Vallario, "Interpolation of Single Beam Echo Sounder Data for 3D Bathymetric Model," International Journal of Advanced Computer Science and Applications, 2019, vol. 10, No 10, pp. 6-13.

[3] I.Parnum, J.Siwabessy, A.Gavrilov,M.Parsons, "A comparison of single beam and multibeam sonar systems in seafloor habitat mapping," Proc. 3rd Int. Conf. and Exhibition of Underwater Acoustic Measurements: Technologies & Results, Nafplion, Greece, 2009, June, pp. 155-162.

[4] C.Parente, M.Pepe, "Bathymetry from worldView-3 satellite data using radiometric band ratio," Acta Polytechnica, 2018, vol. 58, No 2, pp. 109-117.

[5] D.Brčić, S.Kos, S.Žuškin, Navigation with ECDIS: Choosing the proper secondary positioning source. TransNav: International Journal on Marine Navigation and Safety of Sea Transportation, 2015, 9.

[6] IHO, IHO transfer standard for digital hydrographic data - Edition 3.1 - November 2000, Special Publication No. 57, 2000, International Hydrographic Bureau, ONACO.

[7] ESRI, Geostatistical Analyst, ArcGIS 10.3- Help, Redlands, CA, USA https://desktop.arcgis.com/en/arcmap/latest/extensions/geostatistical-analyst/what-is-arcgis-geostatistical-analyst-.htm

[8] Esri, ArcGIS 10.3, Redlands, CA, USA www.esri.com/software/arcgis

[9] W.R.Tobler, "A computer movie simulating urban growth in the Detroit region," Economic geography, 1970, vol. 46, sup1, pp. 234-240.

[10] Columbia University Mailman School of Public Health, Kriging, Columbia University, 722 West 168th St. NY, NY 10032, https://www.mailman.columbia.edu/research/population-health-methods/kriging

[11] G.Bohling, "Introduction to geostatistics and variogram analysis," Kansas geological survey, 2005, vol. 1, pp. 1-20.

[12] G.E. Fasshauer, J.G. Zhang, "On choosing "optimal" shape parameters for RBF approximation," Numerical Algorithms, 2007, vol. 45 no. 1-4, pp. 345-368, https://dx.doi.org/10.1007/s11075-007-9072-8

[13] U.Falchi, C.Parente, G.Prezioso, "Global geoid adjustment on local area for GIS applications using GNSS permanent station coordinates," Geodesy and Cartography, 2018, Vol. 44, no. 3, pp. 80-88, , https://doi.org/10.3846/gac.2018.4356

[14] E.Alcaras, L.Carnevale, C.Parente, "Interpolating single-beam data for sea bottom GIS modelling," International Journal of Emerging Trends in Engineering Research, 2020, vol. 8, No 2, pp. 591-597. https://doi.org/10.30534/ijeter/2020/50822020

8

Special Track
Measuring the sea: the contribution of marine geological research

Marine geological researches achieved major results in the last decades thanks to remarkable technological advancements, particularly for remote-sensing observations (ship- or ROV/AUV-based) and seafloor sampling techniques, which presently allow for the recovery of undisturbed sediments sections at the seafloor. The field of application of such technologies is wide, ranging from thematic map compilation, to geological-geophysical-geochemical observations leading to natural and anthropic impact and risk mitigation, as well as for the preservation of cultural heritages. The common requirement of these studies is the need for high accuracy and resolution in carrying out measurements.

2020 IMEKO TC-19 International Workshop on
Metrology for the Sea
Naples, Italy, October 5-7, 2020

An updated reporting of rhodolith deposits in the offshore of Ischia (Gulf of Naples, Italy)

Gemma Aiello[1]

[1] *CNR-ISMAR of Naples, Calata Porta di Massa Porto di Napoli 80133 Naples Italy, gemma.aiello@cnr.it; gemmaiello@virgilio.it*

***Abstract* – In this work, the occurrence of rhodolith deposits on the sea bottom of the Ischia offshore is highlighted on the base of sedimentological data coming from samples collected during the marine geological mapping of the Ischia Island. These sea bottom samples are rich in bioclasts mainly gravelly sands in size. These deposits prevail in the eastern Ischia offshore, on the relict volcanic edifice of the Ischia Bank and on the genetically related parasitic vent and in the Ischia Channel. Subordinately, these deposits occur also in the northern Ischia offshore, where they unconformably overlie debris avalanches and on the top of the Forio Bank. Seismo-stratigraphic data on the Ischia Bank show that rhodolith deposits correspond to a wide wedge-shaped unit occurring on the top of the volcanic edifice, unconformably overlying the volcanic rocky substratum. In the Ischia Channel they are probably inter-layered in the highstand deposits.**

I. INTRODUCTION

Rhodolith or maërl deposits are represented by either alive or dead aggregations of coralline algae, which cover large coastal areas in the present-day oceans [1-3]. These deposits represent common facies in carbonate platform environments, in some cases indicating the transition from bioclastic-to-rocky sea bottoms [4-5]. The rhodoliths are the main components of the rhodalgal skeletal assemblage that characterizes the carbonate production in the oligophotic zone of Cenozoic and modern carbonate platforms [5-10].

Since Early Cretaceous calcareous red algae (*Rhodophyta*, *Corallinales*) live in the photic zone [11-13] from warm, tropical and temperate regions, to cold, polar and subpolar ones [5; 14-18]. The colonization of red calcareous algae occurs both on the rocky substratum and on the mobile sea bottoms. Their growth-form varies from encrusting forms to erect, articulated or free forms from the rocky substratum [12; 19-25].

Red coral algae play an important ecological role in marine ecosystems as habitat builders and produce important biodiversity peaks [3; 26-29]. The mäerl / rhodolite layers [30-33] and the coralligenous [34-36] represent important examples. Furthermore, these algae significantly contribute to the carbonate production, playing a significant role in the carbon cycle [18; 25; 33].

The maërl facies looks like a deposit of whole and/or fragmented thalli of calcareous algae, which are often collected in the concavities of the substratum [37]. The term “maërl” was documented by Crouan & Crouan [38] as a Breton word for unattached, branched corallines, living or dead, loose-lying, often occurring in extensive deposits or algal gravels found off the northwest coast of France (maërl beds or banks) [3].

This note provides an updated report on the rhodolith deposits present in the offshore island of Ischia (Gulf of Naples, Italy); it is based on data coming from sea bottom samples collected during the CARG project aimed at the realization and informatization of the marine geological cartography of the geological sheet No. 464 [39].

The island of Ischia represents the emerged part of a large volcanic field, which extends from the island of Procida to the submerged volcanoes of the western offshore of Ischia [39-41]. The occurrence of rhodolith deposits in the Gulf of Naples was highlighted by some previous studies. The sedimentological analysis of the sea bottom samples, together with the realization of geological cartography at the 1: 10.000 scale has allowed to give an updated report on the rhodolith deposits occurring in the Ischia offshore and representing both relict deposits and zones of active carbonate sediment production. Although qualitatively, the seismo-stratigraphic data allowed for the calibration of the rhodalgal deposits on previously interpreted seismic Sparker profiles [41].

Previous studies focused on rhodolith deposits in the marine areas surrounding Nisida-Posillipo (Nisida Bank and La Cavallara saddle) and the Gulf of Pozzuoli (Miseno Bank), while only a single sample came from the Ischia Bank [42]. Otherwise the present work is based on a dense network of samples collected in the Ischia offshore. Moreover, the recognition of bioclastic deposits on some Sparker seismic profiles let us to perform a qualitative calibration of data coming from sampling.

Rhodolith deposits have previously been reported in the offshore of Ischia. In particular, Toscano et al. [42] have shown the variability of the rhodalgal facies in the Gulfs of Naples and Pozzuoli, which is closely connected with the location of the platform, with the morpho-bathymetric structure, with the morphology of the sea bottom and with the hydrodynamic conditions on the submerged volcanic banks (Nisida, Miseno and Pentapalummo Banks; Ischia Bank). The top of these submerged volcanic banks is located at water depths of -28 / -30 m and is overlain by the *Posidonia oceanica* meadow, growing up to water depths of -35 / -40 m. In the marine areas where the *Posidonia* meadow is lacking, the action of the currents has controlled the formation of large fields of sandy ripples .

The aim of this work is to improve the knowledge on the rhodolith deposits of the offshore of Ischia based on sedimentological, geological and cartographic data, integrating the previous data, which mainly concern the ecology of these deposits, with a little attention paid to their location and classification within the Quaternary geological structure of the offshore of Ischia.

II. MATERIALS AND METHODS

The geological and geophysical data were acquired in the framework of the realization of the geological map n. 464 "Ischia Island" at the 1:10.000 scale [39]. Detailed geological maps, showing the distribution of sea bottom sediments, were built on the basis of the previous geological survey. Furthermore, the new sedimentological analyses of sea bottom samples allowed to reconstruct the facies distribution of the sea bottom and to compare the obtained sedimentological and geological results with the previous ones [42]. The stratigraphic framework of the investigated area is based on both high resolution seismic profiles calibrated by cores and on high resolution sequence stratigraphy). Geological and geomorphological data collected at the 1: 10.000 and 1: 5000 scales have been reported on the 1:10.000 geological maps of Campania in order to later produce national geological maps at the 1: 50.000 scale. The previously interpreted Sparker seismic profiles available around Ischia [41], were the subject of a new detailed interpretation focused on the Ischia Bank and Ischia Channel areas, aimed at the identification of bioclastic deposits and at the definition of their stratigraphic relationships with the volcanic and other sedimentary seismic units detected in the offshore of Ischia. The location of the samples analyzed to highlight the rhodolith deposits in the Ischia offshore was superimposed on the Ischia Digital Elevation Model (DEM; Fig. 1).

III. RESULTS

Sedimentological analyses were performed with the aim of showing the main compositional and textural characters of sediments sampled at the sea bottom in Ischia (Fig. 1). The sediment fractions recognized at the sea bottom based on particle size analyses include gravel sands, sands, silty sands, muddy sands, sandy silts and silts. Multibeam, Sidescan sonar and seismic data, together with samples, were acquired during the realization of sheet n. 464 "Ischia Island" of the new geological map of Italy.

On the Ischia Bank, a large volcanic edifice located in the south-eastern offshore of Ischia, an extensive meadow in *Posidonia oceanica* covers dark brown heterometric bioclastic sands (sample B1794) interpreted as rhodolith deposits due to the presence of living coralline algae. The sands cover a pebbly deposit consisting mainly of shells of mollusks, with fragments of echinoids, widespread on the *Posidonia oceanica* meadow. A low percentage of mud fraction occurs in these deposits. The rhodolith deposits were also found on the parasitic vent, genetically connected to the main volcanic edifice of

the Ischia Bank (sample B1797). Here bioclastic sands with glassy fragments, bryozoans and coralline algae have been found in a muddy lithoclastic matrix with a volcanic component. Rhodolith deposits were also found in sample B1799, located on the same adventitious cone, in which these deposits are associated with mollusk shells, small gastropods and scarce bryozoans. Rhodolith deposits occur in the Ischia Channel, where they were recovered by sample B1800. Here the rhodolith deposits are covered by an extensive meadow in *Posidonia oceanica*. Coralline algae are associated with fragments of mollusks, small gastropods, rhizomes of *Posidonia oceanica* and branched bryozoans, as well as with small slags and volcanic glass. Rhodolith deposits were also found in the offshore of Casamicciola (Ischia north; sample B1813). Here these deposits grade laterally to sandy and muddy sediments and to the debris avalanche deposits present in Casamicciola. In the western offshore of Ischia, rhodolith deposits occur at the top of the volcanic edifice of the Forio Bank, where they are characterized by coarse-grained sands and bioclastic pebbles in a scarce pelitic matrix. These deposits are completely analogous to those found on the Ischia Bank, given that the fundamental genetic analogy between the two volcanic edifices.

The sampling data on rhodolith deposits have allowed to review previous interpretations of seismic lines in the offshore of Ischia [41]. On the Ischia Bank, the rhodolith deposits are probably inter-layered within a wedge-shaped unit located at the top of the volcanic edifice, which unconformably overlies the volcanic rocky substratum, which characterizes the bank. This unit crops out at the sea bottom and can be interpreted as a unit consisting of bioclastic and partially rhodolith deposits.

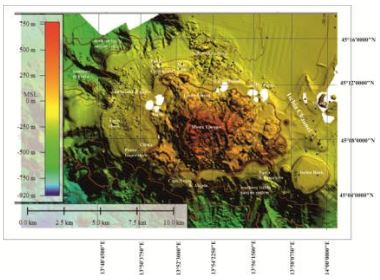

Fig. 1. Onshore-offshore DEM of Ischia reporting the sample location.

REFERENCES

[1] N.A.Kamenos, H.L.Burdett, N. Darrenougue, “Coralline Algae as Recorders of Past Climatic and Environmental Conditions”. In: Riosmena-Rodriguez R, Nelson W & Aguirre J (eds.), Rhodolith/Maerl Beds: A Global Perspective. Coastal Research Library, 2017,15, pp.27-54.

[2] S.Martin, J.M.Hall-Spencer (2017) “Effects of Ocean Warming and Acidification of Rhodolith/Maerl Beds”. In: Riosmena-Rodriguez R, Nelson W & Aguirre J (eds.) Rhodolith/Maerl Beds: A Global Perspective. Coastal Research Library, 2017,15, pp.55-86.

[3] R.Riosmena-Rodriguez, W.Nelson, J.Aguirre (Eds.) “Rhodolith/Maerl Beds: A Global Perspective”. Coastal Research Library, 15, Springer Verlag, Berlin, Germany, pp.1-359.

[4] V.A.Bracchi, D.Basso “The contribution of calcareous algae to the biogenic carbonates of the continental shelf: Pontine Islands, Tyrrhenian Sea, Italy”. Geodiversitas, 34 (1), 2012,pp.61-76.

[5] G..Carannante, M.Esteban, J.D.Milliman, L.Simone(1988) “Carbonate lithofacies as a paleolatitude indicators: problems and limitations”. Sedim. Geol., 60, 1988, pp.333-346.

[6] L.Pomar “Types of carbonate platforms: a genetic approach”. Basin Res.,13 (3), 2001, pp.313-334.

[7] D.Basso, C.Morbioli, C.Corselli (2006) Rhodolith facies evolution and burial as a response to Holocene transgression at the Pontiane Islands shelf break. In: Pedley H. M., Carannante G. (eds.), Cool-water carbonates: depositional systems and palaeoenvironmental control. Geol. Soc. of London Spec. Publ., 255, 2006, pp.23-34.

[8] L.Pomar, J.I.Baceta, P.Hallock, G.Mateu-Vicens, D.Basso”Reef building and carbonate production modes in the west-central Tethys during the Cenozoic”. Mar. and Petrol. Geol., 83, 2017, pp.261-304.

[9] J.Aguirre, J.C.Braga, D.Bassi “Rhodolits and Rhodolith Beds in the Rock Record”. In: Riosmena-Rodriguez R., Nelson W. & Aguirre J. (eds.), Rhodolith/Maerl Beds: A Global Perspective. Coastal Research Library, 2017, 15, pp.105-138.

[10] M.Brandano, I.Cornacchia, L.Tomassetti L. “Global versus regional influence on the carbonate factories of Oligo-Miocene carbonate platforms in the Mediterranean area”. Mar. and Petrol. Geol., 87, 2017, pp.188-202.

[11] H.W.Johansen “Coralline algae, a first synthesis”. CRC Press, Boca Raton, Florida (USA), 1981, pp.1-239.

[12] R.S.Steneck “The ecology of coralline algal crusts: convergent patterns and adaptative strategies”. Ann. Rev. Ecol. Syst., 17, 1986, pp.273-303.

[13] M.M.Littler, D.S.Littler “Algae, Coralline”. In: Hopley D. (ed.), Encyclopedia of Modern Coral Reefs. Structure, Form and Process. Springer Verlag, The Netherlands, 2011, pp.20-30.

[14] M.Brandano, G. Civitelli G. “Non sea-grass meadow sedimentary facies on the Pontian Islands, Tyrrhenian sea: a modern example of mixed carbonate-siliciclastic sedimentation”. Sedim. Geol., 201, 2007, pp. 286-310.

[15] J.C.Braga “Fossil Coralline Algae”. In: Hopley D. (ed.), Encyclopedia of Modern Coral Reefs. Structure, Form and Process. Springer, The Netherlands, 2011, pp.423-427.

[16] Copeland et al. (2011) A.Copeland, E.Edinger, R.Devillers, T.Bell, P.Leblanc, J.Wroblewski “Marine habitat mapping in support of Marine Protected Area management in a subarctic fjord: Gilbert Bay, Labrador, Canada”. Journ. of Coast. Conserv., 17, 2011, pp.225-237.

[17] P.Moissette, E.Koskeridou, J.J.Cornee, J.P.Andre “Fossil assemblages associated with submerged beach rock beds as indicators of environmental changes in terrigenous sediments: Examples from the Gelasian (Early Pleistocene) of Rhodes, Greece”. Palaeogeogr., Palaeoclimatol., Palaeecol., 369, 2013,pp.14-27.

[18] S.Teichert, W.Woerkeling, A.Ruggeberg, M.Wisshak, D.Piepenburg, M.Meyerhofer, A.Form, A.Freiwald A. (2013) “Arctic rhodolith beds and their environmental controls (Spitsbergen, Norway)”. Facies, doi: 10.1007/s10347-013-0372-2, 2013.

[19] J.L.Wray J.L. (1977) “Calcareous Algae”. Elsevier, Amsterdam, The Netherlands, 1977, pp. 1-185.

[20] Keats D.W. (1995) “Lithophyllum cuneatum sp. nov. (Corallinaceae, Rhodophyta), a new species of non-geniculate coralline alga semi-endophytic in Hydrolithon onkodes and Neogoniolithon sp. from Fiji, South Pacific”. Phycolog. Res., 43 (3), 1995, pp.151-160.

[21] Chamberlain Y. M. (1999) “The occurrence of Ezo epiyessoense Adey, Masaki & Akioka (Rhodophyta,

Corallinaceae) in England with a summary of parasitism and endophytism in nongeniculate Corallinaceae". Cryptogam. Algol., 20 (3), 1999, pp.155-165.

[22] R.P.Couto, E.F. Rosas-Alquicira, A.S.Rodrigues, A.I. Neto "Choreonema thuretii and Pneophyllum confervicola (Corallinales, Rhodophyta), new records of coralline algae for the Azores". Cryptogam. Algol., 32 (3), 2011, pp. 293-299.

[23] N.A.Blouin, C.E.Lane C.E. "Red algal parasites: Models for a life history evolution that leaves photosynthesis behind again and again". BioEssays, 34 (3), 2012, pp.226-235.

[24] W.J. Woelkerling, D.Bassi, Y. Iryu (2012) "Hydrolithon braganum sp. nov. (Corallinaceae, Rhodophyta), the first known exclusively fossil semi-endophytic coralline red alga". Phycol., 51 (6), 2012, pp. 604-611.

[25] G. Bressan, L. Babbini, F. Poropat F. (2013) "Corallinales del Mar Mediterraneo: MAK – chiave ed accesso casuale, dalla conoscenza alla conservazione". Biol. Mar. Mediterr., 20 (1), 2013, pp. 54-64.

[26] G.. Bressan, L. Babbini, L. Ghirardelli L., D. Basso "Bio-costruzione e biodistruzione di Corallinales nel Mar Mediterraneo". Biol. Mar. Mediterr., 8 (1), 2001, pp. 131-174.

[27] Z.T. Richards, M. Bryce M., C.Bryce " New records of atypical coral reef habitat in the Kimberley, Australia". Journ. of Mar. Biol., 2013,doi:10.1155/2013/363894.

[28] P.Fong, V.J.Paul V.J. (2011) "Coral Reef Algae". In: Dubinsky Z.& Stambler N. (eds.), Coral Reefs: an ecosystem in transition. Springer Verlag, The Netherlands, 2011, pp. 241-272.

[29] R.Riosmena-Rodriguez, M.A.Medina-López "The Role of Rhodolith Beds in the Recruitment of Invertebrate Species from the Southwestern Gulf of California, Mexico". In: Seckbach J., Einav R., & Israel A. (eds.), Seaweeds and their Role in Globally Changing Environments. Springer Verlag, The Netherlands, 2011, pp. 127-138.

[30] M.S.Foster "Rhodoliths: between rocks and soft places". Journ. of Phycol., 37, 2001, pp. 659-667.

[31] D.L. Steller, R. Riosmena-Rodriguez, M.S. Foster, C.A. Roberts C.A. (2003) "Rhodolith bed diversity in the Gulf of California: the importance of rhodolith structure and consequences of disturbances". Aquatic Conservation Marine Freshwater Ecosystems, 13, 2003, S5-S20.

[32] D.Basso, F.Quaranta, G..Vannucci, M.Piazza "Quantification of the coralline carbonate from a Serravallian rhodolith bed of the Tertiary Piedmont Basin (Stazzano, Alessandria, NW Italy)". Geodiversitas, 34 (1), 2012, pp.137-149.

[33] A.Savini A., D.Basso, V.A.Bracchi, C.Corselli, M.Pennetta "Maërl-bed mapping and carbonate quantification on submerged terraces offshore the Cilento Peninsula (Tyrrhenian Sea, Italy)". Geodiversitas, 34 (1), 2012 pp. 77-98.

[34] E.Gordini, A.Falace, S.Kaleb, F.Donda, R.Marocco, G..Tunis G. "Methane related carbonate cementation of marine sediments and related macroalgal coralligenous assemblages in the Northern Adriatic Sea". In: Harris P.T., Baker E.K. (eds), Seafloor Geomorphology as Benthic Habitat. GeoHAB Atlas of Seafloor Geomorphic Features and Benthic Habitats. Elsevier Science Publishers, 2011, pp.185-200.

[35] M.Bonacorsi, C.Pergent-Martini, P.Clabaut, G.Pergent "Coralligenous atolls: discovery of a new morphotype in the Western Mediterranean Sea". Comptes Rendus Biologies, 335 (10-11), 2012, pp.668 672.

[36] D.Curiel, A.Falace, V. Bandelj, S.Kaleb, C.Solidoro, E.Ballesteros "Species composition and spatial variability of macroalgal assemblages on biogenic reefs in the northern Adriatic Sea". Botan. Mar., 55 (6), 2012, pp.625-638.

[37] D.W.J. Bosence, R.C.L. Wilson "Carbonate Depositional system". In: The Sedimentary Record of Sea-Level Changes, Cambridge University Press, Cambridge, 2003, pp. 209-233.

[38] Crouan P.L., Crouan H.L (1867) "Florule du finistére". Paris, Friedrick Klinksiek, Libraire de l'Institut Imperial de France, Brest, France, 1867.

[39] A.Sbrana, R.M.Toccaceli, G.Biagio, E.Cubellis, C.Faccenna, M.Fedi, G.Florio, P.Fulignati, F.Giordano, G.Giudetti, M.Grimaldi, F.Italiano, W.Luperini, P.Marianelli, M.C.Buia, C.Donadio, M.C.Gambi, M.L.Putignano, G.Aiello, F.Budillon, A.Conforti, B.D'Argenio "Carta geologica di Ischia, scala 1:10.000 – Carta geologica e note illustrative". Regione Campania, Settore Difesa Suolo, Geotermia e Geotecnica, Napoli, Italia, 2011.

[40] P.P.G.Bruno, G.de Alteriis, G.Florio (2002) "The western undersea section of the Ischia volcanic complex (Italy, Tyrrhenian sea) inferred by marine geophysical data". Geophys. Res. Lett., 29 (9), 1343, doi 10.1029/2001GL013904, 2002.

[41] G.Aiello, E.Marsella, S.Passaro "Stratigraphic and structural setting of the Ischia volcanic complex (Naples Bay, southern Italy) revealed by submarine seismic reflection data". Rend. Lincei, 23 (4), 2012, pp. 387-408.

[42] F.Toscano, M.Vigliotti, L.Simone L. (2006) "Variety of coralline algal deposits (rhodalgal facies) from the Bays of Naples and Pozzuoli (northern Tyrrhenian sea, Italy)". In: Pedley H. M. and Carannante G. (eds.), Cool-Water Carbonates: Depositional Systems and Palaeoenvironmental Controls. Geol. Soc. of London, Spec. Publ., 255, 2006, pp.85-94.

High Resolution Volume Magnetic susceptibility correlation as a powerful tool for cryptotephra recognition in marine sediments.

Marina Iorio*, Francesca Budillon, Donatella D. Insinga
Ismar CNR, Calata Porta di Massa,80133 Napoli, Italy,
*marina.iorio@cnr.it

Petrophysical properties of marine deposits provide essential information on their genesis and composition thus representing a powerful tool for correlation purposes. The ISMAR-Naples (former IAMC) provides a dedicated laboratory where petrophysical data on sediment cores are acquired using a fully automated GEOTEK Multi-Sensor Core Logger working at 1/2 cm-step along the archive half, 1 h after the core has been split. The Bartington MS2E Point sensor, in particular, is used to measure the Volume Magnetic Susceptibility (VMS), which has proven to be one of the most effective petrophysical parameter used for an “event stratigraphy” approach to the study of marine records. In this framework, the VMS represents the best tool to detect cryptotephra (tephra not visible at naked eye) in sediments.

In the last decades, scientific projects focused on geological mapping, marine geo-hazards and paleoclimate research along the Campania margin used tephrochronology to date sediments and to constrain events at a high-resolution level, even at centennial scale. Major results have been achieved in the Salerno Bay where the effectiveness of this stratigraphic method for the analysis of marine records is henanced by the high sedimentation rates on the shelf and the mid-proximal location of this basin in respect to the Neapolitan volcanoes. The availability of VMS measurements obtained along the cores allowed to detect a large number of cryptotephra in this basin. In particular, a great detail exists for the Late-Holocene sequence, which is characterized by an almost repetitive and uniform cryptotephra record, from the inner shelf to the slope setting. Once chemically characterized at one site, peak to peak correlation and analyses of the whole VMS patterns along the studied cores allowed to correlate the studied isochron at other sites thus providing its areal distribution. The obtained results have important implications not only for the correct understanding of basin evolution but also for a correct evaluation of the volcanic hazard in the area.

2020 IMEKO TC-19 International Workshop on
Metrology for the Sea
Naples, Italy, October 5-7, 2020

The present-day nearshore submerged depositional terraces off the Campania coast: an analysis of their morpho-bathymetric variability

F. Budillon[1], S. Amodio[2], P. Contestabile[3], I. Alberico[1], S. Innangi[1], F. Molisso[1]

[1] *Istituto per le Scienze Marine, CNR, Calata Porta di Massa, 80133 Napoli,*
francesca.budillon@cnr.it; ines.alberico@cnr.it; sara.innangi@cnr.it; flavia.molisso@cnr.it
[2] *Dip. Scienze e Tecnologie, Univ. Parthenope, Centro Direzionale is.C4, 80143 Napoli,*
sabrina.amodio@uniparthenope.it
[3] *Dip. Ingegneria, Univ. L. Vanvitelli, via Roma 29, 81031 Aversa,*
pasquale.contestabile@unicampania.it

***Abstract* – A census of about 77 nearshore submerged depositional terraces (n-SDT), also known as Infralittoral Prograding Wedges, has been realized along the Campania offshore, in order to verify the correlation of their depths versus their fetch (thus indirectly versus the wave forcing), at a regional scale. The main morphometric parameters of each terrace were derived from high resolution DEMs, by means of a GIS-based software (Global Mapper ®). A moderate correlation occurs between the edge depth and the geographical exposure of all the n-SDT and it improves when the SW- and SE- oriented terraces only are considered; the best correlation versus the geographical exposure is observed between the edge depth of the cluster of n-SDT developed around the rocky cliffs and promontories, while a less reliable correlations have been observed for all the others parameters (slope angle of the foresets, distance from the coasts, grain size of loose sediments). The paper further describes a procedure to analyse the relationship between the depth of n-SDTs and the extreme wave climate. The objective of this study aims to learn more on the morpho-bathymetric variability of these coastal bodies and thus to provide clues on the use of their past counterparts as morphological proxies of past sea level stands.**

I. INTRODUCTION

Nearshore submarine depositional terraces (n-SDT, [1]) otherwise named Infralittoral Prograding Wedges (IPW, [2]) are depositional coastal bodies with internal clinoforms, formed seaward of the lower edge of the submarine beach [3], since the sea-level has attained the present-day position (+/- 1 m), about 6-5 ky BP [4]. These bodies typically form under the combined action of storm waves and across-shore currents, which redistribute littoral sediments below the depth of closure [5]. The position of SDTs' edges is not a direct measure of the sea-level positions because their depth depends on a complex interplay of several factors, such as the base of the storm wave and its variation in response to coastal physiography, as well as the occurrence of subsequent erosional or depositional events.

In this study we analyze a large number of n-SDTs, occurring along the south-eastern Tyrrhenian coast, to identify the controlling factors which may affect their distribution and on their reliability as environmental indicators. As a matter of facts their ancient counterparts have been used as proxies or as marine geomorphic/sedimentary markers for earlier and lower sea-level stands [6,7]. Given that the debate so far has highlighted that a number of controlling factors may affect the depth of the n-SDT, we enlarged our investigations by including also the typology of the coast in the background, the fetch, the coastal orientation, the foresets slope angle and the local wave storm climate.

II. DATA AND METHODS

This study makes use of large-scale marine digital elevation models (DEM), made up of different data set providing a minimum grid cell of about 20 m, which have been acquired over the last twenty years by IAMC-CNR, now ISMAR CNR.

Given the different late Pleistocene-Holocene morpho-structural evolution of the coastal sectors off the Campania region, a correction to the real measures of the rollover point (the break-in-slope point between topset and foresets, visible at the seabed) has been applied, to compensate the recent (historical times) vertical ground movements in unstable coastal sectors, according to the values reported in the literature. The corrected depth of the rollover points (c-ROD) for each n-SDT is a key parameter to describe such morphological coastal features. A large number of corrections derives from the archeological remains along the Campania coast [8-10]. Other correction values derive from biological-sedimentological (fossil coralline and Vermetid reefs, beachrocks, marine and semi-enclosed lagoons) and morphological sea-level indicators (tidal notch, marine terrace) [11-15]. The applied correction values range between -8 m to -1 m. Further, a correction of about -1 m has been applied to the measured depth of the rollover points, taking into account the glacio-eustatic position of sea level at about 2 ky BP, according to the local curves reconstructed along the Campania coast [4]. In coastal areas reported as being mostly stable, only the glacio-eustatic correction has been applied to the measured depth of the rollover point.

A number of 77 n-SDTs lying around Capri, Ischia and Procida islands, and from the Volturno river mouth in the Gaeta Gulf to the Maratea shoreface in the Policastro Gulf (Fig.1) has been analysed. The data set includes morphometric parameters, descriptive of the n-SDT shape (distance from the coast, c-ROD, orientation, slope angle of foresets, length in the alongshore direction) and derived from DEMs, by means of a GIS-based software (Global Mapper ®). The coastal physiography in the terraces' background was also taken into account, and four coastal morpho-types have been distinguished: linear rocky cliffs, rocky promontory, inlet/pocket beach, open shore. In addition, the present-day geographical fetch of each n-SDT has been measured and graphed.

The main idea of this procedure is that the geographical fetch, here considered as the geographical limits of the wave generation areas along a single direction at right angles to the coastline, determines the sea's response to meteorological forces, depending on the wind direction [16]. In other words, the fetch is used as index of wave forcing acting at the site. However, such assumption may fall short. In fact, sites with the same orthogonal fetch extension, and under the same perturbation, can experience very different extreme waves according to the energy dissipation due to local bottom friction and wave-breaking, and other site-specific wave phenomena. To better identify the correlation between the corrected depth of the n-SDTs and the wave hydrodynamic during severe storm condition, a numerical study of the nearshore wave pattern has been carried out. To this purpose, the numerical coastal propagation model (Mike21 SW) has been adopted [17]. The model takes into account the non-dissipative phenomena due to varying depths as refraction and shoaling, local wind generation and the dissipative phenomena due the bottom friction and wave breaking. The model also considers the effects of wave-current interaction. The computational domain was discredited using an unstructured triangulates mesh. The reference bathymetry at grid nodes was interpolated from a gridded bathymetrical data set provided by General Bathymetric Chart of the Ocean [18] with a resolution equal to 30" of arc. Wave input data have been obtained on the wave data records supplied by the pitch-roll type directional buoys operating offshore in Ponza (central Tyrrhenian Sea, 40°52′0.10″ N; 12°57′0.00″ E) actives since July 1989 as part of the Italian Buoys Network [19]. The data set comprises the spectrum zero-moment wave height (Hm0), the mean period (Tm), and wave direction (θm). For Ponza buoys, about 10% missing data, covering about 20 years of observation, have been detected. In order to get a conservative estimation in case of a lack in the time series, missing data or values of wave height of less than 0.2 m for several hours have been considered as errors and removed. The geographic transposition has been applied in the form described for instance by Contestabile et al. [20].

The numerical wave analysis performed in the present work was aimed to evaluate some correlation between the depth of the depositional terraces and the wave hydrodynamic during severe storm condition. According to current coastal engineering practice, extreme events are described in terms of the function HS(TR), which links the significant wave height (HS) of a sea state with different return periods TR [21,22]. To produce a set of extreme significant wave height values, the Peak Over Threshold (POT) method was followed, adopting a Generalized Pareto Distribution.

III. GEOGRAPHY AND COASTAL MORPHOLOGY

The Campanian coast, about 480 km long, shows a variable topography for the occurrence of volcanic areas, islands and due to the NE-SW trending ridges of the Monte Massico, Sorrento Peninsula and Cilento Promontory, which bound the main tectonic depressions of the Campania and Sele Plains (Fig.1).

The coastal physiography of the study area can be mainly subdivided in low and high coasts. The low sandy coasts are open shores and characterise the widest gulfs of the Campania region (Gaeta, Napoli and Salerno) at the seaward edge of the main alluvial plains (Volturno, Sarno and Sele rivers, respectively).

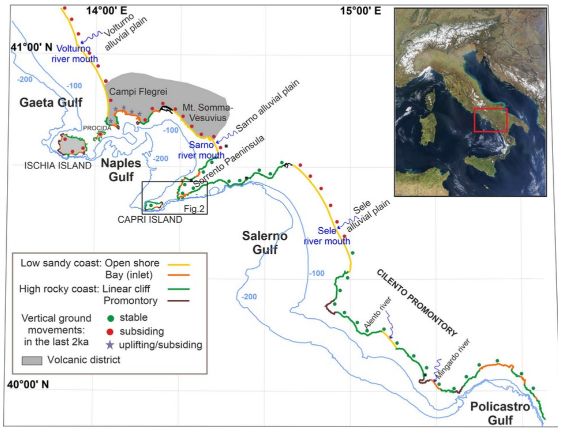

Fig. 1. Location and coastal morphology of the study area

The high coasts occur in the volcanic areas (Ischia Island, Campi Flegrei and Mt. Vesuvius), along the main structural-relieved sectors (Capri Island, Sorrento Paeninsula, Cilento) and are characterised by rocky promontories, small inlets and linear rocky cliffs. The small inlets commonly held pocket beaches, characterised by coarse loose sediments.

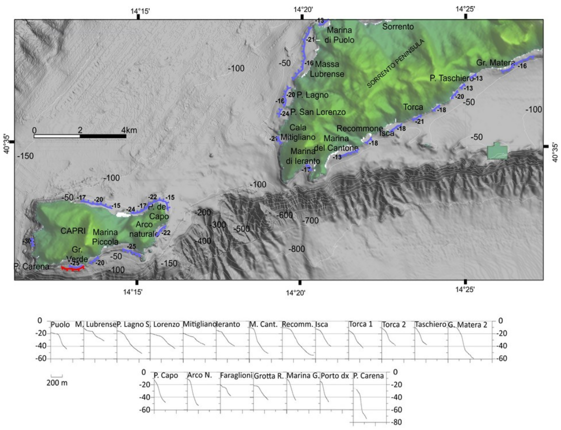

Fig. 2. a) Location of the identified n-SDT (modern terraces in violet, ancient terraces in red) around the Sorrento Paeninsula and Capri Island, a stable area since the last 100 ky [23]; b) topographic profiles of the terraces.

IV. PRELIMINARY RESULTS

The general shape of the n-SDT bodies is convex upwards in shore-normal profile and convex-seaward in plan-view (fig.2a and 2b). They are continuous and elongated prisms, extending hundreds of meters up to kilometers in the shore-parallel direction and are up to tens of metres thick. The c-ROD ranges from -3.5 m to -36 m.

A dimensional remarkable difference comes out between terraces off sediment-starved and high-sediment- supplied coasts (e.g. at river mouth). Off the river mouths (Volturno, Sele, Alento, Mingardo and Bussento rivers) the toplap surface of the n-SDT corresponds to the subacqueous delta top in the inner shelf and the foreset corresponds to the subacqueous delta slope and prodelta environment [24,25]. We observe that the distance from the shoreline of the c-ROD and of the bottomset is much higher (values ranging from hundreds of metres to kilometres) than those along the starved coasts, the rollover point is much smoother and slope angle much gentler, as expected due to the fluvial particle yield.

A. Numerical analysis (depth/fetch)

The first analysis plots the c-ROD of each n-SDT versus the length (km) of the present-day geographical fetch (PDF), regardless the orientation of the terrace. A general direct correlation can be observed and R^2 is moderate (0,39). The correlation increases to $R^2 = 0,42$ if the n-SDT oriented towards the South are excluded from the analysis (Fig.3). The reason of this exclusion is explained in the next paragraph. Three clusters can be observed in the general plot (marked in red, green and violet circles); they are linked to the geographical outline of the coast, which confines the fetch of the n-SDT. The first cluster at about 40 km along the X axis corresponds to the geographical barrier of the coasts of the Napoli Gulf and of the islands which limits the fetch of the NW-, SE-, NE- oriented n-SDT lying in the Napoli Gulf itself; the cluster at 300 km along the X axis is linked to the Calabria-Sicilia geographical boundary with respect to S- and SE-oriented n-STD of the Napoli Gulf and Salerno Gulf; the third cluster at 600 km along the X axis is represented by the geographical boundary of the Algerian-Tunisian coast with respect to the SW-oriented Campania n-SDT and by the geographical boundary of the Liguro-Provencal coast with respect to the ones oriented towards the NW.

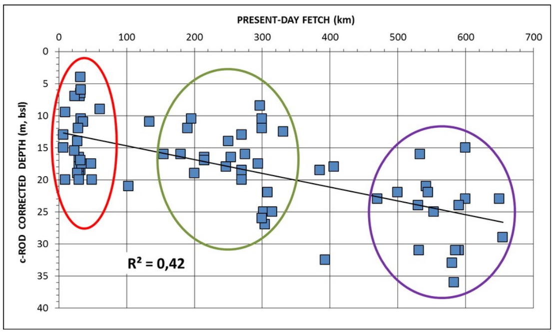

Fig. 3. General correlation between c-ROD versus the present-day geographical fetch (PDF) (R^2= 0,42) for each terrace, regardless the geographical orientation. The three clusters group the geographical fetch of the n-SDT, confined by the Napoli Gulf coast, by the Calabria and Sicily coasts and by the Tunisia and Liguria coasts.

B. Relation c-ROD/ present-day geographical fetch for specific n-SDT orientation

The correlation of the c-ROD versus the present-day geographical fetch (PDF) for each class of orientation (NW, SE, S, NE, SW, SSE, E, N) shows contrasting results with R^2 almost null (R^2 = 0,02 for the group of SSE- and NE- oriented n-SDT) or very low (R^2 = 0,2 for the SE- oriented n-SDTs). The correlation increases to about 0,41 for the SW-oriented terraces and to 0,67 for those NW-oriented (Figs. 4 and 5). Oddly, the correlation between the cluster of the S-oriented terraces is inverse (i.e. the longer the fetch, the shallower the c-ROD) and has no logical explanation, so far. This is the reason why the general correlation in Fig. 3 improves in absence of the S-oriented n-SDTs.

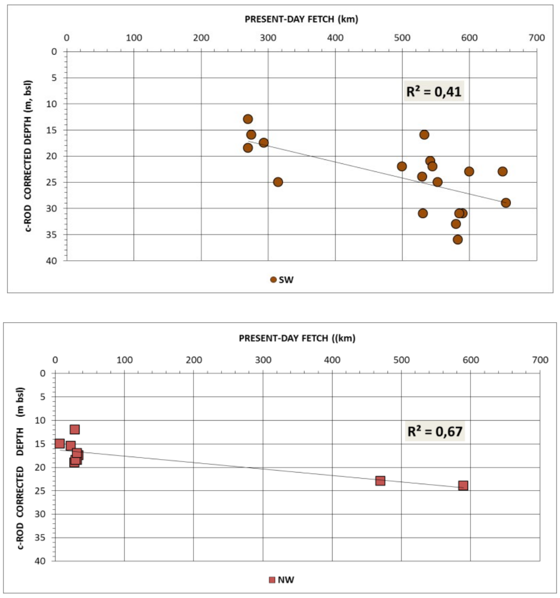

Fig. 4 Correlation between c-ROD versus the present-day geographical fetch (PDF) of the SW- and NW-oriented n-SDTs; a) the two clusters group the n-SDTs, whose geographical fetch is confined by the Calabria-Sicilia coasts and by the Tunisia coast; b)the two clusters group the n-SDTs, whose geographical fetch is confined by the Napoli Gulf and by the Liguria coast.

C. Relation c-ROD/ present-day geographical fetch of terraces grouped in coastal morphotypes.

The analysis of the n-SDTs grouped for the different morpho-types of the coast (*inlet, promontory, rocky cliff, open shore*) shows a moderately good correlation for the first three classes (R^2= 0,37 – 0,46 - 0,43 respectively), and an uncertain result for the *open-shore* category (R^2=0.02). In this last case, the uncertain result is biased by the low number of terraces and also by their belonging to the subset of terraces SW-oriented. It is possible to infer that in the areas where the yield of fine sediments is particularly high (as in this case), the fluvial processes prevail over the storm-wave climate regime and thus the length of the fetch turns to be not relevant. On the contrary, in the coastal sector where the fine-sediment availability in the shore system is limited (as in the case of the n-SDTs formed around the promontories, rocky cliffs and within the isolated inlets), the morphological action of the storm wave regime is more effective on the long term in transferring sediment across-depth and the geographical exposure of the terraces is a relevant factor in their development through the time.

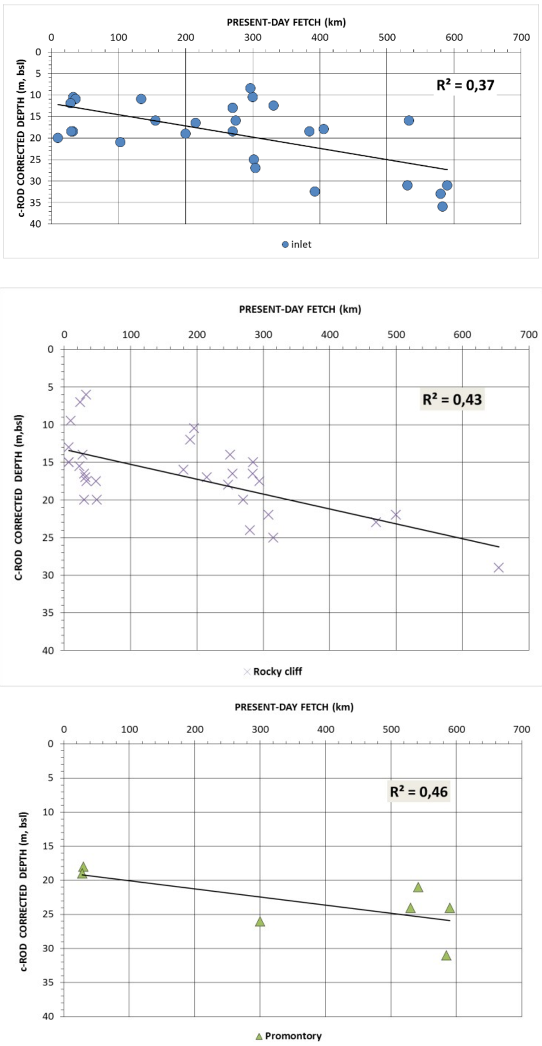

Fig. 5. The c-ROD versus PDF correlation for each morpho-type class displays R^2 ranging from 0,37 to 0,46. The correlation of the open shore morpho-type is inverse and not shown (see text for explanation).

D. Preliminary analysis of relation c-ROD/ extreme significant wave heights.

The analysis of the offshore wave data for the Campania region has allowed the identification of three directional wave sectors (i.e., 70-190° N; 19-250° N; 250-320° N). In order to guarantee directional homogeneity, i.e. by classifying mean sea storm directions into directional sectors, the extreme wave height analysis has been repeated for each directional sector. Results of HS(TR), along with the correspondent peak wave period (TP), are reported in Table 1. The selected value of TR is 200 years, a time span considered long enough to be representative of the environmental conditions over the last 2 ky, and at the same time, compatible with the length of the original time series used to perform the statistical analysis.

Finally, the three extreme sea states have been propagated applying the MIKE 21 SW model under different directions. Results of wave propagation is graphically represented in Fig. 6.

Table 1. Results of Extreme wave height analysis

	Directional wave sector		
	70-190° N	190-250° N	250-320° N
HS(TR=200 years) [m]	6.5	8.3	10.8
TP [s]	11	12.4	14.1

A first attempt to test this approach has been performed on the n-SDTs of Ischia island, exposed to the S-SW. Part of this subset belongs to the category of n-SDTs experiencing the inverse relation observed between c-ROD and PDF (cfr. paragraph IV B). Preliminary results reveal a very good relationship between c-ROD and calculated extreme wave height at each depositional terraces along this coastal area. Such a correlation can be adequately represented by a logarithmic plot (Fig. 7), reporting the local significant wave high during storm conditions and the c-RODs in the area. A relatively high correlation factor can be found, i.e. a root mean squared error, R, higher than 90%. Therefore, a heuristic explanation of the inverse relation c-ROD versus PDF in the subset S-oriented terraces could be proposed. Based on the previous observations of high reliability offered by the local extreme H_S assessment, it is suggested as the use of the fetch as wave forcing indicator could lose its efficiency in some conditions.

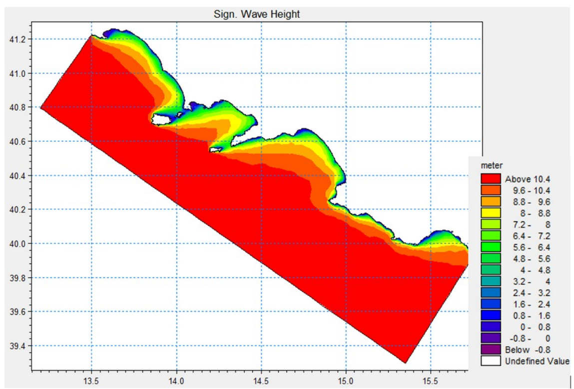

Fig. 6. Example of resulting extreme significant wave height for the Campania region after propagation.

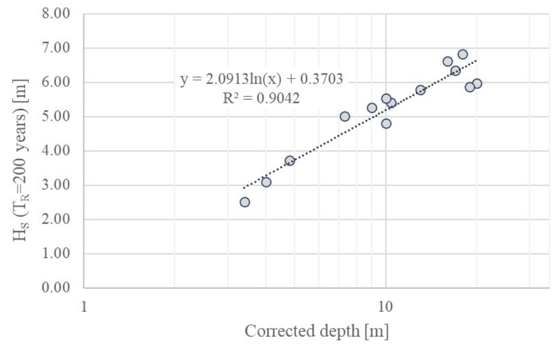

Fig. 7. The correlation between c-ROD and local significant wave height (for a return period of 200 years) for n-SDT in two bays at Ischia island.

V. PRELIMINARY CONCLUSIONS

A census of 77 nearshore submerged depositional terraces (n-SDT) along the Campania offshore has been accomplished, in order to verify the correlation of their depths versus their geographical exposure (thus indirectly versus the wave climate), at a regional scale. The morphometric analysis of key parameters let us to infer that:

- the present-day n-SDTs in the south-eastern Tyrrhenian Sea have extremely variable lateral extensions (from tens of metres to kilometers) and variable depth of the rollover point (ranging from -3.5 m to -36 m); a slight variation in depth can be observed within the same terrace, especially where the coastal morphology in the background, suddenly changes;
- a moderate correlation between c-ROD and the present-day geographical fetch occurs (R^2=0,39) even if the typology of coastal morphology is overlooked; the coefficient improves to R^2= 0,44 if the terraces oriented towards the S are excluded from the analysis;
- the most responsive n-SDTs to the variation of the geographical exposure are those NW- and SW oriented;
- among the cluster of terraces grouped for their coastal morpho-types, the most responsive to the variation of the PDF are those belonging to the *inlets, promontories and rocky cliffs* categories ($0,37 \leq R^2 \leq 0,46$), while the n-SDT off the *open shores* seem to feel the effect of the fluvial processes more than the storm wave climate regime;
- a further analysis performed on a restricted spatial scale – i.e. on the n-SDTs localized S and SW of the Ischia Island- showed a clear logarithmic relationship between the local extreme significant wave height and c-ROD; the outcomes of this approach are promising so that future work will extend the numerical analysis here reported to a larger spatial scale.

REFERENCES

[1] D.Casalbore, F.Falese, E.Martorelli, C.Romagnoli, F.L.Chiocci, "Submarine depositional terraces in the Tyrrhenian Sea as a proxy for paleo-sea level reconstruction: Problems and perspective", Quat. Int., 2020, vol.544, pp. 1-11

[2] F.J.Hernández-Molina, L.M.,Fernández-Salas, F.Lobo, L.Somoza, V.Díaz-del-Río, J.M.Alveirinho Dias, "The infralittoral prograding wedge: A new large-scale progradational sedimentary body in shallow marine environments", *Geo-Mar. Lett.*, vol. 20. No.2, 2000, pp. 109-117.

[3] M.E.Field, P.S.Roy, "Offshore transport and sand-body formation: evidence from a steep, high-energy shoreface, South-eastern Australia" J. Sedim. Petr., 1984, vol. 54, No.4, pp. 1292-1302.

[4] K.Lambeck, F.Antonioli, M.Anzidei, L.Ferranti, G.Leoni, G.Scicchitano, S.Silenzi, "Sea level change along the Italian coast during the Holocene and projections for the future", Quat. Int., 2011, vol. 232, No.1-2, pp. 250-257.

[5] N.C.Mitchell,G.Masselink, J.M.Huthnance, L.M.Fernández-Salas, F.J.Lobo, "Depths of modern coastal sand clinoforms", J. Sediment. Res., 2012, vol. 82, pp. 469–481.

[6] F.L.Chiocci, L.Orlando, "Lowstand terraces on Tyrrhenian Sea steep continental slopes", Mar. Geol.,1996, vol. 134, No.1-2, pp.127-143.

[7] F.Pepe, G.Bertotti, L.Ferranti, M.Sacchi., A.M. Collura, S.Passaro, A.Sulli, "Pattern and rate of post-20 ka vertical tectonic motion around the Capo Vaticano Promontory (W Calabria, Italy) based on offshore geomorphological indicators" Quat. Int. 2014, vol. 332, pp. 85-98.

[8] F.Antonioli, L.Ferranti, A.Fontana, A.Amorosi, A. Bondesan, C.Braitenberg, A.Dutton, G.Fontolan, S. Furlani, K.Lambeck, G.Mastronuzzi, C.Monaco, G. Spada, P.Stocchi, "Holocene relative sea-level changes and vertical movements along the Italian and Istrian coastlines", Quat. Int., 2009, vol. 206, pp.102–133.

[9] M.Anzidei, K.Lambeck, F. Antonioli, S. Furlani, G.Mastronuzzi, E.Serpelloni,G.Vannucci, "Coastal structure, sea-level changes and vertical motion of the land in the Mediterranean", Geol. Soc. London, Spec. Publ., 2014,No. 388, pp. 453-479.

[10] P.Aucelli, A.Cinque, G.Mattei, G.Pappone, A.Rizzo, "Studying relative sea level change and correlative adaptation of coastal structures on submerged Roman time ruins nearby Naples (southern Italy)", Quat. Int., 2019, vol. 501, Part B, pp. 328-348.

[11] G.Buchner, A.Italiano, C.Vita-Finzi, "Recent uplift of Ischia, southern Italy", In W.J. Mc Guire, A.P. Jones, J. Neuberg (Eds.), Volcano Instability on the Earth and Other Planets, Geol. Soc. Spec. Publ., London, 1996, vol. 110, pp. 249-252.

[12] A.Cinque, G.Irollo, P.Romano, M.R.Ruello, L.Amato, D.Giampaola, “Ground movements and sea level changes in urban areas: 5000 years of geological and archaeological record from Naples (Southern Italy)”, Quat. Int., 2011, vol. 232, No.1–2, pp. 45-55.
[13] S.Vogel, M.Märker, F. Seiler, “Revised modelling of the post-AD 79 volcanic deposits of Somma-Vesuvius to reconstruct the pre-AD 79 topography of the Sarno River plain (Italy)”, Geol. Carpatica, 2011, vol. 62, No.1, pp. 5-16.
[14] M.L.Putignano, P.E.Orrù, M.Schiattarella, “Holocene coastline evolution of Procida Island, Bay of Naples, Italy”, Quat. Int, 2014, vol. 332, pp. 115-125.
[15] M.Vacchi, N.Marriner, C.Morhange, G.Spada, A.Fontana, A.Rovere, “Multiproxy assessment of Holocene relative sea-level changes in the western Mediterranean: Sea-level variability and improvements in the definition of the isostatic signal”, Earth-Sci. Rev. 2016, vol.155, pp. 172–197.
[16] S.Corsini, L.Franco, R.Inghilesi, R.Piscopia, “Atlante delle onde nei mari Italiani–Italian”, Waves Atlas, Agenzia per la Protezione dell’Ambiente e per i Servizi Tecnici (APAT) and University of Rome: Rome, Italy, 2004, p. 3.
[17] DHI Water and Environment. Available online: https://www.dhigroup.com/
[18] General Bathymetric Chart of the Oceans. Available online: http://www.gebco.net/
[19] D.Vicinanza, L.Cappietti, V.Ferrante, P.Contestabile, “Estimation of the wave energy in the Italian offshore”, J. Coast. Res. 2011, vol. 64, pp.613-617.
[20] P.Contestabile, F.Conversano, L.Centurioni, U.M.-Golia, L.Musco, R.Danovaro, D.Vicinanza, “Multi-collocation-based estimation of wave climate in a non-tidal bay: The case study of Bagnoli-Coroglio bay (Tyrrhenian Sea)”, Water, 2020, vol.12, N°7, 1936.
[21] F.Dentale, P.Furcolo, E.Pugliese Carratelli, F.Reale, P.Contestabile, G.R.Tomasicchio, “Extreme wave analysis by integrating model and wave buoy data”, Water, 2018, vol.10, N°4, pp. 373.
[22] D.Di Luccio, G.Benassai, G.Di Paola, C.M.Rosskopf, L.Mucerino, R.Montella, P.Contestabile, “Monitoring and modelling coastal vulnerability and mitigation proposal for an archaeological site (Kaulonia, Southern Italy)”. Sustainability, 2018, vol. 10, N°6, 2017.
[23] P.Aucelli, A.Cinque, G.Mattei, G.Pappone, “Historical sea level changes and effects on the coasts of Sorrento Peninsula (Gulf of Naples): New constrains from recent geoarchaeological investigations”, Palaeogeography, Palaeoclimatology, Palaeoecology, 2016, vol. 463, pp. 112-125.
[24] A.Cattaneo, F.Trincardi, A.Asioli, A.Correggiari, “The Western Adriatic shelf clinoform: energy-limited bottomset”, Cont. Shelf Res., 2007, vol.27, pp. 506–525.
[25] S.Patruno, G.J.Hampson, C.A-L. Jackson, “Quantitative characterisation of deltaic and subaqueous clinoforms”, Earth-Sci. Rev., 2015, Vol. 142, pp.79-119.

Tsunamigenic mass-failure scenarios in the Palinuro volcano chain

Glauco Gallotti[1], Guido Ventura[2], Alberto Armigliato[1], Filippo Zaniboni[1], Gianluca Pagnoni[1], Liang Wang[1], Salvatore Passaro[3], Marco Sacchi[3], and Stefano Tinti[1]

[1]University of Bologna, Department of Physics and Astronomy (DIFA), Bologna, Italy (glauco.gallotti2@unibo.it)

[2]National Institute of Geophysics and Volcanology (INGV), Roma, Italy.

[3]Institute of Marine Sciences (ISMAR), National Research Council (CNR), Napoli, Italy.

The Palinuro volcanic chain is located nearly 80 km offshore the Campania coasts (Italy), in the southern sector of the Tyrrhenian Sea. 15 distinct volcanic edifices have been recently detected, covering a 90 km long and 20 km wide belt. The presence of shallow seismicity and active hydrothermal activity suggests that this large volcanic chain is still active. Nevertheless, its associated volcanism is still poorly understood. Specific sectors of the complex show the existence of ongoing slope instability. Thus, the chance of mass movements cannot be ruled out as a consequence of seismic or volcanic activity. In this work, a stability analysis for typical seismic loads in such a volcanic area has been performed through a revised limit equilibrium approach. Three mass failure scenarios have been reconstructed by means of numerical models in the weaker sections found. The tsunami triggered by each slide has been simulated, and considerable waves have been found in two of the three hypothesized scenarios. For the biggest slide of 2.4 km^3, waves as high as 10 m could reach portions of the Calabria coasts.

This study belongs to a series of works focused on the numerous volcanic structures of the Tyrrhenian Sea that are still poorly investigated. Considering scenarios involving mass movements of different sizes and based on geomorphological features seems to be a feasible strategy to evaluate the tsunami hazard in the region.

Indice degli autori

F

G

H

I

K

L

M

N

O

P

Q

R

S

T

V

W

Z